Alteration of Volcanic Glasses in Marine Sediments: Laboratory Experiments and Field Studies

Dissertation

zur Erlangung des Doktorgrades
der Mathematisch-Naturwissenschaftlichen Fakultät
der Christian-Albrechts-Universität
zu Kiel

vorgelegt von

Ulrike Schacht

Kiel 2005

Referent/in: .....

Korreferent/in: .....

Tag der mündlichen Prüfung: .....

Zum Druck genehmigt: .....

Der Dekan

Hiermit erkläre ich an Eides statt, dass ich die vorliegende Doktorarbeit selbständig erstellt und keine anderen als die angegebenen Hilfsmittel verwendet habe. Ferner habe ich weder diese noch eine ähnliche Arbeit an einer anderen Stelle im Rahmen eines Prüfungsverfahrens vorgelegt, veröffentlicht oder zur Veröffentlichung eingereicht.

Ulrike Schacht

“The time has come” the Walrus said
“To talk of many things:
Of shoes - and ships - and sealing wax -
of cabbages - and kings ...
and why the sea is boiling hot
and whether pigs have wings.“

Lewis Carroll (1871)
Throuh the Looking Glass

Preface

This study comprises a general introduction presented in Chapter I, and four stand-alone publishable papers – Chapters II to V. Each of the chapters contains a separate introduction, description of methods, presentation of data and discussion, as well as a separate reference list. The independent publications are in press, submitted for publication, as well as in preparation for submission to international journals or textbooks. They may therefore be subject to revision.

The titles and authors of the Chapters II, III, and IV are briefly listed below:

Chapter II

Alteration of Differently Composed Volcanic Glasses in Marine Sediments: Insights into Alteration Pathways and Dissolution Kinetics

Authors Ulrike Schacht, Steffen Kutterolf, Klaus Wallmann, and Mark Schmidt

Status submitted to *Geochimica et Cosmochimica Acta*

Chapter III

Volcanogenic Sediment-Seawater Interactions and the Geochemistry of Pore Waters

Authors Ulrike Schacht, Klaus Wallmann, Steffen Kutterolf, and Mark Schmidt

Status to be submitted to *Chemical Geology*

Chapter IV

The Influence of Volcanic Ash Alteration on the REE Composition of Marine Pore Waters

Authors Ulrike Schacht, Steffen Kutterolf, Klaus Wallmann, and Mark Schmidt

Status to be submitted to *Geochimica et Cosmochimica Acta*

I contributed to these papers by field work in Costa Rica, by work at sea offshore Nicaragua and Costa Rica, by using an experimental approach – including the set-up of two different experimental build-ups and sample preparation before and after the single experimental runs – by chemical analyses using the EMP, ICP-OES, ICP-MS,

LA-ICP-MS, REM, XRF, and XRD, by processing and interpreting all of the field and experimental data, as well as by writing and preparation of manuscripts.

In addition to the work presented in Chapters II - IV, I cooperated with members of the Sonderforschungsbereich 574 (SP C4) and of the Geological Institute at the University of Copenhagen and contributed to the following publications.

CHAPTER V

Onshore to Offshore Tephrostratigraphy and Marine Ash Layer Diagenesis in Central America

Authors Steffen Kutterolf, Ulrike Schacht, Heidi Wehrmann, Armin Freundt, and Tobias Mörz

Status in press – Alvarado, G. and Buntschuh, J. (eds.): *Central America: Geology, Resources, and Hazards*. Balkema (Lisse, Niederlande, Tokio, Japan)

The following two articles are not included in this study:

High-Speed Ocean Water Fertilisation with Subduction Zone Volcanic Ashes

Authors Svend Duggen, Peter Croot, and Ulrike Schacht (The three authors contributed equally to the study)

Status submitted to *Nature*

Tephrostratigraphy offshore Nicaragua - Implications for Sedimentation Rates and Subduction Input

Authors Steffen Kutterolf, Armin Freundt, Ulrike Schacht, Heidi Wehrmann, and Hans-Ulrich Schmincke

Status to be submitted to *Earth and Planetary Science Letters*

Abstract

Large volumes of mainly felsic volcanic ashes have been repeatedly released during explosive volcanic eruptions along the Central American Volcanic Arc. These ashes are found as up to several centimetres thick ash layers in marine sediments offshore Nicaragua and Costa Rica. Since volcanic ashes constitute such a major fraction of slope sediments and subducted deep sea sediments off Nicaragua and Costa Rica its alteration is significantly affecting the chemical signatures of sediments and pore waters. New results of mafic and felsic glass alteration were derived from extensive field investigations of marine tephra deposits and diagenetic processes in related pore waters as well as laboratory dissolution experiments.

Nearly all glass shards of each mafic ash layer retrieved in marine sediment cores were altered with a variation of the degree of alteration. The initial mafic glass alteration in a marine environment is characterised by the rapid removal of alkali and alkaline-earth metals, commonly referred to as network modifying elements, Si and Al, the active enrichment of H_2O and the passive enrichment of Fe and Mg in the glass surface. The initial stage of congruent dissolution is followed by a second stage of aging when basaltic glass alters to palagonite. Palagonite forms a continuous rim on the glass grains. Electron microprobe (EMP) analyses indicate that it accommodates about 15 wt% of water and is leached in all investigated elements except Fe, Mg and in some cases K. At more advanced stages of alteration, element fluxes are also influenced by the formation of secondary phases such as clay minerals, zeolites, or carbonates.

In contrast, felsic glass shards were generelly fresh looking and coexisted with only some strongly altered shards. Shards showing intermediate stages of alteration were absent. EMP analyses of felsic shards, experimentally altered as well as taken from marine ash layers, show an active uptake of H_2O. Almost constant concentrations for network forming elements such as Si and Al indicate only little replacement of Si and Al. Network modifying elements (K, Na, Ca) show varying concentrations, indicating either loses or gains during alteration and the formation of a leached layer. Its thickness does not exceed a few µm. The stage of hydration can proceed until a saturation point of about 3 wt% of H_2O is reached. Further weakening and breakage of the Si-O-Si bonds of the glass structure results in a nearly complete dissolution of the glass which is illustrated by the well constrained composition of the investigated felsic ash layers. A palagonite-like interstage product is missing, resulting in the apparent unaltered appearance of marine

felsic ash layers. This study confirms that secondary minerals will be formed by the direct precipitation from the leaching solution.

The losses of rare earth elements (REE) during seawater alteration seem to be independent of the glass composition. LA-ICP-MS analyses of naturally as well as experimentally altered glass shards of mafic and felsic composition indicate glass shards are characterised by a systematic decrease in REE concentrations at the outer altered rim. That REE can be significantly mobilised during seawater alteration of volcanic glasses is also shown by pore water data of marine sediment cores. Their dissolution behaviour in marine pore waters indicates that the release of the REE is most effective when open ocean conditions, characterised by low rates of organic matter degradation, prevail. Under this conditions the release of REE results in fluxes of at least 0.04 nmol La cm^{-2} yr^{-1} and 0.09 nmol Ce cm^{-2} yr^{-1}. But pore water investigations also imply that REE generated from volcanic ash alteration are quickly removed removed from the solution. For this phosphate precipitation processes like carbonate fluorapatites may be considered as a major sink.

Besides insights into the chemical evolution of volcanic glasses, the experimental work also provides kinetic data concerning the initial stage of mafic and felsic glass alteration. Within the investigated low temperature (25-50°C) range mafic glass dissolved at about the same rate ($10^{-12.5}$ – $10^{-8.7}$ mol m^{-2} sec^{-1}) as felsic glass ($10^{-12.4}$ – $10^{-9.1}$ mol m^{-2} sec^{-1}). However, at 100°C and 200 bar activation energies (E_a), calculated from the Arrhenius equation, of mafic glass dissolution were significantly larger (84.6 kJ mol^{-1}) than for felsic glass dissolution (66.2 kJ mol^{-1}), implying a greater sensitivity of mafic glass dissolution kinetics to temperature changes. Consequently, the *in-situ* dissolution rate under seafloor conditions (2°C, 200 bar), was lower for mafic glass (1 x 10^{-13} mol m^{-2} sec^{-1}) than for felsic glass (3 x 10^{-13} mol m^{-2} sec^{-1}). More evolved products of volcanism which prevail at most volcanic arcs are therefore highly reactive when exported into the marine environment.

Former studies of dissolution kinetics have revealed many factors, which control glass alteration and the formation of alteration products. These include besides the chemical composition of the contact solution the composition of the starting material, and the temperature. The data presented in this study suggest, that dissolution rates are not only affected by temperature but also by pressure, which was not described so far. Therefore, temperature as well as pressure conditions have to be considered for *in-situ* kinetic calculations.

Previous studies showed that the major element composition of pore fluids recovered from long sediment cores obtained by deep-sea drilling are also significantly affected by volcanic matter alteration. Continuous losses of Mg, Na, and K and an enrichments of Ca and Si in pore waters were documented in these studies. However, no significant effect of ash alteration on the major cation concentrations of the investigated pore fluids could be resolved. This observation implies that ash alteration is a very slow process in marine surface sediments.

Dissolved silica concentrations were, however, clearly enhanced by the dissolution of volcanic ashes. A transport-reaction model was applied to the silica and ash data from these marine sediment cores to constrain the rate of dissolved silica release during volcanic glass alteration. The modelling showed that further silica release is inhibited when the dissolved silica concentration in the pore fluids approaches a saturation value of 450 µmol L^{-1}. Hence ash dissolution occurs mainly in the upper sediment horizons were dissolved silica concentrations are low and smaller than the saturation value. A good fit to the data was obtained applying the following kinetic rate law:

$$R_G = k_{GS} \cdot G \cdot \left(1 - \frac{Si}{Si_{Max}}\right)$$

where R_G is the rate of glass dissolution, G is the glass concentration in the core, Si_{Max} is a saturation concentration of dissolved silica (450 µmol L^{-1}) and Si is the concentration of dissolved silica in the investigated pore fluids. The kinetic constant k_{GS} was determined as 3 x 10^{-5} yr^{-1} by fitting the model to the data.

The rate of silica release recorded in the laboratory short-term studies was at least two orders of magnitude higher than the *in-situ* rate derived from the pore water data. The deviation between field data and experimental results is probably related to the much shorter observation time and the higher water rock ratio applied in the experiments. Moreover, the reactivity of the ash surfaces might have been enhanced by the procedures applied during the experiments and the previous separation of glass samples from the sediment matrix. The rate law and the kinetic constant derived from the field data better reflect the rate of ash dissolution at the seafloor. They should hence be considered in future studies of volcanic glass alteration in marine surface sediments.

Kurzfassung

Große Mengen vulkanischer Aschen, hauptsächlich felsischer Zusammensetzung, werden regelmäßig während explosiver Eruptionen entlang der mittelamerikanischen Vulkankette freigesetzt. Diese Aschen werden als mehrere Zentimeter mächtige Lagen in den marinen Sedimenten vor den Küsten Nicaraguas und Costa Ricas abgelagert. Sie stellen somit einen Hauptbestandteil der marinen Fore-Arc- und subduzierten Tiefseesedimente dar. Da ihre Alteration die chemische Zusammensetzung der marinen Porenwässer und Sedimente maßgeblich beeinflusst, stellt diese Arbeit neue Erkenntnisse über die Alteration mafischer als auch felsicher vulkanischer Gläser vor, die auf intensiver Feld- als auch Laborarbeit beruhen.

Nahezu alle Gläser mafischer Aschelagen aus den untersuchten marinen Sedimentkernen zeigten deutliche Anzeichen von Alteration. Die experimentelle Untersuchung des Lösungsverhaltens mafischer Gläser im Kontakt mit Meerwasser zeigte, dass die anfängliche Alteration mafischer Gläser durch die schnelle Lösung von Alkali- und Erdalkalielementen, sogenannten Netzwerkwandlern, sowie durch die Lösung von Si und Al und die Aufnahme von Wasser gekennzeichnet ist. Dieser anfängliche Schritt der kongruenten Lösung ist begrenzt auf den äußeren Rand der einzelnen Glaspartikel. In einem zweiten Stadium der Alteration erfolgt die kontinuierliche Umwandlung des äußeren Randes in eine Rinde aus Palagonit. Mikrosondenanalysen verdeutlichen, dass eine solche Alterationsrinde aus bis zu 15 Gw% H_2O bestehen kann und in allen untersuchten Elementen, mit Ausnahme von Fe, Mg und gelegentlich auch K, verarmt ist. Mit fortschreitender Alteration erfolgt eine kontinuierliche Umwandlung der einzelnen Gläser. Die oben beschriebenen Elementflüsse werden dann durch die Bildung von Sekundärmineralen beeinflusst. Hierbei handelt es sich typischer Weise um Tonminerale, Zeolithe und Karbonate.

Im Gegensatz zu ihrem mafischen Pendant wirkten die Gläser felsischer Aschelagen frisch und wenig beeinflusst von Alterationsvorgängen. Sie treten gemeinsam mit nur wenigen stark alterierten Gläsern auf. Gläser eines mittleren Alterationsstadiums fehlten völlig. Mikrosondenanalysen einzelner felsischer Glasscherben zeigen auch hier eine deutliche Anreicherung von Wasser als Ergebnis der Alteration. Die Konzentrationen von Si und Al weisen nur geringe Veränderungen auf. Dies ist ein Hinweis darauf, dass Netzwerkbildner bei der Alteration felsischer Gläser nur wenig von den Alterationsvorgängen betroffen sind. Netzwerkwandler (K, Na, Ca) hingegen werden angereichert bzw. abgereichert.

Dies führt zur Ausbildung einer dünnen Alterationsrinde, deren Mächtigkeit jedoch nur wenige Mikrometer erreicht. Der Wassergehalt innerhalb dieser Rinde beträgt maximal 3 Gw%. Eine weitere Wasseraufnahme führt zur Schwächung der Glasstruktur und somit zu einer fast vollständigen Lösung der einzelnen Glaspartikel. Die Ausbildung einer Alterationsrinde, welche aus Sekundärmineralen besteht, fehlt, was das scheinbar frische Erscheinungsbild mariner felsicher Aschelagen zur Folge hat. Die Bildung von Sekundärmineralen erfolgt durch deren Ausfällung aus der alterierenden Lösung.

Die Lösung Seltener-Erd-Elemente (SEE) aus der Glasstruktur scheint unabhängig von der chemischen Zusammensetzung der vulkansichen Gläser statt zu finden. LA-ICP-MS Analysen natürlicher als auch experimentell alterierter, mafischer und felsicher Gläser zeigen deutlich eine Verarmung an SEE innerhalb des äußersten Alterationssaumes. Dass signifikante Mengen an SEE während der marinen Alteration aus vulkanischen Gläsern mobilisiert werden können wird durch die Untersuchungen mariner Porenwässer bestätigt. Dieser Prozess ist besonders dann signifikant, wenn nur geringe Abbauraten organischer Substanz vorherrschen, wie sie in den die ozeanische Platte auflagernden Sedimenten auftreten. Unter diesen Bedingungen resultiert die Mobilisierung der SEE in Flüssen von mindestens 0.04 nmol La cm^{-2} a^{-1} and 0.09 nmol Ce cm^{-2} a^{-1}. Die gelösten SEE werden jedoch fast umgehend wieder aus den Porenwässern entfernt, da sie bei der Bildung authigener Phosphate in großen Mengen fixiert werden.

Neben Einblicken in die chemische Entwicklung vulkanischer Gläser, liefert die experimentelle Arbeit ebenfalls Daten zur Beschreibung der Lösungskinetik alterierender Gläser in marinen Sedimenten. Innerhalb des untersuchten Niedrig-temperaturbereiches (25-50°C) lösten sich mafische Gläser mit etwa den gleichen Raten ($10^{-12.5}$ – $10^{-8.7}$ mol m^{-2} sec^{-1}) wie felsische Gläser ($10^{-12.4}$ – $10^{-9.1}$ mol m^{-2} sec^{-1}). Bei erhöhtenTemperaturen (100°C) und Drücken (200 bar) sind die errechneten Aktivierungsenergien (E_a) für die mafische Glaslösung signifikant höher (84.6 kJ mol^{-1}), als für die felsische (66.2 kJ mol^{-1}). Dies impliziert eine größere Sensibilität der Lösungskinetik mafischer Gläser gegenüber Temperaturänderungen. Für *in-situ* Bedingungen am Ozeanboden (2°C, 200 bar) resultieren daraus, konsequenter Weise, niedrigere Lösungsraten für mafische (1×10^{-13} mol m^{-2} sec^{-1}) gegenüber felsischen Gläsern (3×10^{-13} mol m^{-2} sec^{-1}). Silizium-reiche vulkanische Gläser, wie sie von den meisten Subduktionsvulkanen produziert werden, sind daher hoch reaktiv, sobald sie beim Sinken durch die Wassersäule in Bereiche erhöhten Druckes und niedriger Temperatur geraten.

In der Literatur werden viele mögliche Faktoren diskutiert, welche die Lösungskinetik vulkanischer Gläser beeinflussen. Diskussionsschwerpunkt ist neben der chemischen Zusammensetzung der Gläser und der alterierenden Lösung auch der Einfluss der Temperatur. Die Daten der hier vorgelegten Arbeit zeigen neben einer Temperatur- jedoch vor allem eine Druckabhängigkeit der Alterationsprozesse. Bei der Betrachtung der Lösungskinetik von Gläsern sollte daher sowohl die *in-situ* Temperatur als auch der *in-situ* Druck berücksichtigt werden.

Bisherige Studien an Sedimentkernen der Tiefsee und größer Mächtigkeiten haben gezeigt, dass auch die Hauptelementchemie der Porenwässer wesentlich durch die Alteration vulkanischer Aschen beeinflusst ist. Die Verarmung an Mg, Na und K sowie die Anreicherung von Ca und Si gelten hierbei als typische Indikatoren für die Präsenz von vulkanischen Aschen und deren Alteration. Die Porenwässer, der im Rahmen dieser Arbeit untersuchten Sedimente, zeigten diese Signatur jedoch nicht, was auf einen langsamen Ablauf der Aschenalteration in marinen Oberflächensedimenten schließen lässt.

Einzig die erhöhten Konzentrationen an gelöstem Si beschreiben einen deutlichen Effekt der Aschenalteration auf die Chemie der untersuchten Porenwässer. Basierend auf diesen Daten wurde ein Transport-Reaktions-Modell entwickelt, um die Lösungskinetik vulkanischer Aschen in marinen Sedimenten berechnen zu können. Es beschreibt die Mobilisierung von Si aus den vulkanischen Gläsern und verdeutlicht, dass dieser Prozess nur so lange andauert, bis eine Sättigungskonzentration von 450 µmol L^{-1} im umgebenden Porenwasser erreicht ist. Die Aschenlösung erfolgt daher hauptsächlich in den obersten Sedimenthorizonten, da nur hier die Konzentrationen an gelöstem Si im Porenwasser unterhalb des Sättigungswertes liegen. Die mathematische Beschreibung der kinetische Lösungsrate (R_G) von vulkanischen Aschen im Sediment lautet:

$$R_G = k_{GS} \cdot G \cdot \left(1 - \frac{Si}{Si_{Max}}\right)$$

mit G: der Konzentration vulkanischer Gläser im Sediment, Si_{Max}: der Sättigungskonzentration für gelöstes Si (450 µmol L^{-1}) und Si: der tatsächlichen Si-Konzentration im Porenwasser. Eine gute Übereinstimmung mit den gegebenen Porenwasserdaten konnte bei Verwendung einer kinetische Konstante k_{GS} von 3 x 10^{-5} a^{-1} erzielt werden.

Die auf der experimentellen Arbeit beruhenden Lösungsraten sind mindestens zwei Größenordnungen größer als die, welche auf Porenwasserdaten basierend berechnet wurden. Die Differenz zwischen den Lösungsraten unterschiedlicher Herkunft ist auf die sehr viel kürzeren Reaktionszeiten und dem höheren Aschen-Meerwasser-Verhältnis während der Experimente zurück zu führen. Darüber hinaus wurde wahrscheinlich die Oberflächenreaktivität der einzelnen Glaspartikel durch die Probenpräparation erhöht. Die auf den Porenwasserdaten basierenden Daten geben daher die realistischeren Lösungsraten wieder und sollten bei zukünftigen Untersuchungen der Lösungskinetik vulkanischer Gläser in marinen Sedimenten verwendet werden.

CONTENTS

Chapter I

Introduction

The importance of water and aqueous solutions on the Earth's surface barely needs to be pointed out. Water is the principal agent of erosion and of the transportation of the eroded materials, either by mechanical or by chemical means. The world oceans are the primary medium for sedimentation. They act as a global chemical repository for many substances of geological significance (Gill, 1989). All natural waters obtain their chemical composition due to chemical reactions with contacting rock bodies, sediments etc.. Therefore, the reaction of minerals and glasses with aqueous fluids at low temperatures is one of the major geochemical processes on the Earth's surface and in the crust (Stumm and Morgan, 1996).

Volcanic activity on land and at mid ocean ridge systems produces huge amounts of volcanic glasses. It is a main constituent of pyroclastic fall and flow deposits, volcanic ash beds, tuffaceous sediments, and matrices of various volcanic rocks. Because of its widespread occurrence on the ocean floor and in volcanic terrains, its emission during volcanic eruptions and its relatively rapid dissolution rate, volcanic glass plays a major role in the global flux and cycling of numerous metals, nutrients, and CO_2 fixation. The alteration of glass therefore has become a subject of growing interest in geochemistry (Berger et al., 1987; Crovisier et al., 1987; Ghiara et al., 1993; Gieskes and Lawrence, 1981; Gíslason and Eugster, 1987; Guy et al., 1992; Oelkers and Gíslason, 2001; Seyfried and Bischoff, 1979; Wolff-Boenisch et al., 2004; Yokoyama and Banfield, 2002). Although large explosive eruptions on land commonly produce volcanic glass of andesitic to rhyolitic composition, limited data are available on the short and long term dissolution rates of these glasses. This kind of explosive eruptions, however, may affect significantly the composition of the terrestrial and ocean surface (Frogner et al., 2001), as well as of marine sediments (Straub and Schmincke, 1998).

Moreover, glass has long been recognised as a potentially suitable matrix for diluting and stabilising nuclear waste. The most probable mechanism by which radio-nuclides can be released from the glass to the environment is alteration of these glasses by groundwater (Vernaz and Dussossoy, 1992). In order to guarantee the safety of these storages over time periods measured in tens of thousands of years, the long term behaviour of glass blocks and radioactive transfer phenomena in natural or engineered media have been extensively investigated. Aqueous corrosion studies have received special attention. Most of the glasses which have been studied are borosilicates and basaltic glass which are considered as the natural analogue for aluminoborosilicate nuclear glasses (Lutze et al., 1985; Petit, 1992). Over the past years only few studies were determined on rhyolitic glass, which is

even a better natural analogue because it is enriched in heavy transition elements, that are chemically similar to transuranic elements present in nuclear waste glasses (Fiore et al., 1999). Furthermore, during leaching rhyolitic glass is much more resistant than borosilicate glass (Dickin, 1981; Karkhansis et al., 1980).

1.1. Objectives of This Study

Despite the important role of volcanic glass in weathering, there are very few seawater alteration investigations and dissolution rate data available for mafic glasses and even less for felsic glasses, at typical ocean floor conditions of low temperatures (2°C) and elevated pressures (> 200 bar). Thus, alteration processes of differently composed volcanic glasses are investigated in this study combining kinetic experiments, pore water studies, a range of analytical methods, and kinetic modelling. These data were used:

1) to describe the initial and long term alteration mechanisms of differently composed glasses,
2) to define the chemical evolution of marine pore waters and sediments during glass alteration,
3) to establish for the first time glass dissolution rates at ocean floor conditions, and
4) to characterise the influence of glass alteration on the marine cycling of major as well as trace elements.

Chemical weathering of is a complex process involving coupling and feedback of dissolution, precipitation, and mineral replacement reactions. Of these processes this study focuses on the rates of volcanic glass dissolution, a process that is particularly significant during the early stages of glass alteration.

The research project from which this dissertation emerged, is embedded in the Sonderforschungsbereich (SFB) 574 ”Volatiles and Fluids in Subduction Zones”, hosted at the University of Kiel. One general aim of the SFB 574 is to obtain a better understanding of the material transfer through subduction zones concerning input-output budgets. From a geochemical point of view such cycling processes contain three points of interest:

1) The composition of pore fluids changes due to the alteration of volcanic matter (Gieskes and Lawrence, 1981). The chemical composition of many deep formation fluids and fluids expelled at cold vent sites may thus be influenced by tephra alteration processes.

2) Water enters the subduction zone in different ways, e.g. chemically bound in clay minerals. The amount of water infiltrated into the crust and mantle might be affected, if glass alteration significantly changes the mineralogical composition of the subducting sediment column.

3) The geochemical differences in magmas erupted at the volcanic arc of Nicaragua and Costa Rica appear to be controlled by the chemical variations in input (Patino et al., 2000). Since most elements enriched in pore waters during alteration are largely re-deposited due to secondary mineralisation, glass alteration can affect the geochemical signature of subducted deep sea sediments and therefore also the geochemical characteristics of arc magmas.

1.2. Methods

1.2.1. Tephra Samples

Towards the quantification of the role of volcanic glass in marine alteration processes, glasses of various chemical compositions were sampled along the volcanic front of Nicaragua. Collected glassy scoria material from the Cerro Negro 1999 eruption (CN 99, Fig. 1.1) represents material of basalt-andesitic composition whereas Chiltepe Pumice (HE 116, Fig. 1.1), collected from the Chiltepe Volcanic Complex, is of dacitic composition. These two samples cover onshore material used during alteration experiments to investigate the very initial seawater alteration processes. To also be able to investigate long term alteration processes, one rhyolitic as well as one basaltic marine ash layer (M 54 & SO 173, Fig. 1.1) was retrieved from marine sediment cores, which will be designated as offshore material throughout this study. Detailed descriptions of all samples used are given below.

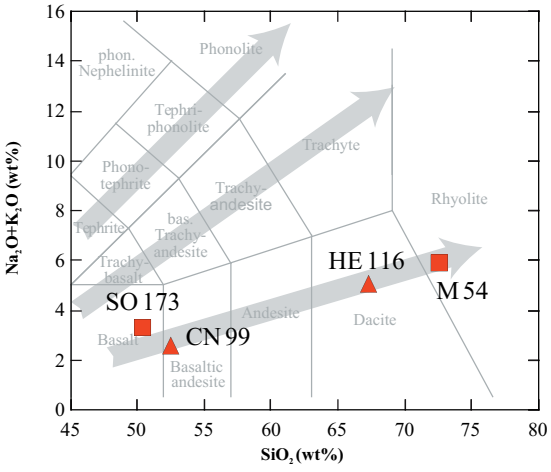

Figure 1.1: TAS-diagramm showing the chemical composition of samples used for experimental work

1.2.1.1. Cerro Negro Glassy Scoria – Cerro Negro volcano is located on the NW flank of El Hoyo-Las Pilas volcanic complex. The volcanic activity at Cerro Negro volcano started in 1850 with initial cone development. Until 1995, more than 20 eruptions were discriminated (McKnight et al., 1994; Simkin and Siebert, 1994) with the youngest activity recorded in 1999.

The 1999 eruption is composed of medium grained (single crystal sizes between 0.5 and 1.8 cm), basaltic scoria, containing clinopyroxene and plagioclase as dominant mineral phases as well as, Fe-Ti oxides and olivine in a vesicular, hypohyaline (50 % crystals – 50 % glass) matrix.

1.2.1.2. Chiltepe Pumince – Chiltepe Pumice is a prominent fallout layer, which is a newly described deposit originating from Chiltepe Volcanic Complex, Nicaragua. This youngest widespread tephra deposit in Western Central Nicaragua affects the nearby area of Chiltepe Peninsula, as well as parts of the Nicaraguan capital (Kutterolf et al. submitted).

Chiltepe Pumice consists of moderate to highly-vesicular white and highly-vesicular pink pumice lapilli. Fine vesicles are often elongated whereas the bubble clusters consists mostly out of rounded bubbles with fine bars between the individual vesicles. Some dense grey and streaky pumices are common (2 %). Chiltepe Pumice is mostly moderate to well sorted and commonly, the pumice clasts are angular to subangular. Lithic (20 %) and crystal (10-20 %) contents are high and their size in the matrix is big. Lithic assemblages contain fresh basalts with unusual angular shape and additionally few rhyolitic clasts. While Plagioclase is the main felsic mineral phase, the heavy mineral assemblage is dominated by large olivin crystals, accompanied by smaller amounts of clinopyroxene, orthopyroxene, and minor amounts of hornblende.

1.2.1.3. Marine Ash Layers – The distal deposits of Central American volcanic eruptions can be found in marine sediments from the Pacific Ocean. During research cruises (RV *Meteor* 54/2, RV *Sonne* 173/3+4) 13 sediment cores were retrieved off Nicaragua and Costa Rica containing about 80 ash layers of 0.5 to 15 cm thickness. The lower contact of the ash beds is usually sharp, whereas the upper contact frequently shows a gradual change from ash to deep marine sediment. In some cores, thin ash layers have been disturbed by bioturbation. Admixtures of ash within terrigenous and pelagic sediments are also common.

Most of the ash layers are white to light-greyish-pink or dark-grey to light grey in colour. Microscopic examination of light-coloured ashes shows mostly clear, colourless, volcanic glass shards and pumice fragments commonly with elongated vesicles. Each of these felsic ash layers is characterised by a distinct modal composition and crystal/glass ratio. Dark-grey ash layers consist predominantly of a mixture of brown glass shards, black, vitreous and opaque particles and numerous light and heavy minerals. Most of the glass shards in the mafic layers have blocky shapes and are poorly vesicular to dense.

The typical grain size of all ash-layers varies in the range of medium silt to medium/coarse sand (< 250 μm). Mineral assemblages comprise plagioclase, pyroxene, hornblende, plus olivine in the mafic, and occasionally biotite in the most-evolved felsic layers. Mafic glass shards constitute > 40 % by volume of the basaltic ash layers, while silicic glass shards make up > 60 vol.% of the felsic layers.

1.2.2. Experimental Procedure

All samples were cleaned ultrasonically using deionised water, dried, mildly scrunched, and sieved to obtain a grain size 0.5-1.5 mm for onshore samples and < 250 μm for marine ash layers. After this procedure single glass shards were carefully picked with the help of microscopy, to obtain samples with the highest portion of glass shards as possible.

Alteration experiments were carried out using synthetic seawater according to the recipe given by Kester et al. (1967). Reaction chambers made of stainless steel were covered with Teflon coatings of 1.5 mm thickness and equipped with Teflon in- and outlets in order to minimise contamination. Experiments were carried out in a closed system for a maximum of 1.5 years at temperatures of 25, 50, and 100°C and pressures of 1, 200, and 400 bar using a water/rock ratio of 10 (10 g seawater/1 g volcanic glass). Filtering was performed using 0.2 μm membrane filters while extracting the fluid from the reactor for chemical analysis. Each experimental series consisted of a sequence of experiments performed on fresh aliquots of the same sample.

For experiments at pressures of up to 200 bar we used a modified accelerate solvent extractor (ASE 200®), an automated system for extracting compounds from a variety of solids by using solvent at elevated temperatures (< 100°C). Pressure is applied via nitrogen supply to the sample extraction cell to maintain the heated solvent in a liquid state during the extraction. After a defined reaction time, the extract is flushed from the sample cell into a standard collection vial and is ready for analysis. High-pressure

experiments at 400 bar were conducted using an autoclave system, where pressure was applied hydrostatically. Glass specimens and seawater were given into inert plastic bags, which were evacuated, and than introduced into the autoclave. The autoclave was placed in an oven and heated to temperatures of up to 50°C. Schematic figures of the experimental set-ups are shown in Figure 1.2.

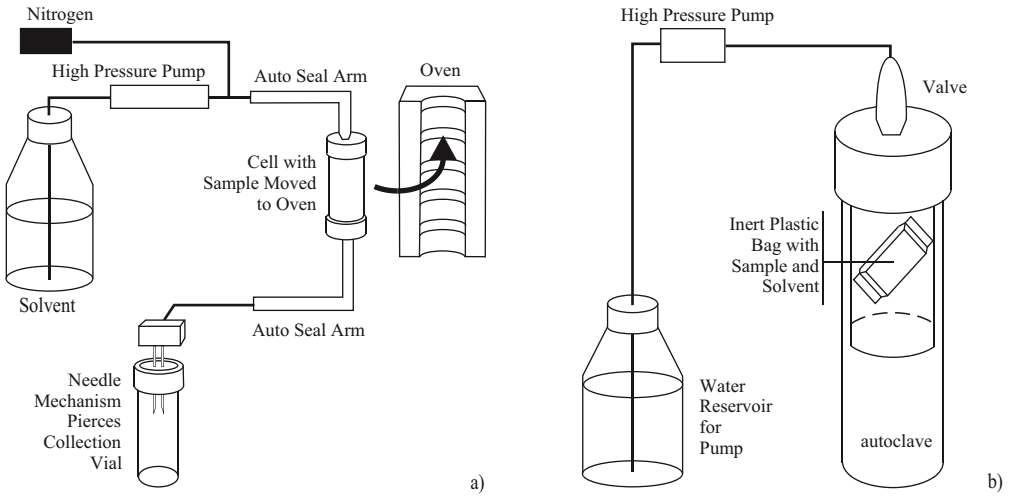

Figure 1.2: Schematic illustration of experimental set-ups used for experiments at pressures of up to 200 bar (a) and 400 bar (b).

The ash-seawater mixtures were not stirred during the experiments, because stirring enhances dissolution rates by several orders of magnitude due to mechanical rupture of solids and the creation of new reactive surface sites (Arvidson et al., 2003). Moreover, we intended to investigate the behaviour of ashes in deep-sea sediments exposed to stagnant pore fluids rather than flowing ground waters.

1.2.3. Obtaining Sediment Samples for Pore Water Analyses

A number of different techniques are available for the retrieval of samples from marine sediments. All in this study discussed sediment cores were retrieved by gravity coring, a technique that yields cores from the upper less solid meters of the sediment column, which are as long as possible and most unperturbed.

Upon using the gravity corer, a steel tube of about 13 cm in diameter is pressed between 6 and 20 m deep into the sediment with the aid of the lead weight weighing about 3 to 4 t. Inside the steel tube, a plastic liner made out of HD-PVC is situated that encompasses the core. Upon extraction from the sediment and raising the tube upwards through the water column, the tubes aperture is kept shut by a valve. Below another valve-like shutter –

a core catcher – prevents the core material from falling out. Generally, cores of about 10-15 m in length are obtained in pelagic sediments (Schulz and Zabel, 2000). This sampling tool can only be operated from the decks of larger ships that are equipped with steel ropes and winches designed for managing weights of 10 to 15 tons but the handling of the gravity corer is easy, safe, and fast.

After the usage of the gravity corer the sediment core obtained is immediately dissected into pieces of 1 m in length within the tube. Usually, the 1 m long tubular pieces, tightly sealed with caps, are stored at in-situ temperature to subsequent further processing which has to be carried out as quickly as possible.

1.2.4. Pore Water Extraction from the Sediment

For extracting pore water from the sediment aboard, a modified appliances after Schlüter (1990) was used. A sediment sample volume of 100 to 200 mL is transferred into a container made out of PE or PTFE which has a piece of round filter foil on the bottom side measuring 5-10 cm in diameter (Fig.1.3).

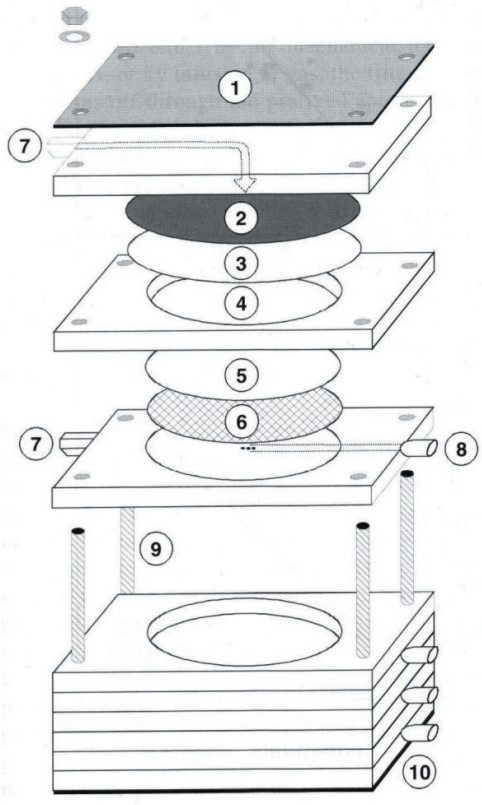

Figure 1.3: Extractor used for the preparation of pore water from low density sediments (modified after Schlüter (1990) and published by Schulz and Zabel (2000)).
1-Top sheet (V2A), 2-Rubberdisk, 3-Parafilm, 4-Chamber for the sediment samples, 5-Filter membrane, 6-Tissue, 7-Pressure supply, 8-Leak, 9-Bottom sheet (V2A), 10-Thread (V2A).

It should be noted that the choice of the filter used in the extraction procedure will determine what will be evaluated as dissolved constituent and what will be evaluated as particle or solid sedimentary phase. On the top the sample is sealed with a rubber cover onto which argon or nitrogen is applied at a pressure of 5-15 atm. The sediment sample is thus compacted and a part of the pore water passes downwards through the filter layer. By this method, a pore water sample comprising 30-50 mL can easily be obtained from the water rich and less solid layers lying close to the sediment surface, generally 15 mL pore water can be obtained.

1.3. Geological Setting

The volcanic chain of Nicaragua and Costa Rica is part of the Central American Volcanic Arc (CAVA) that results from subduction of the Cocos Plate beneath the Caribbean Plate at a rate of up to 90 mm a^{-1} (Kimura et al., 1997) (Fig. 1.4). The dip of the subducting slap underneath the arc volcanoes changes along the arc, with the steepest dip beneath Nicaragua and the shallowest dip beneath Costa Rica (Patino et al., 2000).

At the Nicaraguan segment of the subduction zone bending-related faulting has created a pervasive extensional faulting system that cuts through the crust of the incoming plate, penetrating deeply into the lithospheric mantle. Faulting remains active across the entire ocean trench slope, promoting deep percolation of seawater (Ranero et al., 2003). When proceeding into greater depths, this highly serpentinised, steeply subducting lithosphere is progressively confronted with rising temperatures and pressures, and fluids can be transferred into the overlying mantle wedge (Rüpke et al., 2002), where they facilitate partial melting by lowering of the mantle solidus.

The volcanism resulting from these processes is dominated by explosive activity (Wehrmann, 2005). Thus along the Middle American volcanic chain highly explosive volcanic eruptions generate buoyant eruption columns penetrating up to 40 km into atmosphere where they spread laterally (Kutterolf et al., in press). Because of the prevailing easterly winds (Wehrmann, 2005) most of their ash fraction, which mainly (75 %) is composed of felsic material (Kutterolf et al., in press), is distributed to the west and dropped into the Pacific Ocean (Fig. 1.4). The entire oceanic crust is covered by a ~380 m thick sedimentary sequence (Saffer et al., 2000) and due to the intense explosive volcanism, volcanic matter is one of the major components in marine sediments of the Central American fore-arc. Straub and Schmincke (1998) evaluated the overall tephra input into the Pacific Ocean sediments by arc volcanism going back to Mid-Miocene.

They estimated that approximately 10-13 km^3 of volcanoclastic sediments are produced per km arc length and per million year. An extrapolation over the life-time of major Pacific arcs and hotspot chains, combined with a volume estimate of the distal tephra component, indicates a minimum of 9.3 x 10^6 km^3 of tephra, corresponding to 23 vol.% of existing Pacific oceanic sediments.

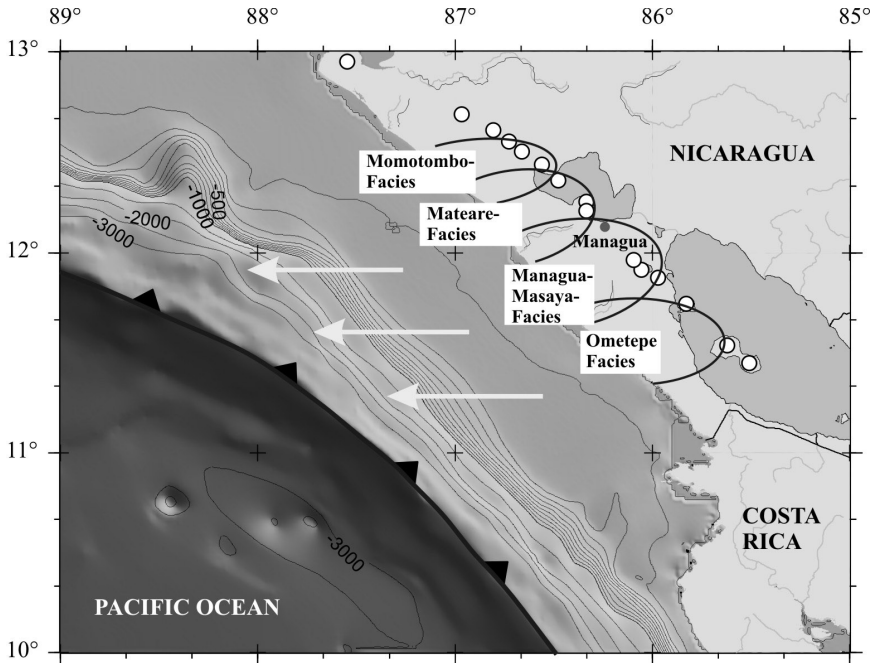

Figure 1.4: Map of the Central American Convergent Margin together with major volcanic centres (white circles) and their related tephra facies. The major wind direction is marked by arrows.

1.4. Thesis Outline

The aims and topics of this PhD thesis as outlined above are presented in four separate articles in Chapter II to V.

Chapter II summarises the experimental investigations. The compositional evolution of the used seawater was determined by ICP-OES and ICP-MS, while electron microprobe analyses were used to describe the chemical evolution of the single glass shards. These data were consulted to describe the initial as well as long-term seawater alteration mechanisms of mafic and, for the first time, felsic composed glasses. Based on the experimentally derived data set apparent dissolution rate constants were calculated, providing insights the evolution of the reactivity of volcanic glass with decreasing temperatures and increasing pressures.

For Chapter III the effects of volcanic glass alteration on the composition of pore fluids in marine surface sediments were investigated while analysing their major as well as trace element composition using ICP-OES. The results of this study are presented and compared to previous investigations of pore waters of deep sea drilling cores. Additionally a transport-reaction model was applied to the pore water data and physical sediment parameters to constrain for the first time a field rate of glass dissolution at ocean floor conditions.

Chapter IV comprises the first study, investigating the pathways of rare earth elements (REE) in surface sediments on the ocean floor due to volcanic ash alteration. Pore water data of dissolved nutrients, major and trace elements, as well as selected REE are presented. To further the knowledge about diagenetic processes occurring during seawater/ash alteration and the related REE behaviour, these investigations were complemented by LA-ICP-MS analyses of fresh and altered glass shards.

The products of highly-explosive eruptions along the Nicaraguan Volcanic Front (NVF) are investigated in Chapter V . This study includes the development of a chronostratigraphy and understanding of the evolution of Quaternary volcanism in Central America, in terms of composition and magnitude. Another aim was to establish stratigraphic correlations of fore-arc sediments along the continental slope with sediments on the incoming plate.

References

Arvidson R., Ertan I., Amonette J., and Luttge A. (2003) Variation in calcite dissolution rates: A fundamental problem. *Geochimica et Cosmochimica Acta* **67**(9), 1623-1634.

Berger G., Schott J., and Loubet M. (1987) Fundamental processes controling the first stage of alteration of a basalt glass by seawater: An experimental study between 200 and 320°C. *Earth and Planetary Science Letters* **84**, 431-445.

Crovisier J.-L., Honnorez J., and Eberhart J. (1987) Dissolution of basaltic glass in seawater: Mechanism and rate. *Geochimica et Cosmochimica Acta* **51**, 2977-2990.

Dickin A. (1981) Hydrothermal leaching of rhyolite glass in the environment has implications for nuclear waste disposal. *Nature* **294**, 342-347.

Fiore S., Huertas F., Tazaki K., Huertas F., and Linares J. (1999) A low temperature experimental alteration of rhyolitic obsidian. *European Journal of Mineralogy* **11**(3), 455-469.

Frogner P., Gíslason S., and Oskarsson N. (2001) Fertilizing potential of volcanic ash in ocean surface waters. *Geology* **29**(6), 487-490.

Ghiara M., Franco E., Petti C., Stanzione D., and Valentino G. (1993) Hydrothermal, interaction between basaltic glass, deionised water and seawater. *Chemical Geology* **104**, 125-138.

Gieskes J. and Lawrence J. (1981) Alteration of volcanic matter in the deep sea sediments: Evidence from the chemical composition of interstitial waters from deep sea drilling cores. *Geochimica et Cosmochimica Acta* **45**, 1687-1703.

Gill R. (1989) *Chemical fundamentals of Geology*. Unwin Hyman.
Gíslason S. and Eugster H. (1987) Meteoric water-basalt interactions. I: A laboratory study. *Geochimica et Cosmochimica Acta* **51**, 2827-2840.
Guy C., Schott J., Destrigneville C., and Chiappini R. (1992) Low-temperature alteration of basalt by interstitial seawater, Mururoa, French Polynesia. *Geochimica et Cosmochimica Acta* **56**, 4169-4189.
Karkhansis S., Bancroft G., Fyfe W., and Brown J. (1980) Leaching behaviour of rhyolite glass. *Nature* **284**, 435-437.
Kester D., Duedall J., Connors D., and Pytkowicz R. (1967) Preparation of artificial seawater: Notes and comment. *Limnology and Oceanography* **12**, 176-179.
Kimura G., Silver E., and Blum P. (1997) Costa Rica accretionary wedge, Sites 1039-1043. *Palaeogeography, Palaeoclimatology, Palaeoecology* **170**, 458.
Kutterolf, S., Freundt, A., Wehrmann, H., Perez, W., and Schmincke H.-U. (submitted) 40,000 years of highly explosive eruptions around Managua, Nicaragua: Time sequence, eruption dynamics, and hazard implications. *Journal of Volcanology and Geothermal Research*
Kutterolf S., Schacht U., Wehrmann H., Freundt A., and Moerz T. (in press) Onshore to offshore tephrostratigraphy and marine ash layer diagenesis in Central America. In *Central America - Geology, Resources and Hazards* (ed. J. Buntschuh). Balkema.
Lutze W., Malow G., Ewing R., Jercinovic M., and Keil K. (1985) Alteration of basalt glasses: implications for modelling the long-term stability of nuclear waste glasses. *Nature* **314**.
McKnight S., Roggensack K., and Williams S. (1994) "Historical eruption dynamics, volumes, and geochemistry of a young volcano, Cerro Negro Nicaragua." *Eos Transactions of the American Geophysical Union* **75**(44), 731.
Oelkers E. and Gíslason S. (2001) The mechanism, rates and consequences of basaltic glass dissolution: I. An experimental study of the dissolution rates of basaltic glass as a function of aqueous Al, Si and oxalic acid concentration at 25°C and pH = 3 and 11. *Geochimica et Cosmochimica Acta* **65**(21), 3671-3681.
Patino L., Carr M., and Feigenson M. (2000) Local and regional variations in Central American arc lavas controlled by variations in subducted sediment input. *Contributions to Mineralogy and Petrology* **138**, 265-283.
Petit J. C. (1992) Natural analogues for the design of performance assessment of radioactive waste forms: A review. *Journal of Geochemical Exploration* **46**, 1-33.
Ranero C., Morgan J. P., McIntosh K., and Reichert C. (2003) Bending-related faulting and mantle serpentinisation at the Middle Americ trench. *Nature* **425**, 367-373.
Rüpke L., Morgan J., Hort M., and Connolly J. (2002) Are regional variations in Central America arc lavas due to differing basaltic versus peridotitic slab sources of fluids? *Geology* **30**(11), 1035-1038.
Saffer D., Silver E., Fisher A., Tobin H., and Moran K. (2000) Inferred pore pressure at the Costa Rica subduction zone: Implications for dewatering processes. *Earth and Planetary Science Letters* **177**, 193-207.
Schlüter M. (1990) Zur Frühdiagenese von organischem Kohlenstoff und Opal in Sedimenten des südlichen und westlichen Weddelmeeres. *Berichte zur Polarforschung* **73**, 156.
Schulz H. and Zabel M. (2000) *Marine Geochemistry*. Springer.
Seyfried W.E. and Bischoff J. (1979) Low temperature basalt alteration by seawater: An experimental study at 70°C and 150°C. *Geochimica et Cosmochimica Acta* **43**, 1937-1947.
Simkin T. and Siebert L. (1994) *Volcanoes of the World*. Geoscience Press.
Straub S. and Schmincke H. (1998) Evaluating the tephra input into Pacific Ocean sediments: Distribution in space and time. *Geologische Rundschau* **87**(3), 461-476.
Stumm W. and Morgan J. (1996) *Aquatic Chemistry*. Wiley and Sons.

Vernaz E. and Dussossoy J. (1992) Current stage of knowledge of nuclear waste glass corrosion mechanisms: The case of R7T7 glass. *Applied Geochemistry* **Suppl. Issue 1**, 13-22.

Wehrmann H. (2005) Volatile degassing and plinian eruption dynamics of the mafic Fontana Tephra, Nicaragua. PhD, University of Kiel.

Wolff-Boenisch D., Gíslason S., Oelkers E. H., and Putnis V. (2004) The dissolution rate of natural glasses as a function of their composition at pH 4 and 10.6, and temperatures from 25 and 74°C. *Geochimica et Cosmochimica Acta* **68**(23), 4843-4858.

Yokoyama T. and Banfield J. (2002) Direct determination of the rates of rhyolite dissolution and clay formation over 52,000 years and comparison with laboratory measurements. *Geochimica et Cosmochimica Acta* **66**(15), 2665-2681.

Chapter II

Alteration of Differently Composed Volcanic Glasses in Marine Sediments: Insights into Alteration Pathways and Dissolution Kinetics

Ulrike Schacht[1,2], Steffen Kutterolf[1,2], Klaus Wallmann[2,1], and Mark Schmidt[3,1]

[1] Special Research Project 574, University of Kiel, Wischhofstr. 1-3, 24148 Kiel, Germany

[2] IFM-GEOMAR, Leibniz Institute of Marine Sciences, Wischhofstr. 1-3, 24148 Kiel, Germany

[3] Institute of Geosciences, University of Kiel, Ludewig-Meyn-Str. 10, 24118 Kiel, Germany

Abstract

The initial alteration stage of mafic and felsic volcanic glasses by seawater has been studied experimentally at temperatures between 25 and 100°C and pressures of 1 to 400 bar, following the chemical evolution of the reacting solution during the experiments and the chemical transformation of the altered glass via microprobe.

Mafic glass alteration is controlled by the selective extraction of cations with respect to Fe leading to the formation of a surface layer enriched in Fe – a palagonite skin. For felsic glass alteration a palagonite-like interstage product is missing, resulting in a nearly complete dissolution of the glass.

The experimental work provides kinetic data concerning the initial stage of mafic and felsic glass alteration indicating that felsic glass dissolves at least as fast as mafic glass under ocean floor conditions (2°C, > 200 bar). It therefore constitutes a major element source, especially in felsic tephra dominated sediments from the Central American fore-arc. Our experimental studies also indicate that dissolution rates are not only temperature but also pressure dependent. Therefore, *in-situ* P/T conditions need to be considered while investigating dissolution kinetics.

2.1. Introduction

Large explosive eruptions in volcanogenic terrains on land commonly produce tephra (glass, ash) of basaltic to rhyolitic composition. These eruptions affect significantly the composition of sediments deposited in the fore-arc of active continental margins and around volcanic islands. The most important seafloor alteration processes include the breakdown and dissolution of primary igneous phases and the precipitation of secondary phases as the solution becomes over saturated with respect to these phases (Berger et al., 1987). Due to the rapid weathering rates of volcanic glass, its alteration may play a significant role in the global cycling of various elements (Alt and Honnorez, 1984; Altaner et al., 2003; Bach et al., 2001; Bednarz and Schmincke, 1989; Berger et al., 1987; Berndt et al., 1986; Clayton and Pearce, 2000; Fiore et al., 1999; Ghiara et al., 1993; Gíslason et al., 1993; Guy et al., 1992; Humphris and Thompson, 1978; James et al., 2003; Lawrence et al., 1979; Philpotts et al., 1969; Seyfried and Mottl, 1982; Staudigel and Hart, 1983; White and Claassen, 1980; Ylagan et al., 1996).

Most experimental studies focus only on dissolution rates of basalts and basaltic glass (e.g. Berger et al., 1987; Crovisier et al., 1987; Daux et al., 1994; Ghiara et al., 1993; Gíslason and Eugster, 1987a; Gíslason and Eugster, 1987b; Gordon and Brady, 2002; Guy et al., 1992; Nesbitt and Wilson, 1992; Seyfried and Bischoff, 1979). The seawater alteration of basaltic glass at low temperatures forms a hydrated layer called palagonite on all exposed surfaces. Recent studies suggest that the palagonite film constitutes a diffusion barrier for reactive species (H_2O, H_3O^+) and reaction products (H_4SiO_4) (Techer et al., 2001). The degree of alteration increases with age and results in the formation of smectites and zeolites (Bach et al., 2001).

In contrast, only few studies were performed investigating alteration rates and mechanisms of intermediate and felsic glass (e.g. Allnatt et al., 1983; Dickin, 1981; Fiore et al., 1999; Jezek and Noble, 1978; Karkhansis et al., 1980; Mungall and Martin, 1994; Wolff-Boenisch et al., 2004; Yokoyama and Banfield, 2002) and most of these studies focus mainly on secondary phases (e.g. Fiore et al., 1999; Hawkins, 1981; Kawano et al., 1993). There are no investigations known to us, dealing with felsic glass alteration under seawater conditions. Detailed knowledge on processes and conditions of felsic glass alteration therefore are still lacking. Felsic glass alteration proceeds, however, somewhat differently. At advanced stage of alteration a palagonite-like interstage product is missing (Fiore et al., 1999; Karkhansis et al., 1980; Schmincke, 1988). Felsic glass alteration seems to result in a complete dissolution of the glass followed by the crystallisation of secondary minerals (Schmincke, 1988).

To better understand volcanic glass-seawater reactions and to quantify the element exchange between sediments and associated pore fluids we conducted a series of experiments at temperatures between 25 and 100°C and pressures between 1 and 400 bar. The geochemical exchange of the main elements during seawater alteration was documented. These data were evaluated to derive rate constants and activation energies of glass dissolution.

2.2. Methods

2.2.1. Starting Material

The volcanic glass samples used in the experiments were collected along the volcanic chain of Nicaragua as well as from ash layers in sediment cores taken during two marine expeditions (RV *Meteor* 54/2 and RV *Sonne* 173/3+4). All samples taken from sediment cores belong to the same alteration environment – they all interacted with seawater – and were retrieved from water depths of about 3250 m (Tab. 2.1).

Table 2.1: Samples used for our experimental work, their main composition, age and sampling locations. Onshore material was collected along the volcanic front of Nicaragua whereas offshore material was taken from marine ash layers.

Sample	Volcanic Name	Location		Age (years)	
		Latitude (N)	Longitude (W)		
onshore					volcano
CN99	basaltic-andesite	13°30.19	86°42.27	3	Cerro Negro
HE116	dacite	12°16.91	86°19.86	~2000	Chiltepe
offshore					water depth
SO173	basalt	11°15.79	88°12.60	~18000	3200 m
M54	rhyolite	11°06.03	87°49.82	21000	3300 m

All samples were cleaned ultrasonically using deionised water, dried, mildly scrunched, and sieved to obtain a grain size 0.5-1.5 mm for onshore samples and < 250 µm for marine ash layers. After this procedure single glass shards were carefully picked with the help of microscopy, to obtain samples with the highest portion of glass shards as possible. Like in many previous studies the specific surface area of the cleaned, scrunched, and picked glass powders was determined by nitrogen adsorption using the BET method. Glass surface area was assumed to be approximately constant over time, therefore it was not measured at the end of the single experimental runs. The chemical composition of

the starting materials, determined by microprobe, as well as its specific surface areas are given in Table 2.2.

Table 2.2: Composition of glass samples and artificial seawater used in the experiments. BET surfaces are given in $m^2\ g^{-1}$.

Glass Samples					Artificial Seawater		
	mafic		felsic				
	onshore	offshore	onshore	offshore			
(wt%)	CN99	SO173	HE116	M54			
SiO_2	53.4	50.9	67.1	71.9	0.00	µmol L^{-1}	Si
Al_2O_3	12.7	14.4	13.6	12.5	1.85	µmol L^{-1}	Al
Na_2O	2.36	2.99	3.55	3.46	489	mmol L^{-1}	Na
K_2O	0.92	1.14	2.21	3.75	10.5	mmol L^{-1}	K
CaO	8.04	8.73	2.27	0.56	10.9	mmol L^{-1}	Ca
TiO_2	1.51	1.16	0.41	0.10	0.27	µmol L^{-1}	Mn
FeO	14.9	12.3	2.28	0.48	54.1	mmol L^{-1}	Mg
MnO	0.29	0.27	0.12	0.06	0.44	µmol L^{-1}	Ba
MgO	3.58	4.44	0.52	0.09	0.82	µmol L^{-1}	Sr
P_2O_5	0.21	0.26	0.06	0.02	2.73	meq kg^{-1}	alk
Total	97.9	96.9	92.1	92.9	7.75		pH
(ppm)							
Ba	382		1500	1240			
Sr	504		185	46			
BET	0.35	5.11	0.75	0.81			

2.2.1.1. Optical Investigations – The volcanic glass samples used for the experimental work were preliminary investigated using smear slides. Smear slides were prepared by dispersing glass shards on microscope slides and fixing the sample with resin (Meltmount). These “thin sections” were then examined under a petrographic and scanning electron microscope (SEM) .

Onshore mafic glass shards reveal a smooth surface free of fine particles, which is consistent with the low specific surface area of sample CN99 (Fig. 2.1a, Tab. 2.2). In contrast the onshore felsic pumice fragments are very porous. The pore shapes are elongated leading to an oriented structure. No alteration could be detected at the glass’ surface (Fig. 2.1a).

As far as offshore samples are concerned we could distinguish felsic ash as mostly clear, colourless, and fresh volcanic glass shards and pumice fragments while mafic ash layers consisted predominantly of smoked to black vitreous glass showing distinct signs of

alteration (Fig. 2.1b). However, up to a defined amount, even for the investigated mafic ash layers we were able to identify microscopically fresh looking single glass shards. Surface areas of mafic glasses tend to increase significantly after 18 kyr of alteration (SO 173 in Tab. 2.1) due to pitting and surface roughness. This explains the elevated surface area for sample SO173 (Tab. 2.2).

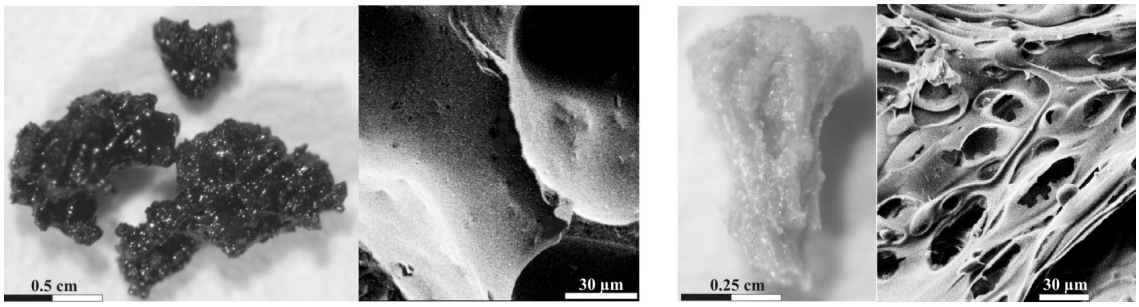

Figure 2.1a: Microscope images of mafic (left) and felsic (right) onshore samples.

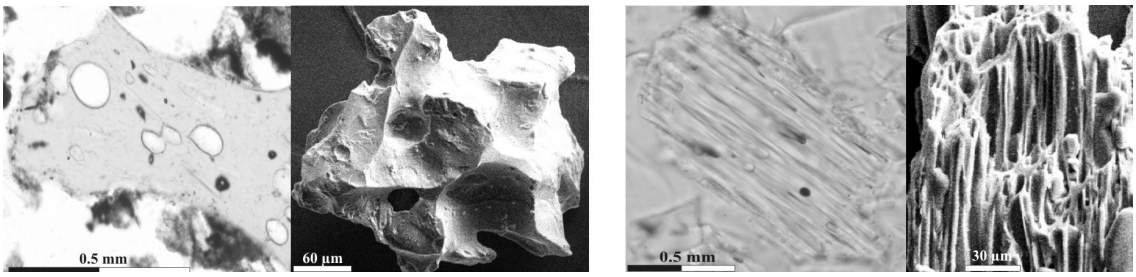

Figure 2.1b: Microscope images of mafic (left) and felsic (right) offshore sample.

2.2.1.2. Age Determination – For age determination offshore volcanic ash samples were chemically correlated with deposits on land (Kutterolf et al., in press). The charcoal contents of these on land deposits and onshore samples were analysed at the Leibniz Laboratory for Radiometric Dating and Isotope Research at the University of Kiel. The selected samples were mechanically cleaned under the microscope, afterwards sieved, and dark organic-looking material < 250 µm was selected for further treatment. The residual material was then extracted with 1 % HCl and 1 % NaOH at 60°C and again with 1 % HCl. The alkali extraction of the organic fraction (humic acid fraction) was precipitated with HCl, washed, and dried. The combustion to CO_2 of all fractions was performed in a closed quartz tube together with CuO and silver wool at 900°C. The ^{14}C concentration of the samples was measured by comparing the simultaneously collected ^{14}C, ^{13}C, and ^{12}C beams of each sample with those of Oxalic Acid standard CO_2 and coal background material. The ^{14}C ages were calculated according to Stuiver and Polach (1977) with a $\delta^{13}C$ correction for isotopic fractionation based on the $^{13}C/^{12}C$ ratio measured by the AMS-system simultaneously with the $^{14}C/^{12}C$ ratio.

2.2.2. Experimental Procedure

Alteration experiments were carried out using synthetic seawater. Its starting composition is given in Table 2.2, the recipe can be found under *www.ifm-geomar.de/index.php?id=mg_analytik*. Reaction chambers made of stainless steel were covered with Teflon coatings of 1.5 mm thickness and equipped with Teflon in- and outlets in order to minimise contamination. Experiments were carried out in a closed system for a maximum of 850 hours at temperatures of 25, 50, and 100°C and pressures of 1, 200, and 400 bar using a water/rock ratio of 10 (10 g seawater/1 g volcanic glass). Filtering was performed using 0.2 µm cellulose acetate membrane filters while extracting the fluid from the reactor for chemical analysis. Each experimental series consisted of a sequence of experiments performed on fresh aliquots of the same sample.

Experiments with blanks were done in order to assess chemical contamination. Blank runs with seawater showed no change in pH, alkalinity or element composition indicating no contamination by leaching the reaction chamber. For experiments at pressures of up to 200 bar we used a modified accelerate solvent extractor (ASE 200®), an automated system for extracting compounds from a variety of solids by using solvent at elevated temperatures (< 100°C). Pressure is applied via nitrogen supply to the sample extraction cell to maintain the heated solvent in a liquid state during the extraction. After a defined reaction time, the extract is flushed from the sample cell into a standard collection vial and is ready for analysis. High-pressure experiments at 400 bar were conducted using an autoclave system, where pressure was applied hydrostatically. Glass specimens and seawater were given into inert plastic bags which were evacuated and than introduced into the autoclave. The autoclave was placed in an oven and heated to temperatures of up to 50°C. Schematic figures of the experimental set-ups are shown in Figure 2.2.

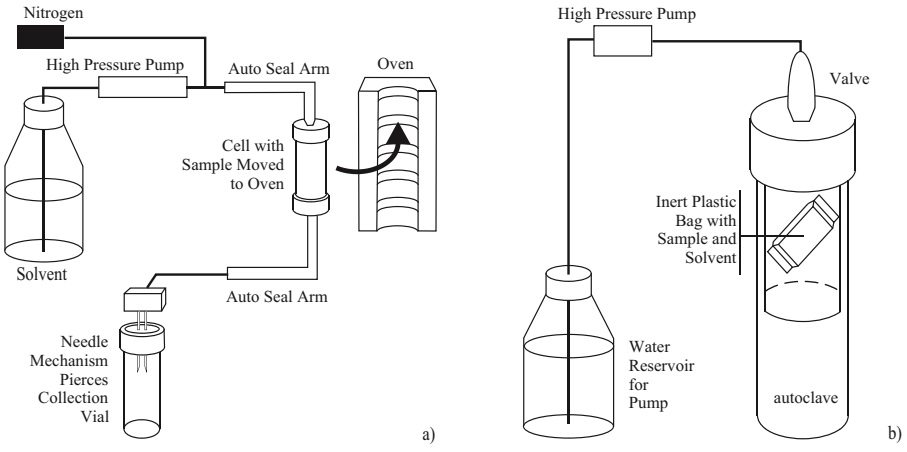

Figure 2.2: Schematic illustration of experimental set-ups used for experiments at pressures of up to 200 bar (a) and 400 bar (b).

Even if it did not appear to be a case in studies performed on glass alteration, by e.g. Gíslason and Oelkers (2003), the ash-seawater mixtures were not stirred during the experiments since mineral dissolution experiments pointed out that stirring causes the mechanical rupture of the solids. The creation of such new reactive surface sites might increase dissolution rates by several orders of magnitude (Arvidson et al., 2003; Metz and Ganor, 2001). Moreover, we intended to investigate the behaviour of ashes in deep-sea sediments exposed to stagnant pore fluids rather than flowing ground waters.

2.2.3. Analytics

Water samples for the total alkalinity measurements were analysed by titration of 0.5-1 mL water with hydrochloric acid (~ 0.02 *N* HCl) according to Ivanenkov and Lyakhin (1978). To remove carbon dioxide during titration the sample was flushed with a continuous stream of pure nitrogen. The equivalence point of the titration was determined colourimetrically, using a mixture of methylene blue and methyl red as an indicator.

Silica concentrations were measured using the Molybdate Blue method (Grasshoff et al., 1999), while *p*H was measured at 25°C on the seawater scale immediately after sampling using appropriate seawater standards (Dickson, 1993). Acidified sub-samples were prepared for ICP-OES analyses of metal ions (Ba, Ca, K, Mg, Na, Mn, Sr) and Al determination by ICP-MS. Detailed descriptions of the used methods are available on: *www.ifm-geomar.de/index.php?id=mg_analytik* and *www.pw-analysen.com*.

At termination of alteration experiments, the weathered glass particles were air dried. To investigate compositional changes of the altered glass shards, electron microprobe (EMP) analyses were conducted on experimentally and naturally altered samples. These samples were epoxy embedded and fixed on polished petrographic thin sections. After carbon coating, rim and core locations on selected glass shards were analysed with a CAMECA SX 50 wavelength dispersive electron microprobe at IFM-GEOMAR, Kiel. Major element compositions were determined at 15 kV accelerating voltage and a beam current of 10 nA for mafic glass and 6 nA for felsic glass, with counting times of 20 sec. The beam was defocused to 10 µm to minimise analytical Na loss. Standardisations was done by using international standards. Standard deviations were less than 0.5 % for major elements and < 3 % for trace elements.

2.3. Results

During our experiments significant reactions between seawater and glass occurred, depending on the experimental conditions. The fluids in the reaction chamber show significant increases and decreases in element concentrations reflecting the dissolution of glass particles and the precipitation of secondary phases. The compositional evolution of seawater during our experiments in contact with mafic and felsic glasses is described below.

The most significant change during dissolution experiments for both, mafic and felsic experiments, is shown by dissolved silica (Fig. 2.3). The concentration of Si increases rapidly in the beginning, and more slowly after the first few hours. In all cases final steady state conditions have not been achieved.

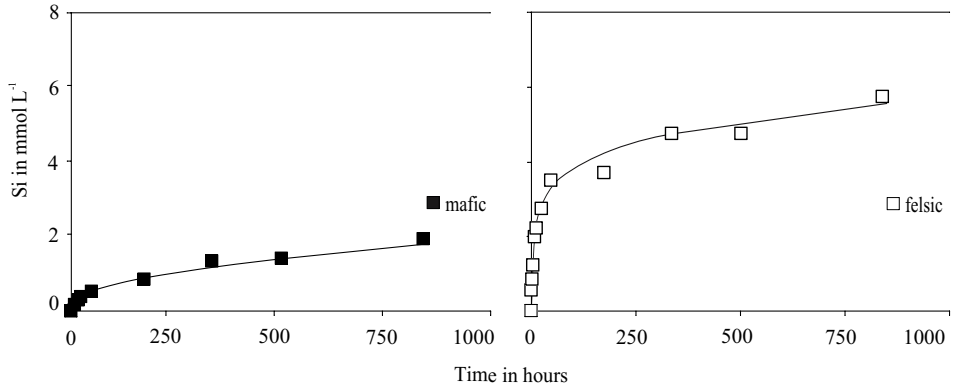

Figure 2.3: Examples of chemical seawater evolution during ash alteration. Data shown above describe silica concentration changes in seawater at 50°C and 200 bar for mafic and felsic onshore samples.

According to Seyfried and Bischoff (1979) the rate and amplitude of *p*H change appear to be sensitive indicators for the extent of alteration. The evolution of *p*H and alkalinity values during our individual experimental runs is shown in Figures 2.4a & b. Alkalinity and *p*H show only small changes at moderate temperatures, but decrease abruptly for experimental runs at elevated temperatures.

Previous studies of basaltic glass alteration (e.g. Crovisier et al., 1983; Gieskes and Lawrence, 1981; Seyfried and Bischoff, 1979; Staudigel and Hart, 1983; Staudigel et al., 1996) describe a slight but continuous loss of Mg, Na, and K and enrichment of Ca and Si in seawater. For most runs only minor changes in concentrations could be seen for these elements due to the high background concentration in the artificial seawater used as starting solution. Experimental runs using felsic glass show slight but

significant concentration changes in Ca at elevated pressures and temperatures (Tab. 2.3). In contrast, mafic glass alteration is only marked by changes in seawater composition, like described for felsic seawater alteration, when exposed to elevated temperatures (100°C, 1 bar). In the literature a significant uptake of Mg, especially during basaltic alteration, is described. Our experiments confirm this observation in experiments under elevated temperature (100°C) and low pressure conditions (1 bar) for both, felsic as well as mafic experimental runs (Tab. 2.3).

Studies focusing on trace element behaviour during alteration are rare and results published are often contradictory (Daux et al., 1994; Menzies and Seyfried, 1979; Patino et al., 2003; Pichler et al., 1999; Staudigel and Hart, 1983). Staudigel and Hart (1983) for instance postulated changes for trace elements becoming either enriched or depleted within the alteration rim whereas Daux et al. (1994) described that trace elements generally become enriched in clay minerals formed during secondary mineralisation. As far as our experiments are concerned, besides the Si release, varying concentrations of Ba, Mn, and Sr are the most evident changes occurring in seawater for felsic alteration experiments (Fig. 2.5a). In contrast, our experiments using mafic glass show no remarkable changes in Ba, Mn, and Sr concentrations but an initial increase in dissolved Al and removal of Al under elevated pressure and temperature conditions (Fig. 2.5b). For all felsic runs dissolved Al concentrations stayed below the detection limit of 1.85 µmol L^{-1}.

2.4. Discussion

2.4.1. Initial Alteration Processes

2.4.1.1. pH and Alkalinity Values – Frogner et al. (2001) ascribed fast *p*H decreases to acid magmatic gases adsorbed at the glass particle surface. These gases dissolve as soon as glass gets in contact with seawater. They therefore attributed their described *p*H decreases to the adsorbed aerosols. However, volcanic ash for their experimental work was sampled only five hours after eruption. Furthermore the collected material was used without any scrunching or cleaning with deionised water, whereas samples used for our experimental runs faced intensive cleaning. Still we observed decreasing seawater *p*H values, but proceeding very much slower, and therefore only clearly displayed at 100°C experimental runs. Thus we can conclude, in our case the rate and amplitude of *p*H change are, like Seyfried and Bischoff (1979) already pointed out, rather caused by glass alteration than being related to dissolved volcanic gases.

Table 2.3: Examples for modification of seawater during felsic and mafic glass alteration expressed by element ratios.

felsic

M54 1bar, 100°C

hours	Ca/Na	K/Na	Mg/Na
0	**0.022**	**0.021**	**0.11**
1	**0.022**	**0.021**	**0.11**
2	**0.022**	**0.021**	**0.11**
4	**0.023**	**0.021**	**0.11**
16	**0.023**	**0.022**	**0.08**
24	**0.023**	**0.022**	**0.08**
33	**0.023**	**0.022**	**0.08**
48	**0.023**	**0.022**	**0.08**

M54 200bar, 24°C

hours	Ca/Na	K/Na	Mg/Na
0	**0.022**	0.021	0.11
2	**0.022**	0.021	0.11
4	**0.022**	0.021	0.11
8	**0.023**	0.021	0.11
16	**0.023**	0.021	0.11
24	**0.023**	0.021	0.11
48	**0.023**	0.021	0.11
168	**0.023**	0.021	0.11
330	**0.023**	0.021	0.11
496	**0.024**	0.021	0.11
836	**0.024**	0.021	0.11

M54 200bar, 50°C

hours	Ca/Na	K/Na	Mg/Na
0	**0.022**	0.021	0.11
2	**0.022**	0.021	0.11
4	**0.022**	0.021	0.11
16	**0.023**	0.021	0.11
24	**0.023**	0.021	0.11
48	**0.023**	0.021	0.11
174	**0.023**	0.022	0.11
336	**0.023**	0.022	0.11
502	**0.024**	0.022	0.11
840	**0.023**	0.021	0.11

M54 400bar, 24°C

hours	Ca/Na	K/Na	Mg/Na
0	**0.022**	0.021	0.11
164	**0.023**	0.021	0.11
331	**0.023**	0.021	0.11
504	**0.023**	0.021	0.11
837	**0.023**	0.021	0.11

M54 400bar, 50°C

hours	Ca/Na	K/Na	Mg/Na
0	**0.022**	0.021	0.11
2	**0.021**	0.020	0.11
4	**0.022**	0.021	0.11
24	**0.022**	0.021	0.11
48	**0.024**	0.021	0.11
330	**0.024**	0.020	0.11

mafic

SO173 200bar, 24°C

hours	Ca/Na	K/Na	Mg/Na
0	0.022	0.021	0.11
1	0.022	0.021	0.11
2	0.022	0.021	0.11
4	0.021	0.021	0.11
8	0.021	0.021	0.11
16	0.021	0.021	0.11
24	0.021	0.021	0.11
48	0.021	0.021	0.11

SO173 400bar, 24°C

hours	Ca/Na	K/Na	Mg/Na
0	0.022	0.021	0.11
2	0.022	0.021	0.11
4	0.021	0.020	0.11
8	0.022	0.022	0.11
16	0.021	0.020	0.11
24	0.022	0.021	0.11
48	0.022	0.021	0.11

SO173 1bar, 100°C

hours	Ca/Na	K/Na	Mg/Na
0	**0.022**	**0.021**	**0.11**
1	**0.022**	**0.021**	**0.11**
2	**0.023**	**0.021**	**0.11**
4	**0.023**	**0.021**	**0.11**
16	**0.022**	**0.021**	**0.08**
24	**0.023**	**0.021**	**0.08**
33	**0.024**	**0.022**	**0.08**
48	**0.023**	**0.021**	**0.08**

SO173 200bar, 50°C

hours	Ca/Na	K/Na	Mg/Na
0	0.022	0.021	0.11
1	0.021	0.021	0.11
2	0.021	0.021	0.11
4	0.021	0.021	0.11
16	0.021	0.021	0.11
24	0.021	0.021	0.11
48	0.021	0.021	0.11

SO173 400bar, 50°C

hours	Ca/Na	K/Na	Mg/Na
0	0.022	0.021	0.11
2	0.022	0.021	0.11
4	0.022	0.021	0.11
8	0.022	0.021	0.11
16	0.022	0.021	0.11
24	0.021	0.020	0.11
48	0.022	0.021	0.11

The dissolution of glass induces an alkalinity increase due to the release and protonation of oxyanions (O^{2-}). In contrast the exchange of oxidisable and/or hydrolisable cations (e.g. Fe, Al, Ti) against seawater cations (e.g. Na, K, Mg) causes a decrease in *p*H and alkalinity due to the proton release during oxidation and hydrolysis. Moreover, protons are released into the solution due to the displacement of adsorbed protons by seawater cations. The observed alkalinity decrease in Figure 2.4b therefore indicates that cation exchange proceeds at much higher rates than ash dissolution under our experimental conditions. Volcanic ashes deposited in marine environments are thus initially equilibrated with seawater via rapid surface exchange processes accompanied by comparably slow dissolution reactions. This process is shown by onshore and even better by offshore samples, even though offshore samples already faced seawater alteration for prolonged periods of time (Kutterolf et al., in press). We attribute this behaviour to their higher specific surfaces, meaning much higher surface roughness, as well as the cleansing procedure with deionised water, rapidly forming new reactive surfaces.

2.4.1.2. Major Elements – Basaltic glass alteration has been described as an important source for Ca. However, only little attention has been paid to felsic volcanics especially as element source for pore fluids. The observed initial and continuous loss of Ca out of felsic glasses as well as the uptake of Mg at elevated temperatures (Tab. 2.3) demonstrate that the composition of pore fluids in felsic tephra dominated sediments may be strongly affected by ash alteration processes.

Accounting for the *p*H, we can point out that chemical changes of seawater for mafic runs are only of the same magnitude as those observed for felsic runs and therefore significant, when seawater reached clearly acid conditions (100°C, 1 bar). This dissolution behaviour displays the *p*H variation described in literature. Gíslason and Oelkers (2003) as well as Oelkers and Gíslason (2001) point out that the dissolution rates of basaltic glass increase significantly with decreasing *p*H under acid conditions but minimise at near neutral *p*H, while obsidian dissolution rates determined by Utzmann et al. (2000) did not show significant changes from *p*H 7 to *p*H 3.

2.4.1.3. Trace Elements – Trace elements like Ba, Mn, and Sr were enriched significantly in the alterating seawater only during experimental runs using felsic glass (Fig. 2.5a) even though the mafic glass samples had higher initial Sr and Mn contents (Tab. 2.2).

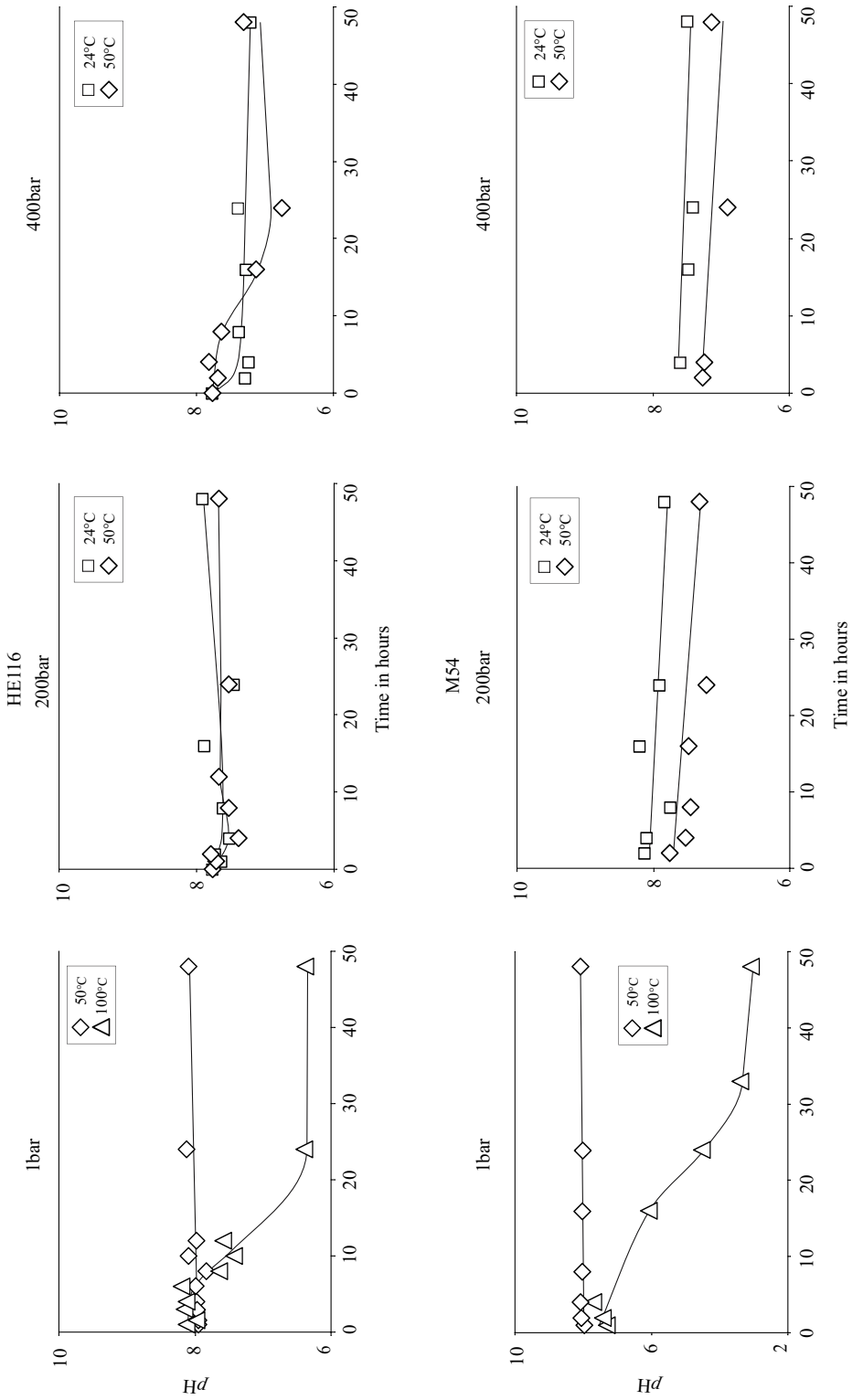

Figure 2.4a: Experimental results. Kinetic experiments with felsic glass show a decrease in solution pH during initial alteration most significantly at 100°C and 1 bar.

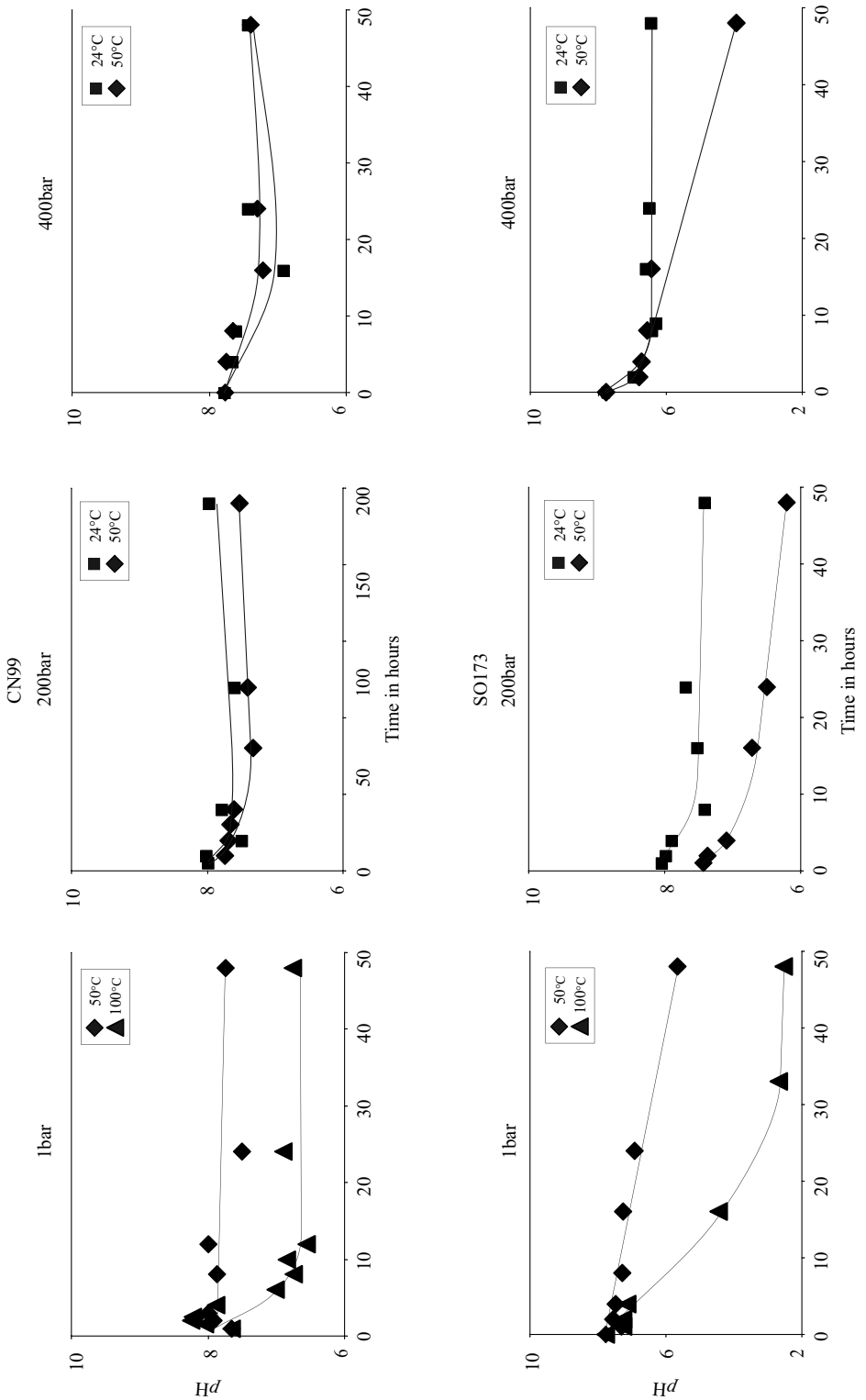

Figure 2.4a continued: Experimental results. Kinetic experiments with mafic glass show a decrease in solution pH during initial alteration most significantly at 100°C and 1 bar.

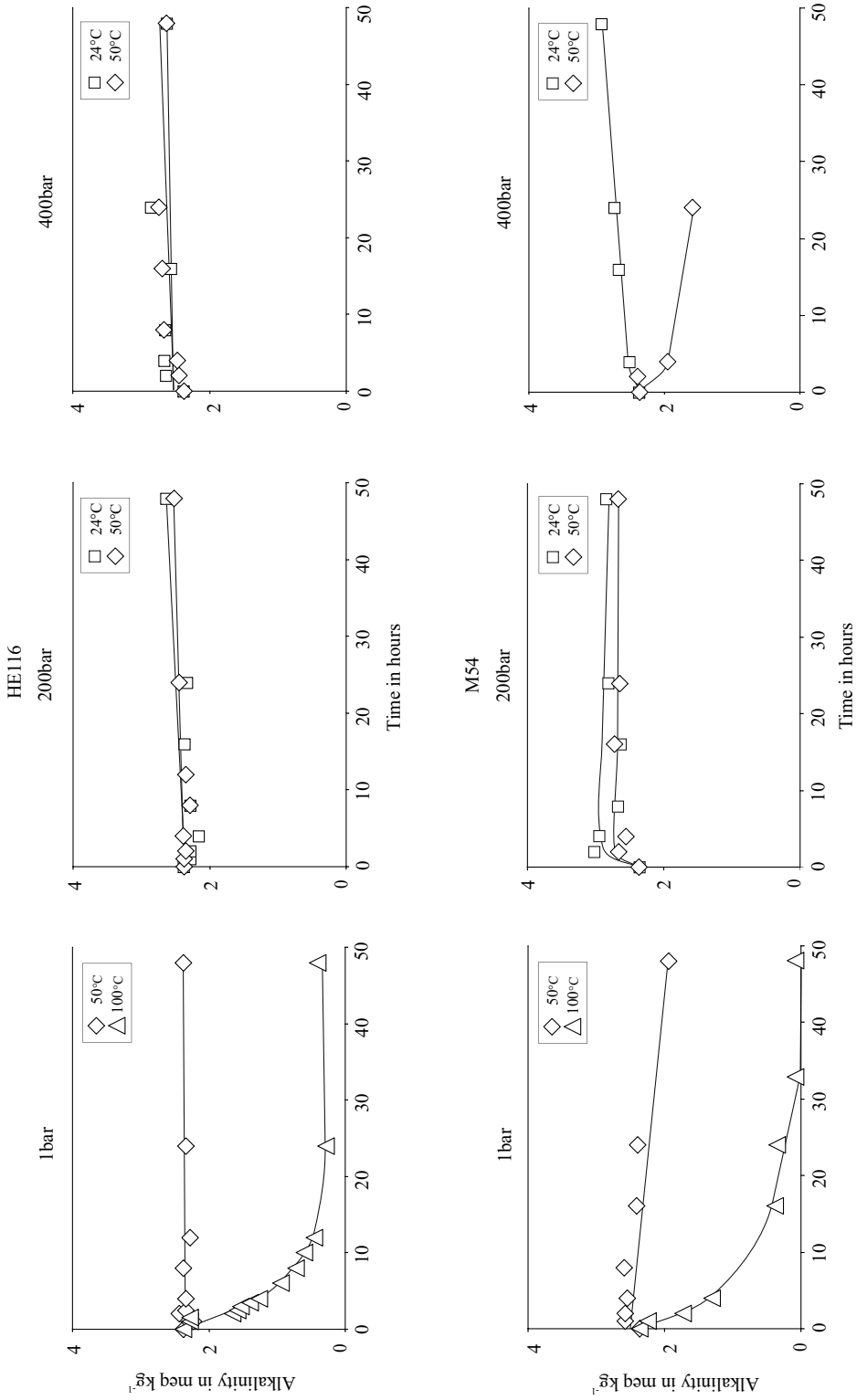

Figure 2.4b: Experimental results. Kinetic experiments with felsic glass show only minor changes in alkalinity during initial alteration, but strong decreases when conducted at 100°C and 1 bar.

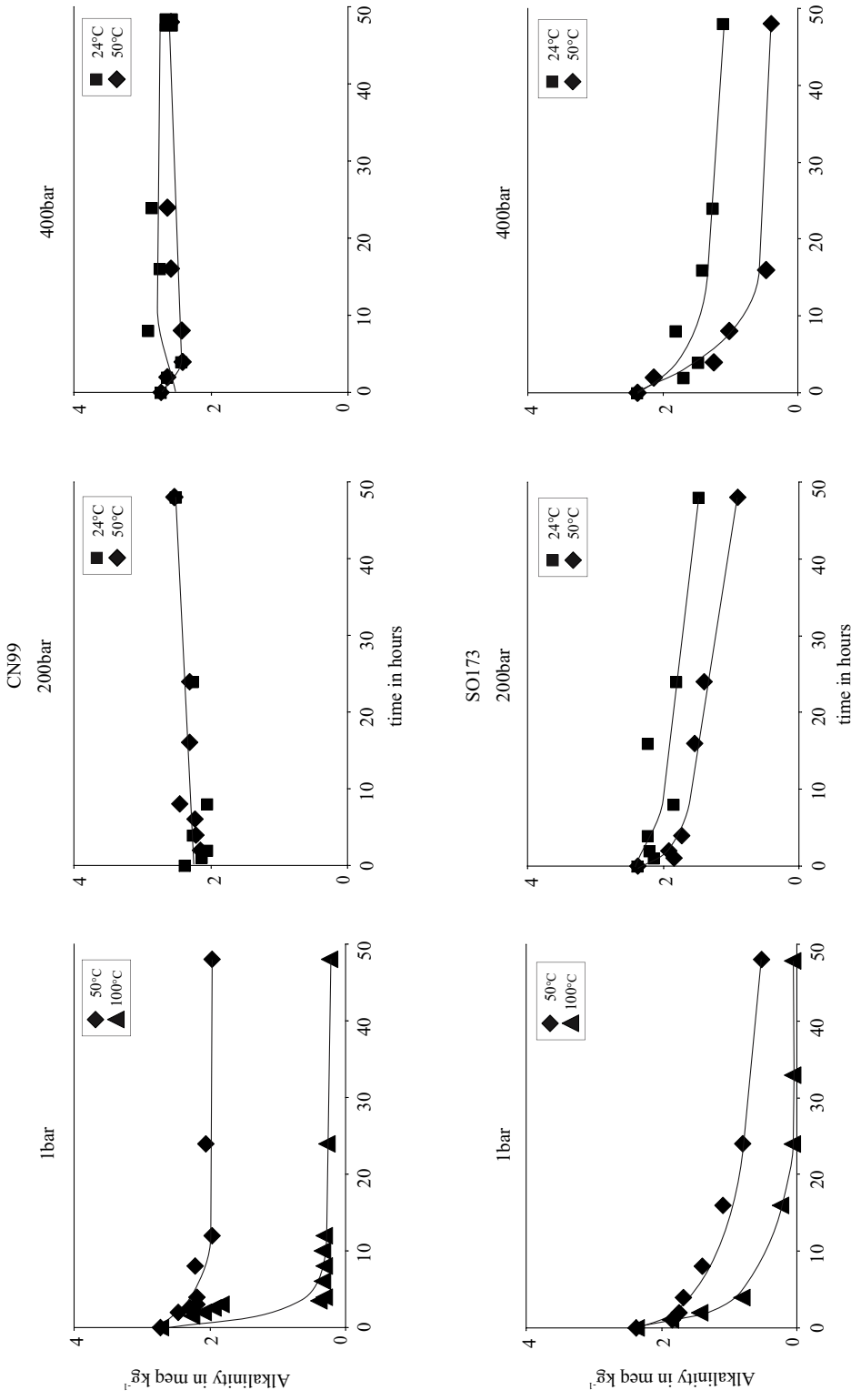

Figure 2.4b continued: Experimental results. Kinetic experiments with mafic glass show strong alkalinity decreases for both, onshore (CN99) and offshore (SO173) material, when conducted at 100°C and 1 bar.

It seems to be possible that these trace elements are efficiently retained in the outer alteration rim of glass shards which is only formed during the alteration of mafic glass.

For mafic runs investigated Al-concentrations decrease, after reaching a maximum value, due to precipitation processes (Fig. 2.5b). Thus for mafic runs it can be concluded that Al concentrations are controlled by an equilibrium with Al-bearing products or phases. However, in all felsic runs Al concentrations stayed below the detection limit (< 1.85 µmol L^{-1}). This marked contrast in the evolution of the seawater composition indicates that mafic ashes release Al into solution to form rather soluble secondary products while during felsic seawater alteration Al is removed from the solution by the precipitation of very insoluble Al-phases, a phenomenon already described by e.g. Kawano et al. (1997).

2.4.2. Dissolution Kinetics

The increase in dissolved silica was used to estimate bulk dissolution rates because Si is the major network component of the investigated volcanic glasses. Considering the different specific surface areas of the used samples, dissolution rates with respect to Si were calculated according to the following equation:

$$Q_{Si} = (C_{Si} \cdot V_{sol})/(A \cdot m) \quad (1)$$

were Q_{Si} gives the moles of Si released per square metre glass surface (mol m^{-2}), C_{Si} (mol L^{-1}) is the Si concentration in the solution, V_{Sol} (L) is the solution volume, A is the initial specific surface area (m^2 g^{-1}), and m is the mass of the glass powder (g). According to Yokoyama and Banfield (2002) dissolution rates are BET normalised, since geometric surface areas cannot be used in the current study because of the high internal porosity of the felsic onshore and offshore samples.

In all experimental runs, released silica (Q_{Si}) showed an initial and rapid increase over the first few hours followed by a slower and approximately linear change extending till the end of the experiments (Figs. 2.6a & b). The rapid initial dissolution step is probably caused by the dissolution of high-energy sites at the glass surface created during sample pre-treatment. Hence it seems to be possible that dissolution is initially promoted because surface groups (Si-OH, $Si\text{-}O^-$, $Si\text{-}M^{n+}$) are not yet equilibrated with the seawater medium and are therefore less stable and more easily detached from the ashes to form dissolved silica.

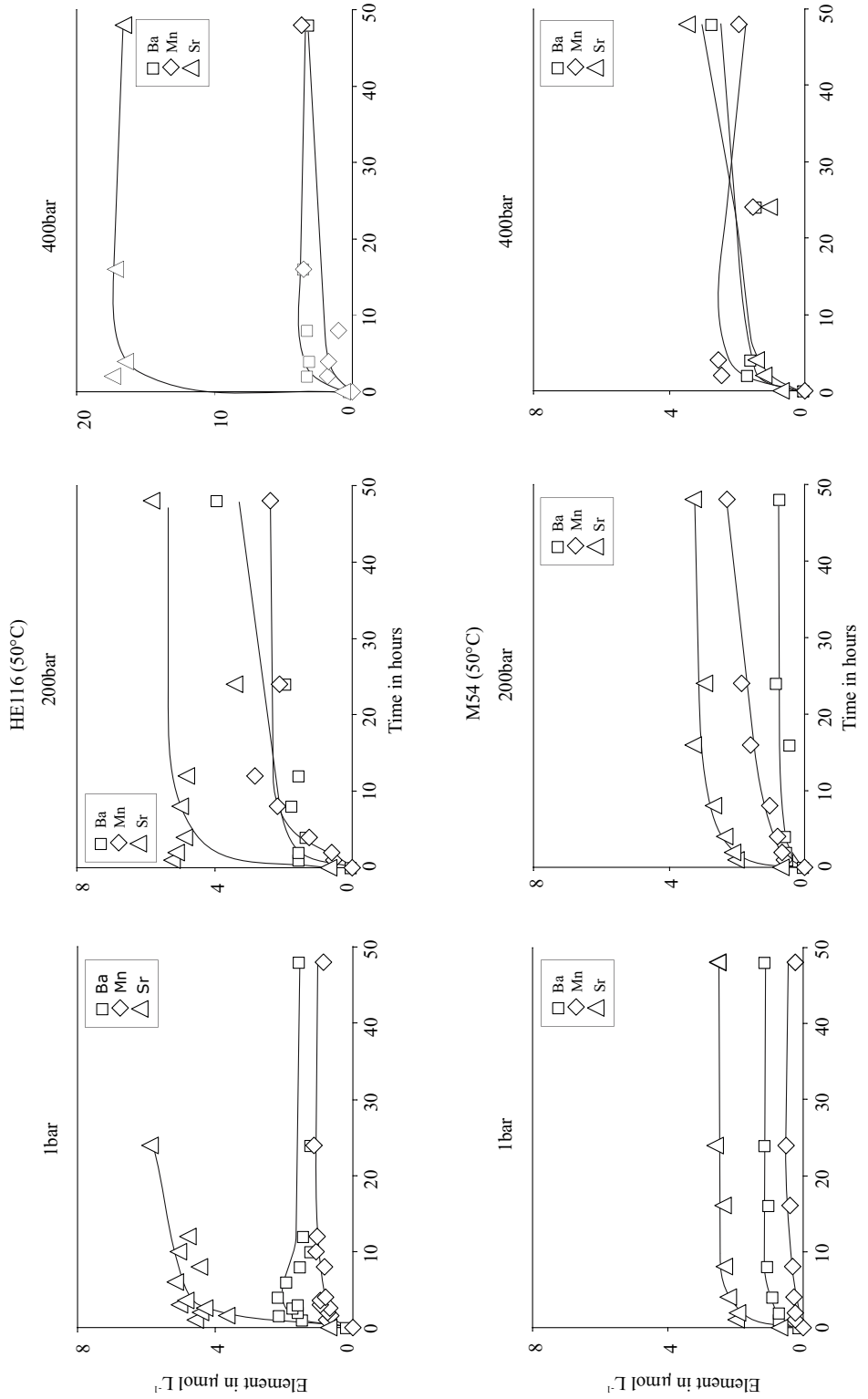

Figure 2.5a: Release of dissolved trace elements during felsic glass alteration.

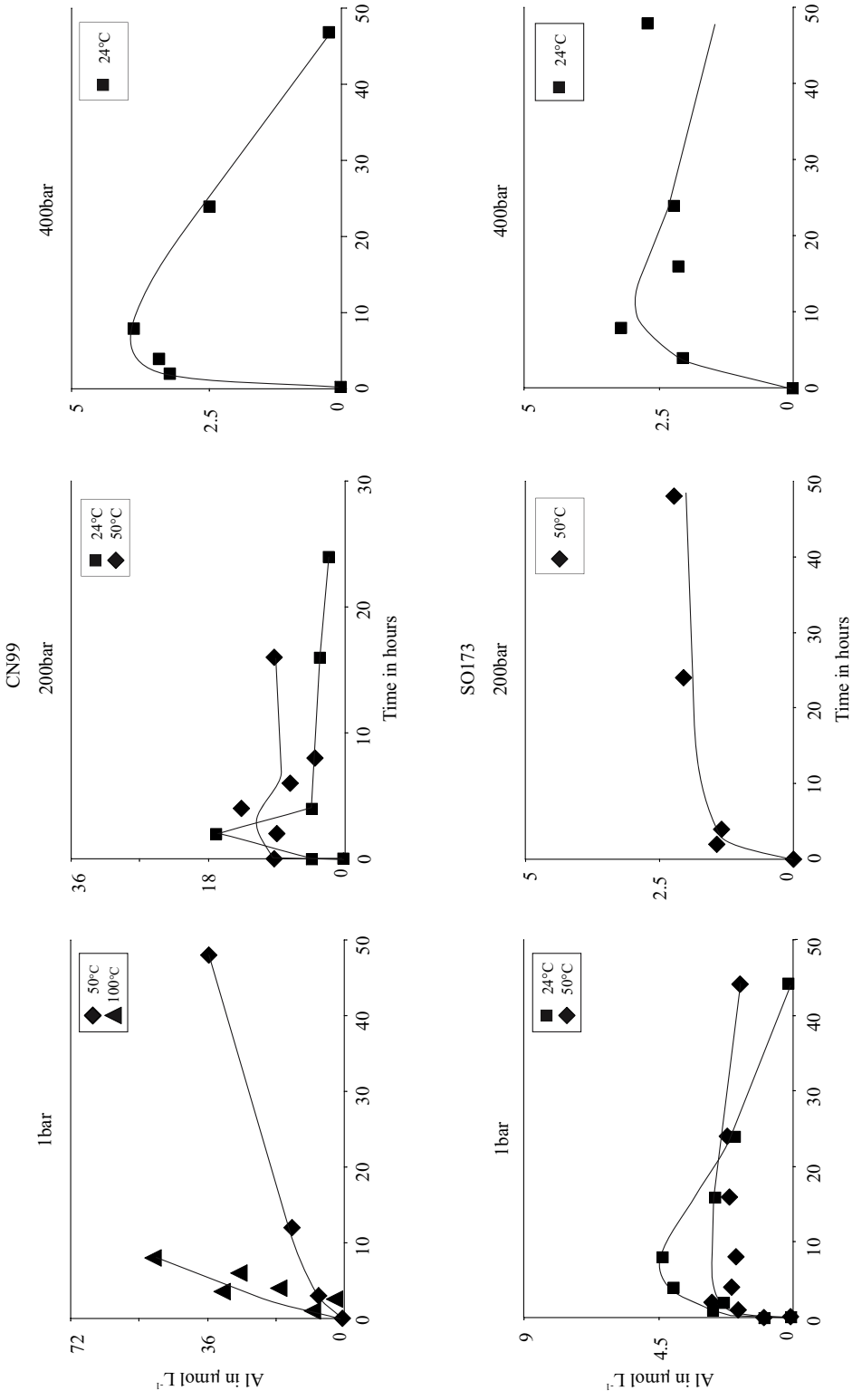

Figure 2.5b: Release of dissolved Al during mafic glass alteration.

Dissolution rates were calculated considering only the slow and linear increase in Q_{Si} following the initial rapid dissolution step. Q_{Si} was assumed to vary with time according to the expression:

$$Q_{Si} = Q_0 + k_{dis} \cdot t \qquad (2)$$

where Q_0 describes the moles released as the result of the initial exchange reaction, k_{dis} is the zero order dissolution constant (mol m^{-2} sec^{-1}), and t is time in seconds. The closeness of the linear fit is indicated by the correlation coefficient (r^2) (Tab. 2.4). In most cases r^2 was greater than 0.96.

Our calculations led to dissolution rate constants given in Table 2.4. Considering the error associated with k_{dis} (± 10%, associated with the used analytical method for Si determination), the uncertainties associated with the BET surface area measurment of the glass specimens (± 25%), and the error within the linear regression, the overall error of the k_{dis}-values reported in this study are in the order of about ± 30 % ($28.1=(0.10^2+0.25^2+0.08^2)^{1/2}$).

2.4.2.1. Temperature Dependence of Dissolution Kinetics – Our experiments confirm that the chemical reactions described above are accelerated with temperature (Tab. 2.4). The data can be applied to the problem of determining whether equilibrium is established under geological conditions or if disequilibria phenomena, like in our experiments, are of importance. The temperature dependence can be evaluated by expressing the rate constant for a reaction by the Arrhenius equation:

$$k_{dis} = A exp^{(-E_a/RT)} \qquad \text{respectively} \qquad ln\, k_{dis} = ln\, A - \frac{E_a}{RT} \qquad (3)$$

where k_{dis} is the linear rate constant (mol m^{-2} sec^{-1}), E_a refers to the activation energy of the dissolution, for a given element (J mol^{-1}), R is the universal gas constant (8.314 J mol^{-1} K^{-1}), T is the absolute temperature (K), and A_a designates the temperature independent pre-exponential factor (mol m^{-2} sec^{-1}). The activation energy E_a for the dissolution reactions was obtained for all experiments from an Arrhenius plot (ln k_{dis} vs. $1/T$) (Fig. 2.7). The results of these calculations are also given in Table 2.4.

For the investigated P/T conditions we can derive for offshore samples that mafic glass dissolution proceeded slightly faster than felsic one. This is in accord with the general observation, that under same experimental conditions silica-poor glasses dissolve faster

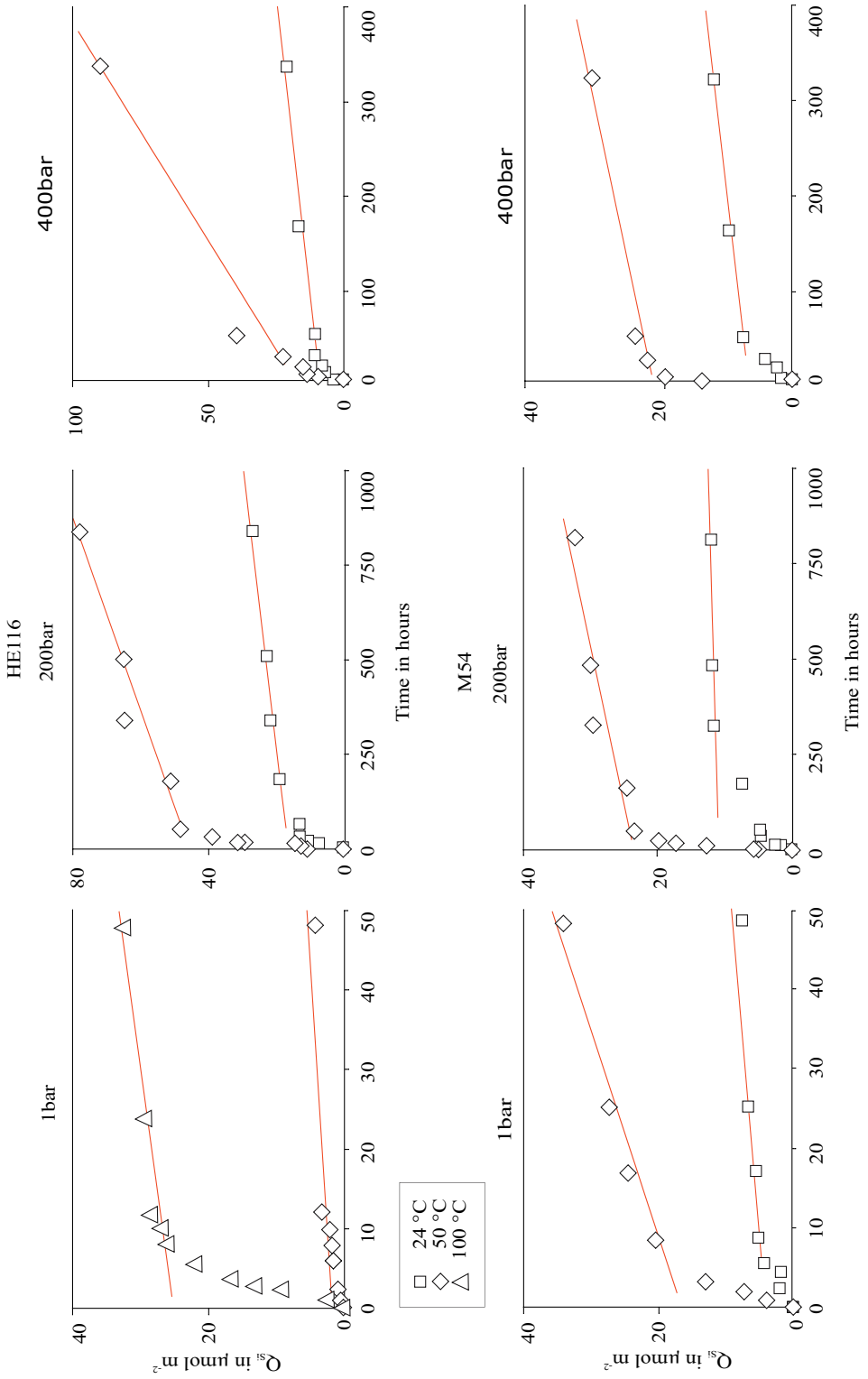

Figure 2.6a: Silica released into solution Q_{Si} (µmol m^{-2}) for felsic experimental runs, straight lines represent regression lines for k_{dis} calculations.

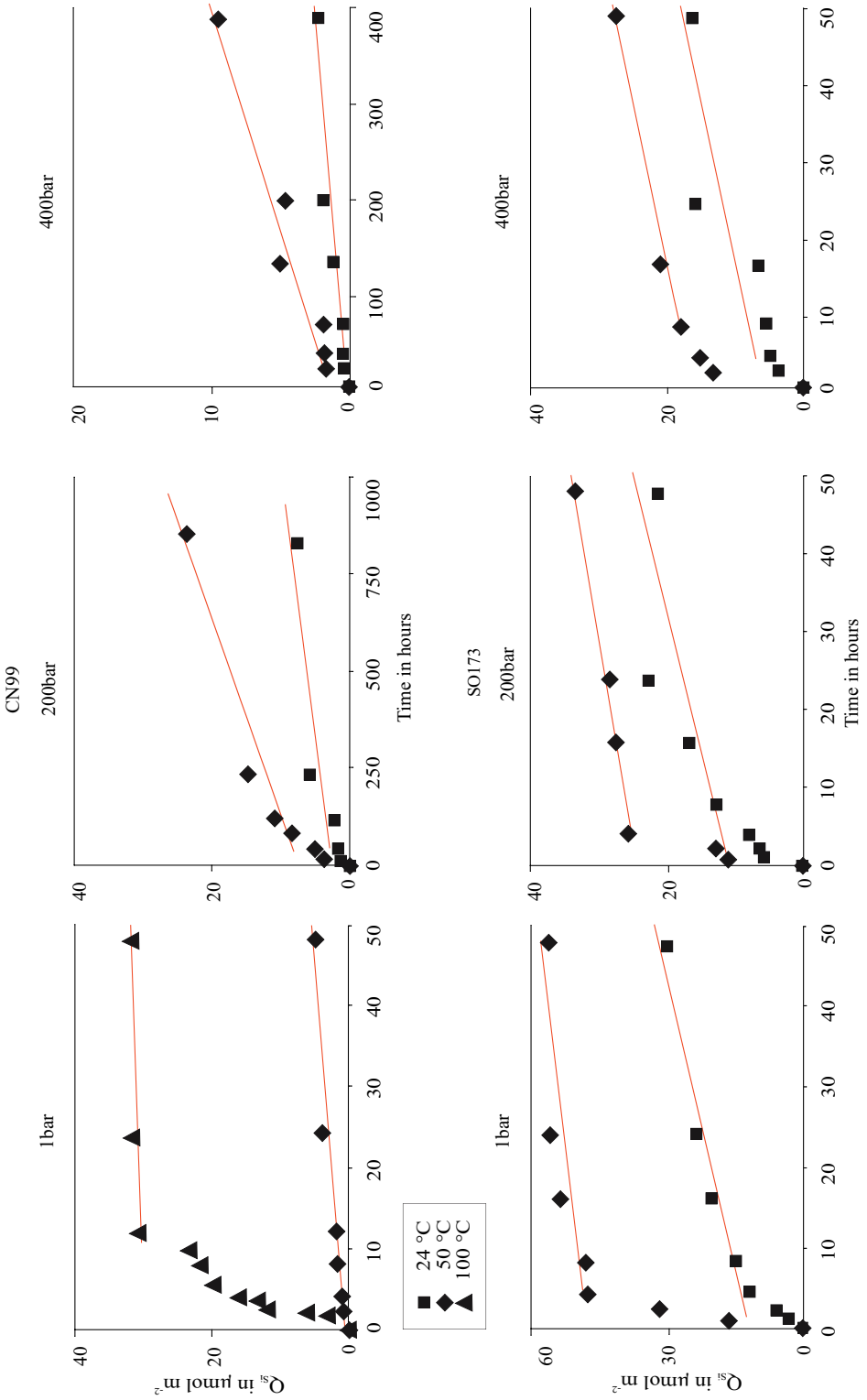

Figure 2.6b: Silica released into solution Q_{Si} (µmol m^{-2}) for mafic experimental runs, straight lines represent regression lines for k_{dis} calculations.

Table 2.4: Values of dissolution constant k_{dis} (mol m^{-2} sec^{-1}), activation energy E_a (kJ mol^{-1}) and pre-exponential term ln A_a (mol m^{-2} sec^{-1}).

	Onshore								Offshore							
	1bar		200bar		400bar				1bar		200bar		400bar			
	log k_{dis}	r^2	log k_{dis}	r^2	log k_{dis}	r^2			log k_{dis}	r^2	log k_{dis}	r^2	log k_{dis}	r^2		
mafic CN99									mafic SO173							
24°C	-12.5	0.96	-11.6	1.00	-11.9	0.99			24°C	-10.1	0.97	-10.3	0.75	-10.5	1.00	
50°C	-11.2	0.88	-10.9	0.98	-10.5	1.00			50°C	-10.2	0.74	-10.3	1.00	-10.2	1.00	
100°C	-10.8	0.76	-8.68	1.00												
		r^2		r^2												
E_a in kJ/mol	45.2	0.83	84.6	0.97												
ln A_a	-9.97		6.59													
felsic HE116									felsic M54							
24°C	-12.4	0.88	-11.4	0.99	-11.4	0.91			24°C	-10.6	1.00	-12.3	0.76	-11.5	0.99	
50°C	-10.9	1.00	-11.0	0.95	-10.2	1.00			50°C	-10.1	0.99	-11.8	1.00	-11.2	1.00	
100°C	-10.5	1.00	-9.14	1.00												
		r^2		r^2												
E_a in kJ/mol	50.2	0.84	66.2	0.95												
ln A_a	-7.55		-0.38													

than silica-rich ones (e.g. Allnatt et al., 1983; Karkhansis et al., 1980; Petit et al., 1990; Wolff-Boenisch et al., 2004). The investigated onshore mafic and felsic glass samples do not show significant differences in dissolution behaviour at low temperatures. Perret et al. (2003) suggested a linear relationship between the logarithmic dissolution rates and silica contents of waste glasses. The Si content of the felsic sample HE116 is rather low and relatively close to the mafic sample CN99 (Tab. 2.2). Thus we ascribe the above described similar dissolution rates to the chemical composition (Si content) of the onshore samples.

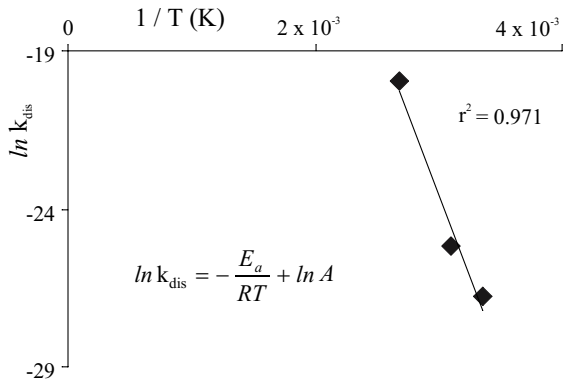

Figure 2.7: Example (CN 99, 200 bar) of an Arrhenius Plot used for activation energy (E_a) determinations.

However, at elevated pressures (200 bar), higher E_a values of the mafic compared to the felsic experiments also have a higher pre-exponential term which result in faster kinetics of the mafic runs at elevated temperatures (100°C) (Tab. 2.4). Higher activation energies for the mafic reactions also imply a greater sensitivity to temperature changes and, at much lower temperatures, slower kinetics. Our estimations for seafloor conditions (2°C, 200 bar) confirm this consideration, since they lead to k_{dis} = 3.1 x 10^{-13} mol m^{-2} sec^{-1} for felsic and 1.1 x 10^{-13} mol m^{-2} sec^{-1} for mafic glasses. Within the range of error, we therefore can estimate that under *in-situ* conditions felsic glass is at least as reactive as mafic glass.

2.4.2.2. Pressure Dependence of Dissolution Kinetics – While it is described in a number of studies that chemical reactions are usually accelerated at high temperatures, Pytkowicz and Fowler (1967) as well as Willey (1974) were the first to describe a similar effect of increasing pressure on the solubility of amorphous silicates in seawater. Though in this study this pressure effect is not observed for all experimental runs. Higher pressures enhanced the dissolution rate constants of mafic and felsic onshore samples and elevated the activation energies. Rate constants of offshore samples were more often diminished at high pressures (Tab. 2.4). Prior to the experiments, onshore samples experienced alteration only under atmospheric pressure conditions while marine samples were deposited and altered at the seafloor under elevated pressures. Thus the reactive surfaces of the marine samples were already adapted to high pressure conditions whereas the surfaces of onshore ashes were equilibrated to atmospheric pressures. The effects of experimental pressure on the dissolution behaviour of volcanic glasses may thus be related to the alteration history of the investigated samples, so that dissolution is enhanced when experiments are run under pressure conditions not previously experienced by the investigated samples. This would imply that the experimental investigation of dissolution kinetics should not only

mimic the prevailing temperatures but should also consider the *in-situ* pressure conditions to avoid an artificial increase in dissolution rate. Moreover, our results suggest that the increase in pressure with water depth accelerates the dissolution of young volcanic ashes deposited at the sediment/water interface.

2.4.2.3. Comparison to Previously Published Dissolution Rates of Mafic and Felsic Glasses – In all cases rate constants for the dissolution of mafic glass determined in this study are smaller than previously determined values (Tab. 2.5). However, it is worth noting that discrepancies of about three orders of magnitude occur, even if experiments were conducted with artificial seawater (Brady and Gíslason, 1997; Crovisier et al., 1987). These discrepancies can mostly be attributed to the differences in duration of experimental alteration, temperature and pressure differences, differences in surface conditions of the used samples, different sample grain sizes, different methods of estimating surface areas, as well as to differences in solution chemistry, if deionised water experiments are concerned.

Rate constants for the dissolution of felsic glass can be compared to the data previously derived by the various authors cited in Table 2.5. The experiments in these studies again were conducted at various conditions of glass- and solution composition etc., but *p*H and temperature are comparable. Since the cited laboratory derived glass dissolution rates are varying it is difficult to to decide which one is directly applicable to complex field conditions. However, as far as field rates are concerned, studies on felsic alteration imply that non-stirring experiments provide data much closer to field rates (Yokoyama and Banfield, 2002). Experimental set-ups, which avoided stirring, thus seem to be appropriate to mimic field conditions and to minimise the artificial creation of high-energy sites at the ash surfaces. This, in fact, represents the advantage of the used experimental approach, since experimentally derived rates can only be applied to predict field dissolution rates if the conditions in the lab are as close as possible to those expected in the field. However, more studies under comparable experimental conditions are needed to further investigate the varying reactivity of felsic glasses in different environments.

2.4.3. Secondary Phases

In order to investigate the chemical evolution of mafic and felsic glasses, microprobe analyses of fresh and experimentally altered glass shards, were conducted.

Figures 2.8a & b compare concentration profiles for selected elements, starting at the rim and proceeding into the fresh glass core, of mafic and felsic glass shards. These data clearly demonstrate, that alteration penetrates much deeper into mafic glasses after only a few hours of alteration. We therefore suggest one of the most significant differences in alteration of differently composed glasses is the formation and the thickness of an alteration skin acts as a sink and source for various elements.

Table 2.5: Dissolution rates (mol m^{-2} sec^{-1}) proposed in this work and in the literature.

Glass	Rate mol m^{-2} sec^{-1}	Weathering Environment	Comments		Reference
basaltic-andesite	10^{-13}	seawater	25°C	non-stirring	This work
basaltic-andesite	10^{-11}	seawater	100°C	non-stirring	This work
basalt	$10^{-14.7}$-$10^{-14.3}$	meteoric	10°C	field rate	Gordon & Brady, 2002
basalt	9.3 x 10^{-7}	deionized water	150°C	stirring	Berger et al., 1994
basalt	$10^{-10.35}$	seawater	25 °C, P_{CO_2}=$10^{-3.5}$	non-stirring	Brady & Gíslason, 1997
basalt	$10^{-9.9}$	seawater	25°C, pH 8	non-stirring	Crovisier et al., 1987
basalt	1.8 x 10^{-11}	demineralized water	25°C, pH 8	stirring	Oelkers & Gíslason, 2001
b-andesite (HZ1-6)	1.3 x 10^{-11}	Millipore™ water	25°C, *p* H 4	stirring	Wolff-Boenisch et al., 2004
b-andesite (HZ1-3)	1.2 x 10^{-10}	Millipore™ water	25°C, *p* H 10.6	stirring	Wolff-Boenisch et al., 2004
dacite	10^{-13}	seawater	24°C	non-stirring	This work
dacite	10^{-11}	seawater	100°C	non-stirring	This work
dacite	10^{-14}-10^{-13}	meteoric	5.5°C	field rate	Dahlgren et al., 1999
rhyolite	6.0 x 10^{-15}	meteoric	20°C	field rate	Yokoyama & Banfield, 2002
rhyolite	3.9 x 10^{-10}	destilled water	82°C, *p* H 6.0	non-stirring	Fiore et al., 1999
vitreous silica	10^{-9}-10^{-7}	NaOH-solution	25°C	stirring	Wirth & Gieskes, 1979
rhyolite	10^{-12}-10^{-11}	deionized water	25°C, *p* H 1.0-6.2	stirring	White & Claassen, 1980; White, 1983
rhyolite (A75F-1)	8.1 x 10^{-12}	Millipore™ water	25°C, *p* H 4	stirring	Wolff-Boenisch et al., 2004
rhyolite (A75-4)	8.7 x 10^{-11}	Millipore™ water	25°C, *p* H 10.6	stirring	Wolff-Boenisch et al., 2004
rhyolite	8.7 x 10^{-13}	deionized water	30°C	non-stirring	Yokoyama & Banfield, 2002

Solid phase observations of glasses at more advanced alteration stages were conducted with naturally altered glass shards taken from marine ash layers. Additional information about the marine ash layers used for long-term alteration investigations are given in Table 2.6. Our EMP analyses of single glass shards taken from those marine ash layers (Fig. 2.8a) again show a significant modification of mafic glass shards from an unaltered core to the surface. An important increase in the Fe_{alt}/Fe_{fresh} ratio is seen at the surface while Mg_{alt}/Mg_{fresh}, and K_{alt}/K_{fresh} ratios increase only slightly and the concentrations of some elements (Ca, Na, Al) decrease significantly (Tab. 2.7). Crovisier et al. (1983) describe the release of Ca to the solution and the addition of Mg from the seawater as the principal chemical exchange between basaltic glass and the leaching solution. We were not able to distinguish this process to be significant on our experimental time scale, but for long term alteration of marine ashes, subjected to *in-situ* alteration at the seafloor, our EMP data confirm that removal of Mg from seawater into the solid occurred and was balanced by the removal of Ca and Na from the mafic glass (Tab. 2.7).

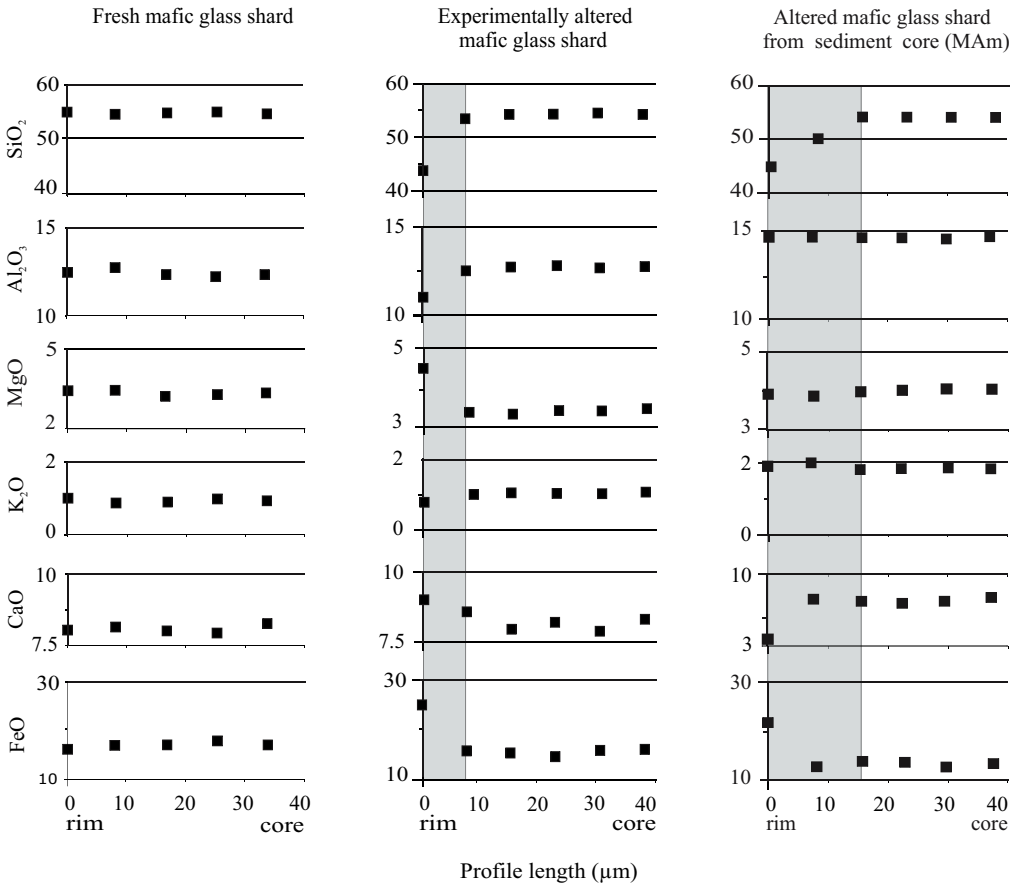

Figure 2.8a: Mafic – EMP-profiles obtained on a fresh onshore glass shard (CN99), on an experimentally altered one (CN99, 24 hours, 100°C, 200 bar), and on a marine ash layer derived one (MAm). The analyses indicate that mafic alteration results in the formation of a fragile altered rim which progressively evolves from a basaltic composition at the center to a palagonit-like composition at the rim.

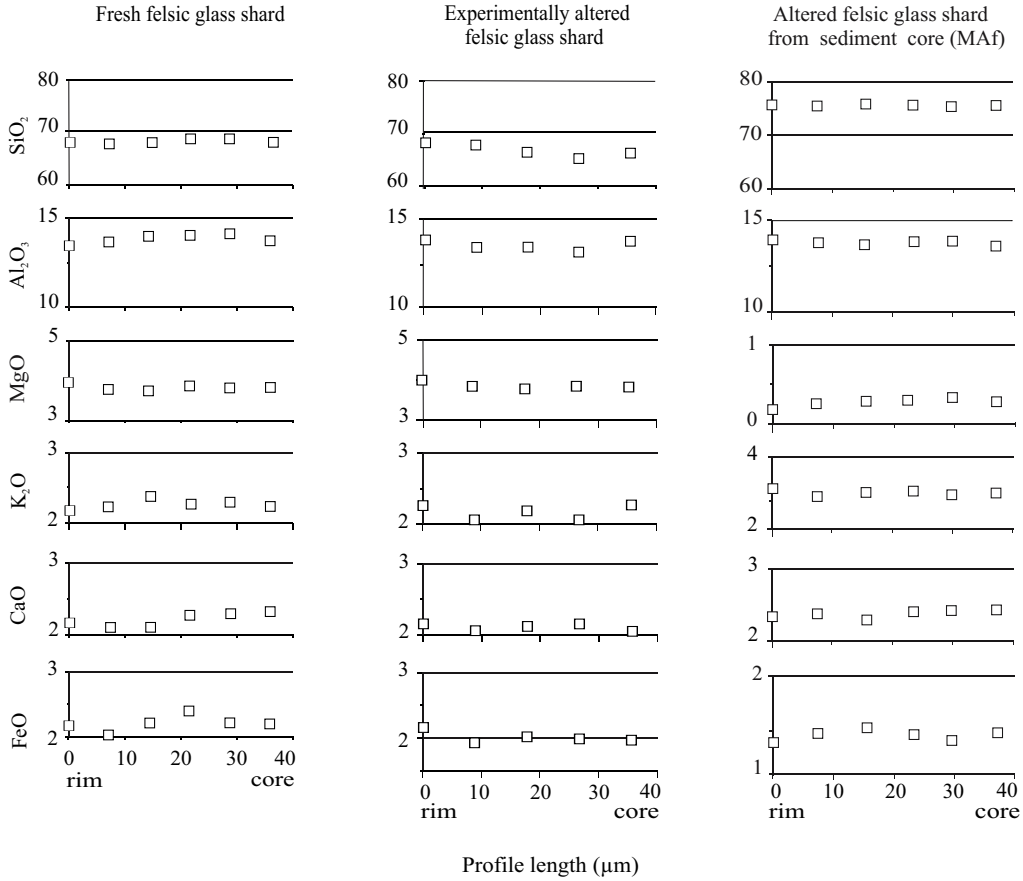

Figure 2.8b: Felsic – EMP-profiles obtained on a fresh onshore glass shard (HE116), on an experimentally altered one (HE116, 24 hours, 100°C, 200 bar), and on a marine ash layer derived one(MAf). The analyses indicate that for felsic alteration a palagonite-like alteration rim is missing, even after long-term alteration under seafloor conditions.

Table 2.6: Marine ash layers used for long-term seawater alteration investigations, their sampling locations and ages.

mafic	location		water depth	sediment depth	age
	latitude (N°)	longitude (W°)	(m)	(cm)	(kyr)
layer1	11°06.03	87°49.82	3334	12	2.1
layer2	11°06.03	87°49.82	3334	267	unknown
layer3	11°20.12	87°18.30	1200	49	16
MAm	11°20.11	87°18.35	1205	661	~40

felsic	location		water depth	sediment depth	age
	latitude (N°)	longitude (W°)	(m)	(cm)	(kyr)
layer1	11°20.11	87°18.35	1205	238	13
layer2	11°06.03	87°49.82	3334	67	~15
layer3	11°20.12	87°18.30	1200	59	24
MAf	11°20.12	87°18.30	1200	283	~34

mafic	CN 99 n=3	Shard1 n=7	Shard2 n=5	Shard3 n=4
SiO_2	0.8	0.9	1.0	1.0
Al_2O_3	0.8	0.9	0.8	1.0
Na_2O	1.1	0.9	0.8	0.8
K_2O	0.8	1.0	1.5	1.2
CaO	1.1	0.6	0.5	0.5
FeO	**1.5**	**1.3**	**1.3**	**1.0**
MnO	0.2	1.0	0.6	0.7
MgO	**1.9**	**1.3**	**1.2**	**1.2**

felsic	Shard1 n=7	Shard2 n=2	Shard3 n=3
SiO_2	1.0	1.0	1.0
Al_2O_3	1.0	1.0	1.0
Na_2O	1.0	0.8	0.5
K_2O	1.1	1.0	1.1
CaO	0.8	1.0	1.6
FeO	**1.2**	**1.2**	**0.9**
MnO	**1.1**	**1.5**	**1.1**
MgO	**2.7**	**1.0**	**1.1**

Table 2.7: Element ratios altered/ fresh determined by EMP of glass shards taken from marine ash layers, indicating chemical gains (bold numbers) and losses (grey bars) during in-situ alteration at the seafloor. "n" describes the number of glass shards that were analysed for each ash layer. Since we were not able to distinguish any chemical changes of experimentally altered felsic glass shards via microprobe this table shows only data for glass taken out of marine felsic ash layers.

Aside from our experimentally observed *breakdown* reactions, which represent sources of elements, EMP data indicate that some elements are released from the glass leaving behind a network enriched in Fe, Mg and water. (We assumed the rate of LOI as corresponding to the weight of H_2O). However, the chosen glass shards representing mafic long term alteration (~ 40 kyr) had developed a rim only slightly thicker than during short term alteration (Figs. 2.8a & 2.9). We see this as an indicator for the preferential alteration of glass shards with enhanced surface features but also as an indicator for the protective role of the altered skin preventing further alteration, a suggestion already made by Techer et al. (2001). The alteration rim can represent a continuous spectrum of composition. Secondary phases evolve out of that alteration rim, acting as a sink for a significant portion of elements released during alteration (Bach et al., 2001; Staudigel and Hart, 1983; Staudigel et al., 1996; Stroncik-Treue, 2000). Such phases include hydrous layer silicates like smectites and zeolites.

Depth profiling of mafic glass shards by Tsong et al. (1978) noted the deepest penetration for H_2O, showing that hydration precedes all other changes in concentration. H_2O initialises the alteration while reacting with the three dimensional Si-O-Si structure of the glass, which can be summarised as:

$$Si - O - Si + H_2O = 2Si(OH) \quad (4)$$

Our EMP analyses of felsic shards, experimentally altered as well as taken from marine ash layers (Tab. 2.6), show almost constant concentrations for network forming elements such as Si and Al, indicating only little replacement of Si and Al (Tab. 2.7). Element ratios for network modifying elements (K, Na, Ca) show varying concentrations, indicating either loses or gains during alteration (Tab. 2.7). It is described that alkalis pass into the leaching solution by hydrogen-ion-exchange (White, 1983):

$$Si - O - Na + H^+ \rightarrow Si - O - H + Na^+ \quad (5)$$

or by inward diffusion of molecular water or by the two mechanisms acting at the same time (Petit et al., 1990; Yang and Kirkpatrick, 1990). The stage of hydration can proceed until a saturation point of about 3 wt% of H_2O is reached (Jezek and Noble, 1978). Further weakening and breakage of the Si-O-Si bonds of the glass structure results in a nearly complete dissolution of the glass (Oelkers, 2001). The absence of a palagonite-like hydrated alteration rim for felsic alteration is illustrated by the *fresh* and well constrained composition of marine felsic ash layers (Figs. 2.1b & 2.9**)**. Additionally to our results, experimental alteration of rhyolitic glass above 100°C presented by Karkhansis et al. (1980) did not display a hydrated layer. X-ray Photoelectron Spectroscopy (XPS) analyses by Fiore et al. (1999) showed as well, that the formation of a leached layer did not take place. However, the formation of a hydrated layer cannot be excluded since opposite results were obtained by Petit et al. (1990) using a similar experimental approach on glass.

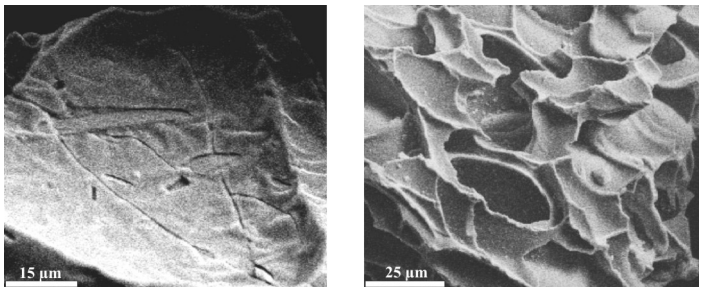

Figure 2.9: SEM images of mafic MAm (left) and felsic MAf (right) ash layers used for long-term alteration behaviour investigations. While the mafic glass shard has clearly developed an a few µm thick alteration skin, the felsic pumice fragment prevails a fresh looking surface, free of secondary mineralisation.

2.4.3.1. Stoichiometric Considerations – The quantity of the possible secondary material formed during our experiments is to small to identify individual phases. However, concentration changes of the dissolved constituents taking part in the formation of secondary phases like Si and Al can be used to characterise possible alteration products.

Since we only could obtain Al-data for our experiments with mafic glasses, the following considerations are limited to these experimental runs.

There are suggestions in literature (e.g. Oelkers and Gíslason, 2001) to use plagioclase as mineral analogue for mafic glass. Thus mafic samples contained approximately 0.5 Al and 7.0 Si per 32 oxygens (numbers of oxygens accroding to Deer et al., 1993). During glass alteration the release rates of Si and Al to the solution were not equal to the proportions of Si and Al in the reactant glass. For stoichiometric calculation of this release, Q_{Al} values were calculated from the Al-concentration data by using the modified Equation 1. Q_{Si} and Q_{Al} were normalised to the Si and Al number of ions in the bulk glass, respectively, to obtain Q_{normSi} and Q_{normAl} (µmol m^{-2}).

Table 2.8: Normalised Al/Si concentration ratios for solutions obtained in different experimental runs with mafic glass samples.

	Q_{normAl}/Q_{normSi}					
	Hours	1bar	Hours	200bar	Hours	400bar
CN 99						
24°C	5040	7.93	2	1.75	4	4.94
	6384	5.45	8	1.33	8	5.32
	9912	3.32	24	0.69	24	
	13104	2.03	48	0.18	48	0.50
50°C	3	9.16	8	0.72	4	0.00
	8		16	0.23	8	0.00
	12	4.93	24	0.41	16	0.00
	48	4.06	174	0.07	48	0.00
100°C	3	0.11	6	0.06		
	4	0.95	8	0.06		
	6	0.42	16	0.06		
	10	1.04	24	0.06		
SO 173						
24°C	4	0.01	4	0.00	4	0.01
	8	0.01	8	0.00	8	
	24	0.00	16	0.00	24	0.00
	48	0.00	24	0.00	48	0.00
50°C	4	0.00	2	0.00	4	0.00
	8	0.00	4	0.00	8	0.00
	24	0.00	24	0.00	24	
	48	0.00	48	0.00	48	0.02

With a ratio of $Q_{normAl}/Q_{normSi} > 1$, Al was released faster than Si and either a Si-rich leached layer was formed on the glass surface or a Si containing precipitate formed. If the ratio was 1 the glass dissolved congruently. With a ratio of $Q_{normAl}/Q_{normSi} < 1$, Si was released faster than Al and either an Al rich leached layer was formed or Al-containing precipitation or adsorption reactions may have occurred. The calculated results of the stoichiometry of release are given in Table 2.8.

The mafic onshore sample shows a preferential release of Al over Si during the initial phase of the experiments performed at 25°C and 50°C. The ratio decreased over time and was smaller than unity at the end of the experiments when elevated pressures of 200 and 400 bar prevailed. In contrast, the marine samples had very small Q_{normAl}/Q_{normSi} ratios already during the initial phase. Considering, that cation exchange is the dominant process during the initial phase of the experiments Al adsorbed to the surface of land ashes is rapidly desorbed when the land ashes are equilibrated with seawater. The marine ashes probably do not contain a significant portion of adsorbed Al because they have been exposed to seawater prior to the experiments for extended time periods. Hence, the different behaviour of land and marine ashes might be related to the abundance of Al adsorbed onto the surface of the glass samples.

EMP-analysis show that Al is not preferentially retained within the alteration rim (Tab. 2.6). Hence, the low Q_{normAl}/Q_{normSi} ratios obtained towards the end of the experiments indicate the precipitation of Al-bearing authigenic phases. These phases could be amorphous Al oxides and hydroxides and/or Al-silicates. Considering, however, that Si is much more abundant than Al in the dissolving glasses (Tab. 2.2), the effect of authigenic mineral formation on the dissolved silica concentrations is probably small, therefore dissolution rates calculated from the evolution of dissolved silica concentrations may not be strongly effected by the formation of secondary minerals. Nevertheless, it should be noted that dissolution rates calculated in this study are net rates reflecting the balance between glass dissolution and the formation of secondary Al-silicate phases.

2.5. Summary and Conclusions

The alteration behaviour of mafic and felsic volcanic glasses in contact with seawater was investigated in a closed system approach over a temperature range of 25 – 100°C and at pressures of 1 – 400 bar. Over the first few hours of the experiments, ion-exchange reactions between seawater and glass surfaces prevailed inducing a significant drop in *p*H

and alkalinity. During this initial phase of alteration, felsic glass released large amounts of dissolved silica, barium, strontium and manganese while mafic glass samples released dissolved silica and aluminium into the solution. These experimental observations indicate that volcanic ashes deposited into marine surface waters after volcanic eruptions and upon erosion may reduce the *p*H and increase the partial pressure of CO_2 in surface waters. Moreover, the released elements (Si, Al, Mn, Ba, Sr) may affect the growth of plankton and the chemical composition of planktonic shells.

After a few hours of equilibration time, the release of trace elements was strongly diminished while the dissolution of glass particles continued at a lower rate. Dissolved silica concentrations showed an approximately linear increase over time which was used to derive zero-order rate constants for glass dissolution. Dissolution rates and rate constants ranged in between 10^{-9} and 10^{-13} mol m^{-2} sec^{-1} and increased with temperature. Activation energies (E_a) calculated from the Arrhenius equation were affected by the prevailing pressure. At 1 bar, E_a was low (E = 45 – 50 kJ mol^{-1}) while significantly higher values (E_a = 66 – 85 kJ mol^{-1}) were obtained under elevated pressures (200 bar). Thus, it seems that the dissolution rate of volcanic glasses depends more strongly on temperature under seafloor conditions where high pressures prevail. Consequently, glass dissolution rates rapidly decrease with water depth both due to the decrease in temperature and the increasing temperature-dependence at high pressures.

Within the investigated low temperature (25 - 50°C) and pressure range (< 200 bar) mafic glass dissolved at about the same rate ($10^{-12.5}$ – $10^{-8.7}$ mol m^{-2} sec^{-1}) as felsic glass ($10^{-12.4}$ – $10^{-9.1}$ mol m^{-2} sec^{-1}). However, at 100°C and 200 bar, E_a of mafic glass was significantly larger (84.6 kJ mol^{-1}) than for felsic glass (66.2 kJ mol^{-1}). Consequently, the *in-situ* dissolution rate under seafloor conditions (2°C, 200 bar), was lower for mafic glass (1 x 10^{-13} mol m^{-2} sec^{-1}) than for felsic glass (3 x 10^{-13} mol m^{-2} sec^{-1}). Thus, the dissolution of felsic ashes in marine sediments deposited at the deep-sea floor and the slope of active continental margins proceeds at least as fast as the dissolution of mafic ashes. More evolved products of volcanism which prevail at most volcanic arcs are therefore highly reactive when exported into the marine environment.

Major ion concentrations in seawater were also affected by the reaction with volcanic glasses. Dissolved calcium concentrations increased over time while dissolved magnesium concentrations were diminished at elevated temperatures. Hence, the composition of pore fluids may change significantly due to ash alteration processes. The exchange between volcanic ashes and pore fluids is accelerated upon burial and subduction of

ash-bearing sediments due to increasing temperatures. Our study confirms that the decrease in dissolved Mg and the increase in Ca observed in many deep formation fluids (Gieskes and Lawrence, 1981) and fluids expelled at cold vent sites (Hensen et al., 2004) may be caused by volcanic ash alteration processes. However, we demonstrate that these changes are not only caused by exchange processes with mafic components but are also due to the alteration of more evolved felsic glasses.

Microscopic observations and microprobe analysis of experimentally altered glass shards and ashes retrieved from marine sediments were used to characterise pathways and modes of persistent ash alteration in the marine environment. The sampled ash layers were exposed to seawater and marine pore fluids over extended time periods (2.1 – 40 kyr) and showed significant changes in major element composition. Mafic glass shards had an extended alteration rim of palagonitic composition (ranging from only 5 µm thickness up to the complete conversion of the single shards), which is characterised by high water and Fe-Mg contents. In contrast, felsic glass shards showed no clear signs of the formation of such an interstage product, but due to the demonstrated chemical exchange one can assume that a leached layer will be formed. As alteration proceeds the weakening and breakage of the glass structure will result in the dissolution of the single glass shards. These investigations go along very well with solid phase observations of marine ash layers via microscope and microprobe showing felsic glass with only little signs of alteration compared to mafic ashes. Nevertheless, our kinetic studies clearly point out that under *in-situ* conditions of low temperatures and elevated pressures dissolution and element release proceed at similar rates for both types of tephra deposits.

Acknowledgments

This work is contribution no. 78 of the Special Research Project SFB 574 “Volatiles and Fluids in Subduction Zones” at the University of Kiel and was supported by the DFG “Deutsche Forschungsgemeinschaft”. Kristin Nass and Regina Surberg performed the ICP-OES analysis and Mario Thoener helped with the microprobe analysis. We would like to thank Carsten Schaffors for the straightforward performing of the Al analyses.

References

Allnatt A., Bancroft G., Fyfe W., Jacobs P., Karkhansis S., Melling P., Nishijima A., Vempati C., and Tait J. (1983) Leaching behaviour and electrical conductivity of natural rhyolite and modified synthetic rhyolites. *Chemical Geology* **38**, 329-357.

Alt J. and Honnorez J. (1984) Alteration of the upper oceanic crust, DSDP site 417: mineralogy and chemistry. *Contributions to Mineralogy and Petrology* **87**, 149-169.

Altaner S., Ylagan R., Savin S., Aronson J., Belkin H., and Pozzuoli A. (2003) Geothermometry, and mass transfer associated with hydrothermal alteration of a rhyolitic hyaloclastite from Ponza Island, Italy. *Geochimica et Cosmochimica Acta* **67**(2), 275-288.

Arvidson R., Ertan I., Amonette J., and Luttge A. (2003) Variation in calcite dissolution rates: A fundamental problem. *Geochimica et Cosmochimica Acta* **67**(9), 1623-1634.

Bach W., Alt J., Niu Y., Humphris S., Erzinger J., and Dick H. (2001) The geochemical consequences of late-state low-grade alteration of lower ocean crust at the SW Indian Ridge: Results from ODP Hole 735B (Leg 175). *Geochimica et Cosmochimica Acta* **65**(19), 3267-3287.

Bednarz U. and Schmincke H.-U. (1989) Mass transfer during sub-seafloor alteration of the upper Troodos Crust (Cyprus). *Contributions to Mineralogy and Petrology* **102**, 93-101.

Berger G., Claparols C., Guy C., and Daux V. (1994) Dissolution rate of basalt glass in silica rich solutions: Implications for long-term alteration. *Geochimica et Cosmochimica Acta* **58**(22), 4875-4886.

Berger G., Schott J., and Loubet M. (1987) Fundamental processes controling the first stage of alteration of a basalt glass by seawater: An experimental study between 200 and 320°C. *Earth and Planetary Science Letters* **84**, 431-445.

Berndt M., Beck W., and Seyfried J., WE. (1986) Hydrothermal alteration of basalt: effect of high temperature Ca fixiation on Sr isotope systematics. *EOS Transactions of the American Geophysical Union* **67**(16), 392.

Brady P. and Gíslason S. (1997) Seafloor weathering controls on atmospheric CO_2 and global climate. *Geochimica et Cosmochimica Acta* **61**(5), 965-973.

Clayton T. and Pearce R. (2000) Alteration Mineralogy of Cretaceous basalt from ODP Site 1001, Leg 165 (Caribbean Sea). *Clay Minerals* **35**, 719-733.

Crovisier J.-L., Honnorez J., and Eberhart J. (1987) Dissolution of basaltic glass in seawater: Mechanism and rate. *Geochimica et Cosmochimica Acta* **51**, 2977-2990.

Crovisier J.-L., Thomassin J., Juteau T., Eberhart J., Touray J., and Baillif B. (1983) Experimental basalt-seawater glass interaction at 50°C: Study of early developed phases by electron microscopy and X-ray photoelectron spectrometry. *Geochimica et Cosmochimica Acta* **47**, 377-387.

Dahlgren R., Ugolini F., and Casey W. (1999) Field weathering rates of Mt. St. Helens tephra. *Geochimica et Cosmochimica Acta* **63**(5), 587-598.

Daux V., Crovisier J.-L., Hemond C., and Petit J. (1994) Geochemical evolution of basaltic rocks subjected to weathering: Fate of major elements, rare earth elements, and thorium. *Geochimica et Cosmochimica Acta* **58**(22), 4941-4954.

Deer W., Howie R., and Zussmann J. (1993) *An introduction to the rock forming minerals*. Longman.

Dickin A. (1981) Hydrothermal leaching of rhyolite glass in the environment has implications for nuclear waste disposal. *Nature* **294**, 342-347.

Dickson A. (1993) pH puffers for seawater media based on the total hydrogen ion concentration scale. *Deep-Sea Research* **40**(1), 107-118.

Fiore S., Huertas F., Tazaki K., Huertas F., and Linares J. (1999) A low temperature experimental alteration of rhyolitic obsidian. *European Journal of Mineralogy* **11**(3), 455-469.

Frogner P., Gíslason S., and Oskarsson N. (2001) Fertilizing potential of volcanic ash in ocean surface waters. *Geology* **29**(6), 487-490.

Ghiara M., Franco E., Petti C., Stanzione D., and Valentino G. (1993) Hydrothermal, interaction between basaltic glass, deionised water and seawater. *Chemical Geology* **104**, 125-138.

Gieskes J. and Lawrence J. (1981) Alteration of volcanic matter in the deep sea sediments: Evidence from the chemical composition of interstitial waters from deep sea drilling cores. *Geochimica et Cosmochimica Acta* **45**, 1687-1703.

Gíslason S. and Eugster H. (1987a) Meteoric water-basalt interactions II: A field study in N.E. Iceland. *Geochimica et Cosmochimica Acta* **51**, 2841-2855.

Gíslason S. and Eugster H. (1987b) Meteoric water-basalt interactions I: A laboratory study. *Geochimica et Cosmochimica Acta* **51**, 2827-2840.

Gíslason S. and Oelkers E. H. (2003) Mechanisms, rates and consequences of basaltic glass dissolution: II. An experimental study of the dissolution rates of basaltic glass as a function of pH and temperature. *Geochimica et Cosmochimica Acta* **67**(20), 3817-3832.

Gíslason S., Veblen D., and Livi K. (1993) Experimental meteoric water-basalt interactions: Characterisation and interpretation of alteration products. *Geochimica et Cosmochimica Acta* **57**, 1459-1471.

Gordon S. and Brady P. (2002) In situ determination of long-term basaltic glass dissolution in the undersaturated zone. *Chemical Geology* **190**, 113-122.

Grasshoff K., Ehrhardt M., and Kremling K. (1999) *Methods of Seawater Analysis*. Wiley-VCH.

Guy C., Schott J., Destrigneville C., and Chiappini R. (1992) Low-temperature alteration of basalt by interstitial seawater, Mururoa, French Polynesia. *Geochimica et Cosmochimica Acta* **56**, 4169-4189.

Hawkins D. (1981) Kinetics of glass dissolution and zeolite formation under hydrothermal conditions. *Clays and Clay Minerals* **29**(5), 331-339.

Hensen C., Wallmann K., Schmidt M., Ranero C., and Suess E. (2004) Fluid expulsion related to mud extrusion off Costa Rica - A window to the subducting slab. *Geology* **32**(3), 201-204.

Humphris S. and Thompson G. (1978) Hydrothermal alteration of oceanic basalts by seawater. *Geochimica et Cosmochimica Acta* **42**, 107-125.

Ivanenkov V. and Lyakhin Y. (1978) Determination of total alkalinity in seawater. In *Methodes of hydrochemical investigations in the ocean* (ed. O. Bordovsky and V. Ivanenkov), pp. 110-114. Nauka Publ.

James R., Allen D., and Seyfried W. J. (2003) An experimental study of alteration of oceanic crust and terrigenous sediments at moderate temperatures (51 to 350°C): Insights as to chemical processes in near-shore ridge-flank hydrothermal systems. *Geochimica et Cosmochimica Acta* **67**(4), 681-691.

Jeschke A. and Dreybrodt W. (2002) Dissolution rates of minerals and their relation to surface morphology. *Geochimica et Cosmochimica Acta* **66**(17), 3055-3062.

Jezek P. and Noble D. (1978) Natural hydration and ion exchange of obsidian: An electron microprobe study. *American Mineralogist* **63**, 266-273.

Karkhansis S., Bancroft G., Fyfe W., and Brown J. (1980) Leaching behaviour of rhyolite glass. *Nature* **284**, 435-437.

Kawano M., Tomita K., and Kamino Y. (1993) Formation of clay minerals during low temperature experimental alteration of obsidian. *Clays and Clay Minerals* **41**(4), 431-441.

Kawano M., Tomita K., and Shinohara Y. (1997) Analytical electron microscopic study of the noncrystalline products formed at early weathering stages of volcanic glass. *Clays and Clay Minerals* **45**(3), 440-447.

Kutterolf S., Schacht U., Wehrmann H., Freundt A., and Moerz T. (in press) Onshore to offshore tephrostratigraphy and marine ash layer diagenesis in Central America. In *Central America - Geology, Resources and Hazards* (ed. J. Buntschuh), Balkema.

Lawrence J., Drever J., Anderson T., and Brueckner H. (1979) Importance of alteration of volcanic material in the sediments of Deep Sea Drilling Site 323: Chemistry, 18O/16O and 87Sr/86Sr. *Geochimica et Cosmochimica Acta* **43**, 573-588.

Menzies M. and Seyfried J., WE. (1979) Basalt-seawater interaction: Trace element and strontium isotopic variations in experimentally altered glassy basalt. *Earth and Planetary Science Letters* **44**, 463-472.

Metz V. and Ganor J. (2001) Stirring effect on kaolinite dissolution rate. *Geochimica et Cosmochimica Acta* **65**(20), 3475-3490.

Mungall J. and Martin R. (1994) Severe leaching of trachytic glass without devitrification, Terceira, Arzores. *Geochimica et Cosmochimica Acta* **58**, 75-83.

Nesbitt H. and Wilson R. (1992) Recent chemical weathering of basalts. *American Journal of Science* **292**, 740-777.

Oelkers E. (2001) General kinetic describtion of multioxide mineral and glass dissolution. *Geochimica et Cosmochimica Acta* **65**(21), 3703-3719.

Oelkers E. and Gíslason S. (2001) The mechanism, rates and consequences of basaltic glass dissolution: I. An experimental study of the dissolution rates of basaltic glass as a function of aqueous Al, Si and oxalic acid concentration at 25°C and pH = 3 and 11. *Geochimica et Cosmochimica Acta* **65**(21), 3671-3681.

Patino L., Velbel M., Price J., and Wade J. (2003) Trace element mobility during spheroidal weathering of basalts and andesites in Hawaii and Guatemala. *Chemical Geology* **202**, 343-364.

Perret D., Crovisier J.-L., Stille P., Shields G., Mäder U., Advocat T., Schenk K., and Chardonnens M. (2003) Thermodynamic stability of waste glasses compared to leaching behaviour. *Applied Geochemistry* **18**(8), 1165-1184.

Petit J., Della Mea G., Dran J.-C., Magonthier M., Mando P., and Paccagnella A. (1990) Hydrated layer formation during dissolution of complex silicate glasses and minerals. *Geochimica et Cosmochimica Acta* **54**, 194-1955.

Philpotts J., Schnetzler C., and Hart S. (1969) Submarine basalts: Some K, Rb, Sr, Ba, REE, H_2O, and CO_2 data bearing on their alteration, modification by Plagioclase, and possible soure materials. *Earth and Planetary Science Letters* **7**, 293-299.

Pichler T., Ridley W., and Nelson E. (1999) Low-temperature alteration of dredged volcanics form the Southern Chile Ridge: Additional information about early stages of seafloor weathering. *Marine Geology* **159**, 155-177.

Pytkowicz R. and Fowler G. (1967) Solubility of foraminifera in seawater at high pressures. *Geochemical Journal* **1**(4), 169-182.

Schmincke H.-U. (1988) Pyroklastische Gesteine. In *Sedimente und Sedimentgesteine* (ed. H. Füchtbauer), pp. 731-778. E. Schweizbart'sche Verlagsbuchhandlung, Stuttgart.

Seyfried J., WE and Bischoff J. (1979) Low temperature basalt alteration by seawater: An experimental study at 70°C and 150°C. *Geochimica et Cosmochimica Acta* **43**, 1937-1947.

Seyfried W.E. and Mottl M. (1982) Hydrothermal alteration of basalt by seawater under seawater-dominated conditions. *Geochimica et Cosmochimica Acta* **46**, 985-1002.

Staudigel H. and Hart S. (1983) Alteration of basaltic glass: Mechanisms and significance for oceanic crust-seawater budget. *Geochimica et Cosmochimica Acta* **47**, 337-350.

Staudigel H., Plank T., White B., and Schmincke H.-U. (1996) Geochemical fluxes during seafloor alteration of the basaltic upper oceanic crust: DSDP Sites 417 and 418. In *Subduction: Top to Bottom* (ed. G. E. Bebout and et al.), pp. 19-38. American Geophysikal Union.

Stroncik-Treue N. (2000) Low-temperature alteration of mafic volcanic glasses - chemical evolution, mass-balancing, and kinetics. PhD, University of Kiel.

Stuiver M. and Polach H. (1977) Discussion: Reporting of ^{14}C Data. *Radiocarbon* **19**(3), 355-363.

Techer I., Advocat T., Lancelot J., and Liotard J.-M. (2001) Dissolution kinetics of basaltic glasses: Control by solution chemistry and protective effect of the alteration film. *Chemical Geology* **176**, 235-263.

Tsong T., Houser C., Yusef N., Messier R., White W., and Michels J. (1978) Obsidian hydration profiles measured by sputter-induced optical emission. *Science* **201**, 339-340.

Utzmann A., van Cappellen P., Schmincke H.-U., and Garbe-Schönberg D. (2000) Experimental determination of low-temperature dissolution kinetics of silicate glasses. *Journal of Conference Abstracts* **5**(2), 1028.

White A. (1983) Surface chemistry and dissolution kinetics of glassy rocks at 25°C. *Geochimica et Cosmochimica Acta* **47**, 805-815.

White A. and Claassen H. (1980) Kinetic model for the short term dissolution of a rhyolitic glass. *Chemical Geology* **28**, 91-109.

Willey J. (1974) The effect of pressure on the solubility of amorphous silica in seawater at 0°C. *Marine Chemistry* **2**, 239-250.

Wolff-Boenisch D., Gíslason S., Oelkers E. H., and Putnis V. (2004) The dissolution rate of natural glasses as a function of their composition at pH 4 and 10.6, and temperatures from 25 and 74°C. *Geochimica et Cosmochimica Acta* **68**(23), 4843-4858.

Yang W.-H. and Kirkpatrick R. (1990) Hydrothermal reaction of a rhyolitic-composition glass: A solid-state NMR study. *American Mineralogist* **75**, 1009-1019.

Ylagan R., Altaner S., and Pozzuoli A. (1996) Hydrothermal alteration of rhyolitic hyaloclastite from Ponza Island, Italy. *Journal of Volcanology and Geothermal Research* **74**, 215-231.

Yokoyama T. and Banfield J. (2002) Direct determination of the rates of rhyolite dissolution and clay formation over 52,000 years and comparison with laboratory measurements. *Geochimica et Cosmochimica Acta* **66**(15), 2665-2681.

Chapter III

Volcanogenic Sediment-Seawater Interactions and the Geochemistry of Pore Waters

Ulrike Schacht[1,2], Klaus Wallmann[2,1], Steffen Kutterolf[1,2], and Mark Schmidt[3,1]

[1] Special Research Project 574, University of Kiel, Wischhofstr. 1-3, 24148 Kiel, Germany

[2] IFM-GEOMAR, Leibniz Institute of Marine Sciences, Wischhofstr. 1-3, 24148 Kiel, Germany

[3] Institute of Geosciences, University of Kiel, Ludewig-Meyn-Str. 10, 24118 Kiel, Germany

Abstract

Four volcanic ash bearing marine gravity cores and one ash-free sediment core were examined during research cruise RV *Meteor* 54/2 offshore Nicaragua and Costa Rica to investigate the chemical composition of pore waters related to volcanic ash alteration.

Sediments were composed of terrigenous matter derived from the adjacent continent and contained several distinct ash layers. Biogenic opal and carbonate were only minor components. The terrigenous fraction was mainly composed of smectite and other clay minerals while the pore water composition was strongly affected by the anaerobic degradation of particulate organic matter via microbial sulphate reduction. The alteration of volcanic matter showed only a minor effect on major element concentrations in pore waters. This is in contrast to prior studies taken on long sediment cores during the DSDP, were deep sediments always showed distinct signs of volcanic ash alteration. The missing signal of ash alteration is probably caused by low reaction rates and the high background concentration of major dissolved ions in the seawater-derived pore fluids. Only, the dissolved potassium concentration was significantly depleted in ash-bearing layers compared to the adjacent ash-free sediment horizons. The marked contrast reflects, however, a sampling artefact. Sediments were significantly heated during core retrieval so that ion exchange equilibria between the clay-rich sediments and the pore fluids were shifted. In response to this effect, dissolved potassium concentrations increase by about 10 % in the clay-rich layers while the concentrations in the ash layers were less affected.

Dissolved silica concentrations were significantly enriched in ash-bearing cores and showed no relation to the low but variable contents of biogenic opal. Hence, the data suggest that silica concentrations were enhanced by ash dissolution. A numerical transport-reaction model was developed to derive the rate of ash dissolution from the data. The following rate law was applied in the modelling:

$$R_G = k_{GS} \cdot G \cdot \left(1 - \frac{Si}{Si_{Max}}\right)$$

where R_G is the rate of glass dissolution, G is the glass concentration in the core, Si_{Max} is a saturation concentration of dissolved silica (450 µmol L^{-1}) and Si is the concentration of dissolved silica in the investigated pore fluids. The kinetic constant k_{GS} was determined as 3 x 10^{-5} yr^{-1} by fitting the model to the data. The in-situ rate of ash dissolution at the seafloor was at least two orders of magnitude smaller than the rate of ash dissolution determined in previous laboratory experiments.

3.1. Introduction

The Middle American subduction zone is among the most dynamic tectonic environments on Earth. In this region highly explosive volcanic eruptions generate buoyant eruption columns penetrating up to 40 km into the atmosphere where they spread laterally (Kutterolf et al., in press). Eruption clouds drift with the wind and gradually drop their ash over areas larger than several 10^5 km^2 (Kutterolf et al., in press). Due to the intense explosive volcanism, volcanic matter is one of the major components in marine sediments of the Central American fore-arc. Volcanogenic components of sediments include both, primary and/or secondary materials that result from volcanic activity (Vallier and Jefferson, 1981).

Studies of pore water composition have revealed that the alteration of volcanic material, dispersed in marine sediments, plays a key role in the submarine cycling and fixation of major elements (Gieskes et al., 1990; Pichler et al., 1999; Spivack and Staudigel, 1994). Hence, changes in dissolved calcium, magnesium, and potassium are primarily due to the alteration of volcanic matter (Gieskes, 1981; Gieskes and Lawrence, 1981; Lawrence et al., 1979) and ash alteration can produce dramatic changes not only in the solution but also in the solid phase (Berger et al., 1987; Crovisier et al., 1983; Guy et al., 1992; Staudigel and Hart, 1983).

The major goal of this work is to study the influence of alteration reactions on the chemical composition of pore waters extracted from volcanogenic surface sediments. During research cruise RV *Meteor* 54/2 a program of sampling and analysis of pore waters from retrieved sediment cores was carried out. Alkalinity, sulphate, calcium, magnesium, potassium and silica concentration-depth profiles of deep-sea sediment cores were measured to define the ash alteration reactions that occur in surface sediments. In this study we present the results of these investigations and apply a transport-reaction model to constrain the rate of ash dissolution at the seafloor.

3.2. Geological setting

Along the Pacific Margin of Nicaragua and Costa Rica the Cocos Plate subducts beneath the Caribbean Plate at the Middle America Trench at a fast subduction rate of up to 90 mm a^{-1} (Kimura et al., 1997). The dip of the subducting slap underneath the arc volcanoes changes along the arc, with the steepest dip beneath Nicaragua and the

shallowest dip beneath Costa Rica (Patino et al., 2000). Offshore the Nicoya Peninsula a triple junction trace divides the subducting Cocos Plate into crust formed at the East Pacific Rise to the north and crust formed at the Cocos-Nazca Spreading Center to the south (Barckhausen et al., 2001) resulting in a smooth northern and a rough southern oceanic plate domain (Fig. 3.1). Important features of the southern domain are the colliding Cocos Ridge and a seamount dominated normal crust segment adjacent to the ridge (von Huene et al., 2000). The incoming sedimentary succession is ~400 m thick and is dominated by pelagic sediments, volcanic ashes, graded sand and silt layers as well as calcareous and diatomaceous oozes (Kimura et al., 1997).

Straub and Schmincke (1998) evaluated the overall tephra input into the Pacific Ocean sediments by arc volcanism going back to Mid-Miocene. They estimated that approximately 10-13 km^3 of volcanoclastic sediments are produced per km arc length and per million year. An extrapolation over the life-time of major Pacific arcs and hotspot chains, combined with a volume estimate of the distal tephra component, indicates a minimum of 9.3 x 10^6 km^3 of tephra, corresponding to 23 vol.% of existing Pacific oceanic sediments.

3.3. Methods

3.3.1. Sediment and Pore Water Sampling

During research cruise RV *Meteor* 54/2 several sediment cores of 1 to 12 m lengths were taken by gravity coring on the continental slope of Nicaragua and Costa Rica and on the incoming oceanic plate off Nicaragua (Fig. 3.1, Tab. 3.1). The gravity corer was equipped with a 2-t-weight attached to the top of a 6 to 12m long steel tube enclosing an inner PVC tube. As soon as the cores arrived on deck they were cut into approx. 1 m long segments and were stored immediately in a container cooled to 8°C.

For the investigation of chemical and physical properties, sediment and pore water was sampled in 10-50 cm intervals. Porosity sup-samples were filled into pre-weighted plastic vials. The pore water was retrieved by pressure filtration through 0.2 µm cellulose acetate membrane filters. The pore water squeezer was operated with argon at a pressure gradually increasing up to 5 bar.

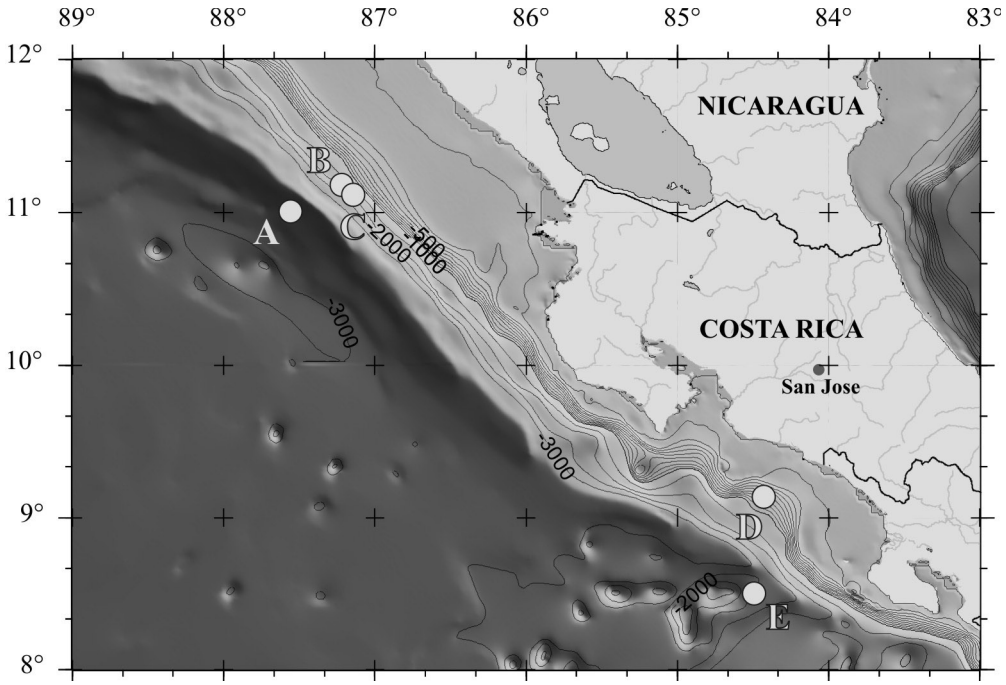

Figure 3.1: Map of the Central American Convergent Margin showing locations (grey circles) of the discussed sediment cores.

Table 3.1: Compilation of all station numbers, geographic positions (NIC=Nicaragua; CR=Costa Rica), and water depths of all gravity cores discussed in this study.

	Core Station	Position				Remarks
		Latitude (N)	Longitude (W)	Geological Setting	Country	
A	54-11.2	11°06.03	87°49.82	Incom. Plate	NIC	Ash Core
B	54-2	11°20.11	87°18.35	Slope	NIC	Ash Core
C	54-13	11°20.12	87°18.30	Slope	NIC	Ash Core
D	54-81.1	09°09.20	84°41.97	Slope	CR	Ref. Core
E	54-57	08°49.70	84°51.21	Slope	CR	Ash Core

3.3.2. Pore Water Analyses

Water samples were analysed for total alkalinity by titration of 0.5-1 mL water with hydrochloric acid (~ 0.02 *N* HCl) according to Ivanenkov and Lyakhin (1978). To remove carbon dioxide during titration the sample was flushed with a continuous stream of pure nitrogen. The equivalence point of the titration was determined colourimetrically, using a mixture of methylene blue and methyl red as an indicator. The titration is complete when the green colour of the solution changes to light pink (*p*H = 5.5). Silica concentrations were measured using the Molybdate Blue method (Grasshoff et al., 1999). The remaining pore waters were later analysed in the IFM-GEOMAR laboratory for dissolved anions

(SO_4^{2-}) and dissolved metals (K, Mg, Ca) using ion chromatography and optical ICP. Accuracies of analytical data are generally better than 2 %. Subsamples for metal analyses were immediately acidified with 10 *N* HNO_3 (supra-pure) to prevent carbonate precipitation and were stored in acid-cleaned plastic vials. Detailed descriptions of the methods are available on: *www.ifm-geomar.de/index.php?id=mg_analytik*.

3.3.3. On-Board Sediment Investigations

The sediment inventory (minerals, glass shards, lithics, biogene material) was preliminary determined using smear slides. Smear slides were prepared by dispersing sediment material on microscope slides and fixing the sample with resin (Meltmount). These "thin sections" were then examined under a petrographic microscope.

3.3.4. Sediment Analyses

At the home laboratory all sediment samples were dry freezed. Samples for analysis of biogenic silica (opal) were ground in an agate mortar. Biogenic opal was determined with a sequential leaching technique (DeMaster, 1981), modified by Müller and Schneider (1993). For total carbon, nitrogen and sulphur analyses the freeze dried samples were grinded in an agate motar (C/N) or in a mill (S). Depending of the C/N/S concentration, 3-20 mg of sample was weighed into a tin cup (C/N/S) or silver cup for the POC measurements. For sulphur determination the same amount of Vanadiumpentoxid is added to the sample. Organic carbon is determined after removing carbonate carbon by acidification with 0.01 *N* hydrochloric acid (Verardo et al., 1990). The analyses were performed using an Carlo Erba Elemental Analyser.

In addition to chemical sediment parameters we analysed the clay phases of the recovered marine sediments. First the samples were divided into a fine (< 63 µm) and a coarse fraction (> 63 µm) by wet sieving. Grain size separation into a silt (2-63 µm) and a clay fraction (< 2 µm) was performed by settling of particles in standing cylinders according to Stokes' Law (Moore and Reynolds, 1989).

Clay mineralogy was determined by X-ray diffractometry using a Philips X-ray diffractometer PW 1710 with monochromatic Co-Kα radiation. Oriented samples were produced by vacuum filtration through a 0.2 µm filter. A range of 2–45° 2Θ and an increment of 0.02° 2Θ were chosen, to obtain the biggest possible amount of reflexes.

This procedure is necessary because mineral assemblages often show coincidences. Measurements were carried out on air-dried and glycol-saturated samples.

3.3.5. Age Determination of Volcanic Ashes

For age determination volcanic ash samples were chemically correlated with deposits on land (Kutterolf et al., in press). The charcoal contents of these on land deposits were analysed at the Leibniz Laboratory for Radiometric Dating and Isotope Research at the University of Kiel. The selected samples were mechanically cleaned under the microscope, afterwards sieved, and dark organic-looking material < 250 µm was selected for further treatment. The residual material was then extracted with 1 % HCl and 1 % NaOH at 60°C and again with 1 % HCl. The alkali extraction of the organic fraction (humic acid fraction) was precipitated with HCl, washed, and dried. The combustion to CO_2 of all fractions was performed in a closed quartz tube together with CuO and silver wool at 900°C. The ^{14}C concentration of the samples was measured by comparing the simultaneously collected ^{14}C, ^{13}C, and ^{12}C beams of each sample with those of Oxalic Acid standard CO_2 and coal background material. The ^{14}C ages were calculated according to (Stuiver and Polach, 1977) with a $\delta^{13}C$ correction for isotopic fractionation based on the $^{13}C/^{12}C$ ratio measured by the AMS-system simultaneously with the $^{14}C/^{12}C$ ratio.

3.3.6. Experimental Method

In addition to pore water extraction and analyses, two long-term experiments were conducted to determine whether volcanic ashes in contact with seawater could achieve dissolved silica concentrations equivalent to or greater than their pore water dissolved silica concentrations. Mafic and felsic volcanic glasses, collected along the volcanic front of Nicaragua were used in these experiments. All experiments were conducted at room temperature (25°C) and pressure (1 bar) for a maximum duration of 80 weeks. Detailed information on experimental set-up, starting seawater composition as well as sample preparation and handling are given in (Schacht et al., submitted).

3.4. Results

3.4.1. Lithology and Geochemical Composition of Sediments

3.4.1.1. Background Sediments – The background sedimentation of ash cores as well as the ash free sediment core D is generally built up through alternating beds of finer (medium silt to silty clay) and coarser (sandy clay to clayey sand) layers (Fig. 3.2). Generally, beyond the clay minerals and lithic content, plagioclase is the most abundant component in the background sedimentation. Additionally, heavy minerals like pyroxene (ortho- and clino), magmatic spinel, olivine, hornblende, and in some cases biotite and magmatic quartz, demonstrate the strong volcanic entry into the marine sediments, whereas the latter three and partly the orthopyroxenes are indicators for more evolved felsic volcanism. Sediments also contain various amounts of pyrite, a very widespread sedimentary mineral, which probably was formed during sediment diagenesis. Biogenic compounds of pelagic origin (organic carbon, carbonate, biogenic opal) contributed only to small amounts (Tab. 3.2 and Appendix).

Table 3.2: Chemical composition of ash-free sediments. All numbers represent average values and are given in wt%.

Core	C_{org}	$CaCO_3$	N	S	Biogenic Opal
A	2.58	1.09	0.26	0.95	7.42
B	3.68	11.1	0.38	1.44	3.53
C	3.51	6.71	0.33	1.78	2.81
D	1.70	7.43	0.17	1.15	2.39
E	1.42	0.95	0.16	0.35	5.06

In general, the sedimentation should be very homogenous and only be disturbed by the varying volcanic input leading to ash layers in the extreme case. Sedimentation rates for all cores described in this paper are between 80 m Myr^{-1} on the incoming plate and 300 m Myr^{-1} at the continental slope (Kutterolf et al., in press). However, the high input of material from the arc leads to increased sedimentation rates, which can cause slumping and slides in the more inclined regions of the deposition area.

3.4.1.2. Volcanic Ash Layers – Volcanic ash, found as up to 20 cm thick ash layers, and dispersed ashes (detectable by microscope) are present throughout the sediment column of ash cores A, B, C, and E. Compared with volcanic ash-free sediment, ash layers show

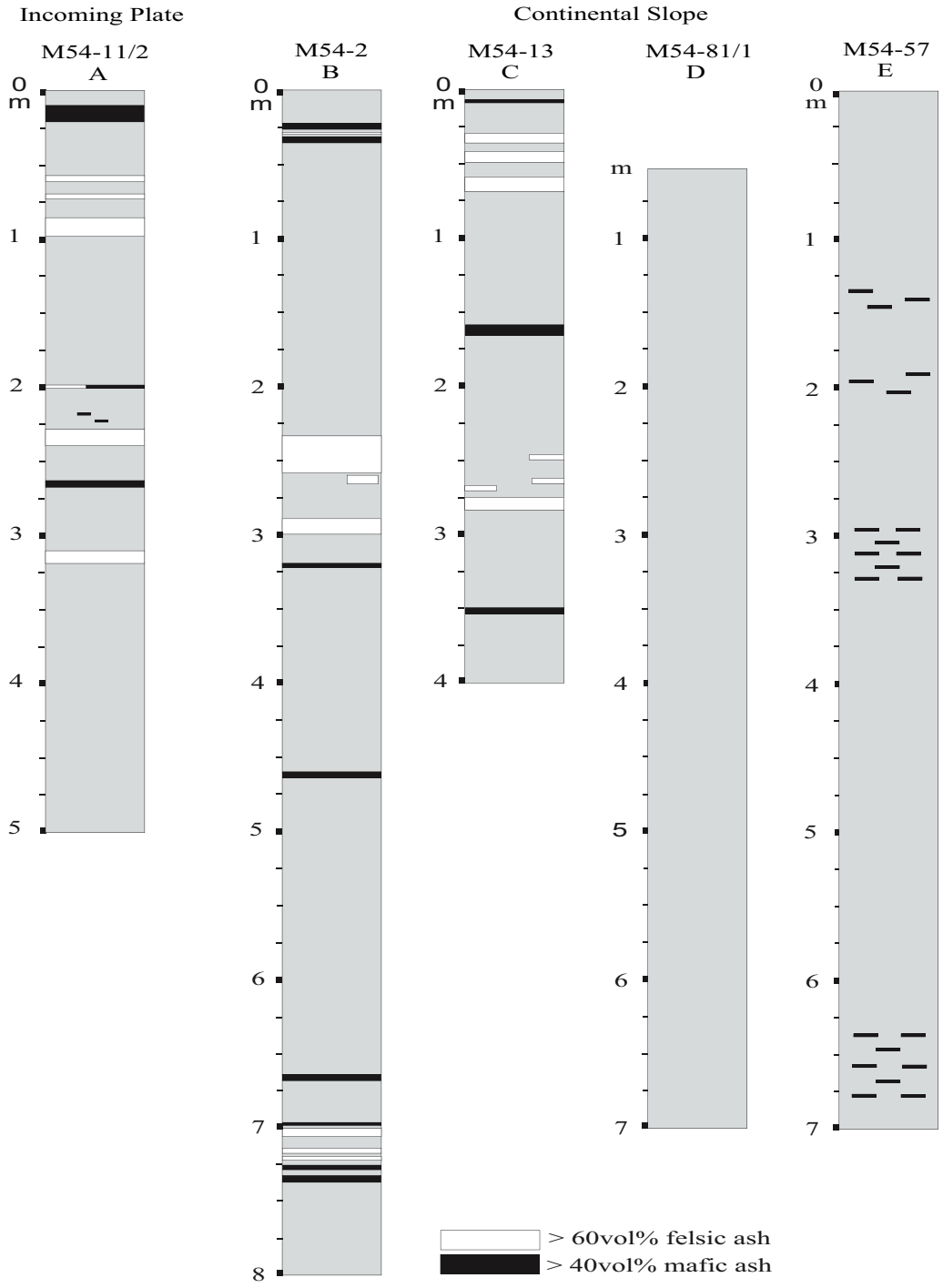

Figure 3.2: Lithologies of described sediment cores, descriptions at full length are given in the text.

marked differences in porosity, water content, and grain size (Appendix). A sharp lower boundary is typical for most of the ash layers and the uppermost part is mostly mixed with background sediment showing a diffuse, relatively large transition zone (up to 50 cm) to the superposed pelagic sediment. Additionally, some ash layers are disturbed through bioturbation at the top and the base of the layer.

Most of the ash layers are white to greyish-pink or dark-grey to pink light-grey in colour. Mostly, dark grey layers are of basaltic to andesitic, and pinkish-white layers are of dacitic to rhyolitic composition. Microscopic examination of light-coloured ashes shows mostly clear, colourless, *fresh* volcanic glass shards and pumice fragments commonly with elongated vesicles. Dark-grey ash layers consist predominantly of a mixture of brown glass shards, black, vitreous particles showing distinct signs of alteration (Fig. 3.3), as well as opaque and numerous light and heavy minerals. The typical grain size of the ash-layers varies in the range of medium silt to medium sand (< 250 µm). Mineral assemblages comprise plagioclase, clinopyroxene, plus olivine in the mafic, hornblende, orthopyroxene in more evolved, as well as occasionally biotite and magmatic quartz in the most-evolved felsic layers. The volcanic material shows glass shards in various stages of alteration. At the scale of optical microscope we could distinguish felsic ash as mostly *fresh* volcanic glass shards while mafic ash layers consisted predominantly of glass, showing distinct signs of alteration and secondary mineralisation.

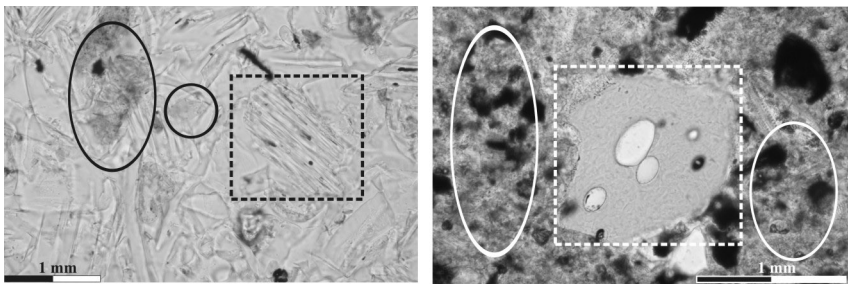

Figure 3.3: Microscopic images of a felsic (left) and a mafic (right) ash layer. Squares mark a pumice fragment and a glass shard, while circles mark alteration products.

3.4.1.3. XRD-Spectra of Clay Separates – We analysed samples from cores C and D to characterise a possible spatial variability of sediment composition offshore Nicaragua as well as Costa Rica. The clay mineral assemblages obtained by XRD are reported in Figure 3.4. The sample of core C is dominated by smectite (probably montmorillonite). Quartz and plagioclase as well as minor amounts of chlorite are also present. Smectite can be characterised very well because the reflection at 12.6 Å shifts to 17.6 Å after glycolation, while all other identified mineral phases stay unaffected by glycol saturation. The clay mineralogy of the sample taken from core D again includes smectite (probably

montmorillonite) as major component together with quartz and plagioclase. Traces of chlorite are also restricted to this sample. However, our investigations go along very well with those made by Spinelli and Underwood (2004) pointing out smectite to be the most dominant clay mineral in surface sediments from the Middle American Pacific Margin.

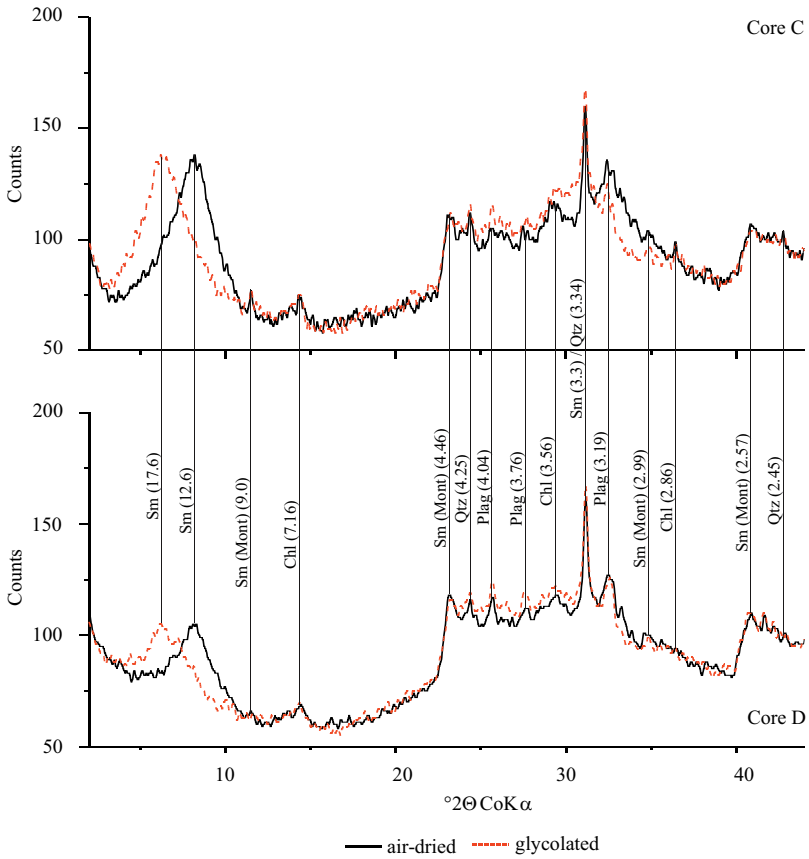

Figure 3.4: XRD patters of < 2 µm-size sediment fraction taken from cores C and D. Numbers in brackets indicate d-spacings. Both samples are mainly composed of smectite, together with minor amounts of quartz and plagioclase as well as traces of chlorite.

3.4.2. Pore Water Composition

The composition of pore fluids measured in the retrieved sediment cores is shown in Figures 3.5a-f. The alkalinity-depth profiles show a regular increase with sediment depth (Fig. 3.5a). The strong alkalinity increase with depth found in cores B, C, D and E is typically for slope sediments obtained in areas of rapid accumulation of organic carbon rich sediments (e.g. Zuleger, 1996). The alkalinity increase is much smaller in core A taken on the incoming oceanic plate. The lower alkalinity values in this core reflect the reduced accumulation of organic carbon which is mainly caused by low rates of terrigenous sedimentation on the oceanic plate (e.g. Zuleger 1996). Dissolved sulphate

concentrations decrease with sediment depth due to microbial sulphate reduction (Fig. 3.5b). The distribution of sulphate mirrors the alkalinity trends.

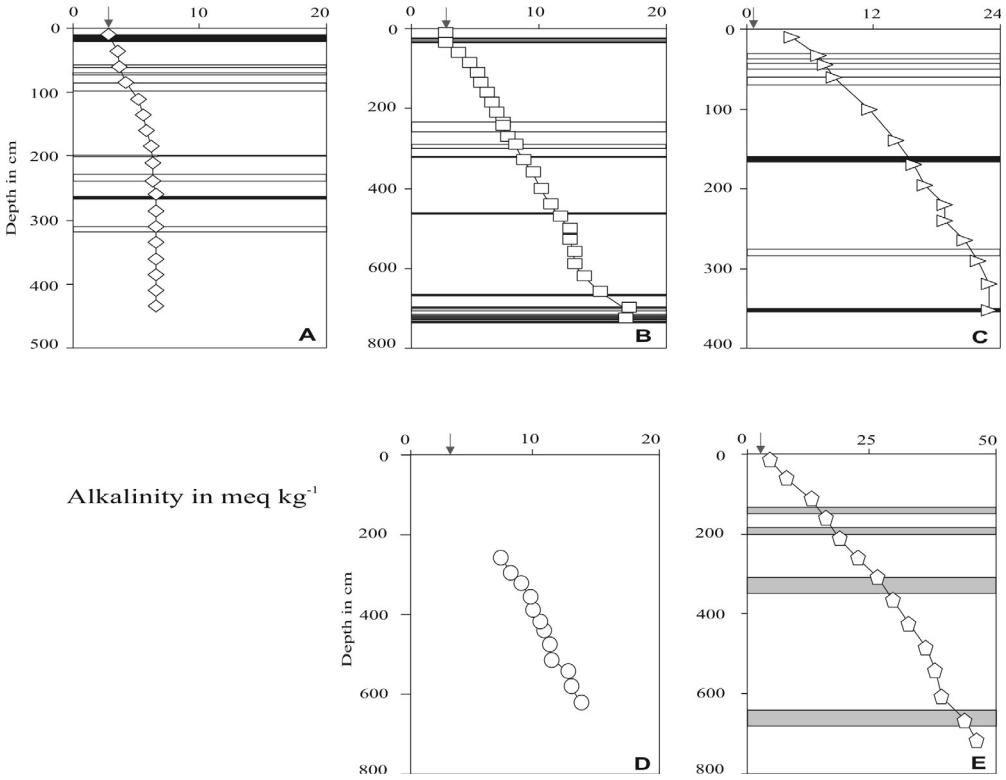

Figure 3.5a: Alkalinity - Pore water concentration-depth profiles for sediment cores A, B, C, D and E. White bars indicate felsic, black bars indicate mafic ash layers, and grey bars indicate high amounts of ash lenses. Arrows define the overlying seawater composition.

Dissolved calcium and magnesium concentrations decrease with sediment depth (Figs. 3.5c & d). As shown in many previous studies (e.g. Manheim, 1976; Presley and Trefry, 1980; Sayles et al., 1973), the bacterial reduction of SO_4 and consequent generation of HCO_3 has evidently led to the precipitation of $CaCO_3$ and Mg-bearing carbonate phases. This reaction may be coupled with the reaction of sulphide (formed from sulphate) with Fe in clays causing the substitution of Mg for Fe in the clay lattice (Drever, 1971).

Dissolved potassium concentrations are significantly enriched relative to the overlying seawater in many cores implying that potassium was released from sediments into the pore solution (Fig. 3.5e). In contrast to the other major cations, dissolved potassium concentrations are characterised by sharp concentration minima which are usually found in the ash-bearing sediment layers. This observation might indicate that potassium is removed from pore waters by ash alteration processes. However, it is also possible that the measured potassium concentrations are affected by sampling artefacts (Mangelsdorf and Wilson, 1969).

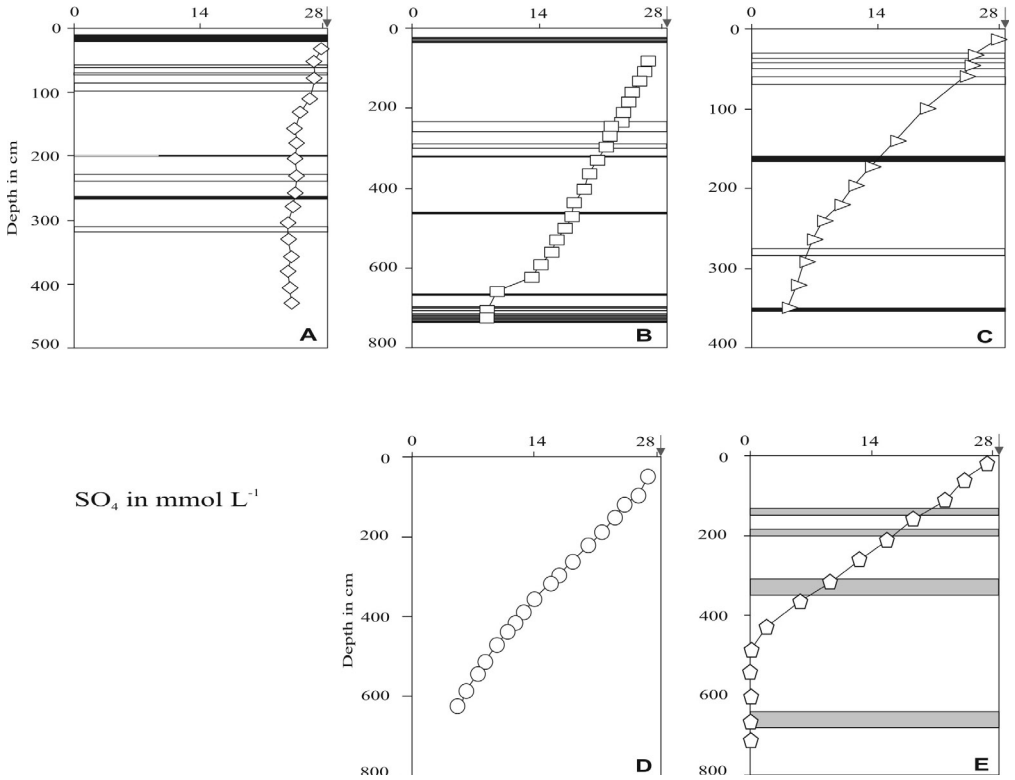

Figure 3.5b: SO_4 - Pore water concentration-depth profiles for sediment cores A, B, C, D and E. White bars indicate felsic, black bars indicate mafic ash layers, and grey bars indicate high amounts of ash lenses. Arrows define the overlying seawater composition.

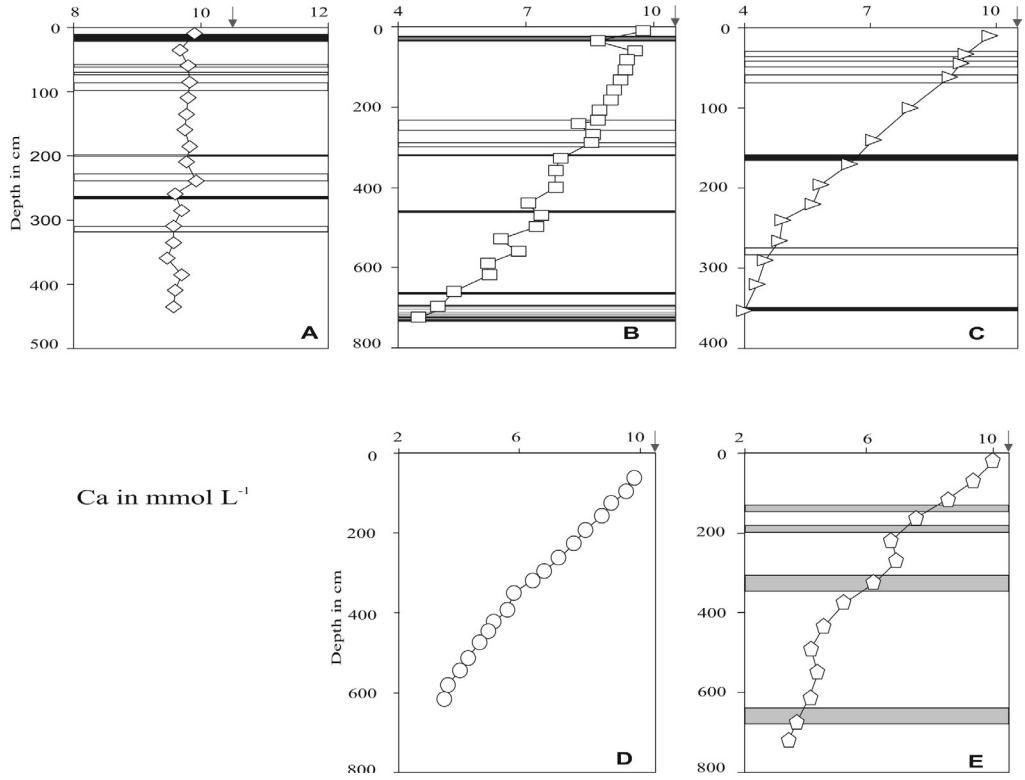

Figure 3.5c: Ca - Pore water concentration-depth profiles for sediment cores A, B, C, D and E. White bars indicate felsic, black bars indicate mafic ash layers, and grey bars indicate high amounts of ash lenses. Arrows define the overlying seawater composition.

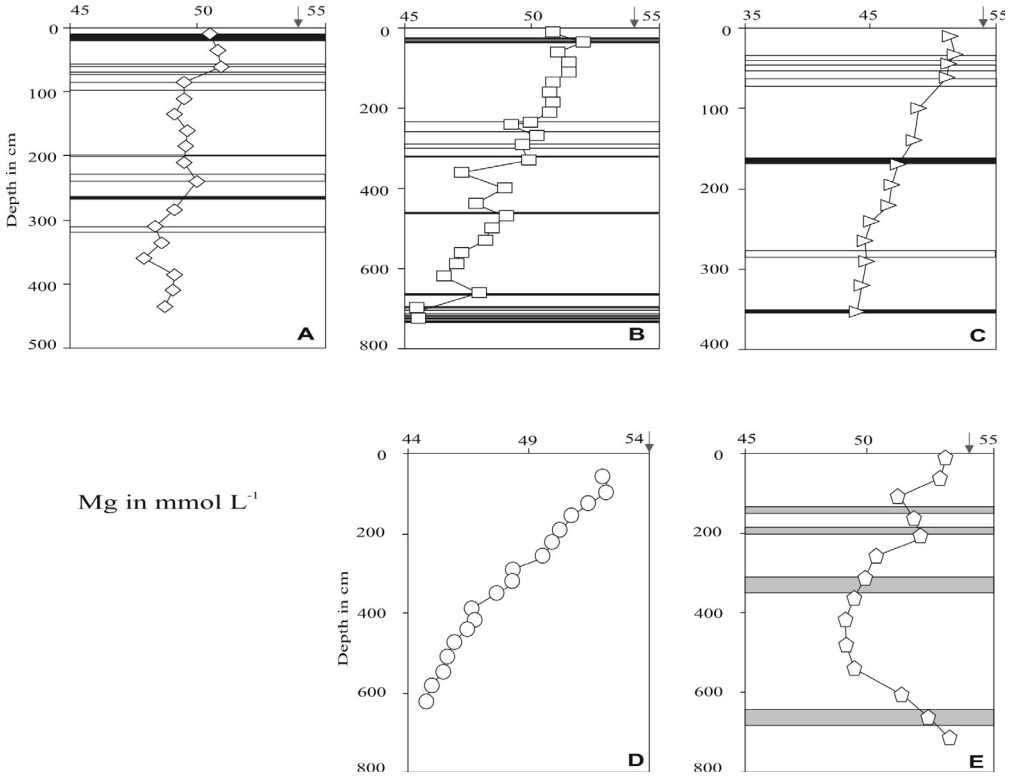

Figure 3.5d: Mg - Pore water concentration-depth profiles for sediment cores A, B, C, D and E. White bars indicate felsic, black bars indicate mafic ash layers, and grey bars indicate high amounts of ash lenses. Arrows define the overlying seawater composition.

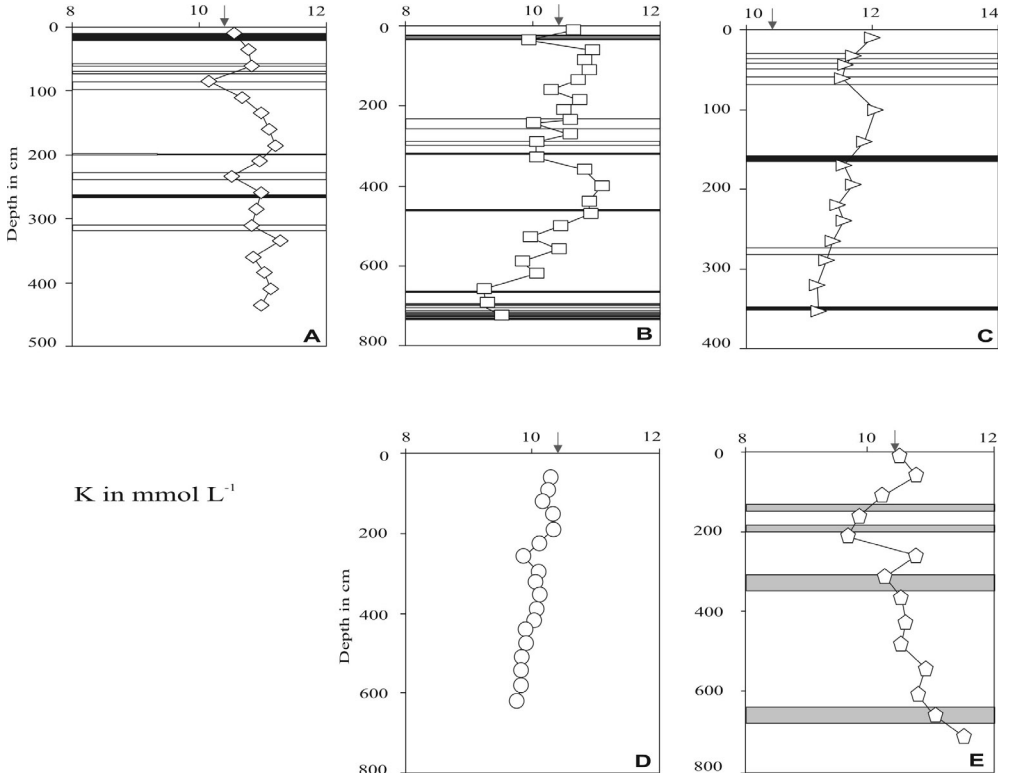

Figure 3.5e: K - Pore water concentration-depth profiles for sediment cores A, B, C, D and E. White bars indicate felsic, black bars indicate mafic ash layers, and grey bars indicate high amounts of ash lenses. Arrows define the overlying seawater composition.

3.4.3. Dissolved Silica, Biogenic Opal, and Volcanic Ashes: Field Data and Experimental Results

The concentration versus depth profiles of dissolved silica in pore waters of the four ash-bearing cores A, B, C, E (Fig. 3.5f) are remarkably similar to each other considering the differences in sedimentary biogenic opal contents given in Figure 3.6. Dissolved silica concentrations varied from approximately 300 µmol L^{-1} near the sediment surface to about 500 µmol L^{-1} at depth but always stayed far below their solubility-controlled concentration of 1000 µmol L^{-1} (Hurd, 1973). Even so biogenic opal contents are different within all four ash-bearing cores, they are still low compared to other marine sediments. It should also be noted that the standard extraction method applied in our study is not very selective, especially when biogenic opal occurs as a minor component in dominantly terrigenous sediments (Schlüter and Rickert, 1998). Some of the silica extracted from the sediments may in fact originate from other silicate phases and the biogenic opal data reported in our study should hence be regarded as maximum estimates. The consistently high dissolved silica concentrations in ash-bearing cores therefore suggest on-going dissolution of volcanic glass, which generally has a higher solubility than other silicates or aluminosilicate minerals.

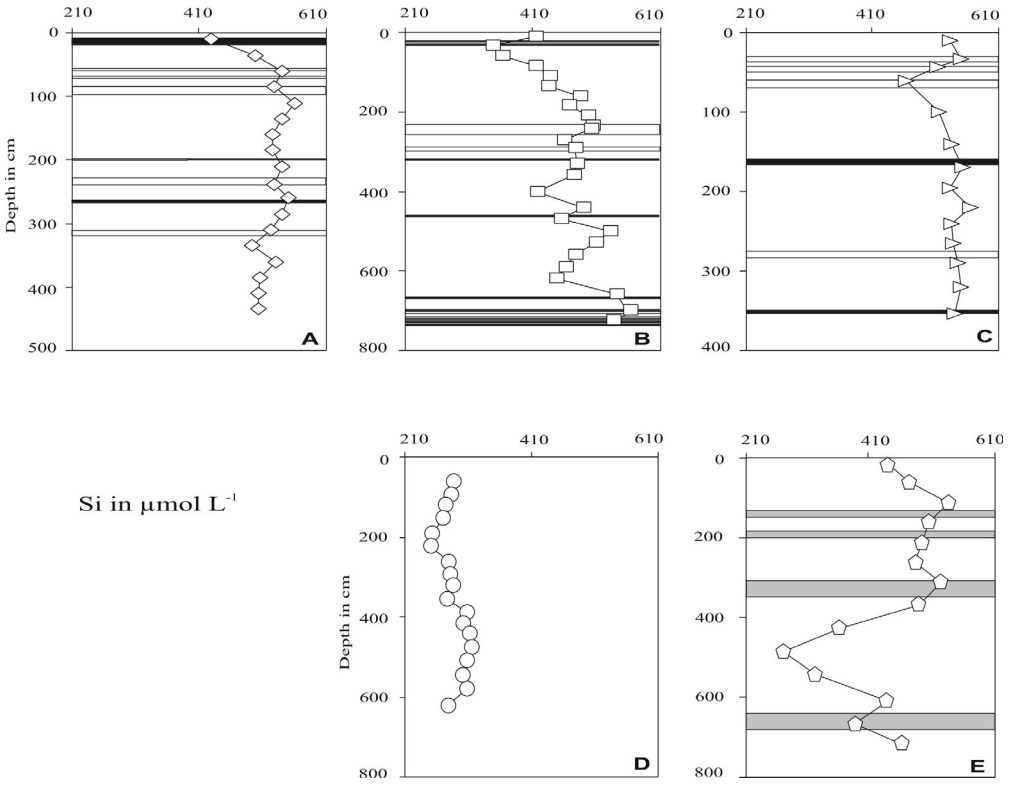

Figure 3.5f: Si - Pore water concentration-depth profiles for sediment cores A, B, C, D and E. White bars indicate felsic, black bars indicate mafic ash layers, and grey bars indicate high amounts of ash lenses.

The silica pore water concentration of sediment core D is rather low, starting around concentrations of 280 µmol L^{-1} for pore waters at the very top of the sediment core, and being relatively stable with only a minor decrease with depth, reaching maximum values of 310 µmol L^{-1} (Fig. 3.5f). The biogenic opal content of core D is within the same range as described above for the ash-bearing cores (Fig. 3.6). This observation confirms that the elevated silica pore water concentrations of up to 600 µmol L^{-1} in ash-bearing cores are probably caused by the alteration of volcanic ashes rather than by biogenic opal dissolution.

During our experiments on the dissolution kinetics of volcanic glasses, the dissolved silica concentrations increased to 980 µmol L^{-1} for mafic and 3800 µmol L^{-1} for felsic runs after 80 and 45 weeks of alteration (Fig. 3.7). The concentrations reached during these experiments were well above the pore water concentration, on one hand indicating especially felsic volcanic ashes to be very reactive phases but on the other hand suggesting that the dissolved silica concentration in our experiments are higher than sediments actually could achieve.

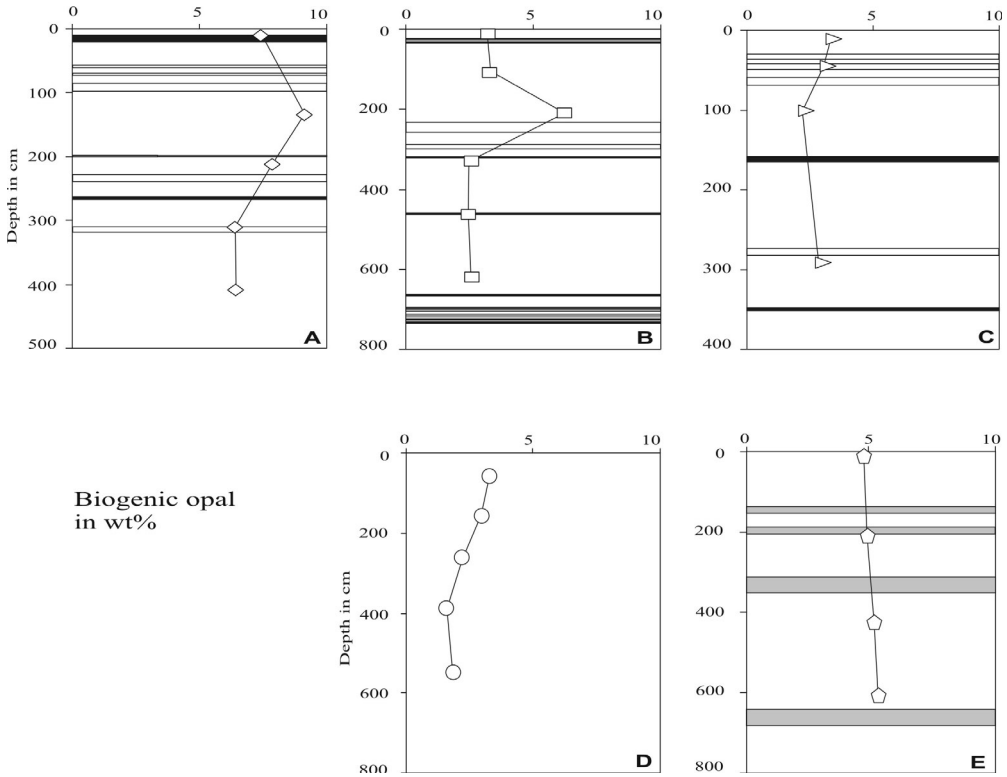

Figure 3.6: Biogenic silica distribution for sediment cores A, B, C, D and E. White bars indicate felsic, black bars indicate mafic ash layers and grey bars indicate high amounts of ash lenses.

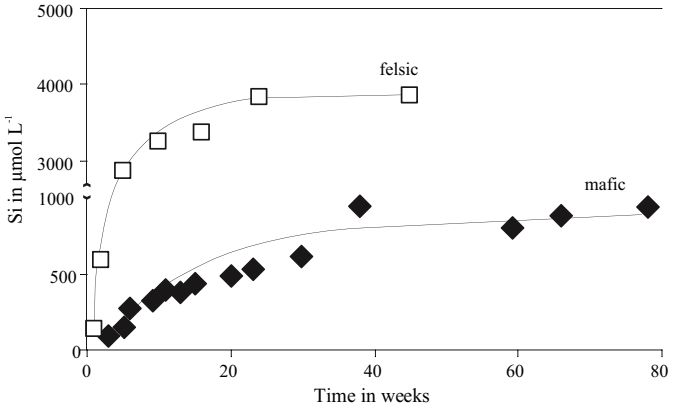

Figure 3.7: Dissolved silica concentration changes during long-term experiments conducted with felsic and mafic material, for a maximum duration of 80 hours at 20°C and 1 bar.

3.5. Discussion

Overall the general pattern in pore waters for all investigated sediment cores is that the depositional rates of particulate organic carbon and the mineralisation intensity decrease from the upper continental slope into the deep sea. More organic matter is deposited and accumulated on the slope where high sedimentation rates favour the accumulation and burial of organic carbon below the bioturbated surface layer. Buried organic matter is further degraded via microbial sulphate reduction as clearly illustrated by the strong SO_4 decreases and alkalinity increases for slope sites B, C, D and E (Fig. 3.5b).

The concentration profiles of major cations showed no clear effects of ash alteration. In contrast, previous studies on long sediment cores taken within the Deep-Sea Drilling Project (DSDP), clearly showed that pore fluids in deep sediments (> 100 m sediment depth) are affected by volcanic ash alteration. The pore waters from these deep-reaching cores are often enriched in dissolved Ca and depleted in Mg and K relative to bottom seawater (Gieskes and Lawrence, 1981; Mottl, 1989). These directions of element transfer between ash/glass and seawater are similar to those observed in laboratory experiments at moderate to elevated temperatures (e.g. Berger et al., 1987; Schacht et al., submitted; Seyfried and Bischoff, 1979; Staudigel and Hart, 1983) and were thus ascribed to ash alteration.

In contrast, the concentration-depth profiles of calcium and magnesium in our sediment cores are mainly controlled by carbonate precipitation processes. We observed no significant difference in dissolved Ca and Mg between the ash-bearing cores and the ash-free reference core confirming that the distribution of alkaline earth elements in the

surface sediments investigated in our study is not significantly affected by ash alteration. Obviously, the rates of Mg-uptake and Ca-release during *in-situ* ash alteration are too low to have a significant effect on the pore water composition in surface sediments.

Apart from the generally low *reactivity* of the investigated sediments, two interesting observations could be made:

1) Potassium pore water concentrations are enriched in background sediments and depleted in ash-bearing sediment layers (Fig. 3.5e).
2) Ash alteration seems to affect dissolved silica contents in pore waters, causing concentrations about two times higher than in the ash-free reference core (Fig. 3.5f).

These two phenomena will be discussed separately below.

3.5.1. Potassium Distribution in Pore Waters

The typical pelagic sediment sample originates at the ice cold (2°C) seafloor. It was brought up through the warmer waters near the surface (up to 30°C), and was subsequently squeezed in a cold room at 8°C. Due to this procedure, sediments were significantly heated prior to pore water separation. The warming caused compositional changes in the pore water by shifting the ion exchange equilibria within the sediment. The pore water concentration of potassium is very sensitive to the temperature of squeezing and potassium is affected far more strongly than any of the other major cations (Sayles et al., 1973). If the temperature during squeezing is 20°C higher than the in situ temperature, than an increase in the potassium pore water concentration of up to 18 % has been reported to occur (de Lange et al., 1992; Presley and Trefry, 1980). This temperature effect seems to be dependent on the type of sediment involved. Clays (like smectite, see Fig. 3.4) and marly sediments are reported to be more sensitive than siliceous oozes, consequently, to give larger deviations from the in situ pore water concentration (Sayles et al., 1973). All potassium pore water concentrations in this study are, therefore, likely to be somewhat higher than in situ concentrations. Most of the more depleted values within ash layers, however, may be considered to be largely unaffected by such artefacts because the ashes have much lower surface areas and cation exchange capacities than the clay-rich sediments. Dissolved potassium concentrations measured in the ash layers probably represent *in-situ* values while the higher concentrations recorded in adjacent ash-free sediment layers are affected by the release of potassium from clays upon core retrieval (Fig. 3.5f).

3.5.2. Modelling of Ash Alteration in Marine Sediments: The Effect on Dissolved Silica Concentrations in Pore Waters

Ash dissolution in the investigated sediments was modelled using the following simple differential equation:

$$\frac{\partial G(x,t)}{\partial t} = -v \cdot \frac{\partial G(x,t)}{\partial x} - R_G(x,t) \quad (1)$$

where the volcanic glass concentration (G) is given in g glass per g of dry solids, v is the burial velocity (0.016 cm yr^{-1}) and R_G is the rate of glass dissolution. In this equation, porosity and density of dry solids are assumed to be constant over the entire sediment column and solids are transported by burial, only. The upper bioturbated surface layer of the sediment is, hence, not included in the model.

Different kinetic equations are applied for the rate expression $R_G(x,t)$. In a first set of model experiments, the rate is assumed to dependent on the ash concentration, only:

$$R_G(x,t) = k_G \cdot G(x,t) \quad (2)$$

where k_G is a kinetic constant (yr^{-1}).

The dissolution of volcanic glass in marine sediments was determined in previous laboratory experiments (Schacht et al., submitted). The experiments showed that dissolved silica was released from felsic ashes at a rate of 3 x 10^{-13} mol Si m^{-2} s^{-1} under seafloor conditions (2°C, 200 bar). The amount of ash did not change considerably over the short-term experiments performed in the laboratory. The investigated ash sample had a specific surface area of 0.81 m^2 g^{-1} and a SiO_2 content of 72 wt% corresponding to a concentration of 12.0 mmol SiO_2 g^{-1}. Hence, the rate of dissolved silica release can be recalculated as 7.67 µmol SiO_2 g^{-1} yr^{-1} and the first order kinetic constant k_G results as 6.4 x 10^{-4} yr^{-1}.

Substituting Eq. 2 into Eq. 1, the general analytical solution of the partial differential equation (Eq. 1) results as:

$$G(x,t) = e^{-\frac{k_G \cdot x}{v}} \cdot F\left(\frac{t \cdot v - x}{v}\right) \quad (3)$$

where F is an arbitrary function.

The following equation is applied as upper boundary condition:

$$G(0,t) = exp\left[-\frac{(t-t_1)^2}{2\cdot w^2}\right] + exp\left[-\frac{(t-t_2)^2}{2\cdot w^2}\right] + exp\left[-\frac{(t-t_3)^2}{2\cdot w^2}\right] + exp\left[-\frac{(t-t_4)^2}{2\cdot w^2}\right] \quad (4)$$

This train of Gauss functions is used to mimic the deposition of four discrete ash layers at the top of the model column. Eq. 4 is set up to simulate ash dissolution in core B which contains four prominent ash layers deposited over the last 40,000 years. The width of the ash layers is defined by w (250 yr = 4 cm at a sedimentation rate of 0.016 cm yr^{-1}) and the times of deposition of the ash layers are given by t_1 to t_4.

Applying the upper boundary condition Eq. 4, the analytical solution of Eq. 1 results as:

$$G(x,t) = exp\left[-\frac{k_G\cdot x}{v}\right]\cdot\left(exp\left[-\frac{\left(\frac{t\cdot v-x}{v}-t_1\right)^2}{2\cdot w^2}\right] + exp\left[-\frac{\left(\frac{t\cdot v-x}{v}-t_2\right)^2}{2\cdot w^2}\right] + exp\left[-\frac{\left(\frac{t\cdot v-x}{v}-t_3\right)^2}{2\cdot w^2}\right] + exp\left[-\frac{\left(\frac{t\cdot v-x}{v}-t_4\right)^2}{2\cdot w^2}\right]\right) \quad (5)$$

The model was run over a period of t_{max} = 42,000 years applying the appropriate volcanic ash ages (t_1 = 2,100 yr, t_2 = 12,500 yr, t_3 = 15,500 yr, t_4 = 40,000 yr) and a wide range of values for the kinetic constant (k_G = 6.4 x 10^{-4} yr^{-1} to 10^{-6} yr^{-1}).

The model results plotted in Figure 3.8a clearly show that only the youngest ash layer would partly survive dissolution while the older ash layers would completely dissolve over the model period if the kinetic constant determined in the laboratory experiments would be valid for field conditions. This is not a surprising result since the half life of the ashes ($t_{1/2}$) calculated as:

$$t_{1/2} = -\frac{ln(0.5)}{k_G} \quad (6)$$

results as only 1,085 yr, while the deepest ash layer in core M54-2 is 40,000 yr old. Considerable ash contents are accumulated only when the value of k_G is reduced by two orders of magnitude to 10^{-5} - 10^{-6} yr^{-1}.

The model was extended to better constrain the *in-situ* rate of ash dissolution. Dissolved silica concentrations are calculated using the following differential equation:

$$\frac{\partial Si(x,t)}{\partial t} = D_S \cdot \frac{\partial^2 Si(x,t)}{\partial x^2} - v \cdot \frac{\partial Si(x,t)}{\partial x} + r_{Si} \cdot R_G(x,t) \qquad (7)$$

where D_S is the molecular diffusion coefficient of dissolved silica in sediments which was calculated from the molecular diffusion coefficient D_M using an empirical equation for the effect of tortuosity and porosity on the diffusion of dissolved species in sediments (Boudreau, 1997):

$$D_S = \frac{D_M}{1 - 2 \cdot \ln(\Phi)} \qquad (8)$$

Applying D_M = 1 x 10^{-5} cm s^{-1} (Wollast and Garrels, 1971) and the average porosity observed in sediment core B (Φ = 0.78), D_S results as 211 cm^2 yr^{-1}.

The rate of glass dissolution was converted into a rate of silica release using the coefficient r_{Si} (8.46 mmol Si cm^{-3}) defined as:

$$r_{Si} = \frac{SiO_2 \cdot d_S \cdot (1 - \Phi)}{\Phi} \qquad (9)$$

where SiO_2 is the SiO_2 content of the volcanic glass (12 mmol SiO_2 g^{-1}) and d_S is the average density of dry solids in the sediment column (2.5 g cm^{-3}).

Equation 7 was solved numerically using the Method-of-Lines approach as implemented in the NDSolve object of MATHEMATICA 5.0. The rate of ash dissolution applied during the modelling of dissolved silica concentrations ($R_G(x,t)$) was calculated as product of the time- and depth-dependent volcanic glass concentration (Eq. 5) and the kinetic constant k_G. Starting with an initial concentration of 300 µmol L^{-1}, the model was run for 42 kyr. A constant dissolved silica concentration of 300 µmol L^{-1} was applied at the top of the model column while a zero gradient condition was prescribed at the base of the sediment column. The initial and upper boundary concentrations correspond to the background concentration of dissolved silica in ash-free sediment cores.

Applying the experimental k_G value of 6.4 x 10^{-4} yr^{-1}, the model produced extremely high concentrations of dissolved silica of almost 3000 µmol L^{-1}. In contrast, a value of k_G = 10^{-6} yr^{-1} resulted in much lower concentrations approaching the measured values

(Fig. 3.8a). Hence, it can be concluded that the *in-situ* dissolution rate is at least two orders of magnitude smaller than the rate obtained in laboratory experiments.

Applying the kinetic Equation 5, ashes continue to be dissolved over the entire sediment column. Consequently, the calculated dissolved silica concentrations show a steady increase with sediment depth when ashes are not completely dissolved at depth (Fig. 3.8a). In contrast, the silica concentrations measured in the ash-bearing cores were constant below a sediment depth of about 200 cm where they approached an upper value of about 450 µmol L^{-1}. This observation and the occurrence of pronounced ash layers in deep sections of the cores suggest that ash dissolution is completely inhibited when the pore water concentration of silica approaches a saturation value of 450 µmol L^{-1}.

Hence, the rate law for ash dissolution was re-defined introducing a saturation term:

$$R_G(x,t) = k_{GS} \cdot G(x,t) \cdot \left(1 - \frac{Si(x,t)}{Si_{Max}}\right) \qquad (10)$$

where the maximum concentration of dissolved silica (Si_{Max} = 450 µmol L^{-1}) represents the solubility of ashes in the investigated sediment cores.

Eq. 10 was introduced into the partial differential Equations 1 and 7 and the coupled system of two equations was solved numerically applying the same boundary conditions and initial values as before. Figure 3.8b shows that the best fit to the dissolved silica data was achieved with a k_{GS} value of 3 x 10^{-5} yr^{-1}. This value is still one order of magnitude lower than the laboratory value indicating that the intrinsic rate of volcanic glass dissolution is much lower in the field than in the laboratory even in undersaturated solutions. Calculated volcanic glass concentrations showed a slight decrease with sediment depth. However, the deepest ash layer still had an ash content of 0.938 g/g (Appendix) indicating that only about 6 % of the ash was dissolved after deposition at the seafloor 40 kyr ago.

3.5.2.1. Field- vs. Laboratory Weathering Rates – Despite the widespread occurrence of volcanic glasses in Pacific Ocean sediments and their role in weathering, there are only very few seawater dissolution rate data available at typical ocean floor conditions of low temperatures (2°C) and elevated pressures (> 200 bar). Schacht et al. (submitted) already pointed out that their experimentally derived dissolution kinetics for volcanic glasses in seawater are about three orders of magnitude slower than rates derived by Crovisier et al. (1987) ($10^{-9.9}$ mol m^{-2} sec^{-1}) as well as by Brady and Gíslason (1997)

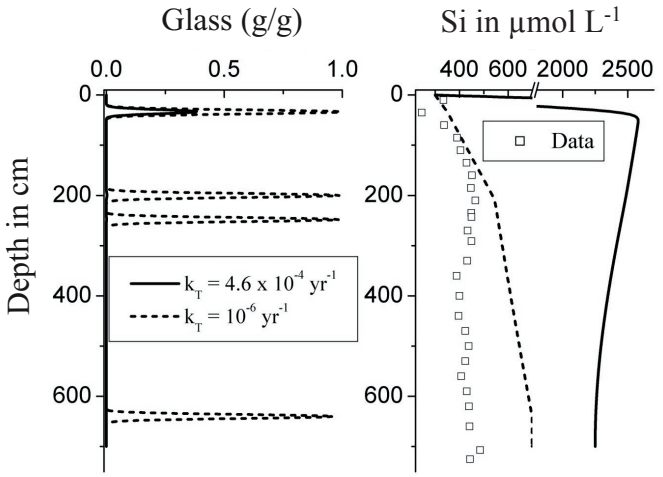

Figure 3.8a: Model results applying the kinetic rate law defined in Eq. 2.

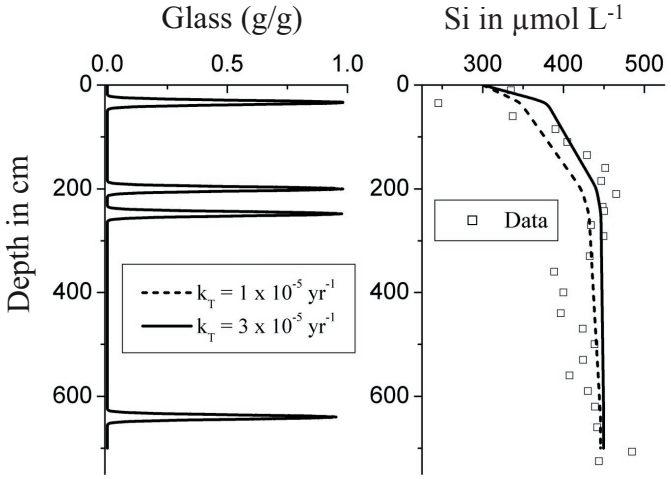

Figure 3.8b: Model results applying the kinetic rate law defined in Eq. 10.

($10^{-10.35}$ mol m^{-2} sec $^{-1}$). Even if all three authors used very similar experimental build-ups to estimate glass dissolution rates in artificial seawater, their data are thus very contradictory. The discrepancies, however, can mostly be attributed to the differences in duration of experimental alteration, temperature and pressure differences, differences in surface conditions of the used samples, and different sample grain sizes, influencing directly or indirectly the elemental geochemical behaviour.

The measurement of glass dissolution rates in the laboratory allow a prediction of dissolution kinetics in the field. However, as noted in this work and by several workers before (Dahlgren et al., 1999; White and Brantley, 2003; Yokoyama and Banfield, 2002) discrepancies exist between field estimates and laboratory measurements of

glass dissolution rates. In particular, no matter if a marine or a meteoric weathering environment is concerned, glass dissolution rates calculated from field data are almost always 1-3 orders of magnitude less than rates measured in the laboratory. For the study presented here as well as for those cited above these differences are attributable to high fluid glass/ratios reacted over short times during laboratory experiments. Therefore solutions are produced that are far from thermodynamic saturation with respect to the reactive phase. Natural weathering involves much lower fluid/glass ratios reacted over longer times what results pore water compositions closer to thermodynamic saturation. Thus experiments produced uncertainties when experimental rates were applied to natural alteration environments.

Moreover, the dissolution of silica during the above described experiments increased rapidly during the very initial stage of alteration to become more slowly after the first few hours (Fig. 3.7). The strong increase of dissolved silica concentrations during felsic experiments points out that during the investigated very initial phase of seawater alteration dissolution seems to occur much faster than precipitation processes. At long time scales the change of dissolution rates will be much less and the formation of secondary mineralisation surly will occur. This explains one more time why the experimentally approach exhibited *pseudo*-dissolution rates. All over, it is essential to always also account for natural processes (in means of field data) since laboratory determined weathering rates greatly over estimates actual rates.

3.6. Conclusions

In this paper we investigated the effects of volcanic ash alteration on the composition of pore fluids in marine surface sediments. Previous studies showed that pore fluids recovered from long sediment cores obtained by deep-sea drilling are significantly affected by volcanic matter alteration. Continuous losses of Mg, Na, and K and an enrichments of Ca and Si in pore waters were documented in these studies. In our ash-bearing cores covering the upper 8 m of the sediment column, dissolved Ca and Mg decreased with sediment depth due to carbonate precipitation processes induced by the anaerobic degradation of organic matter, while dissolved K concentrations were affected by sampling artefacts. Hence, we could not resolve any significant effect of ash alteration on the major cation concentrations in pore fluids. This observation implies that ash alteration is a very slow process in marine surface sediments.

Dissolved silica concentrations were, however, clearly enhanced by the dissolution of volcanic ashes. We applied a transport-reaction model to the silica and ash data from our cores to constrain the rate of dissolved silica release during ash alteration. The modelling showed that further silica release is inhibited when the dissolved silica concentration in the pore fluids approaches a saturation value of 450 µmol L^{-1}. Hence ash dissolution occurs mainly in the upper sediment horizons were dissolved silica concentrations are low and smaller than the saturation value. A good fit to the data was obtained applying the following kinetic rate law:

$$R_G = k_{GS} \cdot G \cdot \left(1 - \frac{Si}{Si_{Max}}\right)$$

where R_G is the rate of glass dissolution, G is the glass concentration in the core, Si_{Max} is a saturation concentration of dissolved silica (450 µmol L^{-1}) and Si is the concentration of dissolved silica in the investigated pore fluids. The kinetic constant k_{GS} was determined as 3 x 10^{-5} yr^{-1} by fitting the model to the data.

In a previous study, we used laboratory experiments to investigate the dissolution kinetics of ash samples from our study area. The rate of silica release recorded in these short-term studies was at least two orders of magnitude higher than the *in-situ* rate derived from the pore water data. The deviation between field data and experimental results is probably related to the much shorter observation time and the higher water to rock ratio applied in the experiments. Moreover, the reactivity of the ash surfaces might have been enhanced by the procedures applied during the experiments and the previous separation of glass samples from the sediment matrix. The rate law and the kinetic constant derived from the field data better reflect the rate of ash dissolution at the seafloor. They should hence be considered in future studies of volcanic glass alteration in marine surface sediments.

Acknowledgements

We wish to thank the captain, crew, and all other participants of RV *Meteor* for their support and good working atmosphere during cruise 54/2. We owe special thank to Nico Augustin for his help while evaluation XRD-data, Jutta Heinze and Petra Fiedler for sample preparation during biogenic silica and clay mineral analyses, Kristin Nass for conducting the ICP-OES analyses, and, last but not least, Bettina Domeyer for performing C/N/S analyses.

References

Barckhausen U., Ranero C., von Huene R., Cande S., and Roeser H. (2001) Revised tectonic boundaries in the Cocos Plate off Costa Rica: Implications for the segmentation of the convergent margin and for plate tectonic models. *Journal of Geophysical Research* **106**(19), 207-220.

Berger G., Schott J., and Loubet M. (1987) Fundamental processes controling the first stage of alteration of a basalt glass by seawater: An experimental study between 200 and 320°C. *Earth and Planetary Science Letters* **84**, 431-445.

Boudreau B. (1997) *Diagenetic models and their implementation - Modelling transport and reactions in aquatic sediments*. Springer.

Brady P. and Gíslason S. (1997) Seafloor weathering controls on atmospheric CO_2 and global climate. *Geochimica et Cosmochimica Acta* **61**(5), 965-973.

Crovisier J.-L., Honnorez J., and Eberhart J. (1987) Dissolution of basaltic glass in seawater: Mechanism and rate. *Geochimica et Cosmochimica Acta* **51**, 2977-2990.

Crovisier J.-L., Thomassin J., Juteau T., Eberhart J., Touray J., and Baillif B. (1983) Experimental basalt-seawater glass interaction at 50°C: Study of early developed phases by electron microscopy and X-ray photoelectron spectrometry. *Geochimica et Cosmochimica Acta* **47**, 377-387.

Dahlgren R., Ugolini F., and Casey W. (1999) Field weathering rates of Mt. St. Helens tephra. *Geochimica et Cosmochimica Acta* **63**(5), 587-598.

de Lange G., Cranston R., Hydes D., and Boust D. (1992) Extraction of pore water from marine sediments: A review of possible artefacts with pertinent examples from the North Atlantic. *Marine Geology* **109**, 53-76.

DeMaster D. (1981) The supply and accumulation of silica in marine environment. *Geochimica et Cosmochimica Acta* **45**, 1715-1732.

Drever J. (1971) Magnesium iron replacement in clay minerals in anoxic marine sediments. *Science* **172**, 1334-1336.

Gieskes J. (1981) Deep-sea drilling interstitial water studies: Implications for chemical alteration of the oceanic crust, layers I and II. *The Society of Economic Paleontologists and Mineralogists* **32**, 149-167.

Gieskes J., Blanc G., Vrolijk P., Elderfield H., and Barnes R. (1990) Interstitial water chemistry - major constituents. *Proceedings of the Ocean Drilling Program, Scientific Results* **110**, 155-177.

Gieskes J. and Lawrence J. (1981) Alteration of volcanic matter in the deep sea sediments: Evidence from the chemical composition of interstitial waters from deep sea drilling cores. *Geochimica et Cosmochimica Acta* **45**, 1687-1703.

Grasshoff K., Ehrhardt M., and Kremling K. (1999) *Methods of Seawater Analysis*. Wiley-VCH.

Guy C., Schott J., Destrigneville C., and Chiappini R. (1992) Low-temperature alteration of basalt by interstitial seawater, Mururoa, French Polynesia. *Geochimica et Cosmochimica Acta* **56**, 4169-4189.

Hurd D. (1973) Interactions of biogenic opal, sediment, and seawater in the central equatorial Pacific. *Geochimica et Cosmochimica Acta* **37**, 2257-2282.

Ivanenkov V. and Lyakhin Y. (1978) Determination of total alkalinity in seawater. In *Methodes of hydrochemical investigations in the ocean* (ed. V. Ivanenkov), pp. 110-114. Nauka Publ.

Kimura G., Silver E., and Blum P. (1997) Costa Rica accretionary wedge, Sites 1039-1043. *Palaeogeography, Palaeoclimatology, Palaeoecology* **170**, 458.

Kutterolf S., Schacht U., Wehrmann H., Freundt A., and Moerz T. (in press) Onshore to offshore tephrostratigraphy and marine ash layer diagenesis in Central America. In *Central America - Geology, Resources and Hazards* (ed. J. Buntschuh). Balkema.

Lawrence J., Drever J., Anderson T., and Brueckner H. (1979) Importance of alteration of volcanic material in the sediments of Deep Sea Drilling Site 323: Chemistry, 18O/16O and 87Sr/86Sr. *Geochimica et Cosmochimica Acta* **43**, 573-588.

Mangelsdorf P. and Wilson T. (1969) Potassium enrichments in interstitial waters of recent marine sediments. *Science* **165**, 171-174.

Manheim F. (1976) Interstitial waters of marine sediments. In *Chemical Oceanography* (ed. R. Chester), pp. 115-186. Academic Press, Inc.

Moore D. and Reynolds R. (1989) *X-ray diffraction and the identification and analysis of clay minerals*. Oxford University Press.

Mottl M. (1989) Hydrothermal convection, reaction and diffusion in sediments on the Costa Rica Rift Flank: Pore-water evidence from ODP Site 677 and 678. *Proceedings of the Ocean Drilling Program, Scientific Results* **111**, 195-209.

Müller P. and Schneider R. (1993) An automated method for determination of opal in sediments and particulate matter. *Deep-Sea Research* **40**(3), 425-444.

Patino L., Carr M., and Feigenson M. (2000) Local and regional variations in Central American arc lavas controlled by variations in subducted sediment input. *Contributions to Mineralogy and Petrology* **138**, 265-283.

Pichler T., Ridley W., and Nelson E. (1999) Low-temperature alteration of dredged volcanics form the Southern Chile Ridge: additional information about early stages of seafloor weathering. *Marine Geology* **159**, 155-177.

Presley B. and Trefry J. (1980) Sediment-water interactions and the geochemistry of interstitial waters. In *Chemistry and Biochemistry of Estuaries* (ed. I. Cato). John Wiley & Sons Ltd.

Sayles F., Manheim F., and Waterman L. (1973) Interstitial water studies on small core samples: Leg 15. *Initial Reports of the Deep Sea Drilling Project* **20**, 783-804.

Schacht U., Kutterolf S., Schmidt M., and Wallmann K. (submitted) Alteration of differently composed volcanic glasses in marine sediments: Insights into alteration behaviour and dissolution kinetics. *Geochimica et Cosmochimica Acta*.

Schlüter M. and Rickert D. (1998) Effect of pH on the measurement of biogenic silica. *Marine Chemistry* **63**, 81-92.

Seyfried J., WE and Bischoff J. (1979) Low temperature basalt alteration by seawater: An experimental study at 70°C and 150°C. *Geochimica et Cosmochimica Acta* **43**, 1937-1947.

Spinelli G. and Underwood M. B. (2004) Character of sediments entering the Costa Rica subduction zone: Implications for partitioning of water along the plate interface. *The Island Arc* **13**, 432-451.

Spivack A. and Staudigel H. (1994) Low-temperature alteration of the upper oceanic crust and the alkalinity budget of seawater. *Chemical Geology* **115**, 239-247.

Staudigel H. and Hart S. (1983) Alteration of basaltic glass: Mechanisms and significance for oceanic crust-seawater budget. *Geochimica et Cosmochimica Acta* **47**, 337-350.

Straub S. and Schmincke H. (1998) Evaluating the tephra input into Pacific Ocean sediments: Distribution in space and time. *Geologische Rundschau* **87**(3), 461-476.

Stuiver M. and Polach H. (1977) Discussion: Reporting of 14C Data. *Radiocarbon* **19**(3), 355-363.

Vallier T. and Jefferson W. (1981) Volcanogenic sediments from Hess Rise and the Mid-Pacific Mountains, Deep Sea Drilling Project Leg 62. *Initial Reports of the Deep Sea Drilling Project* **62**, 545-557.

Verardo D., PN F., and McIntyre A. (1990) Determination of organic carbon and nitrogen in marine sediments using the CARLO ERBA NA-1500 Analyser. *Deep-Sea Research* **37**(1A), 157-165.

von Huene R., Ranero C., and Weinrebe W. (2000) Quaternary convergent margin tectonics of Costa Rica, segmentation of the Cocos Plate, and Central American volcanism. *Tectonics*(19), 314-334.

White A. and Brantley S. (2003) The effect of time on the weathering of silicate minerals: why do weathering rates differ in the laboratory and field? *Chemical Geology* **202**, 479-506.

Wollast R. and Garrels R. (1971) Diffusion coefficient of silca in seawater. *Nature Physical Sciences* **229**, 94.

Yokoyama T. and Banfield J. (2002) Direct determination of the rates of rhyolite dissolution and clay formation over 52,000 years and comparison with laboratory measurements. *Geochimica et Cosmochimica Acta* **66**(15), 2665-2681.

Appendix

Appendix A:
Core A - Chemical composition of pore waters (A1) and sediments (A2).

A1

Core	Depth (cm)	Alkalinity (meq/kg)	SO_4 (mM)	Ca (mM)	Na (mM)	K (mM)	Mg (mM)	Si (µM)
	10	2.82	28.4	9.90	551	10.6	50.5	430
	35	3.48	27.5	9.63	552	10.8	50.8	499
	60	3.62	27.5	9.80	552	10.8	51.0	541
	85	4.12	27.0	9.81	553	10.1	49.5	529
	110	5.19	25.9	9.80	551	10.7	49.5	561
	135	5.53	25.4	9.77	549	11.0	49.1	540
	160	5.80	25.5	9.75	555	11.1	49.6	526
A	185	6.19	25.3	9.82	553	11.2	49.5	525
	210	6.34	25.6	9.77	551	10.9	49.5	539
	235	6.34		9.95	564	10.6	50.0	528
	260	6.58	25.4	9.48	552	11.0		565
	285	6.58	25.1	9.70	549	10.9	49.1	540
	310	6.58	24.5	9.56	549	10.8	48.4	522
	335	6.56	24.5	9.58	550	11.3	48.6	494
	360	6.58	24.9	9.46	552	10.9	47.9	530
	385	6.56	24.6	9.70	551	11.0	49.1	505
	410	6.50	24.8	9.59	552	11.1	49.1	502
	435	6.56	24.9	9.57	553	11.0	48.7	503

A2

Core	Depth (cm)	C_{org} (wt%)	$CaCO_3$ (wt%)	N (wt%)	S (wt%)	H_2O (wt%)	Biogenic Opal (wt%)
	10	2.40	2.30	0.26	0.65	56.5	7.41
	35	3.89	1.29	0.40	0.96	63.1	
	60	2.14	0.01	0.22	0.68	55.4	
	85	0.38	0.10	0.06	0.32	36.6	
	110	1.57		0.18	1.23	44.8	
	135	2.70		0.28	0.81	56.0	9.02
	160	3.02		0.30	1.20	55.7	
A	185	3.12		0.32	1.18	57.3	
	210	2.18		0.23	0.75	56.0	7.9
	235	0.09	0.20	0.04	0.19	32.7	
	260	2.46		0.24	1.07	51.6	
	285	2.90		0.29	1.15	57.4	
	310	1.83	0.12	0.19	0.97	48.3	6.41
	335	1.26	0.37	0.14	2.44	39.7	
	360	2.26	1.67	0.22	0.57	51.3	
	385	2.19	1.50	0.21	0.77	46.8	
	410	2.84	1.41	0.28	1.00	52.8	6.37
	435	2.76	0.56	0.26	0.98	51.7	

Appendix B:
Core B - Chemical composition of pore waters (B1) and sediments (B2).

B1

Core	Depth (cm)	Alkalinity (meq/kg)	SO_4 (mM)	Ca (mM)	Na (mM)	K (mM)	Mg (mM)	Si (µM)
	10	2.61	27.9	9.73	534	10.6	50.8	413
	35	2.56	27.7	8.69	535	9.92	52.0	348
	60	3.64	27.1	9.55	547	10.9	51.0	362
	85	4.54	26.2	9.37	539	10.8	51.4	415
	110	5.07	25.8	9.31	547	10.9	51.4	435
	135	5.39	25.3	9.19	540	10.7	50.8	435
	160	5.85	24.6	9.05	545	10.3	50.7	484
	185	6.26	24.3	8.99	548	10.7	50.8	465
	210	6.66	23.7	8.71	534	10.5	50.7	495
	235	7.10	23.3	8.66	541	10.6	49.9	502
	243	7.13	22.3	8.23	523	9.99	49.2	500
B	270	7.45	22.0	8.55	533	10.6	50.2	460
	291	8.12	21.8	8.53	533	10.0	49.6	475
	330	8.79	20.7	7.80	532	10.1	49.9	477
	360	9.54	19.7	7.67	530	10.8	47.2	473
	400	10.1	19.2	7.70	538	11.1	48.9	416
	440	10.8	18.1	7.06	529	10.9	47.7	487
	470	11.6	17.9	7.34	544	10.9	49.0	452
	500	12.4	17.3	7.22	540	10.4	48.4	529
	530	12.4	16.1	6.41	528	9.94	48.1	507
	560	12.8	15.6	6.80	529	10.4	47.2	476
	590	12.8	14.3	6.08	511	9.82	47.0	461
	620	13.6	13.5	6.11	516	10.0	46.5	447
	660	14.8	9.61	5.29	520	9.22	47.9	539
	707	16.9	8.40	4.92	520	9.27	45.4	560
	725	16.7	8.51	4.47	518	9.50	45.5	535

B2

Core	Depth (cm)	C_{org} (wt%)	$CaCO_3$ (wt%)	N (wt%)	S (wt%)	H_2O (wt%)	Biogenic Opal (wt%)
	10	2.37	11.3	0.26	1.18	50.2	3.19
	35	2.12	10.5	0.24	1.51	52.3	
	60	3.49	13.0	0.37	1.46	62.1	
	85	3.96	10.3	0.40	1.27	63.9	
	110	3.84	11.5	0.39	1.45	62.4	3.32
	135	3.80	12.8	0.39	1.39	63.0	
	160	3.45	13.4	0.37	1.35	61.3	
	185	3.68	14.1	0.39	1.30	62.4	
	210	4.16	13.7	0.42	1.44	61.9	6.15
	235	3.65	11.3	0.36	1.36	58.6	
	243	1.65	4.93	0.17	0.93	47.5	
B	270	3.69	12.5	0.38	1.32	59.6	
	291	0.43	1.80	0.06	0.51	35.9	
	330	3.70	12.2	0.39	1.50	58.0	2.58
	360	3.66	12.2	0.39	1.33	57.5	
	400	3.45	11.3	0.36	1.52	56.0	
	440	3.37	10.5	0.36	1.40	55.2	
	470	3.41	12.4	0.36	1.49	54.2	2.41
	500	3.78	8.23	0.40	1.53	55.9	
	530	3.91	9.94	0.40	1.39	56.5	
	560	4.11	7.53	0.41	1.81	55.8	
	590	3.92	7.61	0.39	1.70	55.4	
	620	4.25	7.69	0.42	1.61	55.8	2.59
	660	2.28	4.53	0.23	2.00	47.3	
	707	2.59	7.31	0.24	1.59	50.6	
	725	2.78	6.55	0.26	2.07	49.1	

Appendix C:
Core C - Chemical composition of pore waters (C1) and sediments (C2).

C1

Core	Depth (cm)	Alkalinity (meq/kg)	SO_4 (mM)	Ca (mM)	Na (mM)	K (mM)	Mg (mM)	Si (µM)
	10	4.93	27.3	9.86	556	12.0	51.3	532
	33	7.24	24.5	9.29	555	11.7	51.7	552
	44	7.89	24.0	9.15	556	11.6	51.2	513
	61	8.67	23.4	8.89	556	11.5	51.1	464
	100	11.7	19.1	7.95	556	12.1	48.8	514
	140	13.9	15.8	7.06	556	11.9	48.4	535
C	170	15.4	13.1	6.49	553	11.5	47.2	554
	195	16.5	11.2	5.84	548	11.7	46.7	534
	220	18.2	9.72	5.64	543	11.5	46.5	566
	240	18.2	7.77	4.91	548	11.6	45.1	536
	265	19.8	6.73	4.82	546	11.4	44.6	538
	290	21.1	5.63	4.50	552	11.3	44.6	546
	320	22.0	4.92	4.30	551	11.1	44.3	552
	353	22.0	3.83	4.00	552	11.1	43.9	542

C2

Core	Depth (cm)	C_{org} (wt%)	$CaCO_3$ (wt%)	N (wt%)	S (wt%)	H_2O (wt%)	Biogenic Opal (wt%)
	10	4.06	8.26	0.38	1.40	63.6	3.36
	33	1.87	4.26	0.19	0.67	49.1	
	44	1.66	6.05	0.17	0.89	46.4	3.13
	61	3.78	10.3	0.39	1.61	57.7	
	100	3.84	9.45	0.38	1.59	55.0	2.26
	140	3.87	9.36	0.39	1.79	54.9	
C	170	4.37	7.20	0.41	1.84	56.0	
	195	3.16	5.40	0.31	1.74	53.9	
	220	2.74	3.72	0.26	2.25	50.5	
	240	2.80	6.22	0.26	1.69	49.7	
	265	4.82	5.92	0.43	1.79	51.9	
	290	3.15	5.64	0.29	1.94	52.9	2.89
	320	2.83	5.35	0.26	1.98	45.5	
	353	3.33	5.99	0.26	1.64	53.1	

Appendix D:
Core D - Chemical composition of pore waters (D1) and sediments (D2).

D1

Core	Depth (cm)	Alkalinity (meq/kg)	SO_4 (mM)	Ca (mM)	Na (mM)	K (mM)	Mg (mM)	Si (µM)
	60		27.0	9.86	472	10.3	52.2	279
	95		25.9	9.61	462	10.2	52.4	282
	120		24.2	9.08	466	10.2	51.8	271
	155		23.3	8.72	474	10.3	50.8	264
	190		21.8	8.19	462	10.3	50.4	253
	225		20.2	7.77	460	10.1	50.0	246
	260	7.36	18.4	7.30	460	9.9	49.4	278
	295	8.00	16.9	6.85	471	10.1	47.9	279
D	320	8.68	15.9	6.51	463	10.1	48.0	283
	355	9.44	14.3	5.97	465	10.1	47.2	281
	390	9.74	13.0	5.62	468	10.1	46.6	304
	415	10.2	12.0	5.26	459	10.0	46.7	302
	440	10.6	11.0	5.01	463	9.89	46.1	316
	475	11.1	9.86	4.71	458	9.87	45.6	317
	510	11.4	8.67	4.43	457	9.81	45.4	304
	545	12.6	7.73	4.17	460	9.81	45.1	303
	580	12.9	6.48	3.91	456	9.84	44.6	299
	620	13.5	5.95	3.83	468	9.74	44.4	279

D2

Core	Depth (cm)	C_{org} (wt%)	$CaCO_3$ (wt%)	N (wt%)	S (wt%)	H_2O (wt%)	Biogenic Opal (wt%)
	60	1.77	7.44	0.19	1.13	54.3	3.29
	95	1.87	7.02	0.19	1.05	55.4	
	120	1.82	5.51	0.17	1.16	54.7	
	155	1.73	7.10	0.17	1.24	53.2	2.96
	190	1.66	9.50	0.17	0.73	51.9	
	225	1.67	7.19	0.17	1.52	51.4	
	260	1.54	13.0	0.17	1.11	47.3	2.20
	295	1.77	8.39	0.18	1.11	50.6	
D	320	1.55	9.89	0.16	1.03	47.9	
	355	1.37	8.37	0.14	0.65	46.7	
	390	1.70	9.05	0.15	1.14	50.6	1.61
	415	1.75	7.40	0.16	1.26	51.1	
	440	1.65	7.80	0.16	1.22	49.2	
	475	1.63	6.37	0.16	1.15	51.2	
	510	1.70	6.17	0.14	1.45	50.4	
	545	1.59	6.07	0.16	1.16	50.3	1.91
	580	1.80	4.33	0.18	1.28	50.3	
	620	1.95	3.16	0.17	1.29	48.9	

Appendix E:
Core E - Chemical composition of pore waters (E1) and sediments (E2).

E1

Core	Depth (cm)	Alkalinity (meq/kg)	SO_4 (mM)	Ca (mM)	Na (mM)	K (mM)	Mg (mM)	Si (µM)
	10	4.21	27.6	10.1	469	10.5	53.0	443
	60	7.72	24.2	9.41	471	10.7	52.8	462
	110	12.7	20.1	8.61	471	10.2	51.0	531
	160	15.5	17.9	7.61	483	9.83	51.7	504
	210	18.4	13.9	6.71	478	9.66	52.1	499
	260	21.9	10.6	6.92	466	10.7	50.2	484
E	310	26.0	7.19	6.31	470	10.3	49.9	507
	365	29.2	3.95	5.30	473	10.5	49.2	486
	425	34.6	0.27	4.63	466	10.6	49.0	359
	485	35.5	0.03	4.18	467	10.5	49.0	257
	545	38.7	0.08	4.39	470	10.9	49.4	325
	605	42.0	0.04	4.17	463	10.7	51.3	430
	665	45.2	0.14	3.81	471	11.1	52.4	396
	725	46.0	0.03	3.64	472	11.6	53.5	452

E2

Core	Depth (cm)	C_{org} (wt%)	$CaCO_3$ (wt%)	N (wt%)	S (wt%)	H_2O (wt%)	Biogenic Opal (wt%)
	10	1.67	0.69	0.20	0.24	66.4	4.70
	60	1.52	0.99	0.18	0.45	59.5	
	110	1.72	1.17	0.21	0.36	59.1	
	160	1.45	1.00	0.17	0.55	57.4	
	210	1.60	2.54	0.18	0.86	56.9	4.90
	260	1.53	1.30	0.18	0.58	58.3	
E	310	1.56	2.39	0.19	0.49	61.7	
	365	1.66	0.47	0.19	0.30	57.0	
	425	1.29	0.63	0.14	0.22	51.0	5.13
	485	1.07	0.06	0.10	0.21	43.2	
	545	1.05	1.41	0.11	0.33	41.5	
	605	1.53	2.03	0.18	0.25	53.6	5.34
	665	1.90	1.73	0.22	0.40	53.1	
	725	1.50	1.47	0.19	0.95	52.0	

Appendix F:
Additional information on petrographic features and ages of ash layers concerning cores A, B, and C.

Core	Depth	Portions ash/sediment	Portions felsic/mafic ash	Portions fresh/altered	SiO_2 (wt%) in glass	Age (kyr)
	14-20	60/40	15/85	90/10	52	2.1
	59-62	70/30	95/5	95/5	68	15.5
	68-69	30/70	95/5		74	reworked
A	83-96	95/5	80/20	90/10	74	21
	200-202	60/40	30/70	70/30	54	~ 40
	234-242	90/10	90/10	98/2	79	86
	267-269	50/50	30/70	65/35	54	n.d.
	311-313	40/60	90/10	75/25	76	n.d.
	30-35	40/60	10/90	75/25	52	2.1
	238-244	80/20	90/10	70/30	75	12.5
	265-269				(felsic)	n.d.
B	295-300	90/10	80/20	80/20	69	15.5
	319-325				(felsic)	n.d.
	661-665	70/30	10/90	60/40	54	~ 40
	707-711	60/40	90/10	60/40	75	n.d.
	725-727	70/30	20/80	55/45	54	n.d.
	06-08	50/50	10/90	90/10	53	2.1
	30-34	90/10	95/5	90/10	75	12.5
	41-46	80/20	85/15	70/30	69	15.5
C	59-65	60/40	80/20	60/40	74	24
	238-240	40/60	75/25	80/20	76	reworked
	282-287	70/30	85/15	70/30	76	n.d.
	350-356	60/40	15/85	65/35	54	~ 40

Chapter IV

The Influence of Volcanic Ash Alteration on the REE Composition of Marine Pore Waters

Ulrike Schacht[1,2], Steffen Kutterolf[1,2], Klaus Wallmann[2,1], and Mark Schmidt[3,1]

[1] Special Research Project 574, University of Kiel, Wischhofstr. 1-3, 24148 Kiel, Germany

[2] IFM-GEOMAR, Leibniz Institute of Marine Sciences, Wischhofstr. 1-3, 24148 Kiel, Germany

[3] Institute of Geosciences, University of Kiel, Ludewig-Meyn-Str. 10, 24118 Kiel, Germany

Abstract

Two volcanic ash bearing deep sea gravity cores were recovered during research cruise *RV Sonne* 173/3 along the Pacific margin offshore Nicaragua. Thick felsic and mafic ash layers dominate the recovered sediments. Pore water samples of these - one incoming plate and one slope site - sediment cores have been analysed for light rare earth elements, alkalinity, sulphate, phosphate, ammonia, calcium, and manganese contents. The data provide a systematic look at changes in REE diagenesis proceeding from open ocean sediments to highly reducing near-shore sediments.

The pore water patterns of all the dissolved species mentioned above suggest that volcanic glass alteration constitutes a major source for REE release in marine sediments when low rates of anerobic degradation of organic matter, like typical for incoming plate/open ocean sediments, prevail. Under this conditions the release of REE results in fluxes of at least 0.04 nmol La cm^{-2} yr^{-1} and 0.09 nmol Ce cm^{-2} yr^{-1}**.**

The shapes of the concentration depth profiles also imply an effective withdrawal of REE from pore waters. Our investigations suggest that phosphate precipitation processes and possibly clay minerals may be responsible for the removal of dissolved REE from the solution.

4.1. Introduction

The group of rare earth elements (REE) is interesting for geochemistry due to the unique similarity of their chemical properties, and to a regular change of these properties from La to Lu (McLennan, 1994 and literature cited afterwards). Thus REE patterns are important diagnostic tools in the investigation of complex geological systems. There is a large database dealing with the partitioning of REE during petrogenesis (e.g. Rollinson, 1993), but much less is known about these elements during low temperature alteration of igneous rocks. However, it is clear that REE have the potential for describing interactions between rocks and fluids in hydrothermal convection cells (Klinkhammer et al., 1994). Therefore the REE can be particularly useful as geochemical tracers in the marine environment.

The interest in the marine geochemistry of the REE is documented by numerous investigations undertaken in the last two decades to determine the distribution and abundance of REE in sediments (Koeppenkastrop and de Carlo, 1992; Strekopytov et al., 1999), and in coastal and oceanic waters (e.g. Elderfield and Greaves, 1982; Klinkhammer et al., 1983; Piepgras and Jacobsen, 1992). However, there are presently only few published pore water profiles for REE (i.e. Elderfield and Sholkovitz, 1987; Haley et al., 2004; Sholkovitz et al., 1989).

In order to understand the pathways of trace and rare earth elements in interstitial waters of marine surface sediments due to volcanic ash alteration, this work presents two geochemical profiles of selected rare earth elements in pore waters retrieved from marine, volcanogenic sediment cores offshore Nicaragua. The elements will be presented in relation to dissolved alkalinity-, sulphate-, phosphate-, ammonia-, Ca-, and Mn concentrations which are used as indicators of the redox conditions on each investigated core site. To further our basic knowledge about diagenetic processes during seawater/ volcanic ash alteration and related rare earth elements, in addition to the pore water program LA-ICP-MS analyses of individual volcanic glass shards were carried out.

4.2. Geological Setting

Our investigation area is located in the Pacific Ocean along the Central American Convergent Margin (CACM) concentrating on the segment of the subduction zone system onshore and offshore Nicaragua (Fig. 4.1). The CACM results from the subduction of the Cocos Plate beneath the Caribbean Plate at a rate of nearly 90 mm yr^{-1}

(Kimura et al., 1997). The angle of subduction, the nature of the incoming plate, and magmatic compositions vary significantly along the volcanic arc (Carr, 1984).

The incoming part of the Pacific plate (Fig. 4.1) has a relatively smooth surface morphology and the age of crust is 22 Myr (Barckhausen et al., 2001). The smooth domain is formed at the N-S trending East Pacific Rise spreading centre which is part of an abandoned precursor of the Cocos-Nazca spreading centre (von Huene et al., 2000). The sedimentary succession of the incoming oceanic plate is ~400 m thick. The upper section is hemipelagic containing a large number of tephra layers while the underlying section is dominated by calcareous oozes (Kimura et al., 1997).

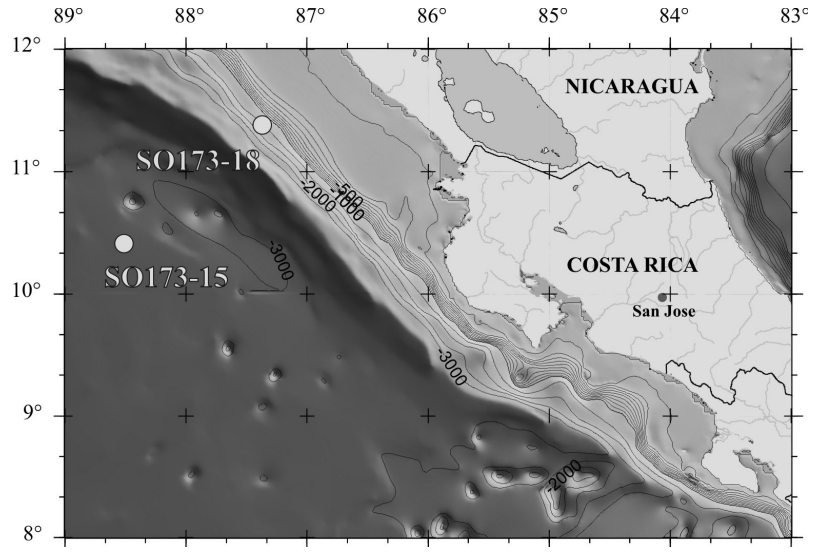

Figure 4.1: Map of Central America showing core locations SO173-15 and 18 (circles).

4.3. Methods

4.3.1. On-Board Sediment and Pore Water Sampling

Both sediment cores investigated in this study were collected by using 2 to 11 m gravity corers during the research cruise RV *Sonne* 173/3 along the continental slope and incoming plate off Nicaragua located between 10°S to 12°S and 87°W to 89°W (Fig. 4.1, Tab. 4.1). After retrieval on board the cores were cut into 1 m segments. To prevent further warming the cores were placed in a cooling laboratory and maintained at a temperature of ~8°C. Generally the cores were cut lengthwise (within the first hours after recovering) and three sediment samples were taken at each depth for pressure (pore water) sampling, subsequent description, and analyses of the solid phase. For

pressure filtration Teflon- and PE-squeezers were used. The squeezers were operated with argon at a pressure gradually increasing up to 5 bar. Pore waters were retrieved through 0.2 µm cellulose acetate membrane filters. Subsamples for ICP-OES and REE analyses were immediately acidified with 10 *N* HNO_3 (supra-pure) to prevent carbonate precipitation and were stored in acid-cleaned plastic vials.

Table 4.1: Listing of the station numbers, geographic positions, water depths and recovery of marine ash cores used for pore water studies.

Station	Location			Water Depth	Recovery
	Latitude (N)	Longitude (W)		(m)	(cm)
173-15	10°43.16	88°54.09	incom. plate	3288	626
173-18	11°36.00	87°36.00	slope	1606	400

4.3.2. Pore Water Analysis

Pore water samples were analysed on-board for total alkalinity by titration of 0.5-1 mL water with hydrochloric acid (~ 0.02 *N* HCl) according to Ivanenkov and Lyakhin (1978). To remove carbon dioxide during titration the sample was flushed with a continuous stream of pure nitrogen. The equivalence point of the titration was determined colourimetrically, using a mixture of methylene blue and methyl red as an indicator. The titration is complete when the green colour of the solution changes to light pink (*p*H = 5.5).

Phosphate (PO_4) and ammonia (NH_4) were determined by photometry according to Grasshoff et al. (1999). Modifications were necessary for samples with high sulphide concentrations. Detailed descriptions fore both methods are available at *http://www.ifm-geomar.de/index.php?id=mg_analytik.*

All pore waters were analysed for calcium and the trace metal manganese as well as the dissolved anion SO_4^{2-} in the IFM-GEOMAR laboratory using optical ICP and ion chromatography. Accuracies of analytical data are generally better than 2 %. When sample size allowed pore waters were analysed by ICP-MS for REE (La, Ce, Pr, Nd, Eu) at the University of Bremen, Germany. Details on the methods and information on precisions and accuracies (1σ values ranging from 6 to 8 %) are given elsewhere (*www.palmod.uni-bremen.de/FB5/Ozeankruste/*).

4.3.3. On-Board Sediment Investigations

The sediment inventory (minerals, glass shards, lithics, biogene material) was preliminary determined and quantitative estimated by using a binocular eyepiece and smear slides. Smear slides were prepared by dispersing sediment material on microscope slides and fixing the sample with resin (Meltmount). The "thin sections" were examined under a petrographic microscope.

4.3.4. Solid Phase Analysis

At the home laboratory all sediment samples (bulk sediments as well as background sediments of ash layers) were freeze dried. For total carbon, nitrogen, and sulphur analyses the freeze dried samples were grinded in an agate mortar (C/N-analyses) or in a mill (S-analyses). Depending of the C/N/S concentration, 3-20 mg of sample was weighed into a tin cup (C/N/S) or silver cup for the POC measurements. For sulphur determination the same amount of Vanadiumpentoxid was added to the sample. Organic carbon is determined after removing carbonate carbon by acidification with 0.01 *N* hydrochloric acid (Verardo et al., 1990). The analyses were performed using an Carlo Erba Elemental Analyser.

REE concentrations (La – Lu) of all solids have been determined by Laser Ablation ICP-MS at the Mineralogical Institute, University of Frankfurt am Main. Small glass grains of marine ash layers as well as of experimentally altered glass shards have been epoxy embedded to prepare polished petrographic thin sections. The main standard used was NIST612. The accuracy is expressed by the difference between the reference values of the geochemical standard and the values measured. Due to higher REE-concentrations in solids accuracies of this measurement are better with 1σ values varying between 1 to 3 %.

4.3.5. Age Determination of Volcanic Ashes

For age determination volcanic ash samples were analysed at the Leibniz Laboratory for Radiometric Dating and Isotope Research at the University of Kiel. The selected samples were mechanically cleaned under the microscope, afterwards sieved, and dark organic-looking material < 250 µm was selected for further treatment. The residual

material was then extracted with 1 % HCl and 1 % NaOH at 60°C and again with 1 % HCl. The alkali extraction of the organic fraction (humic acid fraction) was precipitated with HCl, washed, and dried. The combustion to CO_2 of all fractions was performed in a closed quartz tube together with CuO and silver wool at 900°C. The ^{14}C concentration of the samples was measured by comparing the simultaneously collected ^{14}C, ^{13}C, and ^{12}C beams of each sample with those of Oxalic Acid standard CO_2 and coal background material. The ^{14}C ages were calculated according to Stuiver and Polach (1977) with a $\delta^{13}C$ correction for isotopic fractionation based on the $^{13}C/^{12}C$ ratio measured by the AMS-system simultaneously with the $^{14}C/^{12}C$ ratio.

4.3.6. Glass Dissolution Experiments

In addition to pore water extraction and analyses, laboratory experiments were conducted to determine whether volcanic ashes in contact with seawater could achieve dissolved REE concentrations equivalent to or greater than their pore water dissolved REE concentrations. Mafic and felsic volcanic glasses, collected along the volcanic front of Nicaragua were used in these experiments. The experiments were conducted in a temperature range of 25-100°C and a pressure range of 1-400 bar for a maximum duration of 48 hours using a water/rock ratio of 10 (10 g water/1 g ash). Detailed information on experimental set-up, starting seawater composition as well as sample preparation and handling are given in Schacht et al. (submitted).

4.4. Results and Discussion

4.4.1. Lithology and Geochemical Composition of Sediments

4.4.1.1. Background Sediments – Gravity cores discussed in this work were taken on the incoming oceanic plate (SO173-15) and continental slope offshore Nicaragua (SO173-18) (Fig.4.1, Tab. 4.1). The background sedimentation of all cores is generally built up through alternating beds of finer (medium silt to silty clay) and coarser (sandy clay to clayey sand) layers. Generally, beyond the clay minerals and lithic content, plagioclase is the most abundant component in the background sedimentation. Additionally, heavy minerals like ortho- and clino-pyroxene, magmatic spinel, olivine, hornblende are pervasive. In some cases biotite and magmatic quartz, demonstrate the strong volcanic entry into the marine sediments, whereas the latter three and partly the

orthopyroxenes are indicators for more evolved felsic volcanism. Biogenic compounds of pelagic origin (organic carbon, diatomaceous silica frustules, carbonate) contributed only to small amounts in core SO173-15, while C_{org} concentrations in core SO173-18 are unusually high (Fig. 4.2). Background sediments of both cores also contain various amounts of pyrite.

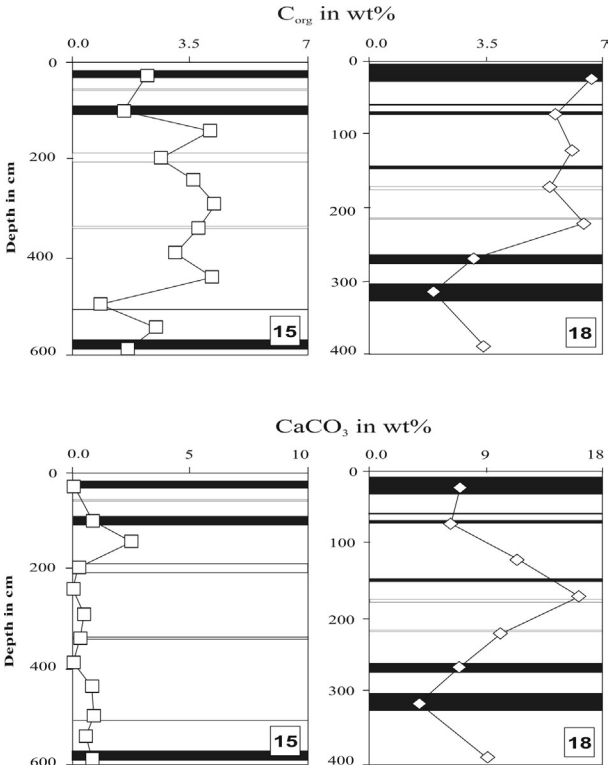

Figure 4.2: Chemical sediment composition of cores SO173-15 and 18. White bars indicate felsic, black bars indicate mafic ash layers.

In general, the sedimentation should be very homogenous and only be disturbed by the varying volcanic input leading to ash layers in the extreme case. Sedimentation rates for all core sites described in this paper are between 80 m Myr^{-1} on the incoming plate and 300 m Myr^{-1} at the continental slope (Kutterolf et al., in press). However, the high input of material from the arc leads to slope instability, which can cause slumping and slides in the more inclined regions of the deposition area.

4.4.1.2. Volcanic Ash Layers – In both sediment cores volcanic ash is found as up to 20 cm thick ash layers (Fig. 4.3). Additionally dispersed ashes (detectable by microscope) are present throughout the sediment column. Compared with volcanic ash-free sediment, ash layers show marked differences in porosity, water content, and grain size (see Appendix). A sharp lower boundary is typical for most of the ash layers and the uppermost part is

mostly mixed with background sediment showing a diffuse, relatively large transition zone (up to 50 cm) to the superposed pelagic sediment. Additionally, some ash layers are disturbed through bioturbation at the top and the base of the layer.

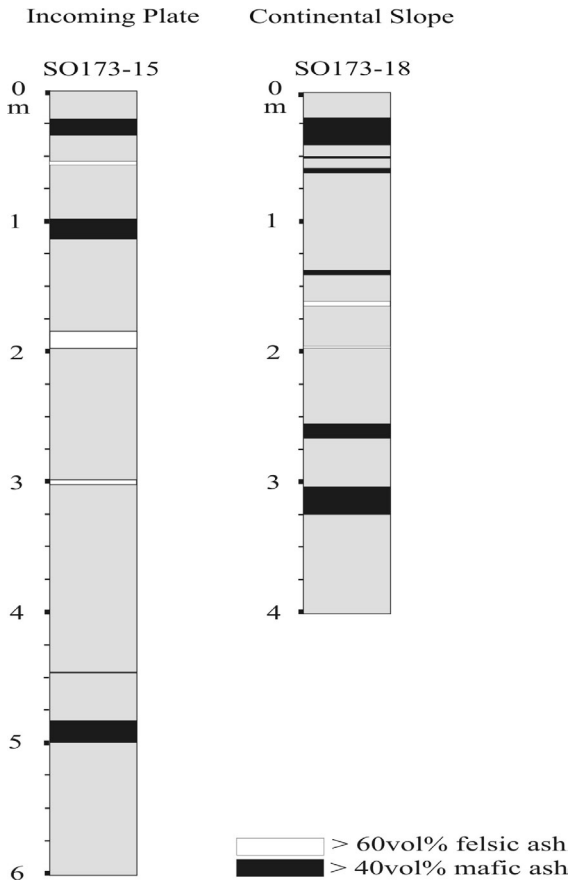

Figure 4.3: Lithologies of described sediment cores SO173-15 and 18. Descriptions in full length are given in the text.

Most of the ash layers are white to greyish-pink or dark-grey to pink light-grey in colour. Mostly, dark grey layers are of basaltic to andesitic, and pinkish-white layers are of dacitic to rhyolitic composition. Microscopic examination of light-coloured ashes shows mostly clear, colourless, volcanic glass shards and pumice fragments commonly with elongated vesicles. Dark-grey ash layers consist predominantly of a mixture of brown glass shards, black, vitreous and opaque particles and numerous light and heavy minerals. The typical grain size of the ash-layers varies in the range of medium silt to medium/ coarse sand (< 250 μm). Mineral assemblages comprise plagioclase, clinopyroxene, plus olivine in the mafic, hornblende, ortho-pyroxene in more evolved, as well as occasionally biotite and magmatic quartz in the most-evolved felsic layers. The volcanic material shows glass shards in various stages of alteration. At the scale of optical microscope we could distinguish felsic ash as mostly *fresh* volcanic glass shards while mafic ash layers consisted predominantly of glass, showing distinct signs of alteration and secondary mineralisation.

4.4.2. Geochemistry of Pore Waters

The composition of pore fluids measured in the retrieved sediment cores is shown in Figure 4.4. The alkalinity-depth profiles show the general pattern of a regular increase with sediment depth due to the microbial degradation of organic matter. The small alkalinity increase with depth found for core SO173-15 is typical for incoming plate sediments near the trench reflecting the reduced input of organic carbon (e.g. Zuleger, 1996). The alkalinity increase with depth is much stronger for core SO173-18 taken in continental slope sediments. The higher alkalinity values in this core reflect the rapid accumulation of organic carbon rich sediments typical for slope site sediments and high degradation rates (e.g. Zuleger, 1996).

The distribution patterns of sulphate mirror the alkalinity trends (Fig. 4.4a). SO_4 concentrations decrease with sediment depth due to microbial sulphate reduction (e.g. (Manheim, 1976; Presley and Trefry, 1980; Sayles et al., 1973). However, sulphate concentrations are still rather high at the base of the core SO173-15 showing that the microbial consumption of sulphate proceeds at rather low rates. The slope site core SO173-18 shows a redox reaction sequence which is characteristic for hemipelagic sediments, with a reaction zone compressed towards the sediment water interface. Sulphate is rapidly consumed below 100 cm depth (Fig. 4.4a).

The very active bacterial sulphate reduction at core site SO173-18 and consequent evolution of HCO_3^- has evidently led to the precipitation of $CaCO_3$, like it is described by other authors (e.g. Gieskes, 1990; Manheim, 1976; Presley and Trefry, 1980; Sayles et al., 1973), resulting in a strong decrease of dissolved calcium concentrations with depth (Fig. 4.4b). Dissolved Manganese concentrations are much lower than in core SO173-15, indicating that Mn is probably also precipitated in carbonate minerals at site SO173-18.

4.4.3. Modelling Rates of Organic Matter Degradation

During the microbial degradation of organic matter, metabolites such as ammonia and phosphate are released into the pore water (Fig. 4.4c) to be transported through the sediment column via diffusion and burial. Assuming steady-state conditions, the turnover

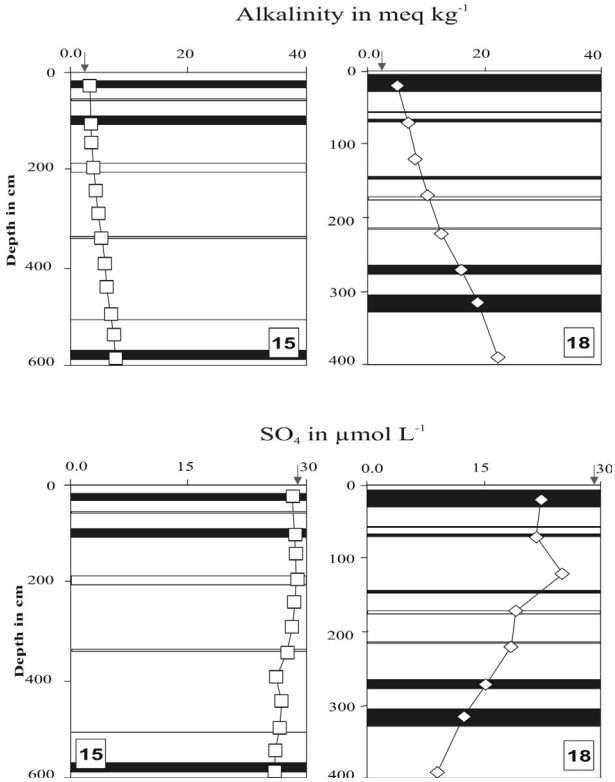

Figure 4.4a: Pore water concentration-depth profiles for sediment cores SO173-15 and 18. White bars indicate felsic, black bars indicate mafic ash layers, while arrows mark overlying seawater composition.

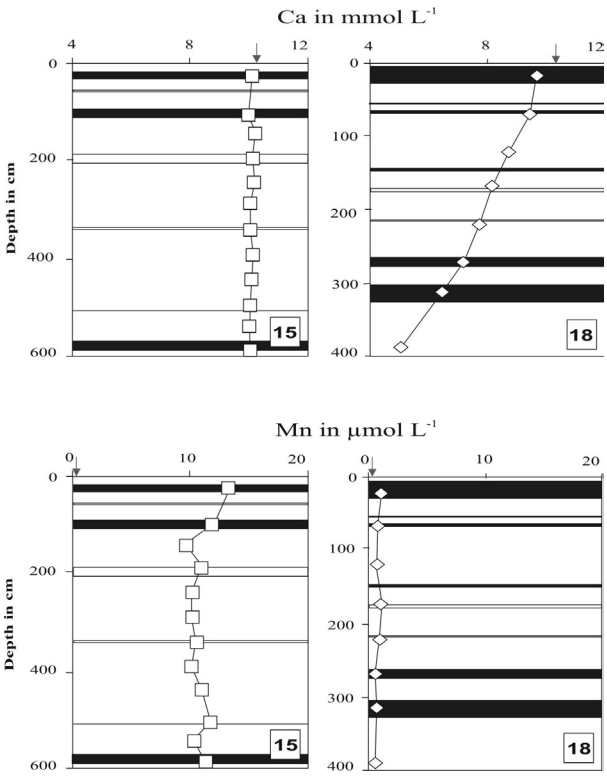

Figure 4.4b: Pore water concentration-depth profiles for sediment cores SO173-15 and 18. White bars indicate felsic, black bars indicate mafic ash layers, while arrows mark overlying seawater composition.

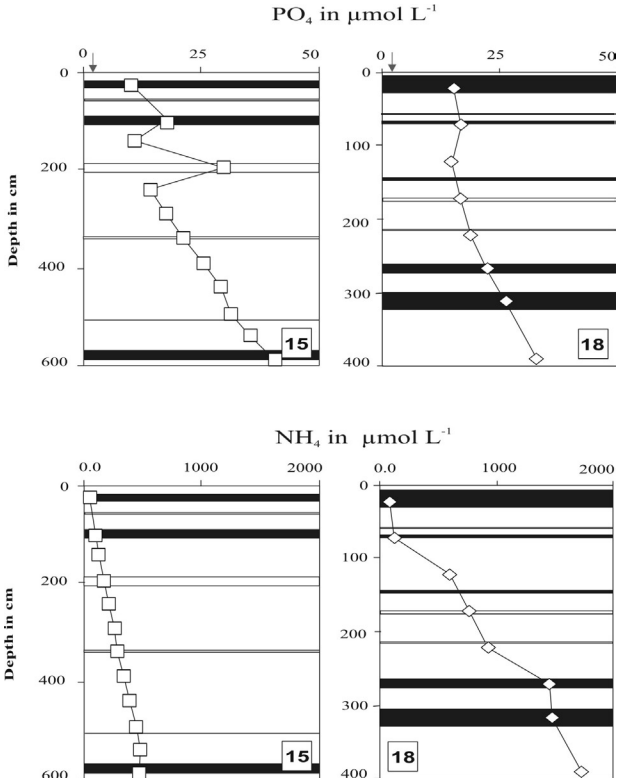

Figure 4.4c: Pore water concentration-depth profiles for sediment cores SO173-15 and 18. White bars indicate felsic, black bars indicate mafic ash layers, while arrows mark overlying seawater composition.

of metabolites in sediments can be described by the following differential equation (Berner, 1980):

$$D \cdot \frac{d^2C}{dx^2} - v \cdot \frac{dC}{dx} + R = 0 \qquad (1)$$

where D is the molecular diffusion coefficient of the dissolved metabolite in the regarded sediment segment, C is the concentration in the pore water, x is sediment depth, v is the burial velocity and R is the rate of metabolite release into the pore water. The equation is valid for a homogenous sediment column with constant porosity.

The concentration and reactivity of organic matter and, hence, the rate of metabolite release usually decrease with sediment depth. Assuming an exponential decay of the release rate with depth:

$$R = r_0 \cdot e^{-p \cdot x} \qquad (2)$$

and the following boundary conditions:

$C(0) = c_0$ and $C'(\infty) = 0$.

The analytical solution of the differential equation results as:

$$C = \frac{r_0 \cdot \left(1 - e^{-p \cdot x}\right)}{p \cdot \left(D \cdot p + v\right)} + c_0 \qquad (3)$$

Applying the equations given in Boudreau (1997), the diffusion coefficient of ammonia in sediments (at a temperature of 2°C, a salinity of 35, and a porosity of 0.8) results as 217 $cm^2\ yr^{-1}$. Dissolved phosphate occurs in sediments mainly as HPO_4^{2-} and $H_2PO_4^-$. The average diffusion coefficient of these two species is used in the calculations and results as 85 $cm^2\ yr^{-1}$ applying the same physical conditions and equations as before. The burial velocity v is 30 cm kyr^{-1} at the slope (core SO173-18) and 8 cm kyr^{-1} on the incoming plate (core SO173-15) (Kutterolf et al., in press).

The degradation rates of organic matter and the corresponding model parameters (r_0: rate of ammonia release at zero depth, p: attenuation coefficient for the exponential decay of degradation rate with depth) were constrained by fitting to the model to the ammonia pore water data (Fig. 4.5a). The same p value of 0.001 cm^{-1} was used for both cores while r_0 values differed significantly between the two cores. A large r_0 value was obtained for the slope core SO173-18 (r_0 = 1.3 mmol NH_4 $cm^{-3}\ yr^{-1}$) while a much smaller value was determined for core SO173-15 taken on the incoming oceanic plate (r_0 = 0.22 mmol NH_4 $cm^{-3}\ yr^{-1}$). The one order of magnitude difference in this model parameter reflects the much higher rate of organic matter degradation prevailing at the continental slope. Sedimentary degradation rates are regulated by the rain of organic matter to the seafloor and the burial of organic matter below the bioturbated surface layer. As export production and sedimentation rates are usually higher at the continental margins, sedimentary degradations are enhanced at the slope compared to open ocean setting. This general trend is also observed in the two sediment cores investigated in our study.

As a next step in the modelling procedure, dissolved phosphate concentrations were calculated using the rate parameters derived from the ammonia data and multiplying the release rates with the P : N ratio (Redfield ratio) of marine organic matter (1/16). The model values obtained for core SO173-15 were usually higher than the measured values. This is not a surprising result since phosphate is known to form authigenic minerals (mainly carbonate fluorapatite) in marine sediments (Ruttenberg and Berner, 1993). The concentration of dissolved phosphate in the pore water is diminished by the precipitation process which is not considered in the modelling. Hence, the difference between the model curve and the data probably reflects the on-going precipitation of phosphate-

bearing minerals. In slope core SO173-18, measured phosphate concentrations were much lower than the model values throughout the entire core (Fig. 4.5b) indicating that most of the phosphate released by the degradation of organic matter was subsequently removed from the pore fluids by the precipitation of phosphate-bearing minerals.

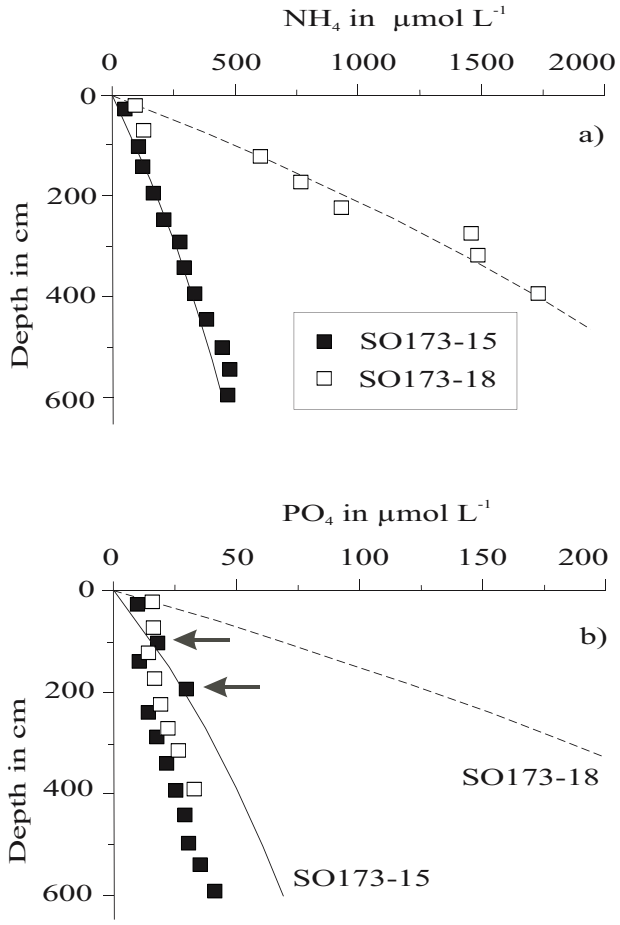

Figure 4.5a-b: Dissolved metabolites of organic matter degradation in sediment pore waters – (a) Ammonia concentrations, (b) Phosphate concentrations. Data are given as solid and open squares and model results are plotted as solid and broken lines for cores SO173-15 and SO173-18, respectively. The two arrows in the lower panel mark the ash layers in core SO173-15 where the highest REE concentrations were observed.

4.4.4. REE Distribution in Pore Waters

At station SO173-18 pore waters are enriched in dissolved REE contents (Fig. 4.6) when compared to the overlying seawater composition given in Table 4.2, demonstrating that REE are mobilised during early diagenesis. However, REE concentrations show no or only minor concentration maxima within ash layers. Like described above core site SO173-18 represents the environment for continental slope sediments. Under this conditions ash layers obviously provide only as little REE input into pore waters as described for the background sediments.

Station SO173-15, the core furthest offshore, represents best the incoming plate environment of mildly reducing conditions. Its REE concentration depth profile shows enriched REE contents in pore waters of background sediments when compared to seawater (Fig. 4.6), but in contrast to SO173-18 the REE concentrations are especially high in pore waters of the volcanic ash layers (note scales in Fig. 4.6). The largest REE enrichment is observed for Ce, which reaches concentrations more than 10^3 higher than the deep ocean water value of 5.89 pmol kg^{-1} according to Piepgras and Jacobsen (1992) (Tab. 4.2).

Table 4.2: Rare earth element composition of North Pacific seawater for two different depth horizons according to Piepgras and Jacobsen (1992).

	La	Ce	Pr	Nd	Sm	Eu	unit
Depth in m			Averg. surface water North Pacific				
0-1000	25.7	5.66	no data	16.2	3.04	0.81	pmol kg^{-1}
Depth in m			Averg. deep water North Pacific				
1000-6000	53.8	5.89	no data	36.2	6.84	1.79	pmol kg^{-1}

4.4.4.1. Standard normalised Patterns – The variation of REE in natural materials can be smoothened out by normalising each REE concentration in the sample to one standard on an element-by-element basis. The standard chosen for our seawater normalisation is an average of REE concentrations in the North American Shale Composite (NASC). Plotting the concentration ratios on a log scale versus atomic number, allows the direct comparison of its REE pattern with that of another sample and slight but significant differences can easily be evaluated.

The NASC-normalised patterns for the measured pore waters are given in Figure 4.7. REE data for overlying seawater are displayed in Figure 4.7a according to Piepgras and Jacobsen (1992). REE patterns of pore water from background sediment are plotted in Figure 4.7b and ash layer related pore water data are given in Figure 4.7c.

All background sediment pore water patterns show the typical negative Ce anomaly (Fig. 4.7b). Goldberg (1961) was the first to suggest an explanation for this, which has not been contradicted. He proposed that Ce^{3+} in the oceans is oxidised to Ce^{4+} and is precipitated from the solution as CeO_2, while the other REE remain in the 3+ state. For ash layer related pore waters of slope core SO173-18 this overall trend is confirmed, reflecting only little REE release during ash alteration. At oceanic plate core site

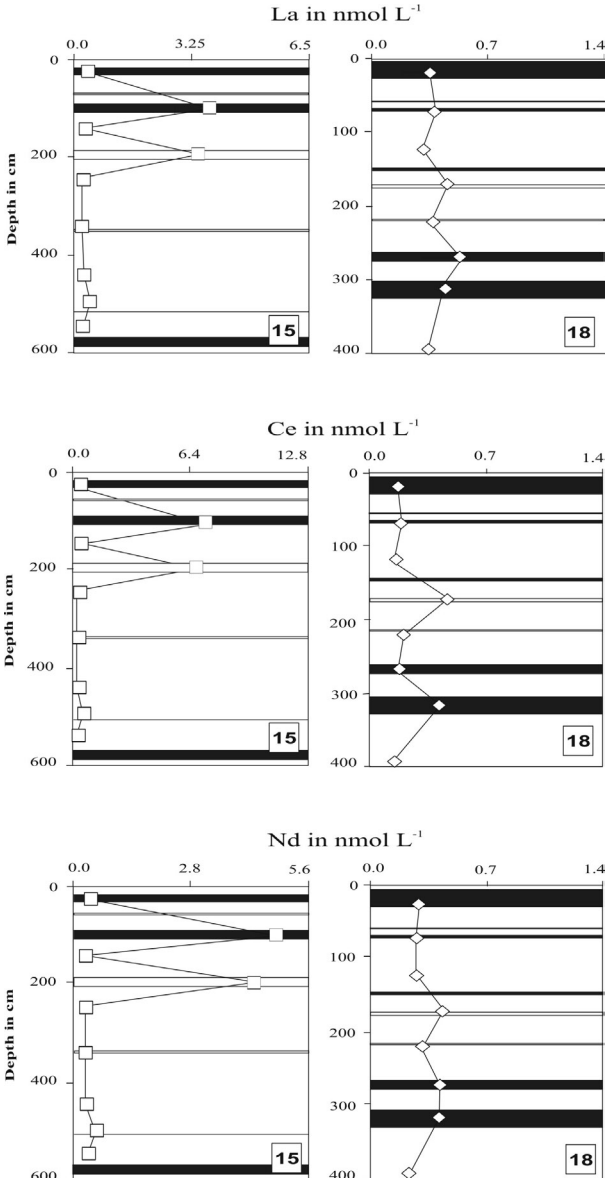

Figure 4.6: Pore water concentration-depth profiles of selected REE for sediment cores SO173-15 and 18. White bars indicate felsic, black bars indicate mafic ash layers.

SO173-15 the above described pattern vanishes and the Ce anomaly becomes positive, resulting in a linear fashion (Fig. 4.7c). This flattening effect was already described by Sholkovitz et al. (1989) and was ascribed to diagenetic processes in slope sediments but without considering single ash layers. Based on our work we consider this to be a common phenomenon in pore waters influenced by ash alteration especially when open ocean diagenetic conditions occur. The significance of this flattening effect is also confirmed by the chemical composition of pore waters derived from our experimental work (Fig. 4.7d). After only 48 hours of alteration at 400 bar and 24°C seawater shows comparable REE pattern like the ash layer related pore waters described above of oceanic plate core SO173-15.

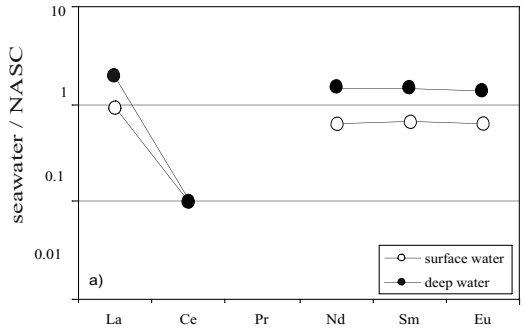

Figure 4.7a: REE patterns normalised to NASC of North Pacific surface and deep water according to Piepgras and Jacobsen (1992).

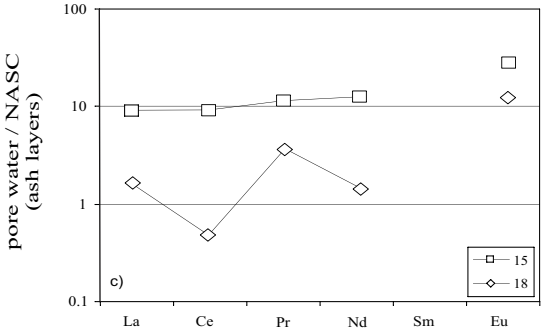

Figure 4.7b: Average of all REE patterns normalised to NASC of pore waters not directly related to the single ash layers within the investigated ash cores.

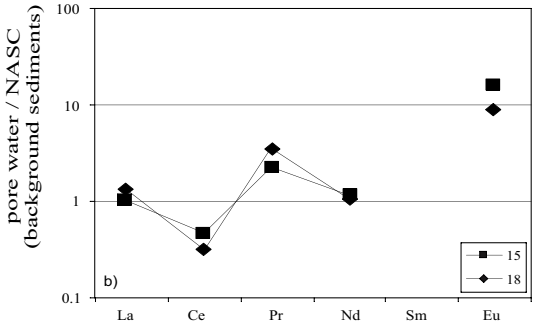

Figure 4.7c: Average of all REE patterns normalised to NASC of pore waters related to the single ash layers within the investigated ash cores. Compared to the typical seawater pattern a clear flattening of the pattern due to the chemical input by ash alteration can be noticed for pore waters of core SO173-15.

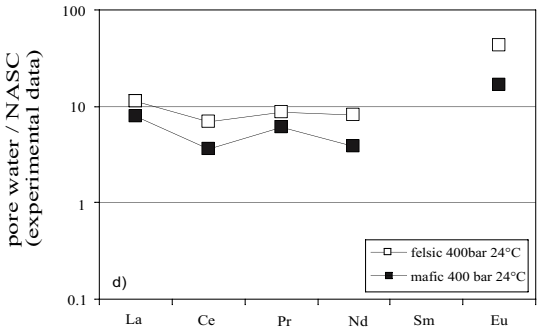

Figure 4.7d: REE patterns normalised to NASC of pore waters derived from tephra alteration experiments. After only 48 houres at 400 bar and 24°C seawater already is marked by a clear flattening of its typicall REE-pattern due to the chemical input by ash alteration.

To specify the REE behaviour during volcanic ash alteration we also conducted solid phase analyses via LA-ICP-MS of mafic and felsic glass shards taken from marine sediment cores (ages: felsic-21 kyr, mafic-18 kyr) and of experimentally altered mafic and felsic ones (24 h, 200 bar, 100°C). Altered rim and fresh centre composition normalised to chondrite are given in Figures 4.8a & b. Figure 4.8a clarifies that during seawater alteration under sea floor conditions (low temperatures about 2°C and elevated pressures > 200 bar), glass shards are characterised by a systematic decrease in REE concentrations at the rim. Figure 4.8b displays a chemical depletion of the glass shard's outer rims, is already shown after only 24 hours, indicating that REE release already starts within the very initial alteration stage. Therefore ashes, when deposited in a marine environment, constitute not only a major but also a continuous sources for rare earth elements.

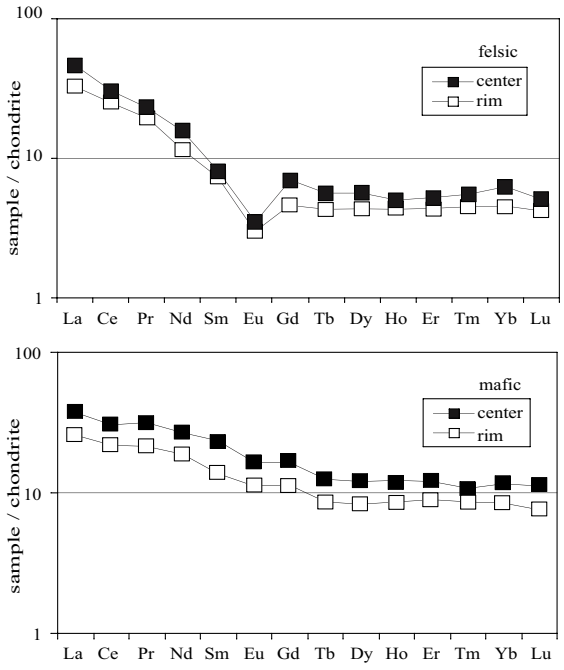

Figure 4.8a: Laser ablation ICP-MS data indicating a systematic release of rare earths out of the rim with respect to the core of volcanic glasses taken from marine ash layers (age: felsic 21 kyr, mafic 18 kyr).

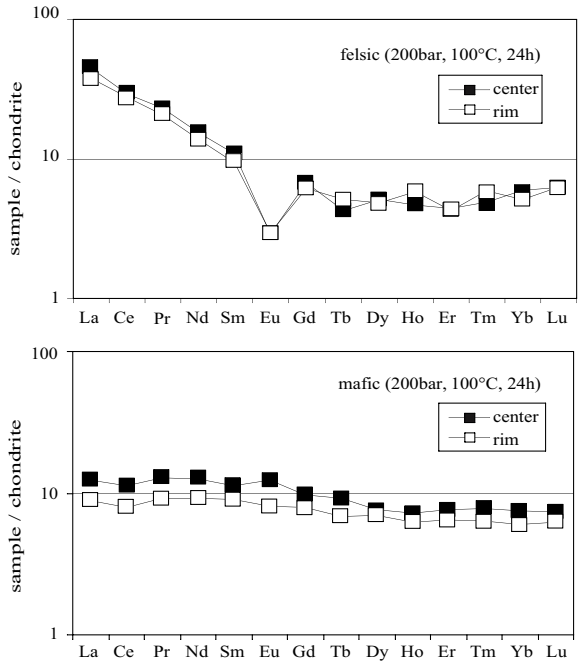

Figure 4.8b: Laser ablation ICP-MS data indicating a systematic release of especially light rare earths at the rim with respect to the core of experimentally altered volcanic glasses, after 24 hours seawater alteration at 200 bar and 100°C.

4.4.5. The Significance of REE Release during Ash Alteration

According to Straub and Schmincke (1998) more than 23 % of the marine sediments in the Pacific Ocean, covering approx. half of the Earth's surface (~49 %), consist of tephra. Since volcanic material constitutes such an important part we discuss below, if the REE release during volcanic ash alteration described in this work will have consequences on the chemical budget of ocean water.

Our investigations point out that the release of REE into pore water by volcanic ash alteration processes is most effective under mildly reducing conditions. Therefore we used the detected concentration gradients of core site SO173-15 (Fig. 4.6) to derive rates of rare earth element releases as a function of depth and pore water chemistry based on the following equation:

$$R_X = \frac{J_1 + J_2}{\Delta x} \tag{4}$$

where R_X describes the element's diffusion rate, J_1 and J_2 are the diffusive fluxes above and below the ash layer and Δx is the thickness of the relevant ash layer (also see Fig. 4.9). Diffusive fluxes were calculated using Fick's first law of diffusion modified for the application in sediments and other porous media by adding the porosity factor Φ (Boudreau, 1997):

$$J_{Sed} = -\Phi \cdot D_{Sed} \cdot \frac{\partial C}{\partial x} \tag{5}$$

Equation 2 was modified to a finite difference equation:

$$J = -\Phi \cdot D_{Sed} \cdot \left(\frac{c_1 - c_2}{\Delta x} \right) \tag{6}$$

and the diffusion coefficients in sediments (D_{sed}) were calculated for the prevailing porosity and temperature using the relations published by Boudreau (1997).

Assuming that the REE diffusive fluxes between ash layers and background sediments reflect the rare earth element fluxes out of an ash layer and can be applied at the sediment/seawater interface, values of at least 0.04 nmol La cm^{-2} yr^{-1} and 0.09 nmol Ce cm^{-2} yr^{-1} into the ocean can be suggested (Tab. 4.3). To estimate the importance of these release rates we compared them to input rates given in literature. These data (Tab. 4.3) illustrate that our minimum release rates are of the same magnitude like input rates, concerning

all possible terrestrial sources, given by Elderfield and Greaves (1982) as well as by Piper (1974).

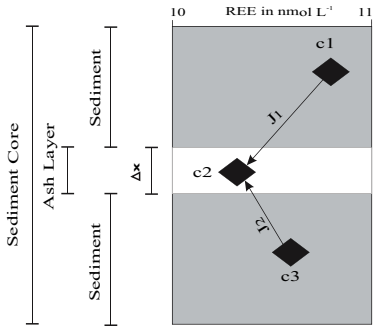

Figure 4.9: Schematic draft for diffusive flux calculations between ash layers and their background sedimentation.

The research work done by Kutterolf et al. (in press) point out that the major part (~75 %) of tephra occurring in Pacific sediments is of felsic composition. Our solid phase analyses of 21 kyr old felsic altered glass shards (Fig. 4.8a) offer data that can be used to calculate the significance of ash alteration processes on the REE Pacific Ocean budget. After 21 kyr of seawater alteration the outer rims (5 µm) of the single investigated felsic glass shards (in average 100 µm in diameter) released portions of lanthanum and cerium correlating to about 30 and 15 percent for the available amount (Fig. 4.8a). Just by assuming a minimum input rate of 10.000 km^3 Myr^{-1} tephra into the Pacific Ocean (Straub and Schmincke, 1998) and that ¼ of this material is deposited on the surface of deep sea sediments, this volcanic ash input would release about 80 g La and 65 g Ce into the ocean each year. As currently understood, the major input of REE into the ocean is river water (Rasmussen et al., 1998). The calculated average river input rates (Tab. 4.3), based on the data published by Elderfield et al. (1990), result in an annual river input of the same magnitude with 103 g La and 188 g Ce.

Table 4.3: Rates of La and Ce input into the ocean taken from literature and calculated for this work. River input rates were calculated based on the data of river water composition published by Elderfield et al. (1990), assuming an annual water flow of 3.6 x 10^{16} L. The term 'total input' summarises all terrestrial La and Ce sources for the ocean. Release rates and -fluxes contribute to ash alteration processes and were calculated in this work based on solid phase analyses as well as pore water data.

	Element		Unit	Reference
	La	Ce		
river input rate	103	188	g yr^{-1}	based on data by Elderfield et al. (1990)
release rate	78.2	66.1	g yr^{-1}	this work
total input flux	0.058	0.101	nM cm^{-2} yr^{-1}	Elderfield & Greaves (1982), Piper (1974)
max. release flux	0.421	0.908	nM cm^{-2} yr^{-1}	this work
min. release flux	0.044	0.090	nM cm^{-2} yr^{-1}	this work

4.4.6. REE Removal from Pore Waters

The highest concentrations of dissolved REE occurred in the two prominent ash layers of core SO173-15 where pronounced maxima in dissolved phosphate were observed (Fig. 4.4c & 4.6). The phosphate concentrations measured in these ash layers were very close to the model curve indicating that phosphate-bearing minerals were not formed in these layers (marked by arrows in Fig. 4.5b). In all other sections of the two studied sediment cores, dissolved REE concentrations were much lower and phosphate precipitation occurred. Hence, the modelling of nutrient data strongly suggests that high concentrations of dissolved REE in marine pore waters can only be maintained in the absence of phosphate precipitation processes (marked by arrows in Fig. 4.5b). The carbonate fluorapatites (CFA) which commonly occur as authigenic minerals in marine sediments may be a major sink not only for dissolved phosphate (Delaney, 1998; Wallmann, 2003) but also for REE released from marine volcanic ash layers.

Our investigations made above imply that the REE generated from volcanic ash alteration are quickly removed from pore waters. This result is in good accommodation with previous works suggesting, on theoretical and experimental grounds, that the precipitation of early diagenetic phosphates should remove REE from marine waters (Byrne and Kim, 1993; Jonasson et al., 1985; Rasmussen et al., 1998). However, Turner and Whitfield (1979) concluded that REE can also be immobilised due to the adsorption on various mineral surfaces. Subsequently, with ongoing diagenesis within the sediments, the REE are incorporated into various authigenic mineral lattices. Based on the research work done by Coppin et al. (2002) the incorporation of REE into clay minerals like smectite can be suggested as a potential sink. Because clay minerals are predominant in sediments entering the Middle American subduction zone (Spinelli and Underwood, 2004) it is possible that these minerals are also of importance for REE fixation within the investigated sediments.

It should be mentioned that according to Sholkovitz (1992) it seems that a non-negligible part of the removed REE (~10 %) is remobilised during diagenesis and may re-enter the water column. Our simple evaluations therefore clarify, that volcanic ash alteration represents a substantial REE supply to pore waters.

4.5. Conclusions

Up to now, it was commonly believed that reactive solid phase REE in marine sediments occur dominantly in particulate coatings composed of Fe-oxides, Mn-oxides and organic matter and in discrete Ce-oxides. However, our study demonstrates, that volcanic ashes provide an additional and very important source of REE in marine sediments. Due to their dissolution behaviour in marine pore waters it seems likely that the release of the REE is linked to anerobic organic matter degradation and most effective when open ocean conditions with low degradation rates prevail. Considering the high REE release rates from marine ash layers (i.e. max. 0.9 nmol Ce cm^{-2} yr^{-1}), it is likely that the REE distribution in ocean waters and sediments is affected by large tephra outfalls due to REE release from reactive volcanic glasses**.**

Certainly conclusions like that can not be directly extrapolated to the case of long-term safety of nuclear waste disposal but the mobility observed here for rare earth elements can also have important consequences for the storage of nuclear waste in the form of glass. It is clear from our results that REE, particulary light REE, can be significantly mobilised during alteration processes. Former studies by Daux et al. (1994) as well as by Mungall and Martin (1994) show that U, Th, and REE behaviours are similar during alteration suggesting that U, Th and other high-field strength heavy elements can be released in significant amounts on short time scales during glass alteration.

Acknowledgments

We thank captain and crew of RV *Sonne* 173/3 for their support during our research cruises as well as the scientific party for the good working atmosphere. Trace element analysis were able due to the accommodating aid by Yann Lahaye and Heike Anders. We owe special thank to Bettina Domeyer, Kristin Nass and Regina Surberg for their help during sample preparation and handling on board as well as in the lab.

References

Barckhausen U., Ranero C., von Huene R., Cande S., and Roeser H. (2001) Revised tectonic boundaries in the Cocos Plate off Costa Rica: Implications for the segmentation of the convergent margin and for plate tectonic models. *Journal of Geophysical Research* **106**(19), 207-220.

Berner R. A. (1980) *Early Diagenesis - A Theoretical Approach*. Princeton University Press.

Boudreau B. (1997) *Diagenetic models and their implementation - Modelling transport and reactions in aquatic sediments*. Springer.

Boudreau B. P. (1997b) *Diagenetic Models and Their Implementation*. Springer-Verlag.

Byrne R. and Kim K.-H. (1993) Rare earth precipitation and coprecipitation behaviour: The limiting role of PO_4^{3-} on dissolved rare earth concentrations in seawater. *Geochimica et Cosmochimica Acta* **57**, 519-526.

Carr M. (1984) Symetrical and segmented variation of physical and geochemical characteristics of the Central American Volcanic Front. *Journal of Volcanology and Geothermal Research* **20**, 231-252.

Coppin F., Berger G., Bauer A., Castet S., and Loubet M. (2002) Sorption of lanthanides on smectite and kaolinite. *Chemical Geology* **182**, 57-68.

Daux V., Crovisier J.-L., Hemond C., and Petit J. (1994) Geochemical evolution of basaltic rocks subjected to weathering: Fate of major elements, rare earth elements, and thorium. *Geochimica et Cosmochimica Acta* **58**(22), 4941-4954.

Delaney M. L. (1998) Phosphorus accumulation in marine sediments and the oceanic phosphorus cycle. *Global Biogeochemical Cycles* **12**(4), 563-572.

Elderfield H., Goddard-Upstill R., and Sholkovitz E. R. (1990) The rare earth elements in rivers, estuaries, and costal seas and their significance to the composition of ocean waters. *Geochimica et Cosmochimica Acta* **54**, 971-991.

Elderfield H. and Greaves M. (1982) The rare earth elements in seawater. *Nature* **296**, 214-219.

Elderfield H. and Sholkovitz E. (1987) Rare earth elements in the pore waters of redusing nearshore sediments. *Earth and Planetary Science Letters* **82**, 280-288.

Gieskes J., Blanc G., Vrolijk P., Elderfield H., and Barnes R. (1990) Interstitial water chemistry - major constituents. *Proceedings of the Ocean Drilling Program, Scientific Results* **110**, 155-177.

Goldberg E. (1961) Chemistry in the oceans. *Oceanography* **67**, 583-597.

Grasshoff K., Ehrhardt M., and Kremling K. (1999) *Methods of Seawater Analysis*. Wiley-VCH.

Haley B., Klinkhammer G., and McManus J. (2004) Rare earth elements in pore waters of marine sediments. *Geochimica et Cosmochimica Acta* **68**(6), 1265-1279.

Ivanenkov V. and Lyakhin Y. (1978) Determination of total alkalinity in seawater. In *Methodes of hydrochemical investigations in the ocean* (ed. V. Ivanenkov), pp. 110-114. Nauka Publ.

Jonasson R., Bancroft G., and Nesbitt H. (1985) Solubilities of some hydros REE phosphates with implications for diagenesis and seawater concentrations. *Geochimica et Cosmochimica Acta* **49**, 2133-2139.

Kimura G., Silver E., and Blum P. (1997) Costa Rica accretionary wedge, Sites 1039-1043. *Palaeogeography, Palaeoclimatology, Palaeoecology* **170**, 458.

Klinkhammer G., Elderfield H., Edmond J., Greaves M., and Mitra A. (1994) Geochemical implications for rare earth element patterns in hydrothermal fluids from mid-ocean ridges. *Geochimica et Cosmochimica Acta* **58**, 5105-5113.

Klinkhammer G., Elderfield H., and Hudson A. (1983) Rare earth elements in seawater near hydrothermal vents. *Nature* **305**, 185-188.

Koeppenkastrop D. and de Carlo E. (1992) Sorption of rare-earth elements from seawater onto synthetic mineral particles: An experimental approach. *Chemical Geology* **95**, 251-263.

Kutterolf S., Schacht U., Wehrmann H., Freundt A., and Moerz T. (in press) Onshore to offshore tephrostratigraphy and marine ash layer diagenesis in Central America. In *Central America - Geology, Resources and Hazards* (ed. J. Buntschuh). Balkema.

Manheim F. (1976) Interstitial waters of marine sediments. In *Chemical Oceanography* (ed. R. Chester), pp. 115-186. Academic Press, Inc.

McLennan S. (1994) Rare earth element geochemistry and the "tetrad" effect. *Geochimica et Cosmochimica Acta* **58**(9), 2025-2033.
Mungall J. and Martin R. (1994) Severe leaching of trachytic glass without devitrification, Terceira, Arzores. *Geochimica et Cosmochimica Acta* **58**, 75-83.
Piepgras D. and Jacobsen S. (1992) The behaviour of rare earth elements in seawater: Precise determination af variations in the North Pacific water column. *Geochimica et Cosmochimica Acta* **56**, 1851-1862.
Piper D. (1974) Rare earth elements in ferromanganese nodules and other marine phases. *Geochimica et Cosmochimica Acta* **38**, 1007-1022.
Presley B. and Trefry J. (1980) Sediment-water interactions and the geochemistry of interstitial waters. In *Chemistry and Biochemistry of Estuaries* (ed. I. Cato). John Wiley & Sons Ltd.
Rasmussen B., Buick R., and Taylor W. (1998) Removal of oceanic REE by authigenic precipitation of phosphatic minerals. *Earth and Planetary Science Letters* **164**, 135-149.
Rollinson H. (1993) *Using geochemical data: evaluation, presentation, interpretation*. Longman Group UK.
Ruttenberg K. C. and Berner R. A. (1993) Authigenic apatite formation and burial in sediments from non-upwelling, continental margin environments. *Geochimica et Cosmochimica Acta* **57**, 991-1007.
Sayles F., Manheim F., and Waterman L. (1973) Interstitial water studies on small core samples: Leg 15. *Initial Reports of the Deep Sea Drilling Project* **20**, 783-804.
Schacht U., Kutterolf S., Schmidt M., and Wallmann K. (submitted) The alteration of felsic and mafic tephra in marine sediments: Insights into alteration pathways and dissolution kinetics. *Geochimica et Cosmochimica Acta*.
Sholkovitz E. (1992) Chemical evolution of rare earth elements: fractionation between colloidal and solution phases of filtered river water. *Earth and Planetary Science Letters* **114**, 77-84.
Sholkovitz E., Piepgras D., and Jacobsen S. (1989) The pore water chemistry of rare earth elements in Buzzards Bay sediments. *Geochimica et Cosmochimica Acta* **53**, 2847-2856.
Spinelli G. and Underwood M. B. (2004) Character of sediments entering the Costa Rica subduction zone: Implications for partitioning of water along the plate interface. *The Island Arc* **13**, 432-451.
Straub S. and Schmincke H. (1998) Evaluating the tephra input into Pacific Ocean sediments: Distribution in space and time. *Geologische Rundschau* **87**(3), 461-476.
Strekopytov S., Dubinin A., and Volkov I. (1999) General regularities in behaviour of rare earth elements in pelagic sediments of the Pacific Ocean. *Lithology and Mineral Resources* **34**(2), 111-122.
Stuiver M. and Polach H. (1977) Discussion: Reporting of ^{14}C Data. *Radiocarbon* **19**(3), 355-363.
Turner D. and Whitfield M. (1979) Control of seawater composition. *Nature* **281**(468-469).
Verardo D., PN F., and McIntyre A. (1990) Determination of organic carbon and nitrogen in marine sediments using the CARLO ERBA NA-1500 Analyser. *Deep-Sea Research* **37**(1A), 157-165.
von Huene R., Ranero C., and Weinrebe W. (2000) Quaternary convergent margin tectonics of Costa Rica, segmentation of the Cocos Plate, and Central American volcanism. *Tectonics*(19), 314-334.
Wallmann K. (2003) Feedbacks between oceanic redox states and marine productivity: A model perspective focused on benthic phosphorus cycling. *Global Biogeochemical Cycles* **17**(3), 1084, doi: 10.1029GB001968.

Zuleger E., Gieskes J., and You C. (1996) Interstitial water chemistry of sediments of Costa Rica accretionary complex off the Nicoya Peninsula. *Geophysical Research Letters* **23**(8), 899-902.

Appendix

A1: Chemical composition of sediments (grey bars mark ash layers).

Core	Depth (cm)	C_{org} (wt%)	$CaCO_3$ (wt%)	N (wt%)	S (wt%)	H_2O (wt%)
SO173-15	25	2.20	0.00	0.24	0.36	68.6
SO173-15	100	1.47	0.87	0.16	1.05	48.5
SO173-15	140	4.08	2.45	0.44	1.30	69.0
SO173-15	193	2.63	0.21	0.27	1.10	59.4
SO173-15	240	3.59	0.00	0.38	1.27	68.3
SO173-15	290	4.20	0.51	0.44	1.43	67.7
SO173-15	340	3.75	0.23	0.42	1.71	67.0
SO173-15	390	3.03	0.00	0.33	1.20	67.8
SO173-15	440	4.15	0.82	0.46	2.03	68.2
SO173-15	496	0.82	0.85	0.10	1.03	41.9
SO173-15	540	2.50	0.48	0.30	1.53	66.3
SO173-15	590	1.58	0.83	0.20	1.03	65.8

A2: Chemical composition of pore waters (grey bars mark ash layers).

Core	Depth (cm)	Alk (meq/kg)	SO_4 (mM)	PO_4 (µM)	NH_4 (µM)	Ca (mM)	Mn (µM)
SO173-15	25	3.15	28.4	9.86	47.2	10.1	13.4
SO173-15	100	3.44	29.0	17.6	102	10.1	12.0
SO173-15	140	3.63	28.7	10.6	121	10.2	9.57
SO173-15	193	3.85	28.8	29.6	166	10.3	10.9
SO173-15	240	4.26	28.4	14.1	203	10.2	10.1
SO173-15	290	4.82	28.0	17.6	269	10.1	10.1
SO173-15	340	5.25	27.7	21.1	289	10.1	10.4
SO173-15	390	5.83	26.2	25.4	330	10.1	10.2
SO173-15	440	6.19	26.9	28.9	377	10.1	10.9
SO173-15	496	6.89	26.6	31.0	444	10.1	11.7
SO173-15	540	7.19	26.1	35.2	474	10.0	10.3
SO173-15	590	7.63	26.0	40.9	465	10.2	10.4

A3: Light REE composition of pore waters (grey bars mark ash layers).

Core	Depth (cm)	La (nM)	Ce (nM)	Pr (nM)	Nd (nM)	Eu (nM)
SO173-15	25	0.40	0.33	0.22	0.37	0.32
SO173-15	100	3.74	7.28	1.20	4.80	0.51
SO173-15	140	0.31	0.29	0.16	0.30	0.18
SO173-15	193	3.45	6.80	1.08	4.29	0.46
SO173-15	240	0.25	0.23	0.15	0.30	0.16
SO173-15	340	0.24	0.19	0.15	0.26	0.16
SO173-15	440	0.27	0.21	0.16	0.29	0.28
SO173-15	496	0.47	0.60	0.22	0.53	0.16
SO173-15	540	0.28	0.24	0.18	0.31	0.18

B1: Chemical composition of sediments (grey bars mark ash layers).

Core	Depth (cm)	C_{org} (wt%)	$CaCO_3$ (wt%)	N (wt%)	S (wt%)	H_2O (wt%)
SO173-18	20	6.67	7.78	0.70	1.07	69.7
SO173-18	70	5.56	6.93	0.55	1.34	66.1
SO173-18	120	6.08	12.7	0.65	1.26	65.1
SO173-18	170	5.40	16.4	0.55	1.18	62.6
SO173-18	220	6.42	11.2	0.66	1.31	65.8
SO173-18	270	3.08	7.64	0.31	1.77	57.7
SO173-18	315	1.88	4.27	0.20	1.79	50.6
SO173-18	390	3.41	9.55	0.35	1.62	59.9

B2: Chemical composition of pore waters (grey bars mark ash layers).

Core	Depth (cm)	Alk (meq/kg)	SO_4 (mM)	PO_4 (µM)	NH_4 (µM)	Ca (mM)	Mn (µM)
SO173-18	20	5.10	22.3	15.4	84.3	9.75	0.51
SO173-18	70	6.98	21.7	16.8	124	9.46	0.38
SO173-18	120	8.25	25.1	14.7	599	8.77	0.33
SO173-18	170	10.3	19.1	16.8	764	8.20	0.49
SO173-18	220	12.7	18.4	18.9	929	7.75	0.41
SO173-18	270	16.0	15.2	22.4	1455	7.17	0.31
SO173-18	315	18.8	12.5	26.6	1482	6.45	0.32
SO173-18	390	22.4	8.98	32.9	1726	5.06	0.31

B3: Light REE composition of pore waters (grey bars mark ash layers).

Core	Depth (cm)	La (nM)	Ce (nM)	Pr (nM)	Nd (nM)	Eu (nM)
SO173-18	20	0.37	0.18	0.23	0.29	0.11
SO173-18	70	0.42	0.20	0.23	0.28	0.20
SO173-18	120	0.35	0.15	0.23	0.27	0.10
SO173-18	170	0.52	0.49	0.28	0.44	0.13
SO173-18	220	0.40	0.21	0.26	0.31	0.13
SO173-18	270	0.62	0.18	0.26	0.41	0.33
SO173-18	315	0.49	0.42	0.28	0.41	0.16
SO173-18	390	0.37	0.15	0.25	0.24	0.16

CHAPTER V

Onshore to Offshore Tephrostratigraphy and Marine Ash Layer Diagenesis in Central America

Steffen Kutterolf[1,2], Ulrike Schacht[1,2], Heidi Wehrmann[1,2], Armin Freundt[2,1], and Tobias Mörz[3]

[1] Special Research Project 574, University of Kiel, Wischhofstr. 1-3, 24148 Kiel, Germany

[2] IFM-GEOMAR, Leibniz Institute of Marine Sciences, Wischhofstr. 1-3, 24148 Kiel, Germany

[3] Research Center Ocean Margins, University of Bremen, Am Fallturm 1, 28359 Bremen, Germany

5.1. Introduction

In Central America, as in other regions on Earth, highly explosive, plinian volcanic eruptions generate buoyant eruption columns capable of penetrating up to 40 km high into the stratosphere, until they reach the level of neutral buoyancy and spread laterally. Such eruption clouds drift with the prevailing wind and gradually drop their ash load over areas sometimes larger than 10^5 km^2. The resulting ash layers are best preserved in non-erosive marine or lacustrine environments which thus provide the most complete record of volcanic activity. Wide aerial distribution across sedimentary facies boundaries, near-instantaneous emplacement, chemical signatures facilitating stratigraphic correlations, and the presence of minerals suitable for radiometric dating make these ash layers excellent stratigraphic marker beds. Marine tephrostratigraphy provides constraints on the temporal evolution of both the volcanic source region and the ash-containing sediment facies. The presence of chemically reactive volcanic glass particles also affects the diagenetic evolution of the sediments.

The Central American land bridge is fairly narrow (c. 100–300 km), allowing prevailing south-easterly surface and north-westerly upper level winds (Carey and Sigurdsson, 2000) to disperse ash erupted at the volcanic front across marginal areas of the Pacific and Caribbean basins. Due to the erosive nature of the subduction process along the western coast of Central America, ash deposited in the Pacific basin may eventually become recycled in the "subduction factory".

SFB 574 scientists are investigating the products of highly-explosive eruptions along the Nicaraguan Volcanic Front (NVF) in order to establish a time sequence of subduction zone magmatic volatile releases into the atmosphere. This approach includes the following three methods:

1) Petrological/geochemical analyses of eruption products with a focus on volatile analyses, using the volatile concentration difference between glass inclusions in minerals and matrix glass to assess the volatile fractions released during an eruption.
2) Regional stratigraphic correlations of tephra deposits on land and offshore with the aid of geochemical analyses, and radiocarbon dating in order to quantify long-term temporal changes in volcanic activity.
3) Mapping of the areal thickness and grain-size distribution of each deposit in order to determine the erupted magma mass, and to apply volcanological modelling tools to constrain eruption parameters such as magma discharge rate,eruption duration, and column height.

In summary, the objectives of this study include the development of a chronostratigraphy and understanding of the evolution of Quaternary volcanism in Central America, in terms of composition and magnitude, and its possible implications for climatic changes. Another aim is to establish stratigraphic correlations of fore-arc sediments along the continental slope with sediments on the incoming plate. In addition sedimentation rates can be determined and shed light on terrestrial erosion rates, tectonic events, and slope stability. The diagenesis of ash-bearing fore-arc sediments and its effect on element exchange with seawater can also be studied by using tephrostratigraphy. Finally, these studies can lead to a better assessment of natural hazards related to volcanic and tectonic activity.

This chapter is a review of marine tephrostratigraphic research in Central America but also uses preliminary results from ongoing research to illustrate the methods, applications, and implications for Central American geology of studying marine tephra layers.

5.2. Methods used in Marine Tephrostratigraphy

Core drilling by the Deep Sea Drilling Project (DSDP), Ocean Drilling Project (ODP), and more recently by the Integrated Ocean Drilling Project (IODP) reaches deep penetration (up to several hundred meters) into the ocean floor and is thus best suited to extend tephrostratigraphy to great ages (in the million-year age range). Unfortunately, its application is limited to few sites. Piston and gravity cores reach only up to 20 m deep in soft sediments and therefore limit tephrostratigraphy to ages less than 10^6 years. However, they can readily be used to obtain lateral profiles or arrays of many sections, thus providing insights into lateral stratigraphic changes or local erosion events.

Visual identification of ash layers is easy when the ash forms mm- to cm-thick distinct and undistorted layers. In slope settings, however, mass wasting processes redistribute the ash and make visual recognition in sediment cores difficult. Core logging techniques facilitate core description by identification of both distinct layers and dispersed ashes in marine sediments. Standard core logging parameters include P-wave velocity, sediment densities from gamma-wave attenuation, and magnetic susceptibility. The most sensitive method to identify volcanic ash is magnetic susceptibility, which is the degree to which a material can be magnetised by an external magnetic field, and is expressed as the intensity ratio of the sediment magnetisation to an external magnetic field. The magnetic susceptibility value of natural samples is proportional to the volume fraction of magnetic minerals (Blum, 1997) and is a measure of the concentration of ash, respectively.

Basaltic ashes are most easily recognised by magnetic susceptibility because they contain concentrations of magnetic minerals (magnetite, chromite, siderite, hematite, titanomagnetite, franklinite, pyrrhotite) much higher than in other sediments and therefore yield high magnetic susceptibility and density values. In contrast, felsic ash is rich in feldspar, glass, and related weathering products which are all characterised by low or even "negative" magnetic susceptibility values (Hunt et al., 1995). As a consequence, core-log signatures of felsic ash show low or lower background magnetic susceptibility values associated with distinct peaks in gamma density.

Petrographic and geochemical analyses are the most powerful tools in marine tephrostratigraphic work to establish correlations between marine and terrestrial tephras. Petrography identifies typical mineral assemblages but also textural characteristics of the ash particles. Bulk-ash chemical analysis is done on slice samples that are easily cut from cm-thick ash layers. Even primary fallout layers, however, commonly contain some biogenic and clastic debris, and thin ash layers are ususally strongly mixed with pelagic sediment. Bulk-ash analyses thus require tedious prior separation of the volcanic material. Microanalytical techniques, in turn, can immediately be applied to the samples except where ash thinly dispersed in sediment necessitates prior enrichment. The most common microanalytical technique is the electron microprobe (EMP), which determines the concentration of major, minor, and some trace elements in volcanic minerals and glasses. Advantages of analysing individual glass shards include the detection of components of compositionally zoned magmas or the identification of material from different eruptions in ash beds mixed by reworking. Many volcanic deposits are sufficiently distinct at the major element level and can thus be distinguished by EMP analysis of glass shards. When variations in major elements are not sufficiently diagnostic, trace element compositions of glass shards can be determined by Laser Ablation Inductively Coupled Plasma - Mass Spectrometry (LA-ICP-MS) or by Secondary-Ion Mass Spectrometry (SIMS, ion probe). Such techniques also allow to determine isotope ratios of glass shards (Clift and Blusztajn, 1999; Schmincke, 2003; Ukstins Peate et al., 2003). Several trace elements and isotopes are immobile during alteration and thus are especially well-suited for geochemical correlation (Clift and Blusztajn, 1999; Pearce et al., 1999; Schmincke, 2003). K-bearing minerals can be used for laser-fused single-crystal $^{40}Ar/^{39}Ar$ radiometric dating of ashes older than some ten-thousand years. The ages of younger marine ash layers can be constrained by their host sediments using established time-scales of micro fossils, oxygen isotopes, and magnetic reversals. Another alternative is the radiocarbon (^{14}C) dating of organic material in correlated tephra on land. Such correlated ash layers then provide excellent time markers across the marine and terrestrial environments.

Widespread volcanic ash and aerosols from highly-explosive eruptions provide a potential tool for correlating stratigraphies from distant environments such as marine and terrestrial successions or polar ice sheets. Volcanic volatiles and resulting aerosols have much longer atmospheric residence times than ash particles and can be distributed globally, as evidenced by sulphurous layers in polar ice sheets (Zielinski et al., 1997; Zielinski et al., 1994).

5.3. Comprehensive Marine Tephrostratigraphic Correlations

Marine tephrostratigraphy is an excellent method that allows to connect terrestrial and marine stratigraphic sequences in the entire region of Central America (Fig. 5.1). Tephra studies along the Central American subduction zone extend back to the early 1980's when DSDP Leg 67 (Cadet et al., 1982a) was drilled off the Pacific Coast of Guatemala (Fig. 5.1). Due to the rotary core drilling technique used, only ash layers in hardened sediments (> 15-20 kyr) were recovered at depths down to 650 m below seafloor. Cadet et al. (1982a) and Cadet et al. (1982b) identified 186 ash layers at seven sites of Leg 67, which can be correlated with Central American eruptions extending back to the Early-Miocene. The tephra sequence from Leg 67 comprises ash layers from several prominent Guatemalan eruptions: the 1902 eruption of Santa Maria volcano, the Los Chocoyos ash from a source near Lake Atitlán, and the Pinos Altos tephra from Ayarza caldera (Cadet et al., 1982a; Drexler et al., 1980; Rose et al., 1982; Rose et al., 1979). A later study by Pouclet et al. (1985) at DSDP Leg 84 (Fig. 5.1) corroborates the observations and conclusions from near-by Leg 67. Two DSDP sites from Leg 68 (502 and 503) (Fig. 5.1), located in the Pacific Ocean and the Caribbean Sea respectively, contain Late-Miocene and Pliocene-Pleistocene ash layers which probably originated from the Central American Volcanic Arc (CAVA) (Ledbetter, 1982) but whose exact sources have not yet been identified.

The Caribbean ODP Leg 165 (Fig. 5.1) revealed 2019 volcanic ash layers, which originated from eruptions in Nicaragua, Guatemala, El Salvador, Costa Rica, and probably the Antilles, Mexico, and even the Andes, since the Early-Miocene (Sigurdsson et al., 1997). Altogether, the volcanic ash layers amount to 1-5 % by volume of the total sediment thickness of Leg 165. These ash layers are composed almost exclusively of ryholitic glass shards texturally resembling co-ignimbrite ash deposits on land, and are considered to mainly represent distal fallout from major ignimbrite-forming

eruptions rather than distal plinian fallout (Sigurdsson et al., 1997). Possible source regions include the Matagalpa sequence (Guatemala, El Salvador, and Nicaragua), which comprises 50-m-thick Miocene dacitic and rhyolitic ignimbrites (Ehrenborg, 1996). Tentative correlations relate other ash layers to voluminous ignimbrites and co-ignimbrite ashes of south-central Guatemala and El Salvador, thick rhyolitic ignimbrites of the Padre Miguel Group in southeast Guatemala and Honduras, and the major siliceous ignimbrites of the Coyol group, Nicaragua (Sigurdsson et al., 2000). Based on the sequence at Site 999, Leg 165, Carey and Sigurdsson (2000) estimated an average ash accumulation rate of 250 cm Myr^{-1} in the marine area adjacent to Central America. The frequency of major eruptions (*c.* >10 km^3 DRE = dense rock equivalent) in the source regions is in the order of one event per 20 kyr. Magnitudes of theses eruptions, as estimated from thickness vs. distance-relationships of tephra layers, are comparable to the largest Quaternary eruptions worldwide such as the 30 kyr Campanian Ignimbrite in Italy (100 km^3 DRE) (Shipboard Scientific Party, 2003) or the 75 kyr Toba eruption on Sumatra (2000 km^3 DRE) (Ninkovich and Sykes, 1975).

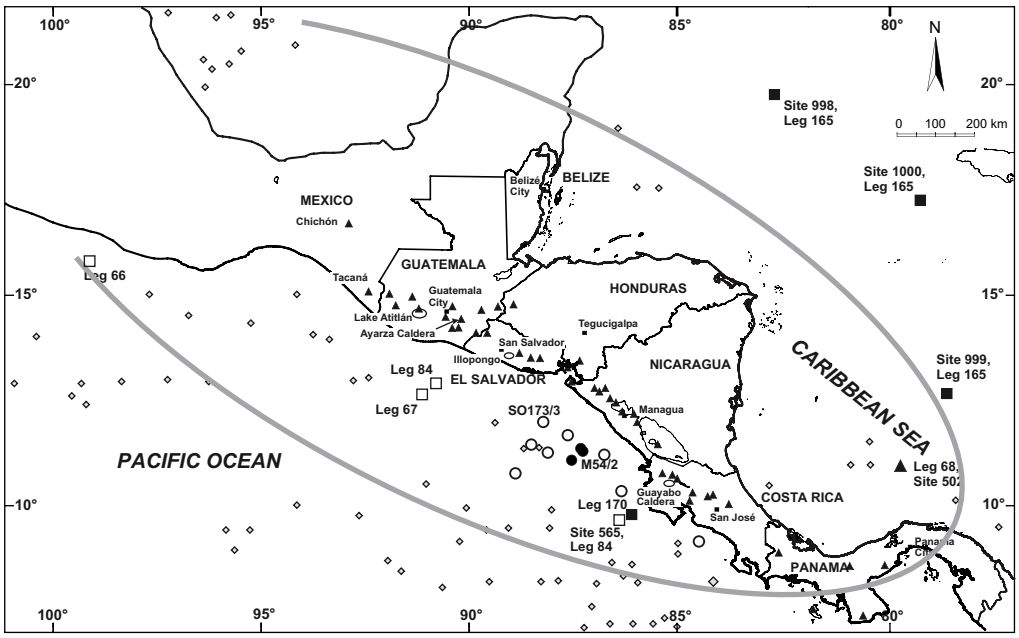

Figure 5.1: Map of Central America showing the CAVA volcanoes (triangles) and core locations of ODP (solid squares), DSDP (open squares), Meteor cruise 54/2 (filled circles), Sonne cruise 173/3 (open circles) and Ledbetter (1985) (diamonds). The bold grey line shows the extent of the Pleistocene Los Chocoyos Ash from Guatemala, the most widespread tephra covering the entire area of Central America and parts of North America.

Few studies have been conducted to obtain a Quaternary volcanic record in marine sediments using piston and gravity corers to drill soft sediments. Based on minor and trace element compositions of 128 volcanic ash samples from 56 piston cores, Bowles et al. (1973) distinguished three principal areas of ash deposition in the eastern equatorial and southeastern Pacific Ocean. Source volcanoes were identified in Guatemala (Tecpán-Chimaltenango Basin), El Salvador (Lake Ilopango), Nicaragua, Colombia, and Ecuador. These ash layers range from < 1 cm to a maximum of 46 cm in thickness and occur at depths ranging from 0 to 16 m. Most, if not all, of the ash layers examined are younger than 300 kyr. Based on tephrostratigraphy, Bowles et al. (1973) estimated a minimum sedimentation rate of 5.4 cm per 1000 years in the northern Pacific area near Central America.

In addition, Ledbetter (1985) determined the areal distribution of eleven tephra layers younger than 300 kyr by evaluating microprobe analyses of glass shards from more than 300 piston cores across the Gulf of Mexico, the Caribbean Sea, and the Pacific Ocean (Fig. 5.1). This sequence includes the two most widespread volcanic deposits known in Central America: the Los Chocoyos ash (84 kyr) and the Worzel Layer-L (230 kyr). Ledbetter (1985) inferred the ages of the ash layers by comparison with dates obtained on land, and by correlation with marine oxygen isotope curves, foraminiferal biostratigraphy, and calcium carbonate stratigraphy. An interesting result of this work is that ash layers can provide time markers that allow to compare age-equivalent sediments of different facies in three ocean basins.

Apart from the Los Chocoyos ash that is found all over Central America, few additional, preliminary chemical correlations were established in this area using data from ODP and DSDP Legs. Chemical analyses allow correlations with older tephra deposits from Guayabo Caldera found near active Rincón del la Vieja volcano in Costa Rica. Tephras from Guayabo Caldera have been correlated with marine ash layers from ODP cores and gravity cores described by Ledbetter (1985), using diagnostic trace element contents (Ti, Ca, Rb, Ba, Sr, Zr). The youngest tephra layer (La Ese; ~600 kyr) (Chiesa et al., 1992) of Guayabo Caldera probably correlates with the layer I2 (core V-15-18, 13 m below seafloor) (Ledbetter, 1985). Additionally, other marine tephras in cores from ODP Leg 170, Site 1039B (78, 88, and 133 m below seafloor), can be correlated with Guayabo volcanic deposits (Tab. 5.2) (Kimura et al., 1997). Some of the uppermost marine tephras show similarities in componentry and composition to deposits from eruptions of Rincón de la Vieja volcano. Time intervals between the dated terrestrial tephras from Rincón de la

Vieja volcano agree well with time intervals between the marine ash layers inferred from average sedimentation rates within the trench environment.

5.4. Periodicity and Cyclicity of Volcanic Activity in the Circum-Pacific Volcanic Belt

Marine tephra research leads to a more comprehensive understanding of the eruptive history of a volcanic region. The great preservation potential of ash markers in non-erosive marine environments results in nearly complete stratigraphic records that are optimal for studying temporal variations in volcanic activity. Eruption chronology can then be correlated with other large-scale or global events such as climatic changes or tectonic movements. Several authors have recognised variations in the frequency of ash layers with depth in cores around the Pacific and postulated that these fluctuations reflect changes in the frequency of explosive volcanic eruptions.

It is now widely accepted that volcanism, especially around the Pacific, operates in large-scale temporal cycles. Kennett et al. (1977) were first to recognise the episodic nature of Circum-Pacific volcanism and identified major episodes of increased activity at 4 Myr and during the past 2 Myr. Sigurdsson et al. (2000) (ODP Leg 165) improved the time-resolution of this first approach. These and other authors recognised peaks of volcanic activity in the Quaternary, middle Miocene (~14-16 Myr), late Miocene (~8-11 Myr) and latest Miocene to early Pliocene (3-6 Myr) in the Northern Pacific and the Bering Sea (e.g. Hein et al., 1978), the Japan Trench (e.g. Cadet and Fujioka, 1980), the Kamchatka and eastern Aleutian Volcanic front (e.g. Prueher and Rea, 2001) and Central America (e.g. Cadet et al., 1982a; Kimura et al., 1997; Ledbetter, 1982; Pouclet et al., 1985; Shipboard Scientific Party, 2002; Sigurdsson et al., 1997). Similar pulses of activity recorded in several DSDP and ODP cores are shown in Figure 5.2, which summarises data for three major episodes of increased Circum-Pacific volcanism. These peaks correlate with increased subduction related volcanism in New Zealand during the Plio-Pleistocene (Shane et al., 1996; Shane et al., 1995), and in the western Pacific from Japan to the Philippines with an activity pulse at 0.3, 0.7 Myr before present, and during the Plio-Pleistocene; (Cambray and Cadet, 1994; Cambray et al., 1995; Pouclet and Scott, 1992). Pliocene-Quaternary and Mid-Miocene pulses of arc volcanism in the pacific area were also detected by Straub and Schmincke (1998), who evaluated the tephra input into the Pacific Ocean sediments in space and time. They estimated that

approximately 10-13 km^3 of volcaniclastic sediment are produced per km arc length and per million year. Extrapolation over the life-time of major Pacific arcs and hotspot chains, combined with a volume estimate of the distal tephra component, indicates a minimum of 9.3 x 10^6 km^3 of tephra, corresponding to 23 vol.% of existing Pacific oceanic sediments (Straub and Schmincke, 1998).

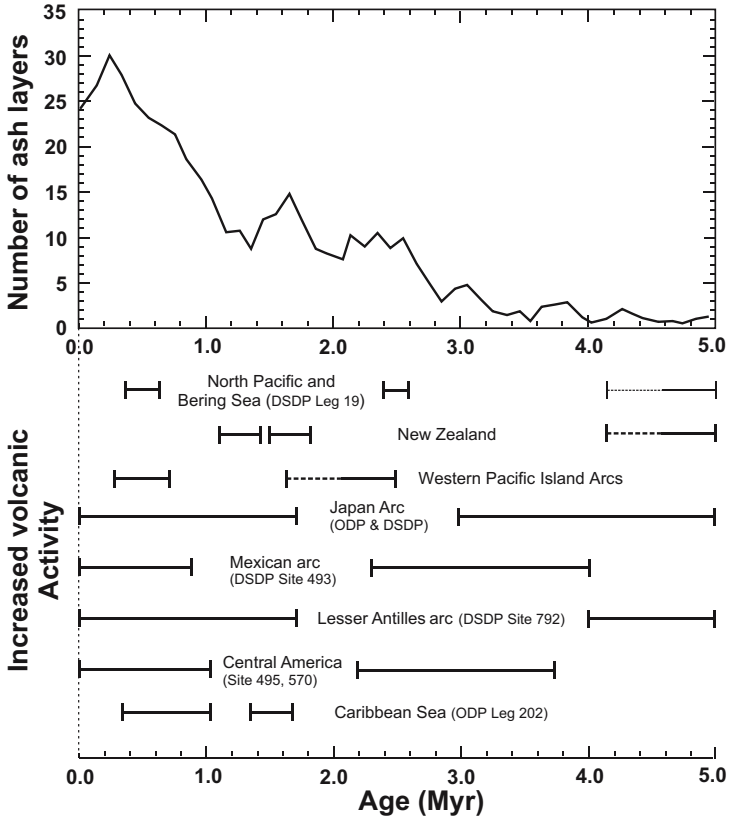

Figure 5.2: Eruption frequency in the Circum-Pacific area over the last 5 Myr after Cambray and Cadet (1994), Prueher and Rea (2001), and Sigurdsson et al. (2000). Top: The frequency of ash layers in ODP Leg 145 near Kamchatka and the Eastern Aleutian Arc increases toward the present.
Bottom: Comparison of periods of increased volcanic activity observed around the Pacific Ocean.

Since these volcanic episodes correlate with subduction related volcanism in many other areas, Kennett et al. (1977) and Cambray and Cadet (1994) suggested that these episodes were global in nature and related to plate tectonics. In contrast, Sigurdsson et al. (2000) pointed out that a global and simultaneous increase of explosive volcanism is too complex and can not be explained by plate tectonics alone. These authors were not able to recognise any ubiquitous mechanism that would be capable of exerting control on volcanic cyclicity on a global scale. They emphasise that any subduction zone, although principally governed by plate-tectonic movement, is also affected by regional

factors including velocity and direction of plate motion and age and composition of the subducting slab. On the other hand, increased sediment subduction during Quaternary time (e.g. von Huene and Scholl, 1991) - which transports large amounts of water to depth where dehydration of the subducted slab leads to hydration of the overlying mantle wedge and enhanced magma production – may explain the high global rate of Quaternary explosive volcanism in support of Cambray´s theory .

Understanding cyclic behaviour is essential to assess broader implications of explosive volcanism such as global climatic effects. Apart from such aspects, analysis and correlation of marine ash layers is important for the study of individual volcanoes or eruptions. In settings such as Central America where volcanoes are situated close to the ocean and wind-driven ash dispersal is dominantly seaward, land-based field work alone would provide incomplete information when it comes to quantifying volcanic eruption processes. In the following section this is illustrated by a case study from Nicaragua.

5.5. Preliminary Results from the Nicaraguan Continental Slope

5.5.1. Sediment Cores and Ash Layers Recovered on RV *Meteor* Cruise M54/2

In summer 2002, during RV *Meteor* cruise M54/2, Sediment cores were collected by gravity coring offshore Nicaragua near 11°30'N / 87°30'W on the lower continental slope (1200 m water depth), and on the opposite flank of the trench (3300 m water depth), i.e., at distances of 150-220 km from the Nicaraguan volcanic front. In autumn 2003, additional sediment cores were taken in the northern part of offshore Nicaragua during RV *Sonne* cruise SO173/3 (Figs. 5.1 & 5.3). Core lengths generally extended to 3.5-11 m below seafloor. Cores M54-2 and M54-13, SO173-11, SO173-11/1, SO173-18, SO173-25 and SO173-35 were taken on the Nicaraguan slope, and cores M54-11/2, SO173-13/1, SO173-15, and SO173-17 were taken on the incoming plate where average sedimentation rates are lower. Here we focus on the three M54 cores which together contain 20 ash layers intercalated with terrigenous and pelagic sediments; the 62 ash layers in the SO173 cores are subject of ongoing analyses. Most of the ash layers are white to greyish-pink or dark-grey to pink light-grey in colour. Six dark grey layers are of basaltic, and 14 pinkish-white layers are of rhyolitic composition. The ash layers were named after the cores M54-11/2, M54-2, and M54-13 and the appending depths of their occurrence in the sediment cores.

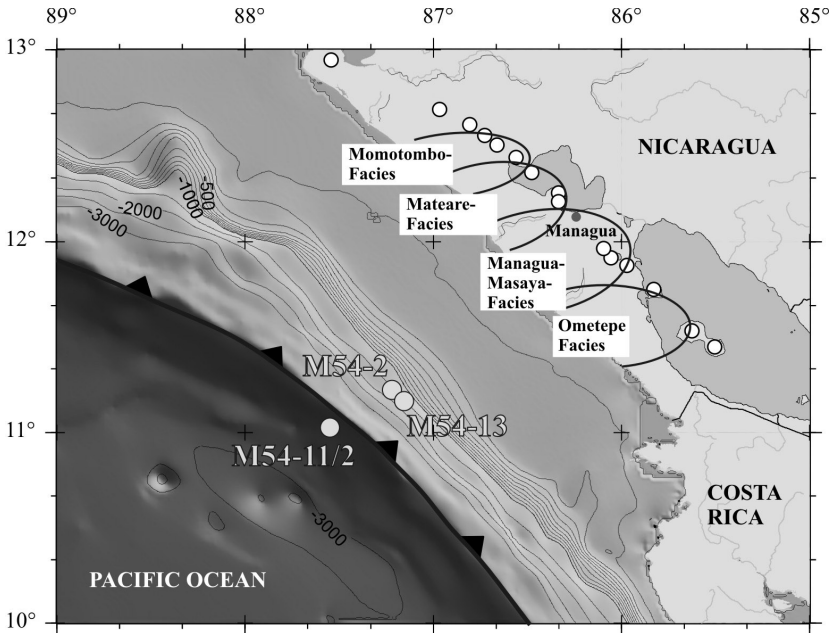

Figure 5.3: The Nicaraguan volcanic front (NVF, circles) and related tephra facies. Grey circles show core positions of Meteor cruise M54/2 across the trench.

Core logging shows mafic ash layers by high magnetic susceptibility and high density values whereas felsic ash shows low or negative magnetic susceptibility values and high densities (Fig. 5.4). Logging identified four ash layers that were not apparent in visual inspection of the cores. In 12 additional beds volcanic ash is dispersed in the clastic sediment. Ash layer thicknesses range from 0.5 to 14 cm (Fig. 5.4). Most of the layers appear to be primary fallout deposits but some are reworked. Discontinuous ash lenses occur in the sediment sequence as well as reworked pumice clasts. The lower contact of the ash beds is usually sharp, whereas the upper contact frequently shows a gradual change from ash to deep marine sediment. In some cores, thin ash layers have been disturbed by bioturbation. Admixtures of ash within terrigenous and pelagic sediments are also frequent.

Microscopic examination of light-coloured ashes shows mostly clear, colourless, volcanic glass shards and pumice fragments (Fig. 5.5a) commonly with elongated vesicles. Each rhyolitic ash layer is characterised by a distinct modal composition and crystal/glass ratio (Tab. 5.1). Dark-grey ash layers consist predominantly of a mixture of brown glass shards, black, vitreous and opaque particles and numerous light and heavy minerals. The typical grain size of the ash-layers varies in the range of medium silt to medium/coarse sand (< 250 μm). Mineral assemblages comprise plagioclase, pyroxene, hornblende, plus

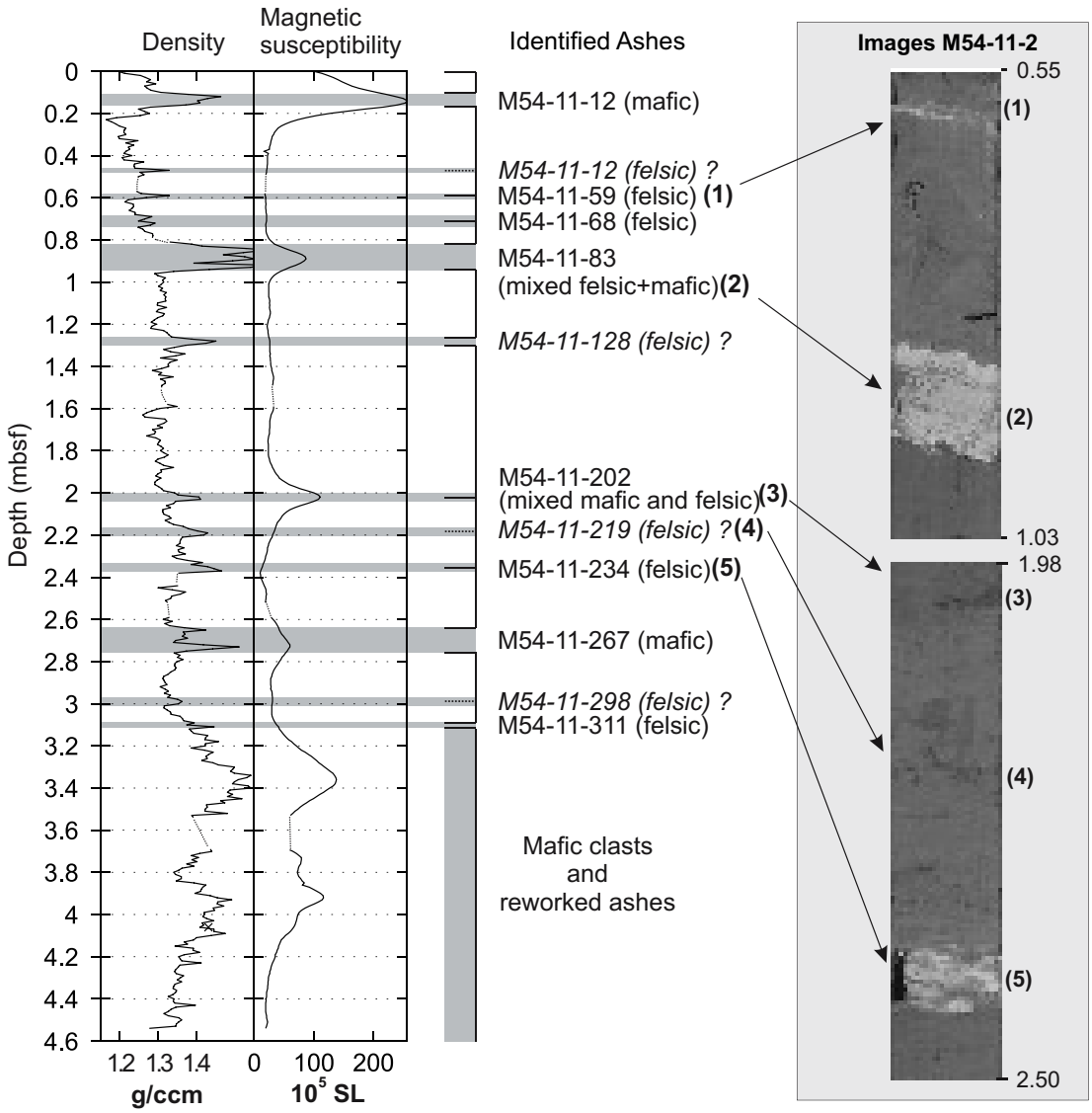

Figure 5.4: Density and magnetic susceptibility log of core M54-11/2 from sediments on the subducting plate offshore Nicaragua and core photographs of selected cores containing macroscopically visible tephras. Log aberrations are due to core segment endings. Some core disturbances are removed and indicated by a dashed line. Mafic ash layers such as (2) and (3) are characterised by high magnetic susceptibility and density values. Felsic ash layers such as (5) show low magnetic susceptibility values and high densities. Four of the ash layers detected in the logging record (e.g. M54-11-12 at the top) were not noted by visual inspection of the core.

olivine in the mafic, and occasionally biotite in the most-evolved felsic layers. Most of the glass shards in the basaltic layers have blocky shapes and are poorly vesicular to dense (Fig. 5.5a). Mafic glass shards constitute < 40 % by volume of the basaltic ash layers, while silicic glass shards make up > 60 vol.% of the felsic layers. Glass-shards in the felsic layers have commonly pumiceous textures with elongated vesicles (Fig. 5.5b, Tab. 5.1).

EMP major element analyses of 555 glass shards (Tab. 5.2) from 20 ash layers in the 3 cores yield compositions ranging from basalt to rhyolite (51-79 wt% SiO_2; Fig. 5.6). Analytical totals amount to 93-96 % in rhyolitic, and 98-99 % in basaltic glass shards, probably reflecting a higher degree of hydration of rhyolitic glass (4-7 wt% H_2O) compared to basaltic glass (1-2 wt% H_2O). Glass-shard compositions of individual ash layers form coherent data fields in variation diagrams that can be used for stratigraphic correlations among the cores and with deposits on land. Silicic ashes can be divided into three compositional groups (Fig. 5.6). Group A ash is rhyolitic in composition (76-80 wt% SiO_2), rich in K (3.5-4.5 wt% K_2O) (Fig. 5.5b) and commonly biotite bearing. Group B ash is K-poor (2.5-3 wt% K_2O) (Fig. 5.5b) calc-alkaline rhyolite (73-77 wt% SiO_2). Finally, group C ash is of dacitic compositions (67-70 wt% SiO_2). Overall, the chemical variations show a pattern consistent with fractional crystallisation from a range of parental compositions.

5.5.2. Identification of Reworked Ash

Glass shards found in the 12-cm-thick layer M54-11/2-234 also occur in small amounts in the stratigraphically higher layers M54-11/2-202 and M54-11/2-83. Similarly, glass shards compositionally belonging to layers M54-13-283 and M54-11/2-83 are also found in the respective younger ash beds. These observations suggest that erosive processes did locally rework older tephra (and sediment) that was subsequently deposited together with new ash. Ash reworking in core M54-11/2 on the incoming plate can be related to step-like scarps of normal bent-faults cutting the oceanic plate in the North-Nicaraguan region of the Middle American Trench (MAT) (Ranero et al., 2003). The reworked ash occurs either as ripped-up clasts of diagenetically hardened older ash or as particle lenses within the newly emplaced ash. We interpret these intra-clasts and ash lenses as a result of mass wasting at nearby fault scarps occurring while deposition of primary, new fallout ash through the water column was in progress.

5.5.3. Correlation between Cores

The chemical composition of the glass shards, the modal composition of the crystal fraction, crystal-glass ratios, and the stratigraphic order of ash layers need to be considered when attempting stratigraphic correlations. Three white ash layers, M54-11/2-59, M54-2-295, and M54-13-41, stand out in chemical variation diagrams (M1)

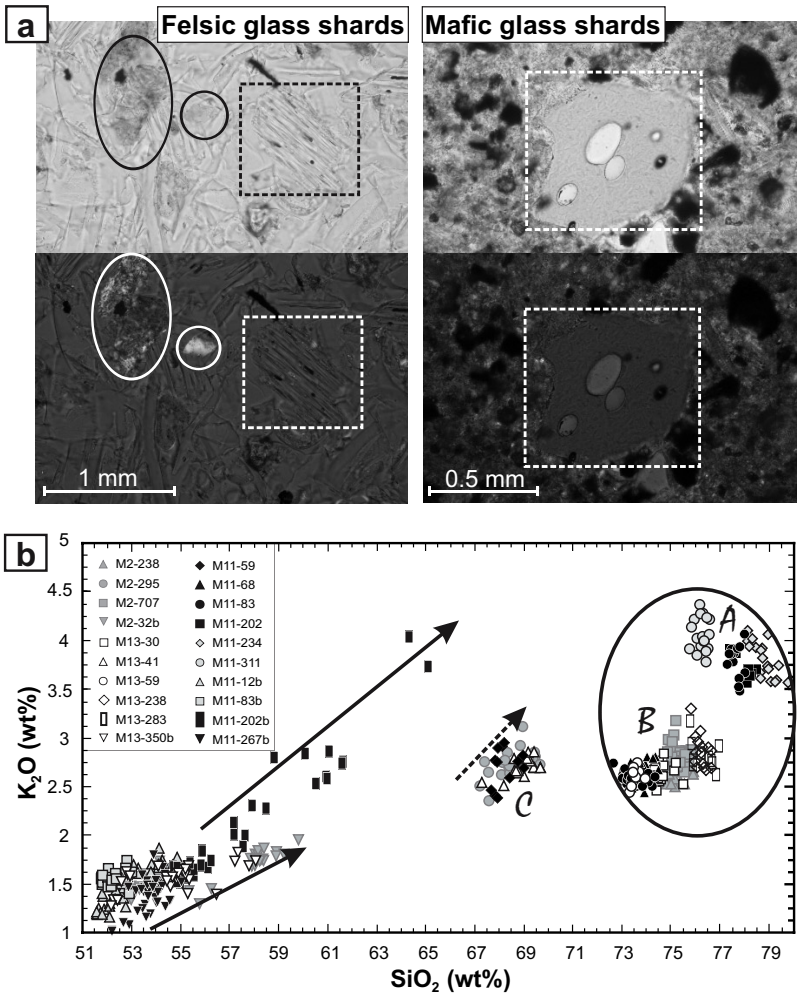

Figure 5.5a: Examples of the petrographic and alteration features from a felsic (left) and mafic (right) ash layer viewed in transmitted light (top) and under crossed polarisers (bottom). Circles show altered areas in felsic ash with secondary minerals visible in polarised light. Squares outline glass shards that appear unaltered under the microscope.

Figure 5.5b: K_2O versus SiO_2 diagram of M54 glass shards from ash layers analysed with EMP. The ellipsoid encircles felsic ashes which are more resistant to alteration. The arrows mark the alteration trends in mafic tephras that contradict the optically fresh appearance in Figure 5.5a. A, B, C marks compositional groups of felsic ash as identified in Figure 5.6.

(Figs. 5.6 & 5.7) by overlapping intermediate silica contents of their glass shards (67.3-69.7 wt% SiO_2; dacitic group C). Their crystal-glass ratios of 0.4-0.6 are identical, as well as their modal compositions comprising plagioclase, augite, and hornblende (Tab. 5.1). Layer thicknesses decrease systematically from 8 cm through 6 cm to 3 cm with increasing distance from the volcanic front. The three ash beds thus represent a

Table 5.1: Petrographic features of different ash layers in cores M54-2, M54-11/2, and M54-13

Ash layers M54-	Grain size of glass shards (sand grades)	Glass content %	Crystal content %	Mineral/ glass ratio	Reworked mafic/felsic glass	Pumice fragments	Fluidal structures	Crystals °° - many, ° - abundant, ? - few					Possible correlations
Felsic								hbl	bi	cpx	opx	ol	
2-238	medium	80-90	10-15	0.15	few	abundant	abundant	°°		°°	°	?	M2
2-290	fine-medium	60-65	25-30	0.44	few	many	abundant	°°		°°	°		M1
2-707	fine-medium	80	10-20	0.19		few	few	?		°°	?	?	
11/2-59	medium	60-70	30-40	0.54		abundant	abundant	°°		°	°		M1
11/2-68	coarse	60-70	30-40	0.54		many	few	?		°°	°	?	
11/2-83	fine-medium	60-70	20	0.31		abund. -many	many			°	°	?	M3
11/2-202	coarse	20	10	0.50	many	few	abund.-many			?	°°		
11/2-234	coarse	90-95	5-10	0.08	few	abundant	few	°°	°°	°			
11/2-311	fine-medium	70-80	20-30	0.33	few	many	few	°°	°	°°	°		
13-29	fine-medium	80-90	10-15	0.15	few	abundant	abundant	°°		°°	°°		M2
13-41	fine	60-65	30-40	0.58	few	many	abundant	°°		°°		?	M1
13-59	coarse	70-80	20	0.27		many	abundant			°°	°	?	M3
13-238	fine-medium	70-80	20-30	0.33	abundant	abundant	many	°°					
13-280	medium	60-70	20-30	0.38		abundant	abundant	°°		°			
Mafic													
2-32	coarse	30-40	10-20	0.43	few-	abundant	few			°°	°		
11/2-12	medium	20-30	10-20	0.60		many	few	?		°°	°°	?	
11/2-83	medium	50-60	20	0.36		few	few			°°	°°	°	
11/2-202	medium	60-70	10	0.15	abundant	few-abundant	few-abundant			?	°°		M4
11/2-267	coarse	60-70	10	0.15	abundant	abundant	abundant			°°	°°	?	
13-350	coarse	60	10	0.17	abundant	abundant-	abundant			°°	°°	?	M4

(hbl= hornblende, bi= biotite, cpx= clino-pyroxene, opx= ortho-pyroxene , ol = olivine)

Table 5.2: EMP data for tephras from RV Meteor cores, from sediment cores investigated by Ledbetter (1985) and from our Nicaraguan field study. Average data from Fontana and Upper Apoyeque pumice are published by Wehrmann et al. (2003) All data are recalculated to 100% anhydrous total. Values in parentheses show maximum deviation of multiple analyses.

Sample	SiO_2	K_2O	Al_2O_3	Fe_2O_3	MgO	CaO	Na_2O
				all data in wt%			
correlated with land tephra or ODP ash layers							
M54-11/2-234	78.86	3.81	12.64	0.53	0.09	0.64	2.89
	(1.66)	*(0.54)*	*(0.47)*	*(0.29)*	*(0.06)*	*(0.25)*	*(1.13)*
Los Chocoyos (Ninkovich	78.12	3.92	12.77	0.65	0.40	0.85	2.99
and Sykes, 1975)	*(1.24)*	*(0.16)*	*(0.48)*	*(0.65)*	*(0.12)*	*(0.15)*	*(0.59)*
M54-11/2-311	76.31	4.06	13.07	1.02	0.13	0.79	3.79
	(0.82)	*(0.59)*	*(0.40)*	*(0.43)*	*(0.09)*	*(0.15)*	*(0.52)*
G- Tephra (Ninkovich and	76.83	4.24	13.25	1.10	0.30	0.34	3.26
Sykes, 1975)	*(0.49)*	*(0.12)*	*(0.26)*	*(0.19)*	*(0.23)*	*(0.03)*	(0.22)
M54-2-290	68.53	2.74	15.90	2.98	0.89	2.79	5.07
	(2.46)	*(0.76)*	*(1.10)*	*(0.78)*	*(0.51)*	*(1.15)*	*(0.08)*
M54-11/2-59	68.24	2.70	16.05	3.15	0.84	2.80	4.75
	(1.33)	*(0.57)*	*(0.96)*	*(0.77)*	*(0.51)*	*(0.76)*	*(0.95)*
M54-13-41	68.97	2.70	15.96	2.86	0.83	2.67	4.93
	(2.39)	*(0.35)*	*(1.11)*	*(0.49)*	*(0.42)*	*(0.91)*	*(0.61)*
L.Ometepe	68.48	2.68	16.04	2.90	0.91	2.87	5.12
	(2.63)	*(0.68)*	*(1.95)*	*(0.61)*	*(0.39)*	*(1.51)*	*(0.45)*
M54-2-238	75.22	2.62	13.21	1.88	0.32	1.99	3.72
	(1.41)	*(0.24)*	*(0.63)*	*(0.49)*	*(0.18)*	*(0.48)*	*(0.72)*
M54-2-707	75.41	2.82	13.54	1.42	0.30	1.32	4.17
	(0.96)	*(0.53)*	*(0.59)*	*(0.45)*	*(0.11)*	*(0.28)*	*(0.40)*
M54-13-29	74.73	2.66	13.57	1.85	0.32	2.04	3.75
	(1.19)	*(0.47)*	*(0.54)*	*(0.48)*	*(0.17)*	*(0.38)*	*(0.98)*
U. Apoyeque	74.63	2.64	13.54	2.01	0.45	2.19	3.82
	(1.28)	*(0.05)*	*(0.73)*	*(0.23)*	*(0.04)*	*(0.34)*	*(0.29)*
M54-11/2-83	73.55	2.59	14.06	2.03	0.45	1.88	4.44
	(1.71)	*(0.26)*	*(1.14)*	*(0.59)*	*(0.17)*	*(0.42)*	*(0.66)*
M54-13-59	73.58	2.59	13.99	2.01	0.47	1.88	4.46
	(1.11)	*(0.31)*	*(1.25)*	*(0.50)*	*(0.26)*	*(0.46)*	*(0.27)*
U. Apoyo	73.79	2.64	13.84	2.02	0.50	2.20	4.28
	(0.89)	*(0.25)*	*(0.56)*	*(0.32)*	*(0.09)*	*(0.46)*	*(0.25)*
M54-11/2-202	55.92	1.74	15.23	10.99	3.32	7.44	3.35
	(4.13)	*(1.14)*	*(1.48)*	*(3.09)*	*(1.37)*	*(2.51)*	*(1.16)*
M54-13-350	54.58	1.50	15.26	11.73	3.87	8.13	3.22
	(6.49)	*(0.88)*	*(1.94)*	*(3.89)*	*(2.55)*	*(3.26)*	*(0.99)*
Fontana	55.70	1.55	15.68	9.94	3.91	8.79	2.47
	(3.89)	(0.87)	*(1.00)*	*(1.35)*	*(1.59)*	*(2.05)*	*(0.80)*

single volcanic fallout deposit (layer M1 in Figs. 5.7 & 5.8) and hence provide a time marker across all three cores.

Table 5.2 continued: EMP data for tephras from RV Meteor cores. All data are recalculated to 100% anhydrous total. Values in parentheses show maximum deviation of multiple analyses.

Sample	SiO_2	K_2O	Al_2O_3	Fe_2O_3	MgO	CaO	Na_2O
				all data in wt%			
			not correlated or reworked				
M54-2-32	53.04	1.61	14.54	12.79	4.15	8.57	3.19
	(3.45)	*(0.95)*	*(2.13)*	*(1.93)*	*(1.64)*	*(2.47)*	*(1.61)*
M54-11/2-12	52.73	1.43	14.88	12.64	4.27	8.89	3.00
	(3.29)	*(0.62)*	*(0.87)*	*(1.63)*	*(1.58)*	*(2.10)*	*(0.51)*
M54-11/2-20 (reworked)	78.23	3.50	12.86	0.70	0.11	0.65	3.60
	(1.54)	*(1.27)*	*(0.67)*	*(0.36)*	*(0.13)*	*(0.40)*	*(0.70)*
M54-11/2-68 (reworked)	73.89	2.68	13.80	2.00	0.38	1.95	4.20
	(1.14)	*(0.37)*	*(0.92)*	*(0.45)*	*(0.16)*	*(0.53)*	*(0.63)*
M54-11/2-83 reworked	52.32	1.55	14.37	13.02	4.52	9.00	3.05
mafic	*(1.23)*	*(0.34)*	*(0.73)*	*(1.20)*	*(0.60)*	*(1.13)*	*(0.35)*
M54-11/2-110 (reworked	77.72	3.79	12.81	0.60	0.11	0.58	3.76
part)	*(0.71)*	*(0.59)*	*(0.72)*	*(0.42)*	*(0.11)*	*(0.21)*	*(0.39)*
M54-11/2-267	53.73	1.39	15.26	11.76	4.11	8.69	3.26
	(2.85)	*(0.73)*	*(1.17)*	*(2.60)*	*(1.37)*	*(1.68)*	*(0.54)*
M54-13-238 (reworked	76.26	2.87	12.96	1.39	0.26	1.38	3.81
from 13-280)	*(0.87)*	*(0.63)*	*(0.62)*	*(0.46)*	*(0.23)*	*(0.17)*	*(0.90)*
M54-13-280	76.33	2.82	13.09	1.35	0.27	1.37	3.77
	(1.16)	*(0.56)*	*(0.60)*	*(0.32)*	*(0.05)*	*(0.12)*	*(0.61)*

The younger layers M54-2-238 and M54-13-29 share compositional characteristics such as SiO_2 content in the glass (74.4-76.0 wt%), crystal-glass ratios of 0.15, and plagioclase, augite and hornblende in the crystal fraction. No equivalent layer was found in core M54-11/2. Thickness of this deposit (layer M2 in Figs. 5.7 & 5.8) decreases from 17 cm in core M54-2 to 5 cm in nearby core M54-13, suggesting partial erosion at the latter site.

We established a third correlation between the black-and-white ash layer M54-11/2-83 and the white layer M54-13-59. The black-and-white layer in core M54-11/2 contains both basaltic and rhyolitic material which is chaotically mixed. It is a primary felsic ash layer mixed with several lenses of older, reworked felsic ash and up to 10 % mafic glass shards. Minor basaltic material (< 5 %) is also found in the white ash layer in core M54-13, which has a sharp lower contact but a gradual transition into the overlying sediment and is interpreted as a primary fallout. The primary rhyolitic material in both layers has the same chemical and modal composition (73.1-74.4 wt% SiO_2 in the glass, crystal-glass ratios of 0.15 and plagioclase and augite in the crystal fraction). Thus, both

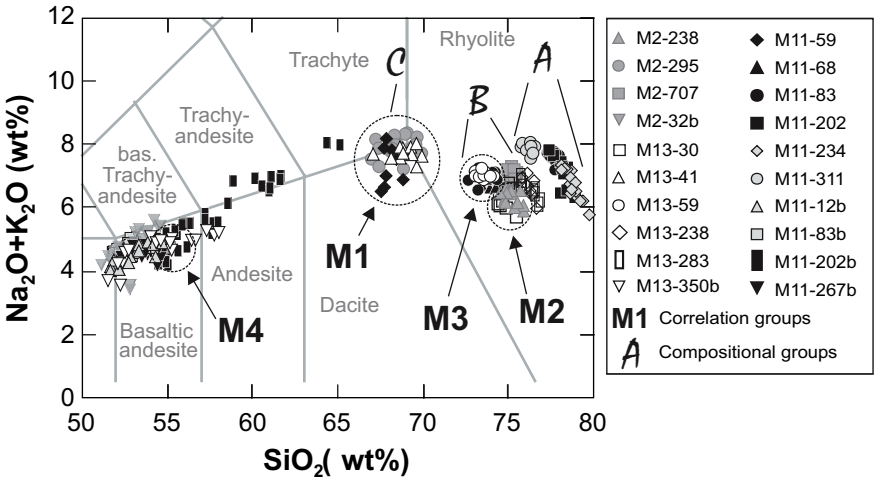

Figure 5.6: Na_2O+K_2O versus SiO_2-diagram of M54 glass shards of ash layers analysed with EMP. Felsic tephras make up three compositional groups A, B, C. M1-M4 identify ash layers correlated with tephras on land in Nicaragua.

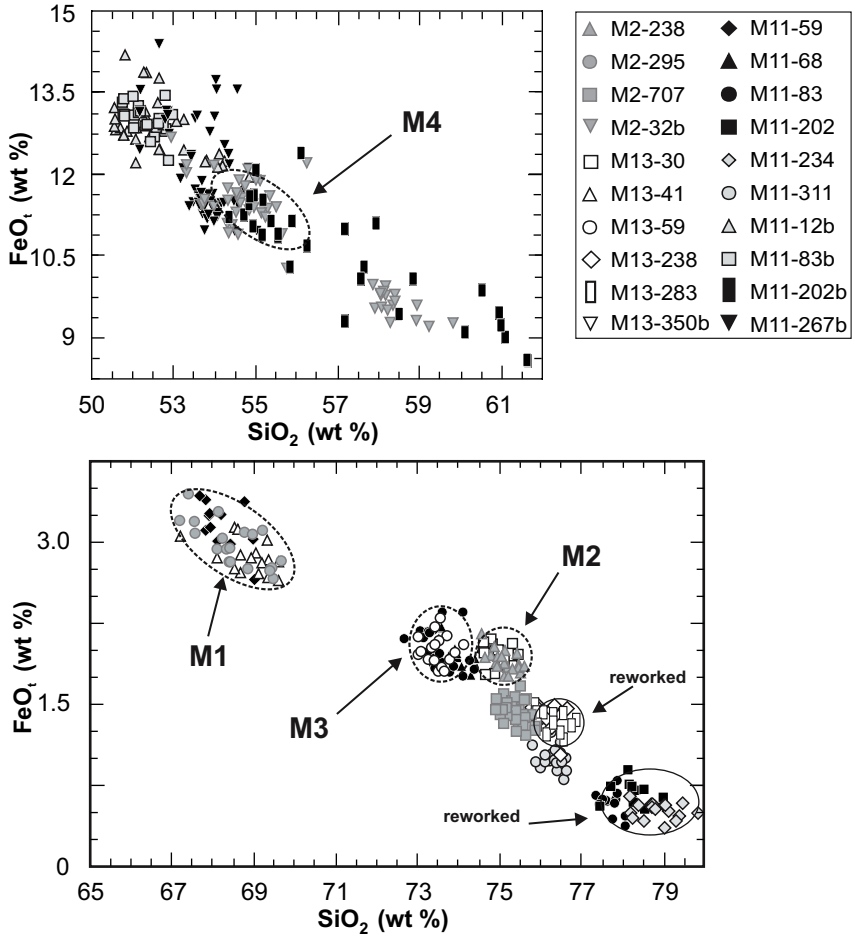

Figure 5.7: The FeO_t versus SiO_2-diagram is particularly useful to compositionally correlate ash layers such as M1-M4, and to identify reworked ash particles mixed with primary fallout as in M2 and M3.

layers probably originated from the same eruption (layer M3 in Figs. 5.7 & 5.8). Another correlation (layer M4 in Figs. 5.7 & 5.8) possibly exists between the basaltic ash layer M54-13-350 and the basaltic material in the black-and-white mixed layer M54-11/2-200, which are quite similar in chemical composition of the glass shards.

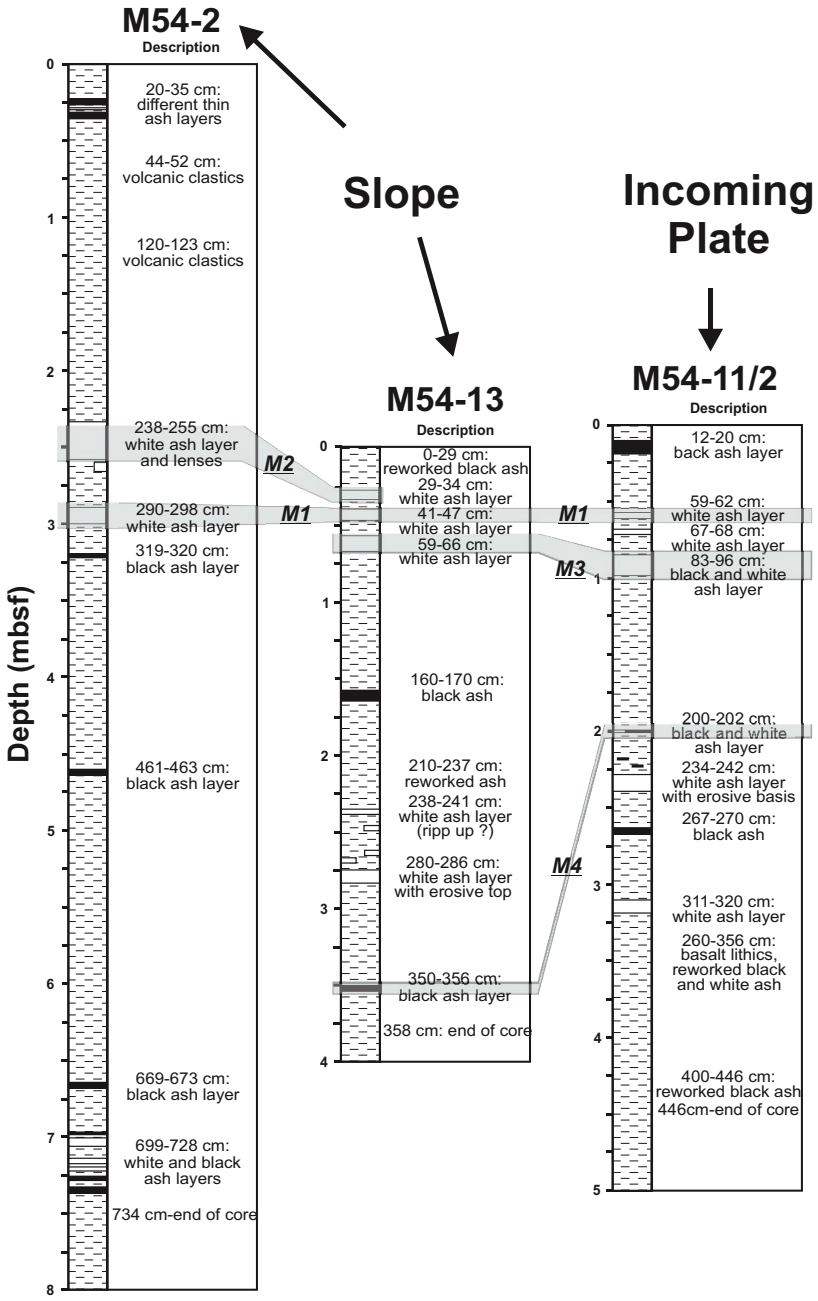

Figure 5.8: Compositionally correlated ash layers M1 through M4 provide stratigraphic links between the three cores M54-2, M54-13, and M54-11/2 across the trench.

5.5.4. Correlations with Tephras On Land

5.5.4.1. Quantifying Explosive Quaternary Volcanism in Nicaragua - Onshore work in Nicaragua concentrated on the area from León in the north to Isla de Ometepe in the south (Fig. 5.3), and on a time interval from 50 kyr BP to the present. We distinguished four interfingering tephra facies by their distinct stratigraphic successions. These are, from north to south, the Momotombo Facies, the Mateare Facies, the Managua-Masaya Facies, and the Ometepe Facies (Fig. 5.3). These successions include products of more than 30 highly-explosive eruptions. The composite succession of deposits from highly explosive eruptions of the Mateare and Managua-Masaya Facies is shown in Figure 5.9. Eruption products range from basaltic through strongly zoned (basaltic andesite to rhyolite) up to dacitic/rhyolitic compositions. Most are fallout deposits but ignimbrites and pyroclastic surge deposits are also present. The most violent rhyodacitic eruptions occurred at Apoyo Caldera and the Chiltepe volcanic complex, while two mafic plinian tephras and a voluminous surge deposit erupted from Masaya Caldera. Extensive isopach (thickness) and isopleth (grain size) mapping yielded erupted tephra volumes (calculated according to Fierstein and Nathenson, 1992) that range between 2 km^3 (Fontana Tephra) and 7 km^3 (Upper Apoyo Tephra). After subtraction of void space and lithic contents, corresponding erupted magma masses are 2 to 7 x 10^{12} kg DRE. Using results from eruption-column modelling (Carey and Sigurdsson, 1989; Woods, 1995), mapping data indicate that eruption columns reached high into the stratosphere (25-38 km) at magma discharge rates in the order of 10^8 kg s^{-1}.

5.5.4.2. Correlations with Nicaraguan Eruptions - The same procedures followed for inter-core correlations were applied to correlate marine ash layers with tephras on land. It should be noted that chemical compositions of marine glass shards must be compared with matrix-glass compositions of on-land pumice, rather than bulk-rock compositions. Among the young (< 50 kyr) products of highly explosive eruptions at the Central NVF (Fig. 5.9), rhyolite glass from Apoyo Caldera reaches the highest silica contents (75.2-75.5 wt% SiO_2). Amphibole only occurs in dacitic to rhyolitic pumices from Chiltepe and Ometepe volcanoes. Two plinian fallout deposits from Masaya Caldera have basaltic (Masaya Triple Layer, 2120 yr. BP) and basaltic-andesitic compositions (Fontana Tephra, *c.* 50 kyr).

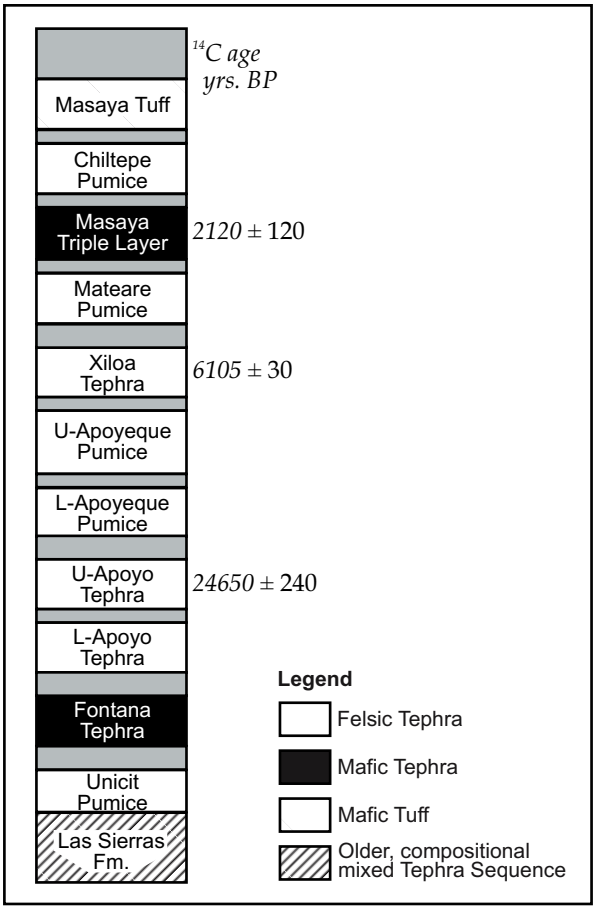

Figure 5.9: Schematic stratigraphic section showing the composite Late Pleistocene/Holocene tephra sequence produced by highly explosive eruptions at the central Nicaraguan volcanic front (Mateare and Managua-Masaya Facies).

Glass-chemical compositions (Fig. 5.10) suggest that marine ash layer M2 corresponds to the Upper Apoyeque Tephra, and layer M3 to the Upper Apoyo Tephra. These correlations are supported by petrographic observations, mineral-chemistry, and glass analyses, as well as X-Ray Fluorescence Spectroscopy (XRF) of bulk-rock samples including trace element analysis (Tab. 5.3a & b). Layer M2 shards have the same type of strongly elongated vesicles that is typical for the Upper Apoyeque Tephra, and amphiboles in layer M2 have a composition almost identical to Upper Apoyeque amphibole phenocrysts (Fig. 5.11). M3 is the only layer lacking amphibole, and Apoyo pumice does not contain amphibole as a mineral phase. These two layers thus bracket the age interval from 21 kyr (Upper Apoyo) to ~12 kyr (Upper Apoyeque). They also bracket the marine ash layer M1, which most closely matches pumice from Ometepe in both glass and mineral compositions (Figs. 5.10 & 5.11). The Ometepe Pumice in Figures 5.10 & 5.11 is the "Tierra Blanca TBL3-Layer" dated at 2720 ± 60 yr BP by Borgia and van Wyk de Vries (2003), and is thus too young to correlate with layer M1. Layer M1 probably represents an older eruption from Ometepe which occurred between 12-21 kyr but had a similar composition. Mafic layer M4 is tentatively correlated with the Fontana Tephra but this correlation needs further support by trace element data.

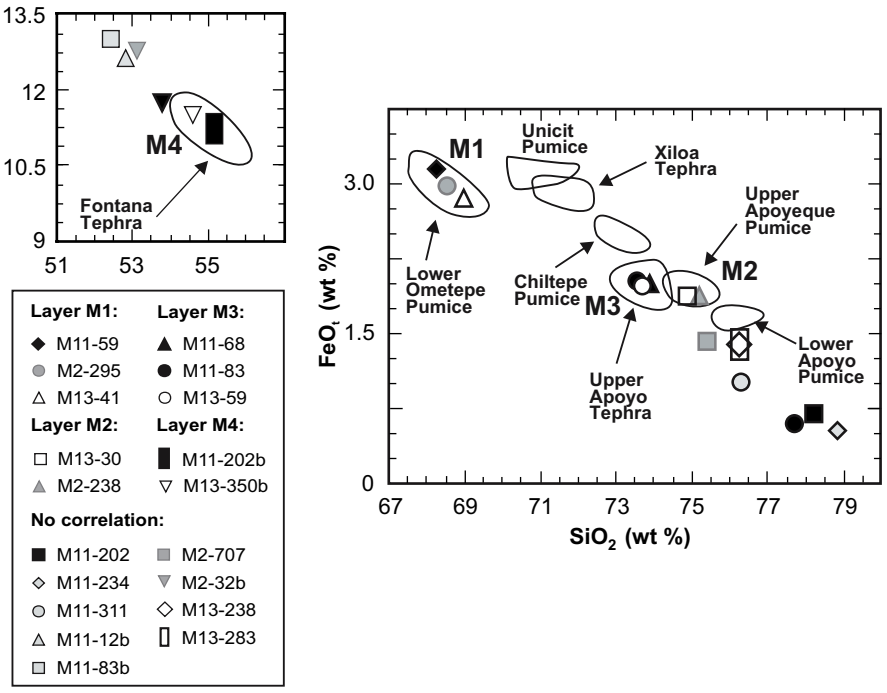

Figure 5.10: Glass shard correlation of marine ash layers (RV Meteor cruise M54/2) with tephras from the Nicaraguan VF in the FeO_t versus SiO_2 diagram.

Table 5.3a: XRF whole-rock analyses of onshore tephras and offshore ash layers.

Sample	SiO_2	TiO_2	Al_2O_3	Fe_2O_3	MgO	CaO	Na_2O	K_2O	total
					all data in wt%				
TBL3 (Borgia & van Wyk de Vries, 2003)	65.7	0.48	16.3	3.87	1.11	3.12	5.04	2.6	101
L. Ometepe	60.6	0.57	17.0	5.05	1.68	4.41	4.49	2.14	96.3
M54-2-290	61.3	0.48	16.7	4.95	1.37	4.26	4.74	2.03	96.1
U. Apoyo	64.1	0.52	15.0	4.07	1.26	3.68	3.87	2.05	94.8
M54-11/2-83	64.3	0.42	16.0	3.82	1.07	3.9	4.27	1.88	95.8
Buena Vista (Chiesa et al., 1992)	74.9	0.24	13.4	1.91	0.63	1.84	2.69	4.25	100
La Ese (0.6 Myr) (Chiesa et al., 1992)	74.5	0.29	13.3	2.09	0.24	2.19	3.13	3.82	100
ODP 170 Site 1039B, 78 m depth	74.8	0.38	13.7	2.39	0.6	1.74	3.21	4.01	101
Salitral (1.5 Myr) (Chiesa et al., 1992)	72.7	0.38	14.4	2.96	0.63	2.28	2.96	3.56	100
ODP 170 Site 1039B, 88 m depth	72.6	0.33	13.8	2.17	0.74	1.54	2.85	4.65	98.8
ODP 170 Site 1039B, 133 m depth	71.6	0.34	14.1	3.49	1.08	1.77	2.83	3.69	99.0
Layer I2 (EMP) (Ledbetter, 1985)	71.8	0.51	15.7	2.56	1.12	1.88	3.07	3.49	100

Table 5.3b: XRF trace element analyses of onshore tephras and offshore ash layers.

Sample	Ce	La	Rb	Ba	Sr	Th	Zr
			all data in ppm				
TBL3 (Borgia & van Wyk de Vries, 2003)			51		425		243
L. Ometepe	70	16	48	1168	537	4	196
M54-2-290	56	14	45	1179	554	7	189
U. Apoyo	27	14	43	1254	342	4	144
M54-11/2-234	51	14	115	979	103	10	67
Buena Vista (Chiesa et al., 1992)			71	1652	299		138
La Ese (0.6 Myr) (Chiesa et al., 1992)			73	1783	215		163
ODP 170 Site 1039B, 78 m depth			74	1457	195		205
Salitral (1.5 Myr) (Chiesa et al., 1992)			56	1657	305		200
ODP 170 Site 1039B, 88 m depth			101	1648	238		135
ODP 170 Site 1039B, 133 m depth			66	1876	242		103
Layer I2 (EMP) (Ledbetter, 1985)			55	1830	210		170
Marine Los Chocoyos (Drexler et al. 1980)	28.4 *(20.0)*	16.0 *(4.00)*	128 *(20.0)*	1104 *(287)*	107 *(15.0)*	10.0 *(3.00)*	82.0 *(20.0)*
M54-11/2-83	19	14	39	1216	378	4	137

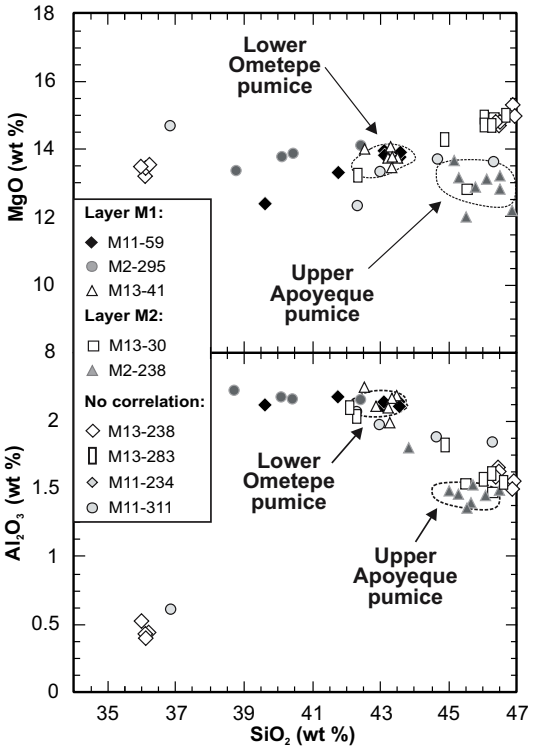

Figure 5.11: The composition of amphiboles in MgO and Al_2O_3 versus SiO_2 diagrams support the correlations of marine ash layers (RV Meteor cruise M54/2) with tephras from the Nicaraguan VF.

The marine ash layers Y-8 and G in the stratigraphy of Ledbetter (1985) (where Y-8 corresponds to the 84 kyr old Los Chocoyos ash from Atitlán volcano, Guatemala, the most important Quaternary marker horizon in Central America) have the same glass compositions as our group A high-silica rhyolites. They also contain biotite and therefore potentially correlate with layers M54-11/2-234 and M54-11/2-311, respectively. This correlation is also supported by trace element data from our XRF-bulk-rock analyses (Tab. 5.3b).

5.5.5. Role of Ash Layers during Fore-Arc Diagenesis

5.5.5.1. Alteration of Volcanic Ash on the Seafloor - Volatiles and fluids penetrating the fore-arc sediment wedge react with the sediments and the resident pore fluids. Fluid compositions thus change in response to chemical reactions and precipitation of diagenetic minerals which serve as transient reservoirs of volatile components. The presence of volcanic material in the sediments, particularly of glassy particles, can have a strong influence on diagenetic processes since volcanic glass is highly reactive. We aim to identify and quantify chemical mass transfer and reactions between volcanic glass of various compositions and seawater under realistic pressure and temperature conditions. Such alteration studies need to be considered when using geochemical signatures of volcanic ash in means of stratigraphic correlations.

While some effort has been devoted to understand dissolution rates and alteration mechanisms of basaltic glass (e.g. Berger et al., 1984; Staudigel and Hart, 1983), only few studies have considered intermediate or felsic ashes (e.g. Fiore et al., 2001). Felsic ashes from highly explosive eruptions, however, dominate the inventory of the fore arc sediments off Central America and are therefore the focus of our alteration studies

5.5.5.2. Methodology and Results - New data of basaltic and felsic glass alteration were derived from both laboratory dissolution experiments of ash and extensive field investigations of marine tephra deposits and diagenetic processes in related pore water. We performed alteration experiments under controlled P-T-X conditions (< 400 bar, < 100°C,< 6 weeks) with ashes taken from the marine cores of M54/2 as well as with their respective terrestrial tephras.

Our experimental data for the very initial stage of felsic and mafic alteration prove that the release of dissolved silica and cations such as $Fe^{2+/3+}$, Mn^{4+}, and Ba^{2+} is always accompanied by a strong decrease in alkalinity and pH (Fig. 5.12). The dissolution of ash induces an alkalinity increase due to the release and protonation of oxyanions (O^{2-}). In contrast, the exchange of oxidisable and/or hydrolysable cations (e.g. $Fe^{2+/3+}$, Al^{3+}, Ti^{4+}) with seawater cations (e.g. Na^{+}, K^{+}, Mg^{2+}) causes a decrease in alkalinity due to the proton release during oxidation and hydrolysis. Therefore, the observed alkalinity decrease clearly indicates that cation exchange proceeds at a much higher rate than ash dissolution. Volcanic ash deposited in the marine environment is thus initially equilibrated with seawater via rapid surface exchange processes accompanied by comparably slow dissolution reactions.

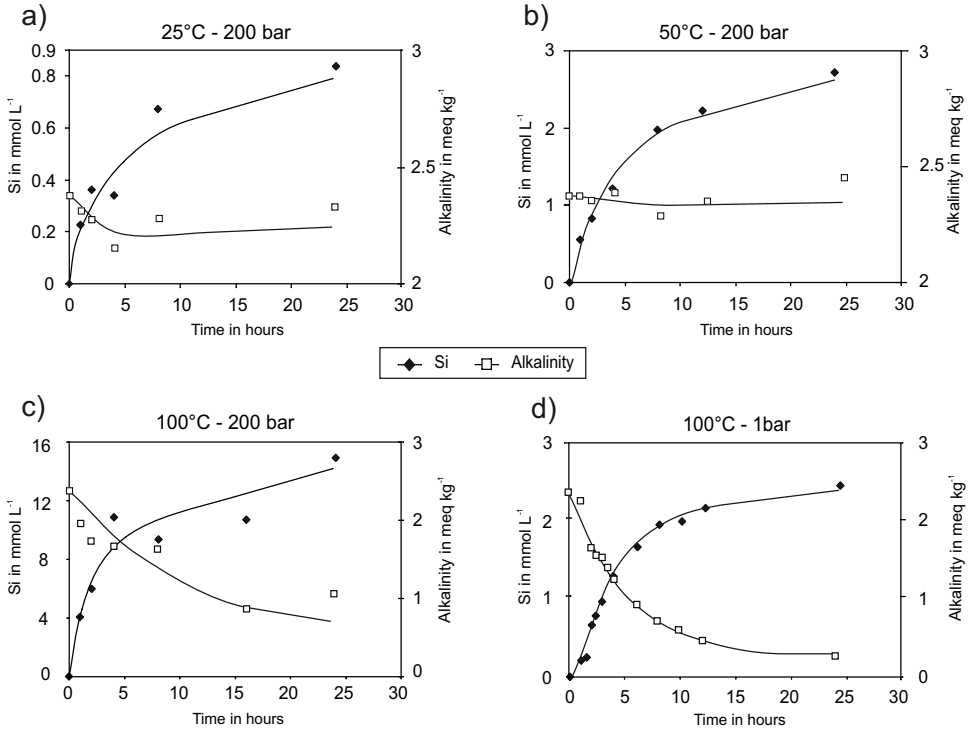

Figure 5.12: Data of kinetic experiments with felsic tephra at three different temperatures (24, 50, 100°C) and pressures of 200 (a-c) and 1 bar (d). The diagrams clearly show the strong increase in dissolved silica over time and document the decrease in alkalinity.

During mafic glass alteration in a marine environment, the loss of Si, Al, Mg, Mn, Ca, Na, and K is accompanied by the active enrichment of H_2O and the passive enrichment of Fe. Microprobe data show that this very initial stage of congruent dissolution is followed by a second stage of aging which includes the uptake of K out of the solution. The behaviour of Ca and Na does not change, still showing depletion, whereas Fe stays immobile and

becomes relatively enriched. EMP analyses indicate that alteration results in a fragile altered shard rim which accommodates about 15 wt% of water, and the shard progressively evolves from a basaltic composition at centre to a palagonite-like composition at the rim. The formation of such a palagonite rim can significantly slow down alteration of the fresh glass (Techer et al., 2001). This is reflected by the strong gradient from only weakly to strongly altered glass shards in the same ash layer. At more advanced stages of alteration, element fluxes are also affected by the formation of secondary phases such as clay minerals, zeolites, or carbonates (Stroncik-Treue, 2000).

Initial felsic glass alteration comprises a selective extraction of elements such as Si, Mg, Mn, Ca, Na, and K from the glass surface and the active uptake of up to 3 wt% of H_2O. Felsic glass alteration, however, operates somewhat differently from that of basaltic ash. Analyses of glass shards using Electron Microprobe indicates that at the advanced stage of alteration, a palagonite-like interstage product is missing. Felsic glass alteration processes result in a nearly complete dissolution of the glass followed by crystallisation of secondary minerals (smectite, phillipsite, analcime) out of the alterating solution (Schmincke, 1988) which is illustrated by the well-constrained composition of felsic ash layers and our experimental data described below.

Figure 5.13 summarises the exchange of selected elements between felsic and mafic ash and seawater during the two stages of alteration. Clearly, mobile elements such as Ca, Na, and Mg must be carefully considered when using chemical composition of ash layers to establish stratigraphic correlations.

Table 5.4: Chemical evolution of basaltic and felsic glass during seawater alteration. (Data for mafic glass alteration were taken from Berger et. al. (1987). Felsic glass composition summarises EMP-data of ash layer M54-2-238).*

Mafic glass *

	Unaltered basaltic glass	Leached glass layer (< 1µm)	Palagonite rim	Clay (smectite)
Chemical contents (wt%)				
SiO_2	55	50	44	48
Al_2O_3	12	10	10	6.5
Na_2O	3.0	2.5	2.5	0.44
CaO	9.5	8.0	8.0	5.4
FeO	15	25	25	17
MgO	3.5	4.1	4.8	5.9
K_2O	0.8	1.5	0.75	0.01
MnO	0.3	0.55	0.55	0.92

Felsic glass

	Unaltered felsic glass	Leached glass layer (< 1µm)	Seawater
Chemical contents (wt%)			
SiO_2	75	75	Precipitation of
Al_2O_3	13	13	
Na_2O	3.7	3.6	
CaO	1.9	1.6	smectite
FeO	1.8	2.1	kaolinite
MgO	0.32	0.69	
K_2O	2.6	2.8	out of the
MnO	0.09	0.10	solution

5.5.5.3. Discussion of Results - As shown in Figures 5.12a-d, seawater is enriched in silica during interaction with volcanic glass at 1 and 200 bar. Van Capellen and Qiu (1997) estimated the saturation concentration of biogenic silica at 1 bar under different temperature conditions using Equation 1:

$$log\, C_s = 6.44 \cdot \left(\frac{968}{T} \right) \quad (1)$$

where C_s describes the solubility of silica (µmol L^{-1}) and T the absolute temperature (K).

Saturation concentrations of silica for our experiments at 1 bar calculated from Equation 1 are given in Table 5.4. Comparison of these results with our experimental data (Tab. 5.4, third column) shows that Equation 1 can be used for basaltic alteration trends. However, data for felsic alteration runs differ (Fig. 5.14). Our experimental data emphasise that the dissolved silica concentration in our experiments are higher than sediments actually could achieve. Felsic ashes seem to be very reactive phases within marine sediments and therefore need to be considered as one of the major silica sources next to biogenic silica when sediment composition is dominated by volcanic ashes of felsic composition.

Table 5.5: Solubility of silica (C_s) at 1 bar under different temperature conditions (after van Capellen and Qiu, 1997) compared to our experimental data (Si_{max}).

Temperature in °C	C_s in µmol L^{-1}	Si_{max} in µmol L^{-1}
24	1520	3840
50	2780	1230
100	7010	2470

Alteration trends of mafic and felsic glasses similar to the experimental results were observed in ash layers which were recovered from sediment cores during RV *Meteor* cruise M54/2. Nearly all glass shards of each mafic ash layer were altered and the degree of alteration was variable, but not seen under the microscope. In contrast, felsic glass shards were generally fresh and coexisted with only some strongly altered shards which can be identified clearly by secondary mineralisation visible in polarised light (Fig. 5.5a). Shards showing intermediate stages of alteration are absent.

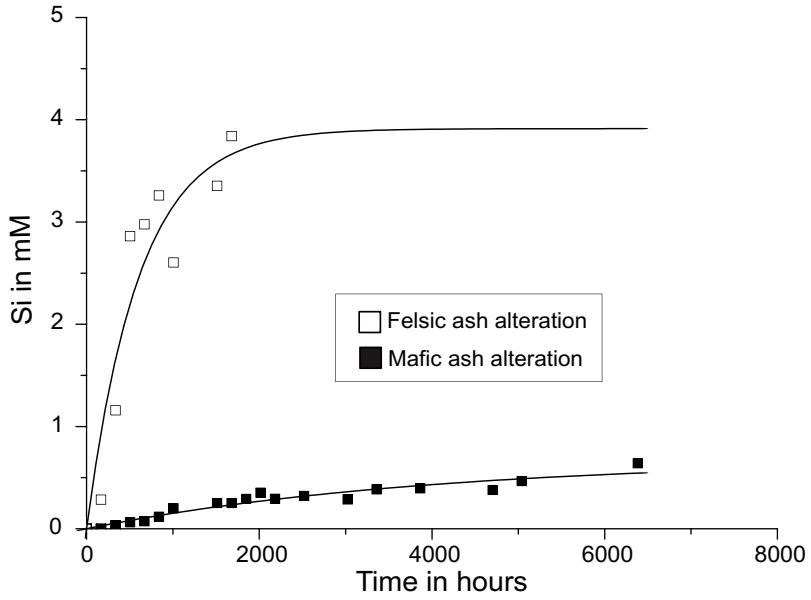

Figure 5.13: Data of kinetic experiments (24°C and 1 bar) using felsic and mafic tephra collected along the VF of Nicaragua. Note the much stronger increase in dissolved silica over time for the felsic experimental run compared to the mafic one.

Most elements enriched in pore water by alteration processes are largely re-deposited due to secondary mineralisation which may also act as a sink for trace elements lost during alteration. Lavas from Central America reflect a strong influence of variably composed Cocos Plate sediments (Patino et al., 2000). Element ratios with large stratigraphic variations in Cocos Plate sediments (e.g. Ba/Th, U/La) indicate that marine stratigraphy exerts some control on geochemical characteristics of the lavas. The knowledge of glass alteration as a sink and source for REE will therefore enhance the understanding of the chemistry of the volcanic input and output in the Central American subduction zone.

5.6. Conclusions and Implications of an Integrated Marine and Terrestrial Tephrostratigraphy in Central America

5.6.1. Implications for Eruption Dynamics and Event Chronology

The marine tephras of the Nicaraguan continental slope extend the reconstructed areal thickness distribution of volcanic fallout deposits from 50 km (as traceable on land) to more than 250 km from source. Calculated erupted tephra volumes including the marine tephra dispersal almost double the volumes estimated from terrestrial data alone (e.g. Upper Apoyo Tephra; Fig. 5.15). More precise assessments of erupted tephra

volumes (or magma masses) are essential when studying various aspects of subduction zone volcanism such as:

1) temporal and regional variations of magma discharge,
2) time-averaged magma discharge as a function of magma composition,
3) volatile input into the atmosphere, and
4) risk assessment from temporal evolution of eruption magnitudes.

Older volcanic deposits are commonly only sporadically exposed on land, leaving the stratigraphic record partially incomplete. This problem can be solved by correlation with marine sediment cores that better preserve the stratigraphic successions. Thus, our RV *Meteor* cores contain ash beds especially in the lower core sections for which corresponding deposits on land have not yet been found.

Several sulphur and chlorine spikes from yet unknown sources were identified in Greenland ice-cores (e.g. Zielinski et al., 1994). Theses peaks fall close to the time periods when volcanoes in Nicaragua produced 22-32 km high eruption columns. Our ongoing work will show if such a correlation can be substantiated.

5.6.2. Implications of Diagenesis

There is a growing interest in the interaction between volcanic glass and seawater, especially in the Central American fore arc sediments, because of the extensive volcanism that occurs along the volcanic chain of Nicaragua and Costa Rica. Natural waters obtain their chemical composition through chemical reactions with the surrounding rock (Stumm and Morgan, 1996). Therefore, the alteration of volcanic glass by seawater in the Central America subduction zone can be considered as one of the most important factor contributing to the subduction process, since altered glass is one of the major sediment fractions that is transported down the slope and into the subduction zone, where it may affect future subduction zone processes including arc volcanism.

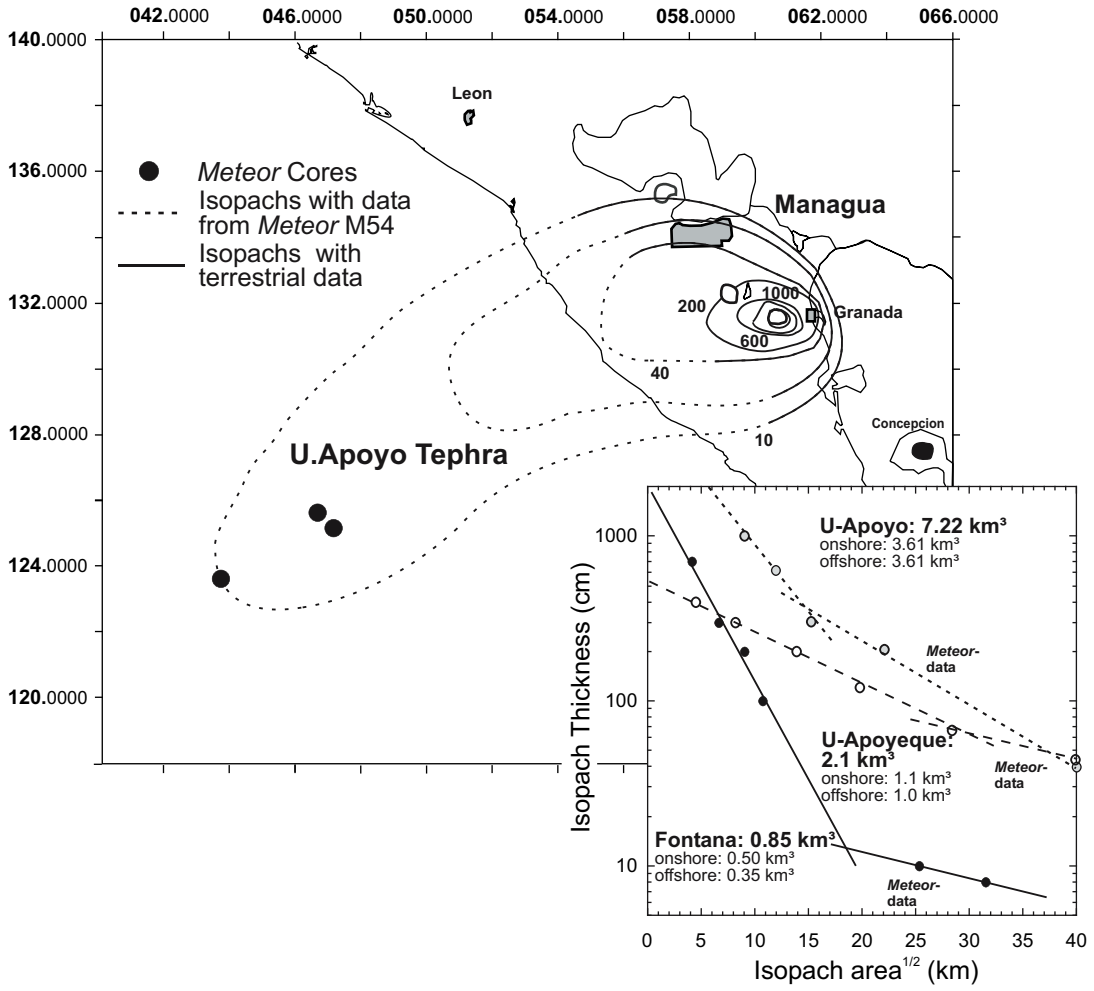

Figure 5.14: Example isopach map of the Upper Apoyo Tephra illustrating the significance of marine tephra data for the areal distribution. The inset figure shows isopach thickness versus square-root of isopach area data from three tephras used to calculate their volumes according to Fierstein and Nathenson (1992). Note how the offshore segments of the lines contribute to the total volume.

5.6.3. Implications for Marine Sedimentation or Erosion Rates

Dated ash layers allow determination of time-averaged sedimentation rates for interbedded sediments. Results obtained from single cores must, however, be regarded with caution. In Nicaragua for example, the 21-11 kyr interval between M2 and M3 in core M54-13 contains 19 cm clastic sediment; the M2 to M1 section of the interval in core M54-2 contains 35 cm sediment, and the M1 to M3 section in core M54-11/2 contains 45 cm sediment. This would suggest that sedimentation rates are highest on the incoming plate rather than on the continental slope. A more detailed investigation of sediment composition and structure is clearly necessary to clarify the reasons for

this phenomenon. It seems reasonable to assume that the seemingly low sedimentation rates on the slope reflect in fact high and locally variable erosion rates and a variable depositional environment. On the other hand, the peculiar morphology of the incoming plate with up to several hundred meter high scarps generated by bent-faults (Ranero et al., 2003) suggests that sedimentation rates may have dramatically increased near M54-11/2 by mass wasting at these scarps.

In summary, marine tephrostratigraphy provides a powerful tool that can be applied in a wide range of geoscientific fields in Central America. Results from the RV *Meteor* cruise M54/2 at the Nicaraguan slope will be extended by more data from new cores obtained during RV *Sonne* cruise SO173 and following research cruises along the Middle American Trench. Such interdisciplinary approaches are necessary to achieve a more comprehensive understanding of past, present, and possibly future geologic processes in Central America.

References

Berger G., Claparols C., Guy C., and Daux V. (1984) Dissolution rate of basalt glass in silica-rich solutions: Implications for long term alteration. *Geochimica et Cosmochimica Acta* **58**(22), 4875-4886.

Blum P. (1997) *Physical properties handbook: A guide to the ship board measurement of physical properties of deep-sea cores.*

Borgia A. and Wyk de Vries van B. (2003) The volcano-tectonic evolution of Concepción, Nicaragua. *Bulletin of Volcanology* **65**, 248-266.

Bowles F. A., Jack R. N., and Carmichael I. S. E. (1973) Investigation of deep-sea volcanic ash layers from equatorial Pacific cores. *GSA Bulletin* **84**, 2371-2388.

Cadet J.-P. and Fujioka K. (1980) Neogene volcanic ashes and explosive volcanism: Japan Trench transect, *Initial Reports of the Deep Sea Drilling Project* **57**(2), 1027-1034.

Cadet J.-P., Pouclet A., Thisse Y., Bardintzeff J. M., and Azéma J. (1982a) Middle America Neogene explosive volcanism and ash layers: Evidence from the Middle America Trench transect. *Initial Reports of the Deep Sea Drilling Project* **67**, 475-491.

Cadet J.-P., Thisse Y., Pouclet A., Bardintzeff J. M., and Stephan J. F. (1982b) Tephra from Deep Sea Drilling Project Leg 66: Middle American Trench Transect (Southern Mexico). In *Initial Reports of the Deep Sea Drilling Project* **66**, 687-698.

Cambray H. and Cadet J.-P. (1994) Testing global synchronism in peri-Pacific arc volcanism. *Journal of Volcanology and Geothermal Research* **63**, 145-164.

Cambray H., Pubellier M., Jolivet L., and Pouclet A. (1995) Volcanic activity recorded in deep-sea sediments and the geodynamic evolution of western Pacific island arcs. In: *Active Margins and Marginal Basins of the western Pacific*, 97-124.

Carey S. and Sigurdsson H. (1989) The intensity of plinian eruptions. *Bulletin of Volcanology* **51**, 28-40.

Carey S. and Sigurdsson H. (2000) Grain size of Miocene volcanic ash layers from Sites 998, 999, and 1000: Implications for source areas and dispersal. In *Proceedings of the Ocean Drilling Program* **165**, 101-113.

Chiesa S., Civelli G., Gillot P.-Y., Mora O., and Alvarado G. E. (1992) Rocas piroclásticas asociadas con La Formación de la Caldera de Guayabo, Cordillera de Guanacaste, Costa Rica. *Revista de la Geología América Central* **14**, 59-75.

Clift P. D. and Blusztajn J. (1999) The trace-element characteristics of Aegean and Aeolian volcanic arc marine tephra. *Journal of Volcanology and Geothermal Research* **92**, 321-347.

Drexler J. W., Rose jr. W. I., Sparks R. S. J., and Ledbetter M. T. (1980) The Los Chocoyos Ash, Guatemala: A Major Stratigraphic Marker in Middle America and in the Three Ocean Basins. *Quaternary Research* **13**, 327-345.

Ehrenborg J. (1996) A new stratigraphy for the Tertiary volcanic rocks of the Nicaraguan Highland. *GSA Bulletin* **108**(7), 830-842.

Fierstein J. and Nathenson M. (1992) Another look at the calculation of fallout tephra volumes. *Bulletin of Volcanology* **54**, 156-167.

Fiore S., Huertas F.-J., Huertas F., and Linares J. (2001) Smectite formation in rhyolitic obsidian as inferred by microscopic (SEM-TEM-AEM) investigation. *Clay Minerals* **36**(4), 489-500.

Hein J. R., Scholl D. W., and Miller J. (1978) Episodes of Aleutian Ridge explosive volcanism. *Science* **199**, 137-141.

Hunt C., Moskowitz B. M., and Banerjee S. K. (1995) Magnetic properties of rocks and minerals. *Rock Physics and Phase Relations* AFU Ref. Shelf 3, 189-204.

Kennett J. P., McBirney A. R., and Thunell R. C. (1977) Episodes of Cenozoic volcanism in the circum-Pacific region. *Journal of Volcanology and Geothermal Research* **2**, 145-163.

Kimura G., Silver E. A., and Blum P. (1997) Costa Rica acrretionary wedge. *Proceedings of the Ocean Drilling Program, Preliminary Reports* **170**, 1-86.

Ledbetter M. T. (1982) Tephrachronology at Sites 502 and 503. In *Initial Reports of Deep Sea Drilling Project* **68**, 403-408.

Ledbetter M. T. (1985) Tephrochronology of marine tephra adjacent to Central America. *GSA Bulletin* **96**, 77-82.

Ninkovich D. and Sykes L. R. (1975) Distribution stratigraphic position and age of ash layer "L" in Panama Basin region. *Earth and Planetary Science Letters* **27**, 20-34.

Patino L. C., Carr M., and Feigenson M. D. (2000) Local and regional variations in Central American arc lavas controlled by variations in subducted sediment input. *Contributions to Mineralogy and Petrology* **138**, 256-283.

Pearce N. J. G., Westgate J. A., Perkins W. T., Eastwood W. J., and Shane P. (1999) The application of laser ablation ICP-MS to the analysis of volcanic glass shards from tephra deposits: bulk glass and single shard analysis. *Global and Planetary Change* **21**, 151-171.

Pouclet A., Cadet J.-P., K. F., and Bourgois J. (1985) Ash Layers from Deep Sea Drilling Project Leg 84: Middle America Trench Transect. In *Initial Reports Deep Sea Drilling Project* **84**, 609-618.

Pouclet A. and Scott S. D. (1992) Volcanic ash layers in the Japan Sea: Tephrochronology of Sites 798 and 799. In *Proceedings of the Ocean Drilling Program, Scientific Results* **127/128**, 791-803.

Prueher L. M. and Rea D. K. (2001) Tephrochronology of the Kamchatka - Kurile and Aleutian arcs: Evidence for volcanic episodicity. *Journal of Volcanology and Geothermal Research* **106**, 67-84.

Ranero C. R., Phipps-Morgan J., McIntosh K., and Reichert C. (2003) Bending, faulting and mantle serpentinisation at the Middle America Trench. *Nature* **425**, 367-373.

Rose W. I., Bornhorst T. J., and Drexler J. W. (1982) Preliminary correlation of quaternary volcanic ashes from the Middle America Trench off Guatemala, Deep Sea Drilling Project Leg 67. In *Initial Reports of the Deep Sea Drilling Project* **67**, 493-495.

Rose W. I. J., Grant N. K., and Easter J. (1979) Geochemistry of the Los Chocoyos Ash, Quezaltenango Valley, Guatemala. *GSA Special Paper* **180**, 87-99.

Schmincke H.-U. (1988) Pyroklastische Gesteine. In *Sedimentgesteine* (ed. H. Füchtbauer), Schweizerbart'sche Verlagsbuchhandlung, 731-778.
Schmincke H.-U. (2003) *Volcanism*. Wissenschaftliche Buchgesellschaft
Shane P., Black T. M., Alloway B. V., and Westgate J. A. (1996) Early to middle Pleistocene tephrochronology of North Island, New Zealand: Implications for volcanism, tectonism, and paleoenvironments. *GSA Bulletin* **108**, 915-925.
Shane P., Froggatt P., Black T., and Westgate J. A. (1995) Chronology of Pliocene and Quaternary bioevents and climatic events from fission-track ages on tephra beds, Wairarapa, New Zealand. *Earth and Planetary Science Letters* **130**, 1241-1254.
Shipboard Scientific Party. (2002) Southeast Pacific paleoceanographic transects. *Proceedings of the Ocean Drilling Program, Preliminary Reports* **202**, 1-80.
Shipboard Scientific Party. (2003) Fluid flow and subduction flux across the Costa Rica Convergent Margin: Implications for the seismogenic zone and subduction factory. *Proceedings of the Ocean Drilling Program, Preliminary Reports* **205**, 1-55.
Sigurdsson H., Kelley S., Leckie R., Carey S., Bralower T., and King J. (2000) History of circum-Caribbean explosive volcanism: $^{40}Ar/^{39}Ar$ dating of tephra layers. *Proceedings of the Ocean Drilling Program, Scientific results* **165**, 299-314.
Sigurdsson H., Leckie R. M., Acton G. D. et al. (1997) Caribbean Volcanism, Cretaceous/Tertiary impact, and Ocean-Climate History: Synthesis of Leg 165. *Proceedings of the Ocean Drilling Program, Initial Reports* **165**, 377-400.
Staudigel and Hart. (1983) Alteration of basaltic glass: Mechanisms and significance for oceanic crust-seawater budget. *Geochimica et Cosmochimica Acta* **47**, 337-350.
Straub S. and Schmincke H.-U. (1998) Evaluating the tephra input into Pacific Ocean sediments: Distribution in space and time. *Geologische Rundschau* **87**(3), 461-476.
Stroncik-Treue N. A. (2000) Low-temperature alteration of mafic volcanic glasses - chemical evolution, mass-balancing and kinetics. PhD, University of Kiel.
Stumm W. and Morgan J. J. (1996) *Aquatic Chemistry*. Wiley.
Techer I., Advocat T., Lancelot J., and Liotard J.-M. (2001) Dissolution kinetics of basaltic glasses: control by solution chemistry and protective effect of the alteration film. *Chemical Geology* **176**, 235-263.
Ukstins Peate I., Baker J. A., Kent A. J. R., Al-Kadasi M., Al-Subbary A., Ajylew D., and Menzies M. (2003) Correlation of Indian Ocean tephra to individual Oligocene silicic eruptions from Afro-Arabian flood volcanism. *Earth and Planetary Science Letters* **211**, 311-327.
van Capellen P. and Qiu L. (1997) Biogenic silica dissolution of sediments in the Southern Ocean, I, Solubility. *Deep Sea Research Part II* **44**(5), 1109-1128.
von Huene R. and Scholl D. W. (1991) Observations at convergent margins concerning sediment subduction, subduction erosion, and the growth of the continental crust. *Reviews of Geophysics* **29**, 279-316.
Wehrmann, H., Kutterolf, S., Freundt, A., Schmincke, H.-U. (2003) Stratigraphy and eruption dynamics of, and volatile release from highly explosive volcanic eruptions in Central Nicaragua during the last 30 kyr. *Abstracts for IUGG 2003 in Sapporo*, **week A**, A532.
Woods A. W. (1995) The dynamics of explosive volcanic eruptions. *Reviews of Geophysics* **33**, 387-414.
Zielinski G. A., Mayewski P. A., Meeker L. D., Grönvold K., Germani M. S., Whitlow S., Twickler M. S., and Taylor K. (1997) Volcanic aerosol records and tephrochronology of the Summit, Greenland, ice cores. *Journal of Geophysical Research* **102**(26), 625-640.
Zielinski G. A., Mayewski P. A., Meeker L. D., Whitlow S., Twickler M. S., Morrison M., Meese D., Alley R., and Gow A. J. (1994) Record of volcanism from the GISP2 ice core (Greenland) since 7000 B.C. and implications for the volcano-climate system. *Science* **264**, 948-952.

Danksagung

Ich möchte allen danken, die mich dabei unterstützt haben, diese Dissertation anzufertigen. Für mich war die Zeit an der Christian-Albrechts-Universität zu Kiel und am IFM-GEOMAR eine sehr anregende und lehrreiche Zeit. Meine Projektleiter PD Dr. Klaus Wallmann und Dr. Mark Schmidt standen mir jederzeit für inhaltliche Diskussionen zur Verfügung und gewährten mir gleichzeitig den Freiraum, der produktives und kreatives Arbeiten erst möglich macht. Mit Dr. Steffen Kutterolf, Oliver Bartdorff, Christoph Beier, Dr. Emanuel Söding und Dr. Svend Duggen führte ich zahlreiche interessante und hilfreiche Diskussionen. Von ihnen bekam ich auch in schwierigen Phasen die notwendige moralische Unterstützung. Inge Dold unterstütze mich viele Male im Labor, war immer mit praktischen Anregungen zur Stelle und achtete vorbildlich darauf, dass künstliches Meerwasser immer in ausreichenden Mengen zur Verfügung stand. Danken möchte ich auch Michael Weiss und Judith Kaatz für ihre unermüdliche Ausdauer beim Picken kleinster Glaspartikel. Mathias Marquardt, Sandra Mansor, Emelina Corrales Cordero und Dr. Warner Brückmann erleichterten und erheiterten mir die vielen, vielen Stunden an der Porenwasserpresse im Kühlcontainer.

Die MitarbeiterInnen der genutzten analytischen Einrichtungen standen mir bei Bedarf mit Rat und Tat zur Seite, insbesondere danke ich Dr. Yann Lahaye, Heike Anders, Carsten Schaffors, Kristin Nass, Anke Bleyer und Mario Thöner.

Mein Dank gilt außerdem dem Korreferenten dieser Arbeit sowie den Mitgliedern der Prüfungskommission, für ihre Bereitschaft, sich mit meiner Arbeit kritisch auseinander zusetzen.

Meinen Eltern möchte ich an dieser Stelle für das über all die Jahre entgegengebrachte Vertrauen und die unermüdliche Unterstützung danken und, last but not least, danke ich meinen FreundInnen für ihre Geduld und Unterstützung in den letzten Jahren.

Die Arbeit wurde von der DFG im Rahmen des SFB 574 „Volatile und Fluide in Subduktionszonen - Klima-Rückkoppelungen und Auslösemechanismen von Naturkatastrophen“ gefördert. Die Christian-Albrechts-Universität zu Kiel hat ebenfalls finanzielle, personelle und materielle Ressourcen beigesteuert.

Lebenslauf

Ulrike Schacht

geboren am 03.04.1977
in Rostock
Staatsangehörigkeit: deutsch

1983 - 1995	Polytechnische Oberschule und Gymnasium in Rostock; Abitur im Juni `95
Okt.`96 - Okt.`01	Technische Universität Berlin; Studium der Geoingenieurwissenschaften und Angewandten Geowissenschaften Vordiplom im November `99 Diplom im Oktober ‘01
seit Nov.`01	Christian-Albrechts Universität zu Kiel, IFM-GEOMAR; Wissenschaftliche Angestellte im Sonderforschungsbereich 574